

The biogeochemical cycle of dissolved aluminium in the Atlantic Ocean



Dissertation

vorgelegt von

Jan-Lukas Menzel Barraqueta

zur Erlangung des akademischen Grades eines Doktors der Naturwissenschaften

- Dr. rer. nat. –

an der Mathematisch-Naturwissenschaftlichen Fakultät der Christian-Albrechts-Universität
zu Kiel

1. Gutachter: Prof. Dr. Eric P. Achterberg

2. Gutachter: Prof. Dr. Martin Frank

Tag der Disputation: 01.06.2018

Contents

Abstract	IX
Kurzfassung	XI
Introduction	15
Frame of the project	20
Dissolved aluminium	22
Sources of dAl to the ocean	24
Removal of dAl from seawater	28
Oceanic distribution of dissolved aluminium	29
Dissolved aluminium as an atmospheric deposition tracer	32
Study areas	34
Aim and objectives of the study	36
Methods	47
Pre-cruise preparation	49
Sampling procedure	50
Analysis of dissolved aluminium	54
Ancillary measurements	63
Chapter 3: Aluminium in the North Atlantic Ocean and the Labrador Sea (GEOTRACES GA01 section): roles of continental inputs and biogenic particle removal	71
Chapter 4: Atmospheric deposition fluxes over the Atlantic Ocean: A GEOTRACES case study	119
Chapter 5: The dissolved aluminium plume of the Congo River	179

Synthesis and future recommendations	203
Acknowledgments	219
Statement of declaration	221
List of Figures	223
List of Tables	227
List of Abbreviations	229
Curriculum Vitae	233

Abstract

Dissolved aluminium (dAl) is the most abundant metal in the Earth's crust and has not known biological function. Dissolved aluminium is supplied to the ocean through several sources which include atmospheric deposition, rivers, sedimentary, and hydrothermal sources. The major removal of dAl from seawater is via adsorption onto particles with subsequent sinking of the particles which are finally buried at the seafloor. Dissolved aluminium concentrations in surface waters can be converted into atmospheric deposition fluxes. Atmospheric deposition fluxes to the surface of the ocean are challenging to determine and present large uncertainties due to the inter-seasonal variability in the mechanisms and sources supplying aerosols to the ocean. Therefore it is important to study the distribution and understand the mechanisms that supply and remove dAl to and from the seawater. The work presented in this thesis has focused on the biogeochemical cycling of dAl in surface waters and water column of the Atlantic Ocean. Chapter 3 presents the largest high-resolution vertical and lateral dataset of dAl that exists in the North Atlantic Ocean (>40°N) and in the Labrador Sea. The latter regions present large phytoplankton blooms and during this study it was found that diatoms directly influence the transfer of the dAl phase into the particulate aluminium phase. In the North Atlantic Ocean (>40°N) and in the Labrador Sea dAl displayed, in general, a recycled type distribution which differs from other regions in the Atlantic Ocean and seems to be coupled with surface uptake and the dissolution of diatoms frustules at depth. In chapter 4 the potential use of dAl as an atmospheric deposition tracer was studied over four different regions along the Atlantic Ocean. The studied regions showed marked regional differences in the concentration of dAl in surface waters as a

consequence of varying degrees of aluminium sources and sinks. The datasets presented in chapter 4 have now filled in gaps for regions where no, or limited, dAl data and atmospheric deposition fluxes were available. These new datasets provide a baseline for future modelling studies to test and improve the mechanisms that influence the biogeochemical cycling of dAl in surface waters. The atmospheric deposition fluxes determined in this study from the concentration of dAl in surface waters show, in general, a good agreement with modelling studies. However, in regions affected by enhanced aluminium inputs from non-mineral dust sources or enhanced removal by suspended particles the atmospheric deposition fluxes calculated show low agreement with previous studies. In chapter 5 the distribution of dAl within the Congo River Plume in the Southeast Atlantic Ocean was studied. Prior to this study, the latter region was largely under sampled and this study represents the largest dataset of dAl in this region and it is the first dataset that has traced the influence that the Congo River Plume has on dAl concentrations, which extends as far as 1300 km from the river mouth. The input of dAl from the Congo River Plume showed a conservative behaviour, as a strong correlation was found between salinity and dAl. In this study the flux of dAl from the Congo River into the Southeast Atlantic was calculated and determined that the Congo River accounts for ca. 7.5% of the global world river to ocean dAl flux.

Overall, the results presented in this thesis have identified processes which control the distribution of dAl in the North Atlantic Ocean, tropical Atlantic, Southeast Atlantic, South Atlantic, and it has determined atmospheric deposition and riverine fluxes of dAl to the ocean.

Kurzfassung

Gelöstes Aluminium (dAl, „dissolved“) ist das am häufigsten vorkommende Metall in der Erdkruste, es übernimmt nach heutigem Kenntnisstand jedoch keinerlei biologische Funktion. Gelöstes Al wird von verschiedenen Quellen in den Ozean eingetragen, vornehmlich durch atmosphärischen Niederschlag, Fluss-, Sediment und hydrothermalen Eintrag. Der größte Entzug von dAl in Meerwasser erfolgt über Adsorption an Partikeln, welche absinken und letztendlich am Meeresboden begraben werden. Die dAl-Konzentration im Meerwasser findet als Indikator für lithogenen ozeanischen Eintrag Verwendung. Ausgehend von dessen Oberflächenkonzentrationen können Berechnungen zu Flussmengen atmosphärischen Eintrags angestellt werden - lithogener Eintrag allgemein ist eine bedeutende Quelle für Mikronährstoffe. Diese Bestimmung von Flussmengen ist allgemein als schwierig zu betrachten. Sie sind mit großer Unschärfe hinsichtlich des Mechanismus der Eintragswege und aufgrund der Saisonalität aerosolbedingter Niederschläge behaftet. Daher ist es entscheidend den Mechanismus zu untersuchen, der dem Eintrag und auch der Abförderung von dAl zu Grunde liegt. Die Arbeit der hier vorliegenden Dissertation konzentriert sich auf den biogeochemischen Zyklus des dAl im Oberflächenwasser und der Wassersäule des Atlantischen Ozeans allgemein. Kapitel 3 präsentiert den bisher umfangreichsten, hochauflösenden Datensatz des gelösten Al (vertikal wie lateral) im Nord-Atlantischen Ozean und der Labradorsee. Letztere ist durch große Algenblüte gekennzeichnet – Diatomeen, die nach dieser Studie maßgeblich dazu beitragen, dAl in die partikuläre Phase zu tragen. Die hier dargestellten Transekte des Nordatlantiks und der Labradorsee zeigen eine Verteilung des dAl, das dem eines recycelten Nährstoffs entspricht. Ein

Befund, der von anderen Regionen des Atlantischen Ozeans abweicht und eher mit der Oberflächenaufnahme durch Diatomeen und deren Frustul-Zersetzung in größerer Tiefe in Verbindung zu stehen scheint. Kapitel 4 diskutiert die mögliche Verwendung des dAl als Marker für atmosphärischen Eintrag innerhalb vier verschiedener Regionen des Atlantischen Ozeans. Die untersuchten Gebiete zeigen regionale Unterschiede in der Oberflächenkonzentration, die eine Konsequenz verschiedener Quellen und Senken ist. Insgesamt füllt der Datensatz des vierten Kapitels Lücken von eingeschränkter Genauigkeit des dAl und des Atmosphäreneintrags, die bisher für die entsprechenden Regionen hingenommen werden musste. Diese erweiterten Datensätze stellen eine Basislinie für zukünftige Studien wie Modellierungen dar und können zum Testen und Verbessern der biogeochemischen Mechanismen des dAl im Oberflächenwasser Verwendung finden. Der auf dieser Grundlage berechnete atmosphärische Teilchenflusseintrag ist in guter Übereinstimmung mit entsprechenden Modellierungsversuchen. Allerdings besteht wenig Übereinstimmung zu vorangegangenen Studien für Regionen, die durch erhöhten nicht-mineralischen Eintrag und/oder durch verstärkten Abtransport an suspendierten Partikeln gekennzeichnet sind. Kapitel 5 untersucht die Verteilung des dAl innerhalb der Congo-Flussfahne des südöstlichen Atlantischen Ozeans. Dieser Region wurde bisher probentechnisch wenig Beachtung geschenkt, sodass der vorgestellte dAl-Datensatz nicht nur der längste innerhalb der Region ist, sondern erstmalig auch den Einfluss des Congoflusses bis in 1300 km Entfernung zur Flussmündung abzeichnet. Der Congo dAl-Eintrag verhält sich konservativ. Es besteht eine große Korrelation zwischen dAl-Konzentration und Salinität. Die Studie berechnet abschließend den dAl-Materiefluss und kommt zu dem Ergebnis, dass der

Congo ca. 7,5% des jährlich-weltweiten Flusseintrags an dAl in den Ozean zur Folge hat.

Diese Studie zeigt Prozesse auf, die der Verteilung des dAl im Nord-Atlantischen Ozean, dem tropischen Atlantik, dem südöstlichen wie auch dem südlichen Atlantik zu Grunde liegen. Des Weiteren wurden atmosphärische als auch fluviale, ozeanische dAl-Einträge bestimmt.

Introduction

1. Introduction

1.1 What is a trace metal? Why study them?

Trace metals are elements which are present at concentrations of less than micromolar (μM) molar in a solution. It is important to study the distribution and behaviour of trace metals in seawater since they play an essential role regulating global ecosystem functioning. Many trace metals are essential nutrients required to sustain life (e.g. Fe, Mn, Zn), others are toxic at elevated concentrations (e.g. Pb, Ag, Hg), and some of the metals are used as tracers or proxies to explain important processes in marine biogeochemistry (e.g. Al, Mn, Cd). Table 1.1 shows key trace elements and isotopes studied in the International GEOTRACES programme (see below) (Anderson et al., 2014) and their respective importance for oceanography.

1.2 Trace metals in the ocean

The distribution and concentration of trace metals in the ocean is controlled by several processes and balanced by their respective sources and sinks. Trace metals are classified according to their oceanic distribution, into three principal different categories: (i) Conservative-type distribution; (ii) Recycled- or nutrient-type distribution; (iii) Scavenged-type distribution.

Chapter 1 - Introduction

Table 1.1: Key trace elements and isotopes and their respective importance in oceanography (www.geotraces.com)

Key parameter	Examples of use
<i>Trace Elements</i>	
Fe	Essential micronutrient
Al	Tracer of Fe inputs (from mineral dust and elsewhere)
Zn	Micronutrient; potentially toxic at high concentration
Mn	Tracer of Fe inputs and redox cycling
Cd	Essential micronutrient; palaeoproxy for nutrient content of waters
Cu	Micronutrient; potentially toxic at high concentration
<i>Stable isotopes</i>	
$\delta^{15}\text{N}$ (nitrate)	Modern and palaeoproxy for nitrate cycling
$\delta^{13}\text{C}$	Modern and palaeoproxy for nutrient content and ocean circulation
<i>Radioactive isotopes</i>	
^{230}Th	Constant flux monitor in sediments; tracer of modern ocean circulation and particle
^{231}Pa	Palaeoproxy for circulation and productivity; tracer of modern particle processes
<i>Radiogenic isotopes</i>	
Pb isotopes	Tracer of natural and contaminant sources to the ocean
Nd isotopes	Tracer of natural sources of TEIs to the ocean

(i) Conservative-type trace metals display a narrow range of concentrations in seawater, have long oceanic residence times ($<10^5$ yr), and show varying concentrations in proportion to salinity. Examples of trace metals showing this type of distribution are molybdenum (Mo), tungsten (W), rhenium (Re), caesium (Cs), and thallium (Tl).

(ii) Recycled- or nutrient-type trace metals are actively or passively assimilated by phytoplankton and typically show depleted concentrations in surface waters (e.g. photic layer) due to biological uptake which increase with depth due to remineralization or dissolution of sinking particles (organic and inorganic). Their oceanic concentrations tend to increase along the flow path of deep water masses. Examples of trace metals showing this type of distribution are cadmium (Cd) and zinc (Zn).

(iii) Scavenged-type trace metals are particle reactive and have relatively short oceanic residence times. Generally, they display enhanced concentrations proximal to their immediate sources and their concentrations decrease along the flow path of deep water masses due to continual removal by particles. An example for a trace metal showing this type of distribution is aluminium (Al).

Besides these three principal distribution categories there are also trace metals which exhibit either a hybrid-type or a mixed-type distribution. Trace metals showing a hybrid-type distribution, such as iron (Fe) and copper (Cu), are strongly impacted by both remineralization and scavenging processes. Trace metals which display a mixed-type distribution exist in several chemical forms which display different distributions. Examples of trace metals which exhibit a mixed-type distribution are germanium (Ge), selenium (Se).

1.3 Frame of the PhD: the GEOTRACES Programme

The GEOTRACES Programme is an international study of the chemistry of trace elements and their isotopes in the ocean (Anderson et al., 2014). Before the GEOTRACES Programme, the progress and knowledge gained in the field of trace elements in the ocean was limited to relatively few, isolated studies. As an example, Figure 1.1 shows the few locations below 2000 m depth, as of the year 2003, where seawater was sampled and analysed for iron concentrations. Thus, it became necessary to develop an international programme where a host of nations would sample the oceans along sections of ocean basins at high resolution. In the year 2000 the first meetings started in order to develop the project, following other effective international collaboration projects such as GEOSECS.

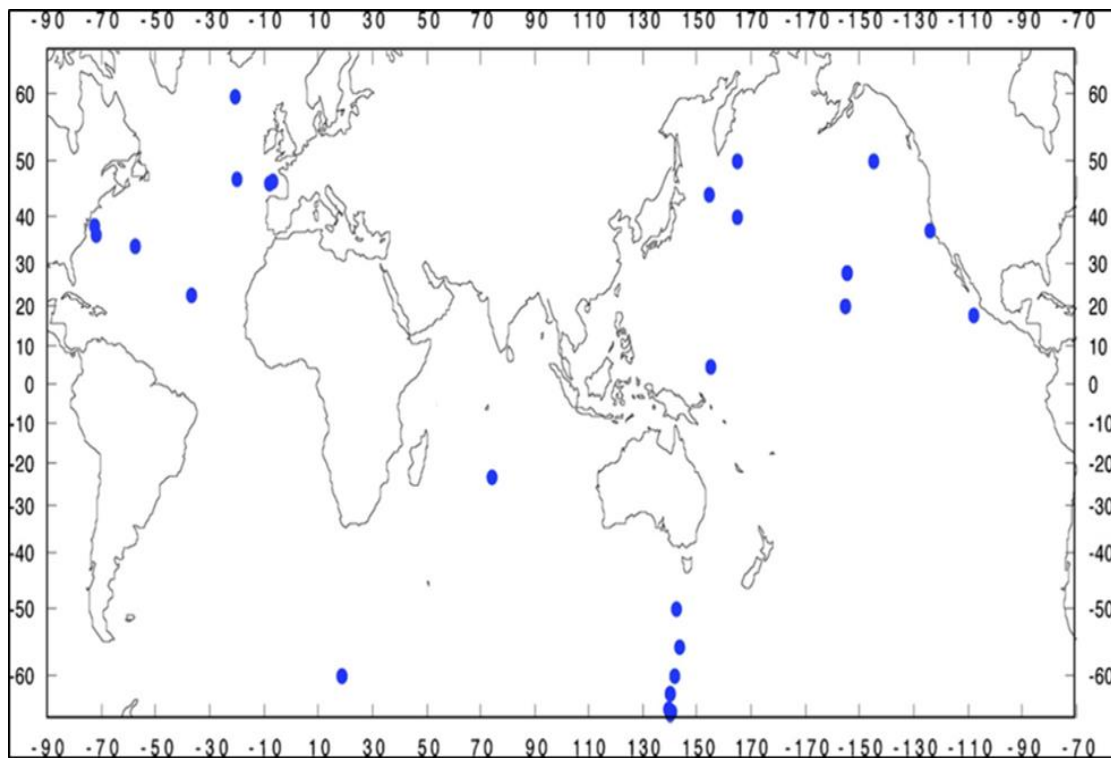


Figure 1.1: Locations where dissolved iron has been analysed below 2000 m (Group, 2007). Permission for reproduction has been obtained by the publisher.

The mission of the GEOTRACES Programme is “to identify processes and quantify fluxes that control the distribution of key trace elements and isotopes in the ocean, and to establish the sensitivity of these distributions to changing environmental conditions” (www.geotraces.com). GEOTRACES implements its mission by means of high resolution sampling strategies undertaken through oceanic sections and process studies. At present, more than 35 different nations collaborate in the project; thus far 99 cruises have been completed and 1054 stations sampled (Figure 1.2, www.geotraces.com; accessed on December 2017).

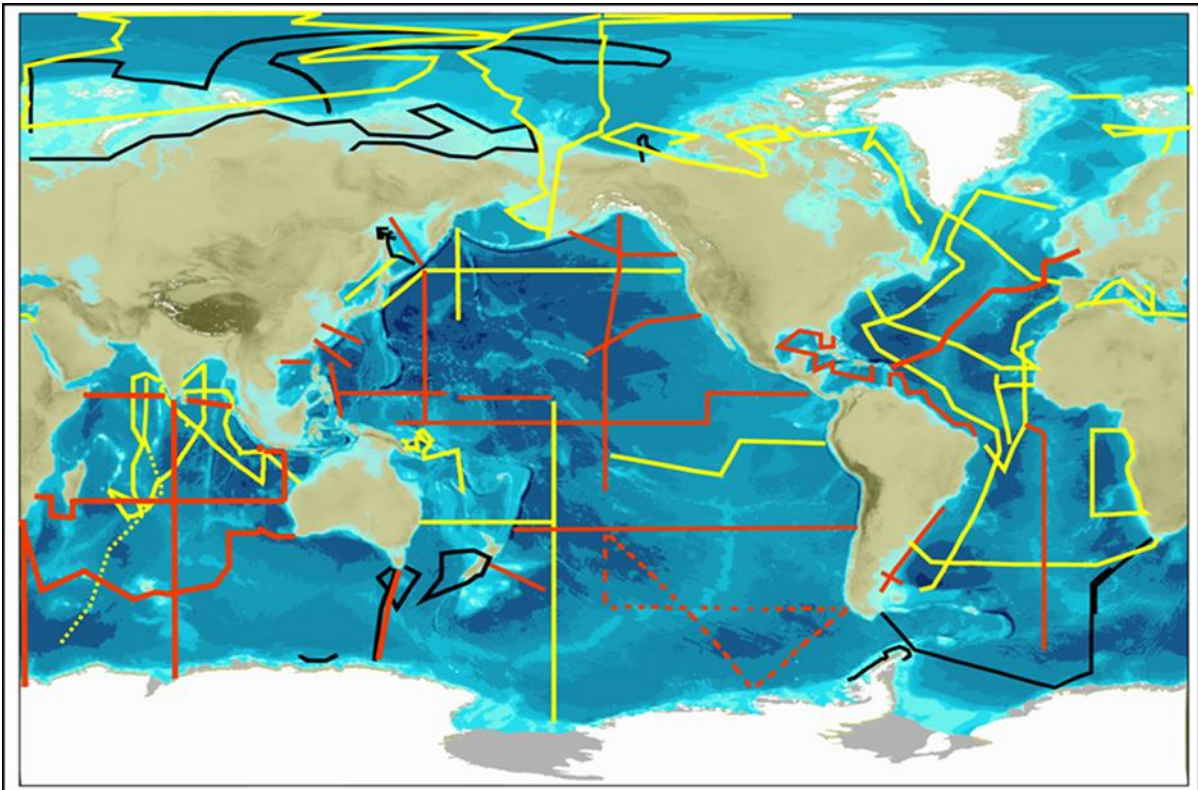


Figure 1.2: GEOTRACES Programme cruise sections plan. Completed sections as for December 2017 are drawn in yellow and black. Planned sections are drawn in red.

In order to obtain high quality results, GEOTRACES scientists are required to intercalibrate their measurements by means of cross over stations occupied by different research expeditions or by double sampling and subsequent analysis of the samples by different laboratories. Each dataset, once successfully intercalibrated, is then stored at international databases such as the British Oceanographic Data Centre (BODC). Every three years, an Intermediate Data Product (IDP) is produced which is the publicly available, quality controlled, data product of the GEOTRACES Programme. Since the start of the project, two IDPs have so far been released, one in 2014 (Mawji et al., 2015) and one in 2017 (Schlitzer et al., submitted). An example for dAl in the Atlantic Ocean for the IDP 2017 is given in Figure 1.3.

1.4 Dissolved aluminium

Aluminium is the third most abundant element (8.23% by weight) of the Earth's crust (Rudnick and Gao, 2003) and is a geochemically reactive element in aquatic environments. However, in seawater, dAl (filtered through 0.4 or 0.2 μm pore size filters) is present at low concentrations (0.1-180 nM). In the marine environment (i.e. in seawater), complex hydrated aluminium hydroxides ($\text{Al}(\text{OH})_3$ and $\text{Al}(\text{OH})_4^-$) are the dominant Al chemical species (32% and 68%, respectively) (Millero et al., 2009; Roberson and Hem, 1969). The latter chemical species are highly particle reactive. Therefore, dAl in seawater is rapidly removed through scavenging processes and is considered a scavenged type element (Bruland et al., 2014). One of the main processes of removal is inorganic adsorption onto particle surfaces either biogenic or non-biogenic which are eventually remineralized at depth or buried in sediments (Chou and Wollast, 1997; Orians and Bruland, 1985). The high affinity of dAl for particles results in short surface and deep ocean residence times of ca. 2-5

and 150-200 years, respectively (Orians and Bruland, 1985). The major sources of dAl to the ocean are atmospheric deposition of aerosols (wet+dry) and rivers (Chester, 2009). Secondary important sources of Al into the ocean are diffusion of Al from sediment pore waters (Hydes, 1983; Stoffyn and Mackenzie, 1982), resuspension of sediments (Moran and Moore, 1991) and hydrothermal vents (Measures et al., 2015; Resing et al., 2015).

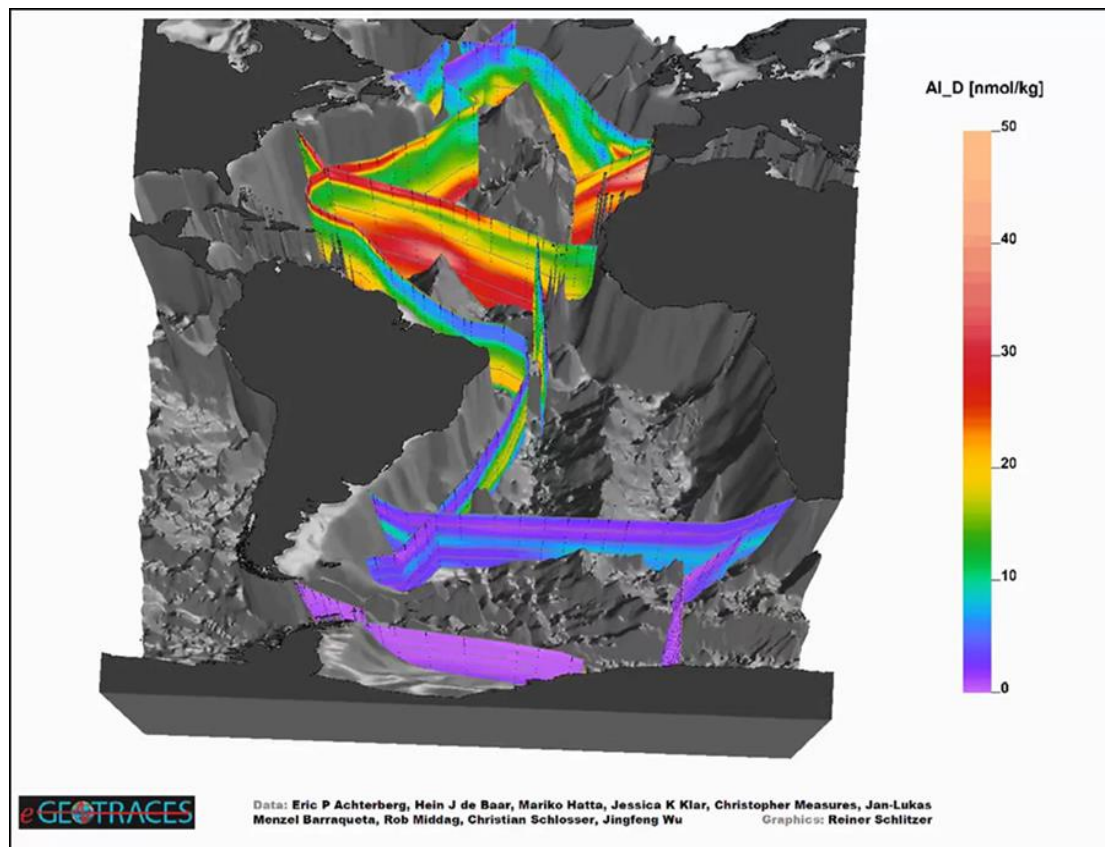


Figure 1.3: Dissolved Al in the Atlantic Ocean from the Intermediate Data Product 2017 (www.geotraces.com).

At present, our understanding of the biogeochemistry of dAl in the ocean is evolving rapidly and in recent years several studies have been published extending the coverage of dAl distributions in the ocean. In the following subsections, an overview and explanation of the sources, removals, and oceanic distribution of dAl is given.

1.4.1 Sources of dissolved aluminium to the ocean

Globally, Al is delivered to the ocean by atmospheric deposition (wet+dry), rivers, hydrothermal activity, and sedimentary sources. The large inter and intra oceanic variability in the distribution of dAl has led to scientific discussions concerning both the sources and removal mechanism controlling its oceanic distribution. Thus, during the 1980's, three main sources were argued to be the main mechanisms delivering Al to the ocean. Caschetto and Wollast (1979) suggested that diffusion of Al from sediment pore waters was the main Al oceanic source whilst Stoffyn and Mackenzie (1982) argued that weathering processes and subsequent riverine transport of Al was the major source of Al to the ocean. However, several authors (Hydes, 1983; Measures and Edmond, 1990; Orians and Bruland, 1985) expressed the opinion that Al derived from the atmosphere may be the major source of Al to the ocean.

1.4.1.1 Atmospheric source

Atmospheric deposition is a major source of Al to the open ocean and accounts for an input of 3.8-6.1 Tg yr⁻¹ (Chester, 2009). Several atmospheric sources of Al to the ocean exist and are grouped into anthropogenic and natural sources. Anthropogenic aerosol sources include anthropogenic particle emissions and products from the conversion of anthropogenic gases (Prospero et al., 1983). Natural atmospheric sources comprise sea-spray residues, volcanic effluvia, biogenic materials, smoke from the burning of land biomass, natural gas-to-particle conversion products, and windblown mineral dust (Prospero et al., 1983). In the early 1980's and based on positive correlations between dAl concentrations in oceanic surface waters and aerosol deposition rates, atmospheric deposition was proposed as the primary source of dAl into the open ocean (Hydes, 1983; Maring and Duce, 1987; Orians and Bruland, 1985). Much of this aerosol mainly originates from arid and semi-arid regions (e.g. North African and Asian desert) and is transported and deposited over large geographical distances and areas (Duce et al., 1991; Mahowald et al., 2005). Figure 1.4 shows atmospheric dust deposition to the ocean from a modelling study (Mahowald et al., 2015). The transport occurs as winds lift erodible particles in the air in a process called soil deflation (Gillett, 1979). Dry deposition is larger closer to the source region due to gravitational settling of larger particles (Prospero, 1996). The atmospheric flux of Al to the surface of the ocean is sporadic, highly variable, and depends on the dust composition and on the soluble Al fraction. The origin of dust plays an important role in dust solubility (Baker and Jickells, 2017; Baker et al., 2006) which is enhanced during atmospheric transport due to chemical processing as well as in wet deposition as a consequence of lower pH in rainwater (Spokes and Jickells, 1995). Several studies have indicated that the soluble fraction of Al in

aerosols is highly variable and range between 0.5% to 100% (Buck et al., 2010; Measures et al., 2010; Prospero et al., 1987; Shelley et al., 2017) with an average aerosol Al fractional solubility in aerosols of 9% for the Atlantic Ocean (Baker et al., 2006).

1.4.1.2 Riverine source

Rivers are a major source of major ions and trace metals to the ocean (Chester, 2009). Globally, dAl concentrations in riverine waters are highly variable (50 nM to $>5 \mu\text{M}$) with an average dAl concentration of $1.18 \mu\text{M}$ (Gaillardet et al., 2003). Thus, riverine dAl concentrations are on average two orders of magnitude higher than seawater dAl concentrations (Chester, 2009). Rivers transport Al mainly in the particulate form with less than 1% being in the form of dAl (Martin and Meybeck, 1979).

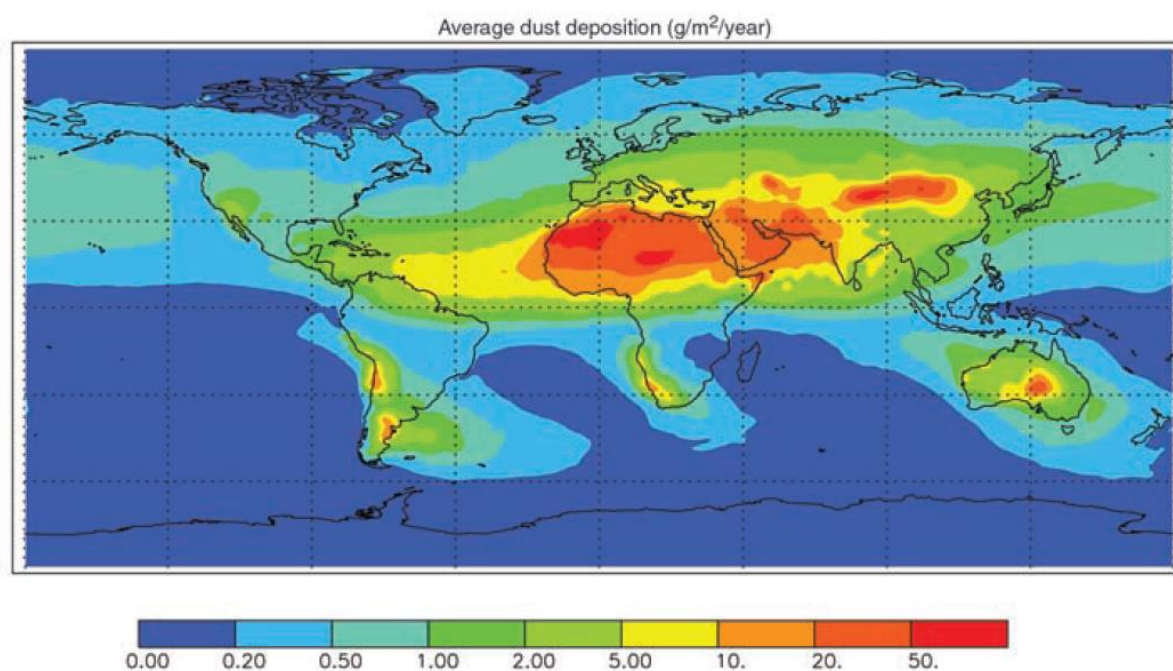


Figure 1.4: Atmospheric dust deposition from a modelling study (Mahowald et al., 2005). Permission for reproduction has been obtained from the publisher.

The riverine Al source was found to significantly influence coastal ocean Al distributions (Brown et al., 2010; Grand et al., 2015b; Hydes and Liss, 1977) and rivers were considered as the major source of Al to the ocean with an estimated global dAl riverine flux of 3 Mt yr⁻¹ (Stoffyn and Mackenzie, 1982). However, in rivers, dAl is to a large extent associated with colloids. Therefore, the net riverine flux of dAl to the ocean is much lower than the gross riverine flux due to enhanced removal of Al in estuarine mixing zones (Chester, 2009). The processes responsible for removing Al during estuarine mixing are flocculation of microcolloids (Sholkovitz, 1978), adsorption onto suspended sediments (Morris et al., 1986) and authigenic aluminosilicate formation (Mackin and Aller, 1984b).

1.4.1.3 Sedimentary sources

Dissolved Al can be added to oceanic waters through diffusion from sediment pore waters (Hydes, 1977) as has been observed for the Southern Ocean (Van Beueskom et al., 1997) and through resuspension and dissolution of shelf and bottom clay sediments via deep slope convection (Mackin and Aller, 1984a; Middag et al., 2009; Middag et al., 2015; Moran and Moore, 1991). The latter mechanism appears to be of great importance for constraining oceanic element budgets, including dAl (Jeandel et al., 2011). Ultimately, resuspension of sediments can act either as a source or as a sink of Al and can produce near to offshore gradients in dAl concentrations.

1.4.1.4 Hydrothermal sources

Hydrothermal venting was generally not considered a significant source of Al to the ocean (Hydes et al., 1986) and thus it was not been used as an input parameter in global oceanic Al models (van Hulst et al., 2014; van Hulst et al., 2013). However, enhanced dAl concentrations have been reported for the TAG hydrothermal plume in the tropical Atlantic Ocean (Lunel et al., 1990), and recent discoveries in the Pacific (Resing et al., 2015) and Atlantic Ocean (Measures et al., 2015) within the GEOTRACES Programme have shown that hydrothermal vents are a significant source of dAl, and other trace metals to the deep ocean. It has been shown that the dAl input from hydrothermal vents can be transported over distances of >3000 km (Resing et al., 2015).

1.4.2 Removal of dissolved aluminium from seawater

Removal of dAl from the water column to marine sediments occurs primarily through two mechanisms. These two mechanisms are: (i) adsorption onto particles (passive removal); (ii) biological uptake by phytoplankton (active removal). To date our understanding on the role of particles either as a source or sink of dAl in the open ocean and whether or not dAl is actively or passively incorporated into diatoms frustules is still limited.

1.4.2.2 Active removal

Biological uptake of dAl occurs in the upper water column and has been associated, in the field and in mesocosmos studies, with diatoms (Moran and Moore, 1988a; Moran and Moore, 1988b). However, it is still unknown if dAl is being actively taken up or passively incorporated (I will refer to this process as active uptake

throughout the thesis). Stoffyn (1979) gave experimental evidence for dAl incorporation into the opal skeleton of diatoms and similar observations were made by Van Bennekom et al. (1991). Gehlen et al. (2002) provided direct evidence for structural association between biogenic opal (diatoms frustules) and dAl. Indirect evidence for active uptake of dAl by phytoplankton is given by nutrient type depth profiles of dAl (Hydes et al., 1988; Kramer et al., 2004) and by positive correlations between dAl and Si in the water column (Middag et al., 2009) and in surface waters (Mackenzie et al., 1978). Dissolved Al has no known role as a nutrient for marine phytoplankton. However, a recent incubation study (Zhou et al., 2017) in the South China Sea shows that the addition of Al can enhance nitrogen fixation rates and the growth of diatoms and the cyanobacteria *Trichodesmium* but it inhibited the growth of dinoflagellates and the cyanobacteria *Synechococcus*. The latter still requires further investigation as it would mean that dAl could have a biological function. However, it could have been that dAl had a negative effect on the grazing potential of zooplankton and thus indirectly allowing phytoplankton net growth.

1.4.3 Oceanic distribution of dissolved aluminium

Dissolved Al concentrations in the ocean, vary by over 3 orders of magnitude between sub-nanomolar levels (<0.2 nM) in the Pacific, Arctic, and Southern Oceans (Middag et al., 2009; Middag et al., 2011; Orians and Bruland, 1985) to more than 150 nM in the Mediterranean Sea (Hydes et al., 1988; Rolison et al., 2015).

1.4.3.1 Surface waters distribution of dissolved aluminium

In the Atlantic Ocean, maximum surface water dAl concentrations occurred across the equatorial Atlantic (Measures et al., 2015; Middag et al., 2015; Schlosser et al.,

2014) and decreased north and southwards (Middag et al., 2015; Middag et al., 2011). This surface water dAl distribution has been noticed before by several authors (Bowie et al., 2002; Vink and Measures, 2001) and coincided with the pattern of maximum deposition of aerosols in the Atlantic Ocean (Jickells et al., 2005). Similarly, Orians and Bruland (1985) suggested that the observed high dAl surface concentration in the North Pacific resulted from Asian dust carried over the Pacific Ocean. Enhanced dAl surface water concentrations are observed in the Mediterranean Sea as a consequence of high dust deposition loads (Rolison et al., 2015). The differences for the dAl surface water concentrations in the open ocean strongly support an atmospheric Al origin. Thus, dAl in surface waters of the ocean has been successfully used as an atmospheric deposition tracer (Measures and Brown, 1996).

1.4.3.2 Vertical distribution of dissolved aluminium

Figure 1.5 displays the vertical distribution of dAl in the Atlantic and Indian Ocean's and in the Mediterranean and Labrador Seas. The vertical distribution of dAl is controlled by the relative magnitude of the sources and the balance between scavenging and remineralization processes. Dissolved Al concentrations in the Pacific (Orians and Bruland, 1985) and Indian Oceans (Thi Dieu Vu and Sohrin, 2013) are generally lower than in the Atlantic Ocean (Measures et al., 2015) and Mediterranean Sea (Rolison et al., 2015) as a consequence of less atmospheric input and continuous scavenging of dAl from the water column along their transport (Figure 1.5). This is strong evidence for the scavenging type behaviour of dAl in the ocean, which is the opposite to the major nutrients which show enhanced concentrations in the Pacific compared to the Atlantic Ocean as a result of

rem mineralization of organic matter. In the early literature, the general description of the vertical oceanic distribution of dAl displayed elevated levels in surface waters due to atmospheric aerosol deposition, a decrease in dAl concentrations with depth due to scavenging onto particles and an increase in concentration towards the sediment interface due to resuspension of sediments and/or diffusion from sediment pore waters (Orians and Bruland, 1985; Hydes, 1983; Measures and Vink, 1990). Figure 1.5c in the equatorial Atlantic is an example of the general distribution explained above. Recent discoveries, specifically due to the GEOTRACES Programme have shown that the distribution of dAl with depth shows large differences in concentrations within and between ocean basins (Measures et al., 2015; Middag et al., 2015; Rolison et al., 2015). Dissolved Al can also display a nutrient type profile in regions, for example of high primary productivity and relatively young waters (Figure 1.5a). This indicates that in regions of high productivity the net remineralization of dAl can exceed the net scavenging of dAl onto particles. In Figure 1.5b (yellow) and we can also observe the influence of horizontal advection of water masses at a depth of ca. 1200 and 2000 m, respectively. The large variability in the vertical distribution (shape and concentrations) of dAl makes this element of special interest as it can trace sources of trace metals at surface and depth.

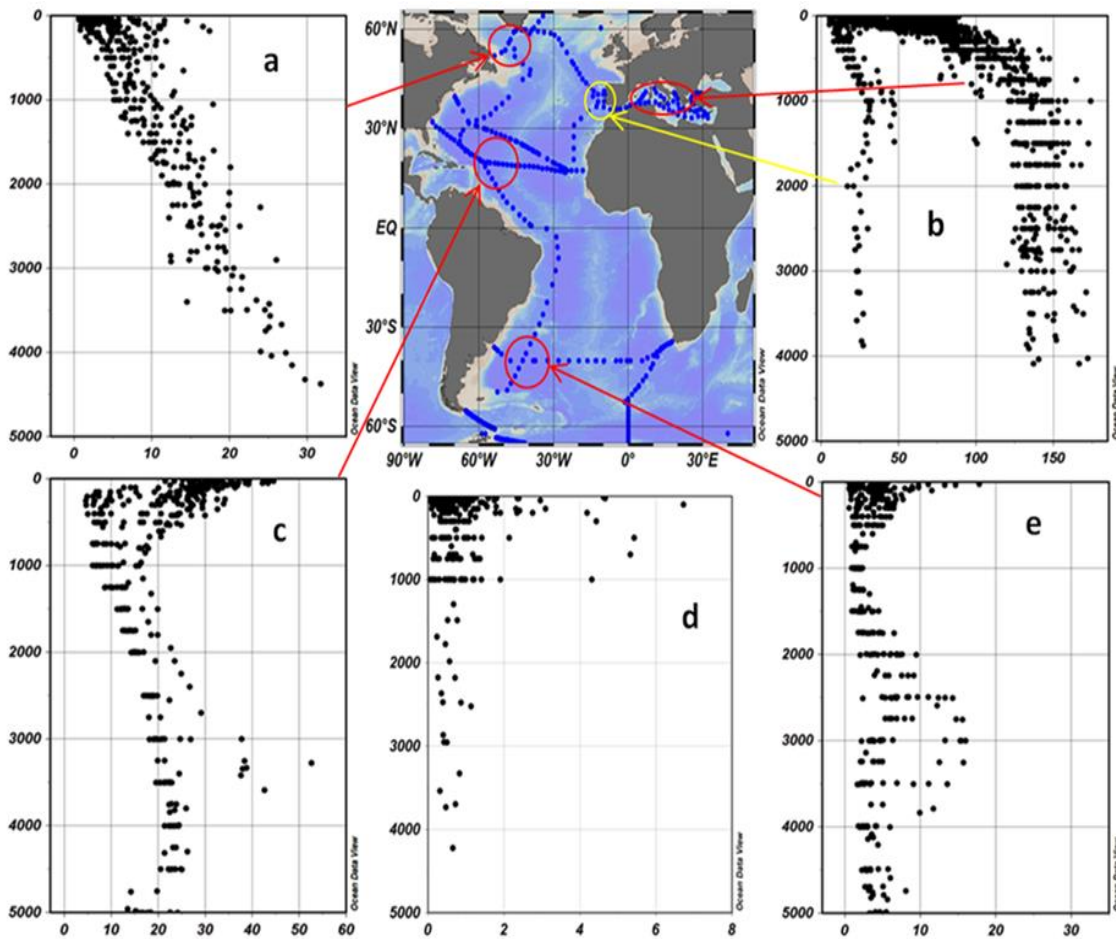


Figure 1.5: Distribution of dAl with depth in the Atlantic Ocean (a,b,c,e) and the Indian Ocean (d). Data are from the IDP 2017(www.geotraces.com) (Mawji et al., 2015).

1.4.4 Dissolved aluminium as an atmospheric deposition tracer

As a result of the apparent positive correlation between dAl concentrations in surface waters and atmospheric dust deposition, Measures and Brown (1996) developed a simple one box model (Model of Aluminium for Dust Calculation in Oceanic Waters, MADCOW) to derive atmospheric deposition fluxes from the dAl concentrations measured in surface waters. The MADCOW model has been shown to provide reliable atmospheric deposition fluxes (Grand et al., 2015a; Measures et al., 2005; Vink and Measures, 2001). The MADCOW model calculates the annual

atmospheric deposition (dry+wet) required to maintain the dAl concentrations found in surface waters. The MADCOW model assumes steady state conditions and thus the sole input of Al to surface waters occurs through atmospheric deposition and the only removal is via scavenging. Therefore, the processes of advection and mixing are considered insignificant due to dAl having a relatively short residence time in the surface mixed layer. However, a recent study (van Hulst et al., 2014), using a global circulation model, has shown that horizontal advection may play a significant role in equatorial regions and that MADCOW atmospheric deposition fluxes may not be reliable in the latter regions. The model assumes: (i) a fixed dAl residence time in the surface mixed layer of 5 years (yr) which, in fact, only applies to certain regions and can vary regionally and seasonally depending on the amount of particles present in surface waters which can scavenge dAl (Damshäuser et al., 2011). For example, in the Bay of Bengal, Grand et al. (2015a) adjusted the residence time of dAl in the surface mixed layer to 1.1 yr as this region is characterized by high productivity and export of organic material. (ii) A surface mixed layer depth of 30 m which was first chosen for the equatorial Atlantic but is not suitable for regions of highly variable atmospheric forcing (e.g. wind stress, heat exchange, evaporation and precipitation) like the North Atlantic Ocean (north of 40°N); (iii) an invariant aerosol Al fractional solubility from dust particles of between 3-5%. However, since the first application of MADCOW several studies have reported a large variability (0.5% to 100%) on aerosol Al fractional solubility with an average for the Atlantic Ocean of 9% (Baker et al., 2006; Buck et al., 2010; Measures et al., 2010; Shelley et al., 2018). Therefore the influence of biological productivity on the removal of dAl, the additional dAl inputs from advection and mixing sources, and the huge range in aerosol Al fractional solubility may bias the quantification of atmospheric inputs

derived from measured surface seawater dAl concentrations. As a consequence, spatial variations in the latter assumptions have to be considered and adjusted in order to improve the calculated atmospheric deposition fluxes.

1.5 Study areas

The global ocean has been divided into five different parts which are the Antarctic, Arctic, Atlantic, Indian, and Pacific Ocean. The Atlantic Ocean is the second largest ocean (in size) after the Pacific Ocean. The Atlantic Ocean covers ca. 17% of the Earth and has an average depth of ca. 3340 m. During this study, samples for the analysis of dAl were collected in the North Atlantic and Southeast Atlantic Ocean. In the following two subsections we will give a general description for each of these study areas.

1.5.1 The North Atlantic Ocean

The North Atlantic Ocean plays an important role regulating Earth's climate and the global oceanic thermohaline circulation (Broecker, 1992). In this region, the meridional overturning circulation (MOC) takes place. Warm and salty surface waters are transported from the tropical Atlantic northwards into the North Atlantic and high latitude North Atlantic. These warm and salty surface waters interact with the atmosphere and are transformed into colder waters (García-Ibáñez et al., 2015). Thus density increases and deep waters are formed which are then transported southwards by mode waters and by the North Atlantic Deep Water (NADW). In addition, in the North Atlantic Ocean, pronounced phytoplankton blooms take place every year (Figure 1.6) (Henson et al., 2009). As a result of the enhanced primary productivity, a strong removal of particle reactive trace metals is expected.

Moreover, the North Atlantic Ocean is a major sink for anthropogenic CO₂ (Humphreys et al., 2016; Sabine et al., 2004) which in turn leads to acidification of the North Atlantic (Gattuso et al., 2015) and the deep Atlantic Ocean through the MOC (Perez et al., 2018). Due to the importance of the North Atlantic Ocean in regulating climate it has received significant research attention. Most of the research undertaken in the North Atlantic Ocean has been to understand the role that the North Atlantic Ocean plays in the MOC and, in recent years, the role of iron as a limiting nutrient (Achterberg et al., 2013; Achterberg et al., 2018). However, the knowledge of the distribution, sources and sinks of trace metals, especially dAl, in the North Atlantic Ocean is still poorly constrained.

1.5.2 The Southeast Atlantic Ocean

The Southeast Atlantic Ocean (SEAO) has received much less attention than other regions in the Atlantic Ocean. The annual chlorophyll a concentration in the SEAO is on average lower compared to the North Atlantic Ocean (Figure 1.6). However, the South East Atlantic Ocean is home to one of the largest and more important pelagic fisheries due to the high productive waters associated to the Benguela upwelling region (Hutchings et al., 2009). The relative importance that the SEAO plays in the distribution and cycling of trace metals is still unknown (Moore et al., 2009). A recent study has investigated at high spatial resolution the distribution of Mn, Fe, and Co in the SEAO (Noble et al., 2012). However, dAl data for the SEAO are scarce with just a few studies published (Bowie et al., 2002; Measures, 1995; van Bennekom and Jager, 1978). The SEAO region is influenced by active exchange of trace metals at the ocean boundaries.

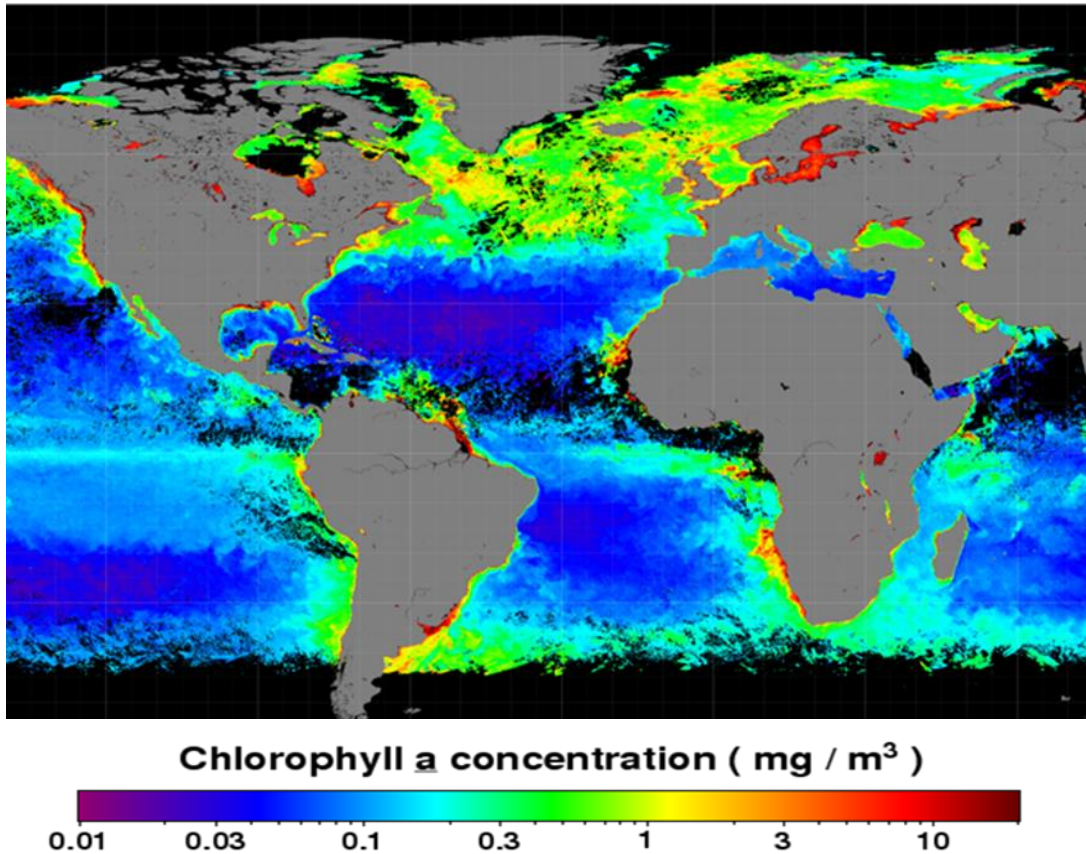


Figure 1.6: Global satellite summer average of chlorophyll a concentration (MODIS Aqua from <http://oceancolor.gsfc.nasa.gov>)

This exchange include sources of trace metals from the atmosphere (South African dust plume), rivers (Congo and Orange), and shelf sediments (continental margins). In addition, the SEAO is host to a significant oxygen minimum zone centered around the Benguela upwelling region (Mohrholz et al., 2008).

1.6 Aim and objectives of the study

The aim of this study is to expand the knowledge on the cycling and distribution of dAl in surface and deep waters of the Atlantic Ocean. Moreover, specific objectives are: (i) to study the distribution and behaviour of dAl in the North Atlantic Ocean in order to elucidate the sources and sinks of Al in this region; (ii) to understand and investigate the role that phytoplankton plays in controlling dAl in surface waters;

Chapter 1 - Introduction

(iii) to assess the suitability of dAl as a tracer for atmospheric aerosol deposition from the North Atlantic to the South Atlantic Ocean; (iv) to investigate the significance of riverine Al input to the South East Atlantic Ocean.

References

Achterberg, E. P., Moore, C. M., Henson, S. A., Steigenberger, S., Stohl, A., Eckhardt, S., Avendano, L. C., Cassidy, M., Hembury, D., and Klar, J. K.: Natural iron fertilization by the Eyjafjallajökull volcanic eruption, *Geophysical Research Letters*, 40, 921-926, 2013.

Achterberg, E. P., Steigenberger, S., Marsay, C. M., LeMoigne, F. A., Painter, S. C., Baker, A. R., Connelly, D. P., Moore, C. M., Tagliabue, A., and Tanhua, T.: Iron Biogeochemistry in the High Latitude North Atlantic Ocean, *Scientific reports*, 8, 1283, 2018.

Anderson, R. F., Mawji, E., Cutter, G. A., MEASURES, C. I., and Jeandel, C.: GEOTRACES: changing the way we explore ocean chemistry, *Oceanography*, 27, 50-61, 2014.

Baker, A. R. and Jickells, T. D.: Atmospheric deposition of soluble trace elements along the Atlantic Meridional Transect (AMT), *Progress in Oceanography*, 158, 41-51, 2017.

Baker, A. R., Jickells, T. D., Witt, M., and Linge, K. L.: Trends in the solubility of iron, aluminium, manganese and phosphorus in aerosol collected over the Atlantic Ocean, *Marine Chemistry*, 98, 43-58, 2006.

Bowie, A. R., Whitworth, D. J., Achterberg, E. P., Mantoura, R. F. C., and Worsfold, P. J.: Biogeochemistry of Fe and other trace elements (Al, Co, Ni) in the upper Atlantic Ocean, *Deep Sea Research Part I: Oceanographic Research Papers*, 49, 605-636, 2002.

Broecker, W. S.: The great ocean conveyor, 129-161, 1992.

Brown, M. T., Lippiatt, S. M., and Bruland, K. W.: Dissolved aluminum, particulate aluminum, and silicic acid in northern Gulf of Alaska coastal waters: Glacial/riverine inputs and extreme reactivity, *Marine Chemistry*, 122, 160-175, 2010.

Buck, C. S., Landing, W. M., Resing, J. A., and Measures, C. I.: The solubility and deposition of aerosol Fe and other trace elements in the north atlantic ocean: observations from the A16N CLIVAR/CO 2 repeat hydrography section, *Marine Chemistry*, 120, 57-70, 2010.

Chester, R.: *Marine geochemistry*, John Wiley & Sons, 2009.

Dammshäuser, A., Wagener, T., and Croot, P. L.: Surface water dissolved aluminum and titanium: Tracers for specific time scales of dust deposition to the Atlantic?, *Geophysical Research Letters*, 38, 2011.

Duce, R., Liss, P., Merrill, J., Atlas, E., Buat-Menard, P., Hicks, B., Miller, J., Prospero, J., Arimoto, R., and Church, T.: The atmospheric input of trace species to the world ocean, *Global biogeochemical cycles*, 5, 193-259, 1991.

Gaillardet, J., Viers, J., and Dupré, B.: Trace elements in river waters, *Treatise on geochemistry*, 5, 605, 2003.

García-Ibáñez, M. I., Pardo, P. C., Carracedo, L. I., Mercier, H., Lherminier, P., Ríos, A. F., and Pérez, F. F.: Structure, transports and transformations of the water masses in the Atlantic Subpolar Gyre, *Progress in Oceanography*, 2015. 2015.

Gattuso, J.-P., Magnan, A., Billé, R., Cheung, W. W., Howes, E. L., Joos, F., Allemand, D., Bopp, L., Cooley, S. R., and Eakin, C. M.: Contrasting futures for ocean and society from different anthropogenic CO₂ emissions scenarios, *Science*, 349, aac4722, 2015.

Gehlen, M., Beck, L., Calas, G., Flank, A.-M., Van Bennekom, A., and Van Beusekom, J.: Unraveling the atomic structure of biogenic silica: evidence of the structural association of Al and Si in diatom frustules, *Geochimica et Cosmochimica Acta*, 66, 1601-1609, 2002.

Gillett, D.: Environmental factors affecting dust emission by wind erosion, Saharan dust, 1979. 71-94, 1979.

Grand, M. M., Measures, C. I., Hatta, M., Hiscock, W. T., Buck, C. S., and Landing, W. M.: Dust deposition in the eastern Indian Ocean: The ocean perspective from Antarctica to the Bay of Bengal, *Global Biogeochemical Cycles*, 29, 357-374, 2015a.

Grand, M. M., Measures, C. I., Hatta, M., Hiscock, W. T., Landing, W. M., Morton, P. L., Buck, C. S., Barrett, P. M., and Resing, J. A.: Dissolved Fe and Al in the upper 1000 m of the eastern Indian Ocean: A high-resolution transect along 95°E from the Antarctic margin to the Bay of Bengal, *Global Biogeochemical Cycles*, 29, 375-396, 2015b.

Henson, S. A., Dunne, J. P., and Sarmiento, J. L.: Decadal variability in North Atlantic phytoplankton blooms, *Journal of Geophysical Research: Oceans*, 114, 2009.

Humphreys, M. P., Griffiths, A. M., Achterberg, E. P., Holliday, N. P., Rérolle, V., Menzel Barraqueta, J. L., Couldrey, M. P., Oliver, K. I., Hartman, S. E., and Esposito, M.: Multidecadal accumulation of anthropogenic and remineralized dissolved inorganic carbon along the Extended Ellett Line in the northeast Atlantic Ocean, *Global Biogeochemical Cycles*, doi: 10.1002/2015GB005246, 2016. 2016.

Hutchings, L., Van der Lingen, C., Shannon, L., Crawford, R., Verheye, H., Bartholomae, C., Van der Plas, A., Louw, D., Kreiner, A., and Ostrowski, M.: The

Benguela Current: An ecosystem of four components, *Progress in Oceanography*, 83, 15-32, 2009.

Hydes, D.: Dissolved aluminium concentration in sea water, *Nature*, 268, 136, 1977.

Hydes, D., De Lange, G., and De Baar, H.: Dissolved aluminium in the Mediterranean, *Geochimica et Cosmochimica Acta*, 52, 2107-2114, 1988.

Hydes, D. and Liss, P.: The behaviour of dissolved aluminium in estuarine and coastal waters, *Estuarine and Coastal Marine Science*, 5, 755-769, 1977.

Hydes, D. J.: Distribution of aluminium in waters of the North East Atlantic 25°N to 35°N, *Geochimica et Cosmochimica Acta*, 47, 967-973, 1983.

Jeandel, C., Peucker-Ehrenbrink, B., Jones, M. T., Pearce, C. R., Oelkers, E. H., Godderis, Y., Lacan, F., Aumont, O., and Arsouze, T.: Ocean margins: The missing term in oceanic element budgets?, *Eos, Transactions American Geophysical Union*, 92, 217-218, 2011.

Jickells, T. D., An, Z. S., Andersen, K. K., Baker, A. R., Bergametti, G., Brooks, N., Cao, J. J., Boyd, P. W., Duce, R. A., Hunter, K. A., Kawahata, H., Kubilay, N., laRoche, J., Liss, P. S., Mahowald, N., Prospero, J. M., Ridgwell, A. J., Tegen, I., and Torres, R.: Global iron connections between desert dust, ocean biogeochemistry, and climate, *Science*, 308, 67-71, 2005.

Kramer, J., Laan, P., Sarthou, G., Timmermans, K. R., and de Baar, H. J. W.: Distribution of dissolved aluminium in the high atmospheric input region of the subtropical waters of the North Atlantic Ocean, *Marine Chemistry*, 88, 85-101, 2004.

Mackenzie, F. T., Stoffyn, M., and Wollast, R.: Aluminum in seawater: control by biological activity, *Science*, 199, 680-682, 1978.

Mackin, J. E. and Aller, R. C.: Diagenesis of dissolved aluminum in organic-rich estuarine sediments, *Geochimica et Cosmochimica Acta*, 48, 299-313, 1984a.

Mackin, J. E. and Aller, R. C.: Processes affecting the behavior of dissolved aluminum in estuarine waters, *Marine Chemistry*, 14, 213-232, 1984b.

Mahowald, N. M., Baker, A. R., Bergametti, G., Brooks, N., Duce, R. A., Jickells, T. D., Kubilay, N., Prospero, J. M., and Tegen, I.: Atmospheric global dust cycle and iron inputs to the ocean, *Global Biogeochemical Cycles*, 19, 2005.

Maring, H. B. and Duce, R. A.: The impact of atmospheric aerosols on trace metal chemistry in open ocean surface seawater, 1. Aluminum, *Earth and Planetary Science Letters*, 84, 381-392, 1987.

Martin, J.-M. and Meybeck, M.: Elemental mass-balance of material carried by major world rivers, *Marine chemistry*, 7, 173-206, 1979.

Mawji, E. and Schlitzer, R. and Dodas, E. M. and Abadie, C. and Abouchami, W. and Anderson, R. F. and Baars, O. and Bakker, K. and Baskaran, M. and Bates, N. R. and Bluhm, K. and Bowie, A. and Bown, J. and Boye, M. and Boyle, E. A. and Branellec, P. and Bruland, K. W. and Brzezinski, M. A. and Bucciarelli, E. and Buesseler, K. and Butler, E. and Cai, P. and Cardinal, D. and Casciotti, K. and Chaves, J. and Cheng, H. and Chever, F. and Church, T. M. and Colman, A. S. and Conway, T. M. and Croot, P. L. and Cutter, G. A. and de Baar, H. J. W. and de Souza, G. F. and Dehairs, F. and Deng, F. and Dieu, H. T. and Dulaquais, G. and Echegoyen-Sanz, Y. and Lawrence Edwards, R. and Fahrbach, E. and Fitzsimmons, J. and Fleisher, M. and Frank, M. and Friedrich, J. and Fripiat, F. and Galer, S. J. G. and Gamo, T. and Solsona, E. G. and Gerringa, L. J. A. and Godoy, J. M. and Gonzalez, S. and Grossteffan, E. and Hatta, M. and Hayes, C. T. and Heller, M. I. and Henderson, G. and Huang, K.-F. and Jeandel, C. and Jenkins, W. J. and John, S. and Kenna, T. C. and Klunder, M. and Kretschmer, S. and Kumamoto, Y. and Laan, P. and Labatut, M. and Lacan, F. and Lam, P. J. and Lannuzel, D. and le Moigne, F. and Lechtenfeld, O. J. and Lohan, M. C. and Lu, Y. and Masqué, P. and McClain, C. R. and Measures, C. and Middag, R. and Moffett, J. and Navidad, A. and Nishioka, J. and Noble, A. and Obata, H. and Ohnemus, D. C. and Owens, S. and Planchon, F. and Pradoux, C. and Puigcorbé, V. and Quay, P. and Radic, A. and Rehkämper, M. and Remenyi, T. and Rijkenberg, M. J. A. and Rintoul, S. and Robinson, L. F. and Roeske, T. and Rosenberg, M. and van der Loeff, M. R. and Ryabenko, E. and Saito, M. A. and Roshan, S. and Salt, L. and Sarthou, G. and Schauer, U. and Scott, P. and Sedwick, P. N. and Sha, L. and Shiller, A. M. and Sigman, D. M. and Smethie, W. and Smith, G. J. and Sohrin, Y. and Speich, S. and Stichel, T. and Stutsman, J. and Swift, J. H. and Tagliabue, A. and Thomas, A. and Tsunogai, U. and Twining, B. S. and van Aken, H. M. and van Heuven, S. and van Ooijen, J. and van Weerlee, E. and Venchiarutti, C. and Voelker, A. H. L. and Wake, B. and Warner, M. J. and Woodward, E. M. S. and Wu, J. and Wyatt, N. and Yoshikawa, H. and Zheng, X.-Y. and Xue, Z. and Zieringer, M. and Zimmer, L. A.: The GEOTRACES Intermediate Data Product 2014, *Marine Chemistry*, 177, Part 1, 1-8, 2015.

Measures, C.: The distribution of Al in the IOC stations of the eastern Atlantic between 30° S and 34° N, *Marine chemistry*, 49, 267-281, 1995.

Measures, C., Hatta, M., Fitzsimmons, J., and Morton, P.: Dissolved Al in the zonal N Atlantic section of the US GEOTRACES 2010/2011 cruises and the importance of hydrothermal inputs, *Deep Sea Research Part II: Topical Studies in Oceanography*, 116, 176-186, 2015.

Measures, C., Sato, T., Vink, S., Howell, S., and Li, Y.: The fractional solubility of aluminium from mineral aerosols collected in Hawaii and implications for atmospheric deposition of biogeochemically important trace elements, *Marine Chemistry*, 120, 144-153, 2010.

Measures, C. I. and Brown, E. T.: Estimating Dust Input to the Atlantic Ocean Using Surface Water Aluminium Concentrations. In: *The Impact of Desert Dust Across the*

Mediterranean, Guerzoni, S. and Chester, R. (Eds.), Springer Netherlands, Dordrecht, 1996.

Measures, C. I., Brown, M. T., and Vink, S.: Dust deposition to the surface waters of the western and central North Pacific inferred from surface water dissolved aluminum concentrations, *Geochemistry, Geophysics, Geosystems*, 6, 2005.

Middag, R., de Baar, H. J. W., Laan, P., and Bakker, K.: Dissolved aluminium and the silicon cycle in the Arctic Ocean, *Marine Chemistry*, 115, 176-195, 2009.

Middag, R., Van Hulten, M., Van Aken, H., Rijkenberg, M., Gerringa, L., Laan, P., and De Baar, H.: Dissolved aluminium in the ocean conveyor of the West Atlantic Ocean: effects of the biological cycle, scavenging, sediment resuspension and hydrography, *Marine Chemistry*, 177, 69-86, 2015.

Middag, R., van Slooten, C., de Baar, H. J. W., and Laan, P.: Dissolved aluminium in the Southern Ocean, *Deep Sea Research Part II: Topical Studies in Oceanography*, 58, 2647-2660, 2011.

Millero, F. J., Woosley, R., Ditrolio, B., and Waters, J.: Effect of ocean acidification on the speciation of metals in seawater, *Oceanography*, 22, 72-85, 2009.

Mohrholz, V., Bartholomae, C., Van der Plas, A., and Lass, H.: The seasonal variability of the northern Benguela undercurrent and its relation to the oxygen budget on the shelf, *Continental Shelf Research*, 28, 424-441, 2008.

Moore, C. M., Mills, M. M., Achterberg, E. P., Geider, R. J., LaRoche, J., Lucas, M. I., McDonagh, E. L., Pan, X., Poulton, A. J., and Rijkenberg, M. J.: Large-scale distribution of Atlantic nitrogen fixation controlled by iron availability, *Nature Geoscience*, 2, 867-871, 2009.

Moran, S. and Moore, R.: Temporal variations in dissolved and particulate aluminum during a spring bloom, *Estuarine, Coastal and Shelf Science*, 27, 205-215, 1988a.

Moran, S. B. and Moore, R. M.: Evidence from mesocosm studies for biological removal of dissolved aluminium from sea water, *Nature*, 335, 706-708, 1988b.

Moran, S. B. and Moore, R. M.: The potential source of dissolved aluminum from resuspended sediments to the North Atlantic Deep Water, *Geochimica et Cosmochimica Acta*, 55, 2745-2751, 1991.

Morris, A., Howland, R., and Bale, A.: Dissolved aluminium in the Tamar Estuary, southwest England, *Geochimica et Cosmochimica Acta*, 50, 189-197, 1986.

Noble, A. E., Lamborg, C. H., Ohnemus, D. C., Lam, P. J., Goepfert, T. J., Frame, C. H., Casciotti, K. L., DiTullio, G. R., JENNINGS, J., and Saito, M. A.: Basin-scale inputs of cobalt, iron, and manganese from the Benguela-Angola front to the South Atlantic Ocean, *Limnology and oceanography*, 57, 989-1010, 2012.

Orians, K. J. and Bruland, K. W.: Dissolved aluminium in the central North Pacific, *Nature*, 316, 427-429, 1985.

Perez, F. F., Fontela, M., García-Ibáñez, M. I., Mercier, H., Velo, A., Lherminier, P., Zunino, P., de La Paz, M., Alonso-Pérez, F., and Guallart, E. F.: Meridional overturning circulation conveys fast acidification to the deep Atlantic Ocean, *Nature*, 2018. 2018.

Prospero, J.: Saharan dust transport over the North Atlantic Ocean and Mediterranean: an overview. In: *The impact of desert dust across the Mediterranean*, Springer, 1996.

Prospero, J., Charlson, R., Mohnen, V., Jaenicke, R., Delany, A., Moyers, J., Zoller, W., and Rahn, K.: The atmospheric aerosol system: An overview, *Reviews of Geophysics*, 21, 1607-1629, 1983.

Prospero, J. M., Nees, R. T., and Uematsu, M.: Deposition rate of particulate and dissolved aluminum derived from Saharan dust in precipitation at Miami, Florida, *Journal of Geophysical Research: Atmospheres*, 92, 14723-14731, 1987.

Roberson, C. E. and Hem, J. D.: Solubility of aluminum in the presence of hydroxide, fluoride, and sulfate, USGPO, 1969.

Rolison, J., Middag, R., Stirling, C., Rijkenberg, M., and De Baar, H.: Zonal distribution of dissolved aluminium in the Mediterranean Sea, *Marine Chemistry*, 177, 87-100, 2015.

Sabine, C. L., Feely, R. A., Gruber, N., Key, R. M., Lee, K., Bullister, J. L., Wanninkhof, R., Wong, C. S., Wallace, D. W., Tilbrook, B., Millero, F. J., Peng, T. H., Kozyr, A., Ono, T., and Rios, A. F.: The oceanic sink for anthropogenic CO₂, *Science*, 305, 367-371, 2004.

Schlosser, C., Klar, J. K., Wake, B. D., Snow, J. T., Honey, D. J., Woodward, E. M. S., Lohan, M. C., Achterberg, E. P., and Moore, C. M.: Seasonal ITCZ migration dynamically controls the location of the (sub)tropical Atlantic biogeochemical divide, *Proceedings of the National Academy of Sciences*, 111, 1438-1442, 2014.

Shelley, R. U., Landing, W. M., Ussher, S. J., Planquette, H., and Sarthou, G.: Characterisation of aerosol provenance from the fractional solubility of Fe (Al, Ti, Mn, Co, Ni, Cu, Zn, Cd and Pb) in North Atlantic aerosols (GEOTRACES cruises GA01 and GA03) using a two stage leach, *Biogeosciences Discuss.*, 2017, 1-31, 2017.

Shelley, R. U., Landing, W. M., Ussher, S. J., Planquette, H., and Sarthou, G.: Regional trends in the fractional solubility of Fe and other metals from North Atlantic aerosols (GEOTRACES cruises GA01 and GA03) following a two-stage leach, *Biogeosciences*, 15, 2271-2288, 2018.

Sholkovitz, E. R.: The flocculation of dissolved Fe, Mn, Al, Cu, Ni, Co and Cd during estuarine mixing, *Earth and Planetary Science Letters*, 41, 77-86, 1978.

Spokes, L. J. and Jickells, T. D.: Factors controlling the solubility of aerosol trace metals in the atmosphere and on mixing into seawater, *Aquatic Geochemistry*, 1, 355-374, 1995.

Stoffyn, M.: Biological control of dissolved aluminum in seawater: experimental evidence, *Science*, 203, 651-653, 1979.

Stoffyn, M. and Mackenzie, F. T.: Fate of dissolved aluminum in the oceans, *Marine chemistry*, 11, 105-127, 1982.

Thi Dieu Vu, H. and Sohrin, Y.: Diverse stoichiometry of dissolved trace metals in the Indian Ocean, *Scientific Reports*, 3, 1745, 2013.

Van Bennekom, A. J., Buma, A., and Nolting, R.: Dissolved aluminium in the Weddell-Scotia Confluence and effect of Al on the dissolution kinetics of biogenic silica, *Marine Chemistry*, 35, 423-434, 1991.

van Bennekom, A. J. and Jager, J. E.: Dissolved aluminium in the Zaire river plume, *Netherlands Journal of Sea Research*, 12, 358-367, 1978.

Van Beueskom, J., Van Bennekom, A., Tréguer, P., and Morvan, J.: Aluminium and silicic acid in water and sediments of the Enderby and Crozet Basins, *Deep Sea Research Part II: Topical Studies in Oceanography*, 44, 987-1003, 1997.

van Hulst, M. M. P., Sterl, A., Middag, R., de Baar, H. J. W., Gehlen, M., Dutay, J. C., and Tagliabue, A.: On the effects of circulation, sediment resuspension and biological incorporation by diatoms in an ocean model of aluminium*, *Biogeosciences*, 11, 3757-3779, 2014.

Vink, S. and Measures, C. I.: The role of dust deposition in determining surface water distributions of Al and Fe in the South West Atlantic, *Deep Sea Research Part II: Topical Studies in Oceanography*, 48, 2787-2809, 2001.

Zhou, L., Liu, J., Xing, S., Tan, Y., and Huang, L.: Phytoplankton responses to aluminum enrichment in the South China Sea, *Journal of Inorganic Biochemistry*, doi: <https://doi.org/10.1016/j.jinorgbio.2017.09.022>, 2017.

Methods

1. Methods and data analysis

In order to avoid contamination of samples from atmospheric sources of trace elements, several pre-sampling and post-sampling protocols need to be followed (GEOTRACES cookbook, www.geotraces.com). In the following subsections, we described the procedures undertaken during this study to collect uncontaminated trace metal seawater samples.

1.1 Pre-cruise preparation

1.1.1 Cleaning of sample bottles and laboratory material

All bottles and laboratory material used to store samples, prepare reagents, standards, etc. needed to pass a three step cleaning protocol. During this study, 125 ml low density polyethylene bottles (LDPE, Nalgene) were used to collect seawater samples.

(i) First, in order to remove any grease attached to the walls of the LDPE bottles, all bottles were soaked in 5% detergent solution (Mucosol Universal detergent) diluted with deionised water (Millipore Milli-Q deionised water $R=18.2\text{M}\Omega\text{ cm}^{-1}$) for 24 hours. The following day, bottles were rinsed with warm tap water to allow the removal of detergent and subsequently rinsed (filled completely and emptied) 5 times with deionised water.

(ii) Second, all the bottles were soaked in a 20% hydrochloric acid (HCl, Sigma Aldrich, Reagent grade 37%) diluted with deionised water for 4 or 7 days. Once the second step was completed, the bottles were rinsed 5 times with deionised water.

(iii) Third, the bottles were filled with and soaked in a 20% diluted nitric acid bath (HNO_3 , Sigma Aldrich, Reagent grade 37%) for 4 or 7 days. Following the third step, the bottles were rinsed 5 times with deionised water, double packed in zip-lock bags, and stored until utilization at sea. All the laboratory equipment used (measuring cylinders, vials, reagent bottles, connectors etc.) for the analysis of dAl was cleaned in the same manner. Pipette tips followed a two-step cleaning procedure prior to any use. They were rinsed 3 times with a 10% diluted HCl solution and rinsed 3 times with deionised water. Cleaning procedures were undertaken in a clean laboratory (ISO class 100) and all the samples were handled under a laminar flow hood.

1.2 Sampling procedure

1.2.1 Surface sampling

Surface sampling was undertaken using a towfish (Figure 2.1). This system is designed to sample surface trace metal clean seawater, at ca. 2-3 m depth, while the ship is steaming (Achterberg, 2000). The towfish was deployed off the side of the ship using the ship's crane and a Kevlar wire. Seawater was collected through Teflon tubing connected to acid cleaned polyvinylchloride (PVC) tubing. The seawater was pumped into the clean container using a polytetrafluorethylene (PTFE) Teflon diaphragm pump (Almatec A15) connected to an oil-free air compressor. Typically one sample was taken every 50 nautical miles and also just before arriving at a station where a deep water column profile was undertaken. The reason for taking this surface sample close to a station relies in that the first sample taken with the CTD is at ca. 15-20 m to avoid contamination from the ship.

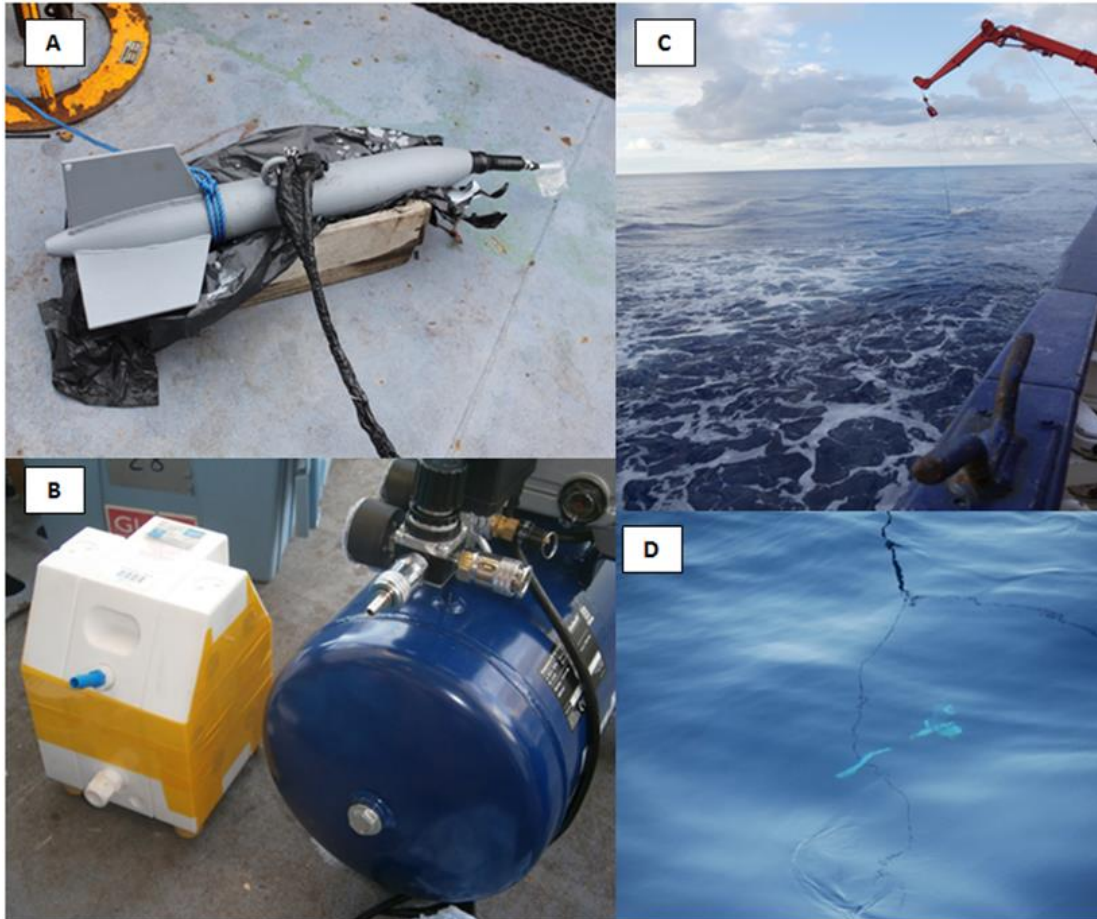


Figure 2.1: Surface sampling with a towfish. A) towfish; B) Teflon pump and air compressor used to pump the water; C) crane used to deploy the fish; D) towfish under the water.

1.2.2 Deep sampling

In the North Atlantic Ocean, samples were collected from 24 x 12 L GO-FLO bottles attached to a Trace Metal Clean Rosette (TMR, General Oceanics Inc. Model 1018 Intelligent Rosette) (Figure 2.2). The TMR was attached to a 6 mm Kevlar line. In the Southeast Atlantic Ocean samples were collected from 24 x 12 L OTE bottles and the TMR was attached to a plastic coated conducting cable. Before the start of each cast, all the GO-FLO bottles were covered, at the top and bottom, with plastic shower caps while the spigots were covered with plastic gloves. The latter step minimized contamination while the GO-FLO bottles were on deck. Just before the TMR was sent down, the shower caps and plastic gloves were removed.

The GO-FLO bottles were sent down open since it has been shown that seawater samples do not get contaminated by this procedure. However, the GO-FLO bottles were designed to be sent down closed. Once the GO-FLO bottles were lowered into the water column, a hydrostatic pressure mechanism caused the pressure release valve to pop in and the top and bottom ends of the GO-FLO open. Once the TMR had reached 5 m above the seafloor, recovering of the TMR started at a speed of 1-3 m min⁻¹. While the TMR was being recovered, each GO-FLO bottle was closed at the desired depth by sending a signal, using Seabird software, which triggered the GO-FLO bottle closing mechanism. Upon recovery of the TMR, the top and bottom ends of each GO-FLO were covered with plastic shower caps and transported into the clean container for seawater sampling (Figure 2.2D). The process of TMR GO-FLO bottles loading, deployment of the clean TMR and recovery of the GO-FLO bottles for the GEOVIDE cruise is available, as a video format, under the following link: <https://www.youtube.com/watch?v=L-JiqpVPTXY>.

1.2.3 Sample collection

Seawater samples were collected, either from the GO-FLO bottles or from the towfish, in 125 mL LDPE bottles. All the samples were collected in a clean container over pressurized with HEPA filtered air (Figure 2.3). Dissolved Al samples were filtered on-line through 0.2 µm capsule filters (SARTOBRAN® 300, Sartorius) or 0.45 µm polyethersulfone filters (Supor®, Pall Gelman) under a slight overpressure (0.2 bar; filtered (Acrovent) N₂ (Air Liquide)). Samples collected from the towfish were under pressure from the Teflon bellows pump. Each sample bottle was rinsed 3 times with sample before being filled. The cap of each sample bottle was rinsed with the seawater used to rinse the bottle.

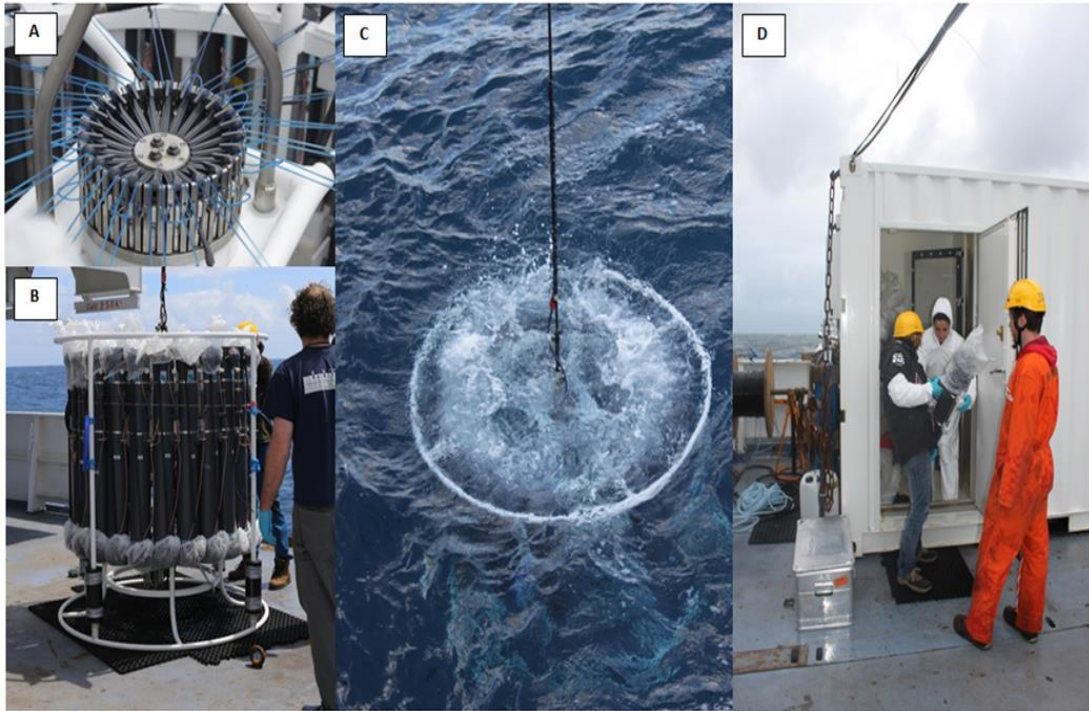


Figure 2.2: Clean Rosette used to sample seawater during GEOTRACES section GA01. A) Release mechanism to close the GO-FLO bottles; B) Set up before deployment; C) Clean rosette making his way on deck; D) Transfer of full GO-FLO bottles.



Figure 2.3: GO-FLO bottles attached to the wall of the clean container and ready to be sampled.

Once all the samples from one cast were collected, each sample was acidified to a pH 1.8 with HCl (Ultra-pure Acid (UpA), Romil) and double bagged for storage. Seawater samples for dAl need to be stored upright since it has been noticed that the polypropylene (PP) caps can, occasionally, contaminate the sample overtime.

1.3 Analysis of dissolved aluminium

Dissolved Al was analysed using two different methods. Both methods used the same chemistry in order to form a fluorescent Al-lumogallion complex which is detected on by fluorometer. (i) The first one is Flow Injection Analysis (FIA) with fluorescence detection. The Al-FIA method was first described by Resing and Measures (1994). An improved version of the Al-FIA method, described by Brown and Bruland (2008) was used in this study. In this study a commercially available metal binding resin was used (Toyopearl AF-650); (ii) The second method employed was the batch lumogallion method, developed by Hydes and Liss (1976). Samples from the GEOVIDE and M121 cruise were analysed following the Al-FIA and Al-Batch lumogallion method, respectively. The reason for changing the analytical method was due to poor functioning of the Al-FIA system.

1.3.1 Flow Injection Analysis

1.3.1.1 Equipment

The equipment (Figure 2.4) consisted of a one two-port position valve (VICI, Valco), a 6 channel peristaltic pump (Gilson), a six-port position valve (VICI, Valco), an oil bath (in-house), a de-bubbler (Omnifit), a fluorescence detector

(Shimadzu RF-10A XL), a 20 port valve position (VICI, Valco), and a laptop to control the FIA system and store the data.

1.3.1.2 Reagent preparation

All the reagents were prepared in deionised water in a class 100 clean air laboratory.

All the plastic laboratory ware used was acid cleaned as described in section 1.1.1.

- Aluminium stock standard solution: A 0.1 μM Al stock standard solution was prepared from a commercially available 1000 ppm Al standard solution (Merck Millipore).
- Ammonium acetate buffer (2M, $\text{pH}=6\pm 0.1$): To prepare 1 L of ammonium acetate buffer: To 500 ml deionised water, 110 ml Acetic acid (UpA, Romil) was added followed by the addition of 120 ml of deionised water and then 150 ml ammonia (UpA, Romil). The reagents were mixed thoroughly and the pH of the buffer adjusted to 6 ± 0.1 by adding small amounts of NH_4OH or HAc.

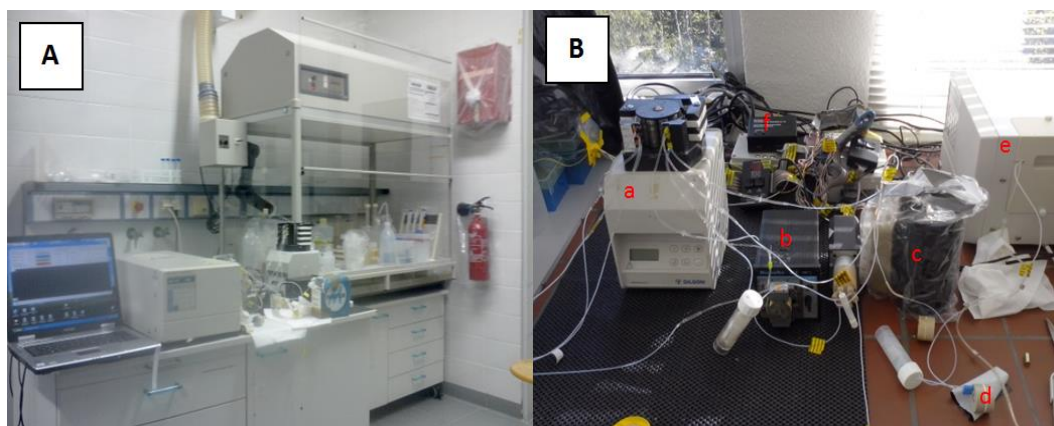


Figure 2.4: A) General setting for the FIA system. B) Close up to the FIA system. a b, peristaltic pump; c, oil bath; d, bubble trap; e, fluorimeter; f, actuator.

- Acidic carrier ($\pm 0.1\text{M HCl}$). 5 ml of concentrated HCl (UpA, Romil) was diluted in 500 ml deionised water.
- Lumogallion stock solution. The Lumogallion working solution was prepared by dissolving 50 mg of Lumogallion (TCI) in 25 ml deionised water in a 30 ml acid cleaned sterilin tube (Carl Roth). To facilitate the dissolution of the lumogallion, an ultrasonic bath was used. This solution was stable for 2 months and was kept refrigerated and in the dark.
- Ammonium acetate buffer Lumogallion work solution: 5 ml of Lumogallion stock solution was diluted in 500 ml ammonium acetate buffer. This solution was stable for 2 days but it is recommended to be freshly prepared before each analysis day.
- 2.5% Brij-35 solution: For 1 L 84 ml of brij-35 to 1000 ml of deionised water.

1.3.1.3 Analysis set up

At the beginning of an analysis day, the different equipment parts were switched on, followed by the detector and the computer. It was important to wait ca. 30 min to allow the oil bath to reach 60°C . Before a new run was started, all the system lines (sample and reagent lines) were acid cleaned with 1M HCl (Reagent grade, Sigma Aldrich) and rinsed with deionised water. For cleaning and rinsing purposes, the software was set up with the following settings: Sample=24, Loops=1, Rinse=5, Load=5, Rinse=5 and Elute=5 (2X, one for acid clean and one for deionised water rinse). At this point, all the system needed to be checked for steady flow-through of

all reagents and no blocking through back pressure. If the back-pressure needed to be adjusted, the tubing clamp placed before the detector was used.

The next step was to set up a system-software baseline as any signal below 0 or above 1000 (arbitrary units) was not recorded in the results file (.txt file). This step was critical since the baseline should not be close to 0 (to allow baseline movement during the run) and not very high (to allow larger range in Al concentrations to be measured). A recommended baseline was at 150 arbitrary counts. For this purpose, each reagent line was placed in each corresponding reagent and the system was set as follow: Sample=1, Loops=10, Rinse=80, Load=120, Rinse=80 and Elute=150. Once the signal was constant (e.g. 300 counts), the peristaltic pump was stopped (not the run), the reagent lines were taken out, rinsed with deionised water, placed in deionised water, and the peristaltic pump was re-started. When the signal was again constant (0 counts), the previous process was repeated but deionised water was replaced by reagents. As the baseline increased again to 300 counts, the ZERO button on the detector was pressed once 150 counts were reached. This way a baseline was set up at ca. 150 counts and the analysis run could be started.

A typical analysis day started with a set of calibration standards, manifold blanks, buffer blanks, followed by samples (reference seawater and seawater samples). For this purpose, each sample line was placed in the right order, the reagent lines were placed correctly in each reagent and the sequence of samples was written down. Normally, after 14 samples, a new 3 point calibration was placed between the samples. This allowed monitoring of a possible system drift. Once the amount of samples to be analysed was known the software was set as follow: Samples=X (sum of samples, standards, and blanks), Loops=2, Rinse=80 s, Load=120 s, Rinse=80 s

and Elute=150 s. It was important to set up an additional sample in order that the last sample was recorded in the result file.

1.3.1.4 Procedure

Acidified seawater was buffered online to pH 5.1-5.2 with Ammonium acetate buffer (2M, pH=6±0.1). The buffered seawater sample was loaded onto a column containing a metal binding resin (IDA, AF-Toyopearl 650). The resin binds and concentrates transition metals while interfering alkali and earth alkali ions pass through. The concentrated Al was eluted from the resin with an acidic carrier (0.1M HCl, UpA, Romil). On the way to the detector, the carrier was mixed with an ammonium acetate buffer Lumogallion reagent (TCI) and heated up to 60°C to facilitate the formation of the Al-lumogallion complex. Before detection, the reaction stream was mixed with a surfactant (Brij-35, Sigma Aldrich) which magnifies the fluorescent signal. As a last step, the reaction stream flows into a detection cell inserted in the fluorescence spectrophotometer. After detection the reaction stream flows into a waste container.

1.3.1.5 System calibration

The system was calibrated using the internal standard addition approach utilising seawater. Typically, a 5 point calibration range was prepared in the range of expected sample concentrations to be analysed. During this study, typical dAl concentrations used in the calibration were: 0, 4, 8, 16, and 32 nM. For this purpose, 20 ml seawater batches were prepared and the required amount to reach the desired Al calibration concentration was added from the 1µM Al stock standard.

It is important to clean the pipette tip between each use in order to not contaminate the next standard.

1.3.1.6 Manifold and buffer blank

The manifold blank was assessed by the analysis of two acidified (pH=1.8) seawater samples without buffering. For this purpose, the buffer line was loosed from the peristaltic pump. The average count (arbitrary units) of the two acidified seawater samples was used. The buffer blank was assessed by the analysis of three acidified seawater samples spiked with increasing amounts of buffer (1x, 2x, and 3x amounts of buffer). The difference between the counts of the three acidified seawater samples spiked with increased amounts of buffer was taken as the buffer blank. The total system blank was then calculated as the addition between the manifold and the buffer blank.

1.3.1.7 Data processing

The AI-FIA results were stored in a text file which contained two different columns, one with time in seconds and one with counts. This result file was then processed using MATLAB. The code used to process the file is given as supplementary information at the end of the chapter. The matlab code output was a text file (Figure 2.5) containing peak number (peak N), peak time (Time peak), corrected signal (raw signal - baseline signal), raw signal, and baseline signal. This output file was then combined into excel for further processing. An example of the Excel spreadsheet used is given in figure 2.6. In the excel file, a graphic representation is presented, with the calibration regression line and the blank values

peak N	Time Peak	Corrected Signal	Raw Signal	BaseL Signal
1	229	95.2367642	330.564265	235.327501
2	654	92.2499419	327.337082	235.08714
3	1127	90.507057	325.21698	234.709923
4	1552	89.8990496	324.282751	234.383702
5	2000	23.2501262	255.687771	232.437645
6	2406	24.3649971	257.201131	232.836134
7	2833	207.032746	443.152091	236.119346
8	3257	206.777766	445.894322	239.116556
9	3683	115.513447	354.282494	238.769047
10	4108	109.954311	347.510597	237.556286
11	4535	134.464832	372.93329	238.468459
12	4959	139.11503	378.10464	238.98961
13	5387	107.940918	345.796929	237.856011
14	5815	109.723881	348.197972	238.474092
15	6238	164.455294	403.82278	239.367485
16	6666	165.49873	405.629075	240.130345
17	7096	84.6824998	324.738234	240.055734
18	7518	86.4379933	325.160957	238.722964
19	7943	166.780161	405.769677	238.989517
20	8367	159.020622	399.511643	240.491022
21	8793	144.717613	384.989633	240.27202
22	9216	144.046623	383.916621	239.869998
23	9643	162.788401	402.849524	240.061123
24	10065	161.391987	402.314861	240.922874
25	10494	216.923655	458.844439	241.920784
26	10919	215.36555	458.452608	243.087058
27	11347	194.821121	436.963067	242.141946
28	11771	187.537656	429.933805	242.39615
29	12197	213.065179	455.795382	242.730203
30	12620	212.41451	455.840269	243.425759
31	13049	87.6111519	330.229184	242.618032
32	13479	82.840787	323.835563	240.994776
33	13900	323.160564	565.96007	242.799506
34	14325	325.791956	572.393179	246.601224
35	14751	270.58057	517.514074	246.933504
36	15176	265.884431	512.151223	246.266792
37	15604	226.646752	472.823544	246.176791
38	16030	226.064455	471.276489	245.212034

Figure 2.5: Output file after processing the raw data acquire with the fluorescence spectrophotometer.

2.3.2 Batch lumogallium method

The basics of this method are the same as for the Al-FIA. In the following we give just a brief description of the method as the procedure described in section 1.3.1 is very similar.

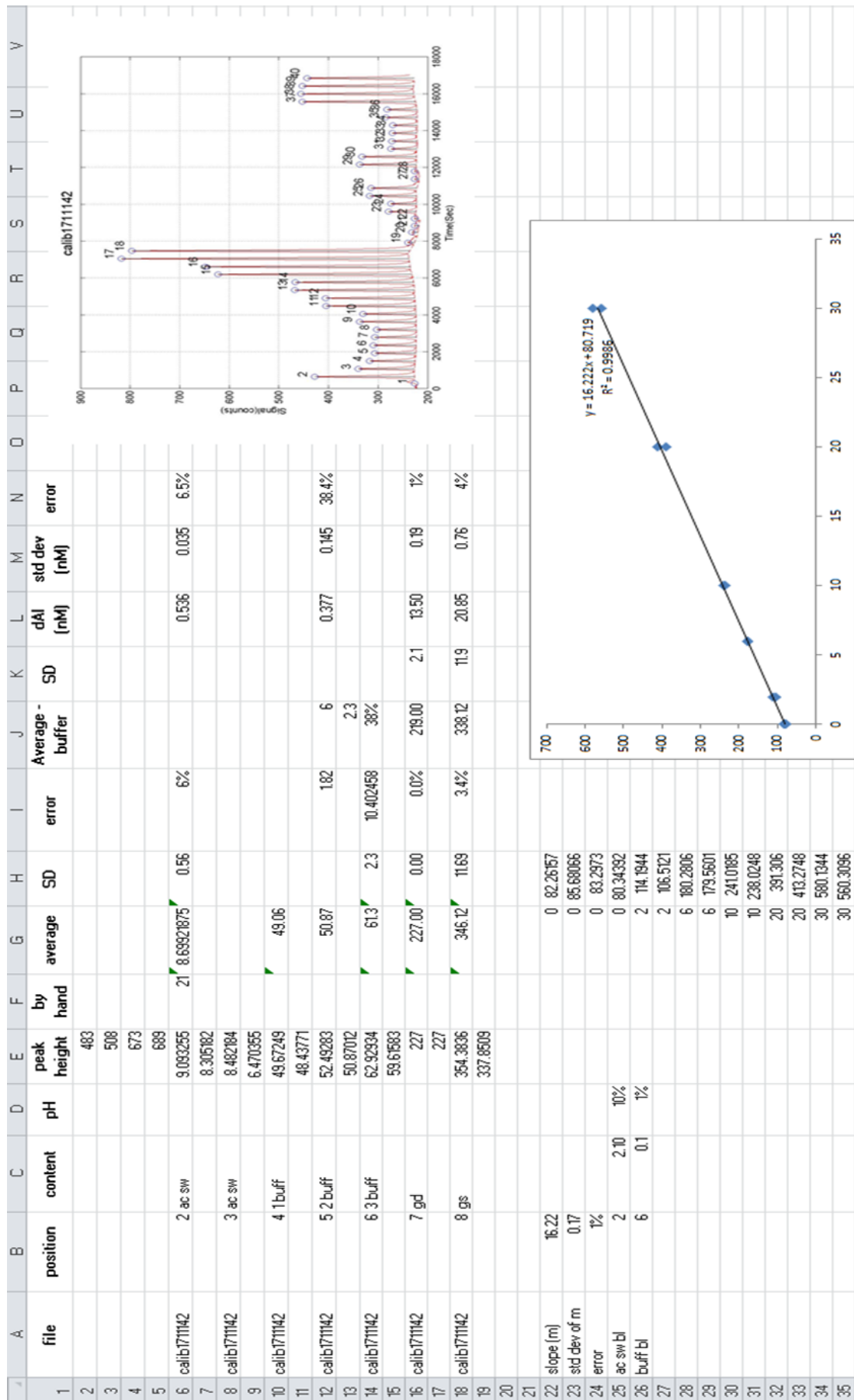


Figure 2.6: Example of excel spreadsheet used to process the daily analysis run.

2.3.2.1 Procedure

The Batch Lumogallion method uses the same chemistry as the Al-FIA method (section 1.3.1), based upon formation of an Al-Lumogallion complex. Indeed, the Al-FIA method was adapted from the Batch-Lumogallion method. The difference between both methods is that in the latter one every sample is manually prepared. This means that acidified seawater is mixed together with Lumogallion work solution and ammonium acetate buffer in a polystyrene tube. After that, each sample was heated for 1.5 hours at 80°C in an oven (Heratherm, Thermo Scientific) and left to cool down at room temperature to facilitate the formation of the fluorescent complex. All the samples were then measured on the following day using a fluorescence spectrophotometer (Cary Eclipse, Agilent). The system was set up with an excitation wavelength and emission wavelength of 465 nm and 555 nm, respectively.

2.3.2.2 Data processing

For each sample run, a .csv file with the signal measured along a wavelength spectrum was recorded. It is important to know at which wavelength the maximum signal was observed. Figure 2.7 shows a calibration example. As observed (Figure 2.7) the maximum signal was observed between wavelengths 575-585 nm. To process each sample file a MATLAB code (supplementary information) was used which gives as an output the average signal intensity measured between 575-585 nm (Figure 2.7, regression line of the calibration).

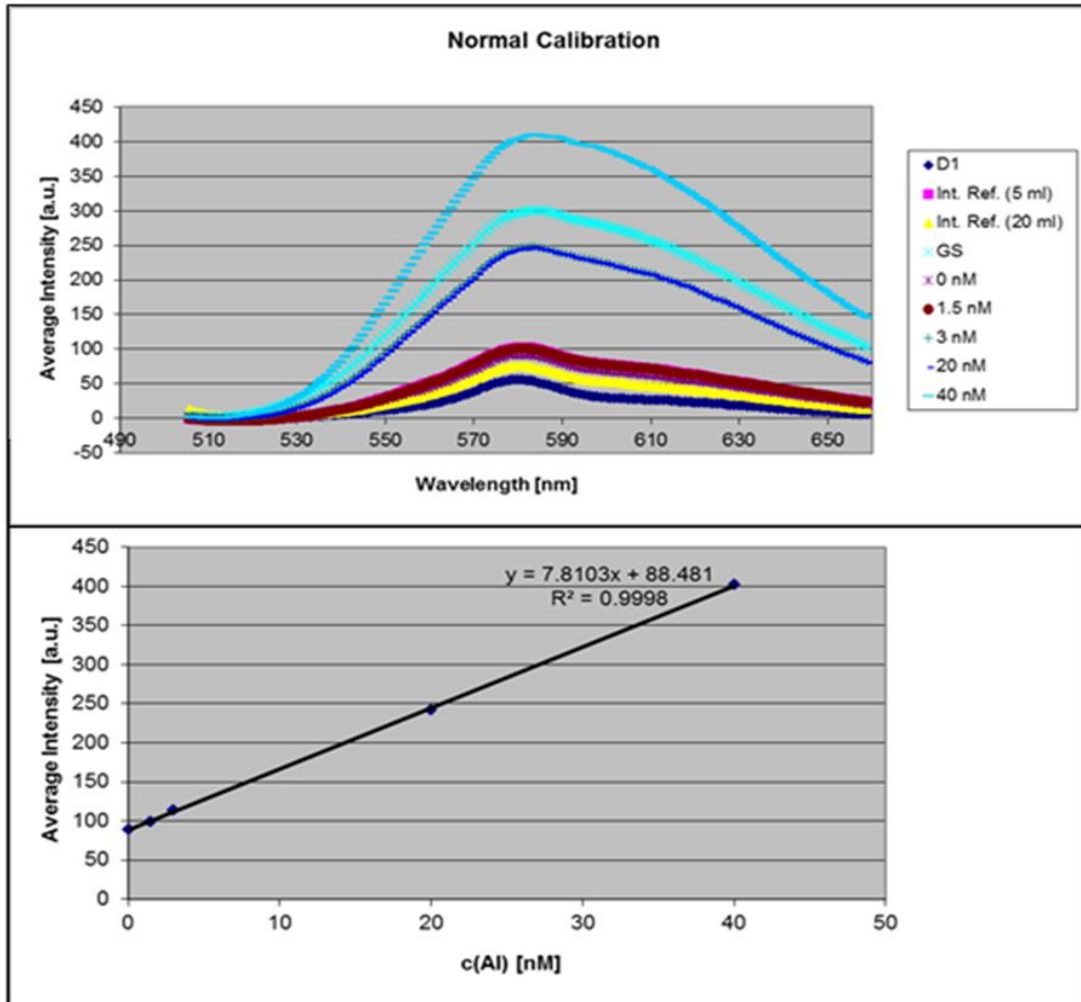


Figure 2.7: Example for a calibration using the Batch Lumogallion method.

1.4 Ancillary measurements

- Particulate Aluminium

Suspended particles were collected from the GO-FLO bottles on 0.45 μm pore size polyethersulfone filters (Supor®, Pall German) and stored frozen until processing and analysis in LEMAR (Brest, France). The filters were digested and analysed for particulate Al following the protocol of Planquette and Sherrell (2012).

- Orthosilicic acid

Seawater samples for nutrient analysis were collected from the GO-FLO bottles and analysed on board using a Bran+Luebbe AA III autoanalyser following the protocol described in Aminot and K  rouel (2007).

- Biogenic Silica

Samples for biogenic silica (BSi) were collected on the regular CTD from Niskin bottles and filtered through 0.4 μM polycarbonate filters immediately after collection. Analysis for BSi was done in LEMAR (Brest, France) by measuring the Si and Al content of two sequential alkaline digestions and a third digestion in hydrofluoric acid of the material collected on the filters following Ragueneau et al. (2005).

- Seabird sensor

Seabird sensor package 991 mounted to the CTD frame recorded pressure, temperature and salinity data, while a Seabird sensor 43 was used for dissolved oxygen. Salinity and oxygen data were calibrated against discrete samples with a salinometer (Guildline) and the Winkler method (Carpenter, 1965).

Supplementary information

AI-FIA data processing MATLAB code:

```
function AI_FIA
%%parametros adquisicion de datos:
%Rinsing
%Loading
%Rinsing
%Elution
id_ans = 1;

while id_ans ==1
prompt={'Rinsing1 (sec)', 'Loading (sec)', 'Rinsing2 (sec)', 'Elution (sec)'};
name='Time acquisition set up';
numlines=1;
defaultanswer={'70', '110', '80', '150'};
answer=inputdlg(prompt, name, numlines, defaultanswer);
texto={prompt{1}, ': ', answer{1}}; [prompt{2}, ': ', answer{2}]; [prompt{3}, ': ', answer{3}]; [prompt{4}, ': ', answer{4}];
button = questdlg(texto, 'Correct?', 'yes', 'no', 'yes');

switch button
case 'yes'
id_ans=0;
case 'no'
id_ans=1;
end

end

for j= 1: length(answer)
T_sec(j)=str2num(answer{j});
end
T_peaks = (sum(T_sec))*0.8; % limit for id peaks 80% of the time

%% file identification and data loading
[file2work, path]= uigetfile('*.txt', 'Choose txt file with your data');

file2open =[path, file2work];
DATA = load (file2open);
%% reduce the data to 1/4 of total, resolution too high.
%Time = DATA(1:4:end,1);
Time = DATA(:,1);
%Signal_Raw = DATA(1:4:end,2);
Signal_Raw = DATA(:,2);
%peak_dist = round(T_peaks / 4);
peak_dist = round(T_peaks);

%% data smooth
Signal_S = smooth (Time, Signal_Raw, 30, 'rloess'); %suavizado de datos

[yy,xx]=findpeaks(Signal_S, 'MINPEAKDISTANCE', peak_dist); %fx para encontrar los peaks

id_num = 1:1:length(xx);

%% find minimum in between peaks for baseline correction

for R = 1: length(xx)-1

vector = Signal_S(xx(R):xx(R+1));
[BL_val, BL_pos]=min(vector);
```

```

    BL_pos = BL_pos+xx(R)-1;
    BaseLineT(R)= Time(BL_pos);
    BaseLineVal(R) = BL_val;
end

%%
for pp = 1: length(xx)

    if pp ==1
        PeakBase(pp) = BaseLineVal(pp);
    else
        if pp == length(xx)
            PeakBase(pp) = BaseLineVal(pp-1);
        else
            X_B = [BaseLineT(pp-1),BaseLineT(pp)];
            Y_B = [BaseLineVal(pp-1),BaseLineVal(pp)];
            b_adj = ezfit(X_B,Y_B,'poly1');
            slopeB=b_adj.m(2);
            intpB =b_adj.m(1);
            PeakBase(pp)= Time(xx(pp))*slopeB + intpB;

        end

    end
end

h=figure;

%plot(Time,Signal_Raw,'k');hold on;
plot(Time,Signal_S,'-r'); grid on; hold on
plot(Time(xx),Signal_S(xx),'ob','markersize',7);
plot(BaseLineT,BaseLineVal,'--r');hold on;
%plot(Time(xx),YY,'--b');
title(file2work(1:end-4),'FontSize',15);hold on;
xlabel('Time (Sec)'); ylabel('Signal (counts)');hold on;
for jj = 1: length(xx)

    plot([Time(xx(jj)) Time(xx(jj))],[Signal_S(xx(jj)) PeakBase(jj)],'-k');hold
on;

end

for k = 1:length(id_num)
text(Time(xx(k)),Signal_S(xx(k))+max(Signal_S)*0.03,(num2str(id_num(1,k))),'FontSi
ze',13)
end

peakT=Time(xx);
SignalP_correc = Signal_S(xx) - PeakBase';
Signal_Rawb= Signal_S(xx);

DATA2save = [id_num', peakT, SignalP_correc, Signal_Rawb, PeakBase']
header = {'peak N' 'Time Peak' 'Corrected Signal' 'Raw Signal' 'BaseL Signal'};
matrix=[header;num2cell(DATA2save)];

xlswrite(([path,'DATA FIA AL Menzel.xlsx']),matrix,file2work(1:end-4));
saveas(h, ([path,file2work(1:end-4),'.jpg']))
saveas(h, ([path,file2work(1:end-4),'.fig']))
end

```

AI Batch-lumogallion data processing MATLAB code:

```
directory=uigetdir('','Select the folder containing the data');
cd(directory);

dirOut=uigetdir('','Select the folder where saving outputs');
D=dir(strcat(directory,'\','*.csv')); % Leo nombre archivos *.csv de la carpeta
D=struct2table(D);

prompt = {'Enter initial time LR:','Enter final time LR:'};
dlg_title = 'Input';
num_lines = 1;
def = {'575','585'};
answer = inputdlg(prompt,dlg_title,num_lines,def);

t_limits=zeros(1,2);
for i=1:length(t_limits);
    t_limits(1,i)=str2num(answer{i});
end

for i=1:length(D.name)

    test=csvread(D.name{i},2);
    [ind1 t1]=min(abs(test(:,1))-t_limits(1,1));
    [ind2 t2]=min(abs(test(:,1))-t_limits(1,2));
    mean_al(i,1)=mean(test(t1:t2,2));

end

% final=struct('file',D.name,'mean',mean_al);

final.file=D.name;
final.mean=mean_al;

final_t=struct2table(final);

cd(dirOut)

prompt = {'Enter name output file'};
dlg_title = 'Name Output file';
num_lines = 1;
def = {'Prueba.csv'};
answer = inputdlg(prompt,dlg_title,num_lines,def);
writetable(final_t,answer{1},'Delimiter','')

```

References:

Achterberg, E. P.: Automated techniques for real-time shipboard determination of dissolved trace metals in marine surface waters, *International Journal of Environment and Pollution*, 13, 249-261, 2000.

Aminot, A. and K erouel, R.: Dosage automatique des nutriments dans les eaux marines: m ethodes en flux continu, Editions Quae, 2007.

Brown, M. T. and Bruland, K. W.: An improved flow-injection analysis method for the determination of dissolved aluminum in seawater, *Limnol. Oceanogr. Methods*, 6, 87-95, 2008.

Carpenter, J. H.: The accuracy of the Winkler method for dissolved oxygen analysis, *Limnology and Oceanography*, 10, 135-140, 1965.

Hydes, D. and Liss, P.: Fluorimetric method for the determination of low concentrations of dissolved aluminium in natural waters, *Analyst*, 101, 922-931, 1976.

Planquette, H. and Sherrell, R. M.: Sampling for particulate trace element determination using water sampling bottles: methodology and comparison to in situ pumps, *Limnology and Oceanography: methods*, 10, 367-388, 2012.

Ragueneau, O., Savoye, N., Del Amo, Y., Cotten, J., Tardiveau, B., and Leynaert, A.: A new method for the measurement of biogenic silica in suspended matter of coastal waters: using Si: Al ratios to correct for the mineral interference, *Continental Shelf Research*, 25, 697-710, 2005.

Resing, J. A. and Measures, C. I.: Fluorometric Determination of Al in Seawater by Flow Injection Analysis with In-Line Preconcentration, *Analytical Chemistry*, 66, 4105-4111, 1994.

Chapter 3

Aluminium in the North Atlantic Ocean and the Labrador Sea (GEOTRACES GA01 section): roles of continental inputs and biogenic particle removal

**A reviewed version of this manuscript has been submitted to
Biogeosciences after minor revisions**

Jan-Lukas Menzel Barraqueta¹, Christian Schlosser¹, H el ene Planquette², Arthur Gourain^{2,3},
Marie Cheize², Julia Boutorh², Rachel Shelley^{2,4,5}, Leonardo Contreira Pereira ⁶, Martha
Gledhill¹, Mark J. Hopwood¹, Pascale Lherminier⁷, Geraldine Sarthou², Eric P. Achterberg¹

¹ GEOMAR, Helmholtz Centre for Ocean Research Kiel, Germany

² LEMAR, UMR 6539, Plouzan e, France

³ Earth, Ocean and Ecological Sciences-School of Environmental Sciences, University of Liverpool, UK

⁴ Earth, Ocean and Atmospheric Science, Florida State University, Tallahassee, Florida, USA

⁵ Geography, Earth and Environmental Sciences, University of Plymouth, UK

⁶ Universidade Federal do Rio Grande-FURG, Rio Grande, Brazil

⁷ Ifremer, Laboratoire d'Oc eanographie Physique et Spatiale (LOPS), IUEM, Plouzan e, France

Abstract

The distribution of dissolved aluminium (dAl) in the water column of the North Atlantic Ocean and Labrador Sea was studied along GEOTRACES section GA01 to unravel the sources and sinks of this element. Surface water dAl concentrations were low (median of 2.5 nM) due to low aerosol deposition and removal by biogenic particles. However, surface water dAl concentrations were enhanced on the Iberian and Greenland shelves (up to 30.9 nM) due to continental inputs (rivers, glacial flour and ice melt). Dissolved Al in surface waters scaled negatively with chlorophyll *a* and biogenic silica (opal) concentrations. The abundance of diatoms exerted a significant ($p < 0.01$) control on the surface particulate Al (pAl) to dAl ratios by decreasing dAl levels and increasing pAl levels. Dissolved Al concentrations generally increased with depth and correlated strongly with silicic acid ($R^2 > 0.76$) west of the Iberian Basin, suggesting net release of dAl at depth during remineralization of sinking opal containing particles. Enrichment of dAl at near-bottom depths was observed due to the resuspension of sediments. The highest dAl (up to 38.7 nM) concentrations were observed in Mediterranean Outflow Waters, which act as a major source of dAl to mid depth waters of the eastern North Atlantic. This study clearly shows that the vertical and lateral distributions of dAl in the North Atlantic differ when compared to other regions of the Atlantic and global ocean. Responsible for these large inter- and intra-basin differences are the large spatial variabilities in the main Al source, atmospheric deposition, and the main Al sink, particle scavenging by biogenic particles.

1. Introduction

Aluminium (Al) in the oceans has been used as a tracer for mineral dust deposition (Han et al., 2008; Measures and Vink, 2000; Measures and Brown, 1996) and water masses (Measures and Edmond, 1990). Aluminium is the third most abundant element in the Earth's crust (Rudnick and Gao, 2003), but concentrations of dissolved Al (dAl; filtered through 0.4 or 0.2 μm pore size filters) in the world's ocean are at nanomolar to low micromolar levels. In seawater, Al undergoes rapid hydrolysis resulting in the formation of species such as $\text{Al}(\text{OH})_3$ and $\text{Al}(\text{OH})_4^-$, which are insoluble (Roberson and Hem, 1969) and particle reactive (Orians and Bruland, 1985), especially in association with silicon-rich particles (Moran and Moore, 1988).

A major source of Al to the surface ocean is dry atmospheric deposition of terrigenous material (Kramer et al., 2004; Measures et al., 2005; Orians and Bruland, 1986) which can be carried thousands of kilometres in the atmosphere before deposition into the ocean (Duce et al., 1991; Prospero and Carlson, 1972). Wet atmospheric deposition (rain, fog and snow) also plays an important role in supplying Al to both the North Atlantic (Schlosser et al., 2014; Shelley et al., 2017) and the global ocean (Guerzoni et al., 1997; Vink and Measures, 2001). Glacial runoff has been reported as a pronounced source for Arctic and Antarctic surface waters (Brown et al., 2010; Statham et al., 2008), but its impact beyond the immediate source regions has not yet been established. Fluvial inputs were historically considered a dominant source of Al to the surface ocean (Stoffyn and Mackenzie, 1982), but Al removal through particle scavenging during estuarine mixing processes appears to strongly reduce the riverine Al outflows (Hydes, 1989). However, recent publications have indicated significant fluvial sources for Al

(Brown and Bruland, 2009; Brown et al., 2010; Grand et al., 2015). Sediment resuspension represents an important source of Al to the deep ocean, especially along ocean margins with strong boundary currents (Jeandel et al., 2011) and in areas with benthic nepheloid layers (Middag et al., 2015b; Moran and Moore, 1991). Recently, hydrothermal vents (Measures et al., 2015; Resing et al., 2015) were noted as Al sources to the deep Atlantic and Pacific Oceans, with plumes extending at depth over 3000 km in the Pacific Ocean.

Removal of Al in oceanic waters occurs through particle scavenging with subsequent sinking of the particulate matter (Orians and Bruland, 1986). This removal occurs via both active and passive scavenging processes. Active scavenging occurs when dAl is incorporated into the atomic structure of opaline diatom frustules, a process which has been demonstrated in laboratory experiments and is also supported by positive correlations between silicic acid (Si(OH)_4) and Al in depth profiles as a result of the sinking and remineralization of diatomous material (Gehlen et al., 2002; Hydes et al., 1988; Hydes, 1989; Middag et al., 2009; Middag et al., 2015b; Moran and Moore, 1988a). Passive scavenging is defined as dAl being adsorbed onto any particle surface without being intrinsically incorporated into cellular structures. This is inclusive of adsorption onto biogenic particles. Evidence for *post-mortem* incorporation (e.g. passive scavenging) of Al into diatoms frustules and concomitant removal from the dissolved phase is given by Koning et al. (2007) and Vrieling et al. (1999).

In the North Atlantic (40°N-65°N) vertical dAl profiles combined with high resolution sections were scarce prior to the GEOTRACES era (Mawji et al., 2015). In the western North Atlantic reported dAl concentrations range from 1 nM in surface waters to 27 nM

near the seafloor (Hall and Measures, 1998; Middag et al., 2015b). In the eastern North Atlantic dAl concentrations in surface waters range between 1-5 nM (Measures et al., 2008), and a dAl mid-depth maximum (>30 nM) is observed associated with Mediterranean Outflow Waters (MOW) (Measures et al., 2015; Rolison et al., 2015). Globally, the highest dAl concentrations have been measured in the Mediterranean Sea (up to 174 nM) (Chou and Wollast, 1997; Hydes et al., 1988; Rolison et al., 2015) and the subtropical North Atlantic (up to 60 nM) (Schlosser et al., 2014), while the lowest concentrations (< 1nM) were found in the Southern Ocean (Middag et al., 2011), the Pacific Ocean (Orians and Bruland, 1986) and the high latitude North Atlantic (Middag et al., 2015b).

This manuscript provides an overview of the surface and water column distribution of dAl in the North Atlantic Ocean and Labrador Sea along GEOTRACES section GA01. The sources and sinks of Al for the surface and deep ocean are discussed, and the controls that regulate dAl are examined in light of Si(OH)_4 and particulate Al (pAl) distributions.

2. Methods

2.1. Sampling and processing

The GEOVIDE cruise was conducted as part of the GEOTRACES programme (GA01 section), and sailed on May 15 (2014) from Lisbon (Portugal), passed by the most southern tip of Greenland (June 16, 17) and arrived in St. John's (Canada) on June 30 (Figure 3.1). A total of 32 stations were sampled for dissolved and particulate trace metals. Seawater was collected using a trace metal clean rosette (TMR, General Oceanics Inc. Model 1018 Intelligent Rosette) attached to a Kevlar

line and fitted with 24×12 L GO-FLO bottles (General Oceanics). After recovery, GO-FLO bottles were transferred to a clean container for sampling.

Dissolved Al samples were filtered using 0.2 µm capsule filters (Sartobran 300, Sartorius) or 0.45 µm polyethersulfone filters (Supor®, Pall Gelman), under a slight overpressure (0.2 bar; filtered (Acrovent) N₂ (Air Liquide)). Seawater samples were collected in 125 mL low density polyethylene bottles (LDPE; Nalgene), cleaned using a three-step protocol (as per Cutter et al., 2017). After collection, the samples were acidified to pH~1.8 with HCl (Ultra-pure Acid (UpA), Romil) and double bagged. Samples were then stored upright in order to minimize contact and potential contamination arising from the polypropylene caps. Samples were shipped to GEOMAR (Kiel, Germany) and analysed in a class 100 clean laboratory. Samples for particulate trace metals (Gourain et al., special issue) were collected on 0.45 µm pore size polyethersulfone (PES) filters (Supor®, Pall Gelman) and stored frozen until analysis at LEMAR (Brest, France). Additionally, total dissolvable Al (TdAl) samples (unfiltered) were collected (May 2014) by hand in 125 mL acid cleaned LDPE bottles (Nalgene) from icebergs (n=11) and surface waters in Godthåbsfjord (n=6) (SW Greenland), acidified to pH1.8 by addition of HCl (UpA, Romil) and stored for 6 months prior to analysis at GEOMAR. After collection, ice samples were defrosted at room temperature in LDPE bags, with the first meltwater discarded to minimize contamination from sample collection, as described by Hopwood et al. (2016).

2.2 Dissolved aluminium analysis

Dissolved seawater samples were analysed for dAl using flow injection analysis (FIA) with fluorescence detection as developed by Resing and Measures (1994), and modified by Brown and Bruland (2008). A slight modification of the method published by Brown

and Bruland (2008) is the use of a 2M ammonium acetate buffer instead of a 4M buffer in the reaction stream. In short, acidified samples were buffered online to pH 5.1 ± 0.1 with a 2M ammonium acetate buffer (UpA, Romil), and passed over a chelating iminodiacetic acid resin (IDA, Toyopearl AF-Chelate 650M). The loading time was normally adjusted to 120 s (2.5 mL/min) and was extended up to 180 s for samples with low dAl concentrations (< 2 nM). After sample loading, the column was rinsed for 70 s (2.5 mL/min) with deionised water (18.2 M Ω cm, Milli-Q, Millipore) to remove the seawater matrix which interferes with the analysis. Subsequently, the preconcentrated dAl was eluted (120 s, 0.6 mL/min) from the resin using 0.1 M HCl solution (UpA, Romil) and passed into the reaction stream. Next, the eluent was combined with Lumogallion (TCI) in 2M ammonium acetate buffer. The eluent and Lumogallium mixture was passed through a 5 m long reaction coil with external heating to 60°C, supporting the formation of the fluorescent complex. After that, the reagent stream was combined with a 2.5% (volume : volume deionised water) Brij 35% solution (Sigma Aldrich) prior to detection using a fluorometer (Shimadzu RF-10A XL). Emission and excitation wavelengths were set to 484 nm and 502 nm, respectively. All samples were analysed in duplicate and the concentrations calculated using fluorescence peak heights.

Calibration was undertaken using standard additions prepared in low trace metal seawater. The different standards were prepared from a stock standard solution of 1 μ M prepared from a 1000 ppm Al standard (Merck Millipore). Typically, a calibration was set up with the following standards additions: 0, 2, 4, 12, 20 and 30 nM. The buffer blank was determined as the difference in counts (arbitrary units) between three identical samples treated with increasing amounts of buffer (single, double and triple buffer addition). The system manifold blank was determined as the mean value of two acidified (pH1.8) samples analysed without buffering. The total blank

contribution was calculated as the sum of the buffer and the manifold blank. The total blank (Mean=0.23±0.1 nM; n=28) was subtracted from the results obtained. The detection limit (0.4 nM) was calculated as three times the standard deviation of the manifold blank.

The accuracy and precision of the measurements was evaluated by analysis of consensus seawater samples as well as internal reference seawater. GEOTRACES deep (GD) and SaFe S reference seawater were analysed (n=4 and n=9) yielding an average concentration of 17.79±0.26 and 1.85±0.33 nM, respectively, and were in good agreement with the GEOTRACES consensus values as of May 2013 (www.geotraces.org) (SaFe S=1.67±0.1 nM; GD=17.7±0.2 nM). A second validation approach of the results was obtained by the comparison of two stations sampled in close proximity in the Iberian Basin by the GEOVIDE cruise (Station 11, 40.33°N, 12.22°W) and the GEOTRACES section GA04N (Station 1, 39.73°N, 14.17°W) (Rolison et al., 2015). Dissolved Al was analysed, based on the same method, using similar analytical techniques in different labs. It is noteworthy that samples for dAl during GA04N and GA01 were analysed at sea and on shore, respectively. The dAl data from waters deeper than 1000 m were used to exclude seasonal variations and based on the salinity profiles which matched below this depth. The Fisher's exact test was used for comparison between profiles as both flow injection data sets were measured with replicates (Middag et al., 2015a). This test calculates an integrated p-value as an objective metric to determine how far two profiles are consistent between each other within a given depth interval. The test determined no significant difference (i-p-value=0.2-0.3) within analytical uncertainty comparing the two profiles. The dAl dataset has thus been successfully intercalibrated through GEOTRACES, included in the Intermediate Data Product

2017 and submitted to the British Oceanographic Data Center (BODC) (www.bodc.ac.uk).

2.3 Ancillary data

Suspended particles were digested at LEMAR following the protocol of Planquette and Sherrell (2012) and analysed for particulate Al exactly as described in Gourain et al. (this issue). Silicic acid concentrations were analysed on board using a Bran+Luebbe AA III autoanalyser following Aminot and K  rouel (2007).

A Seabird sensor package 911 mounted to the CTD frame recorded pressure, temperature and salinity data, while a Seabird 43 was used for dissolved oxygen. Salinity and oxygen data were calibrated using analysis of discrete samples with a salinometer (Guildline) and the Winkler method (Carpenter, 1965), respectively.

3. Results and discussion

3.1 Regional and hydrographical settings

Along the GEOVIDE section, three biogeochemical provinces defined by Longhurst (2010) were studied: (i) the North Atlantic Subtropical (NAST) region, including the Iberian Basin (IB, Stations 1 to 19); (ii) the North Atlantic Drift (NADR) region, including the Eastern North Atlantic Basin (ENAB, Stations 21 to 26) and the Iceland Basin (IcB, Stations 29 to 38); (iii) the Subarctic North Atlantic (SANA), including the Irminger Basin (IrB, Stations 40 to 60) and the Labrador Basin (LB, Stations 61 to 71) (Figure 3.1a). The salinity distribution and the main water masses in the North Atlantic and Labrador Sea are shown in Figure 3.1b.

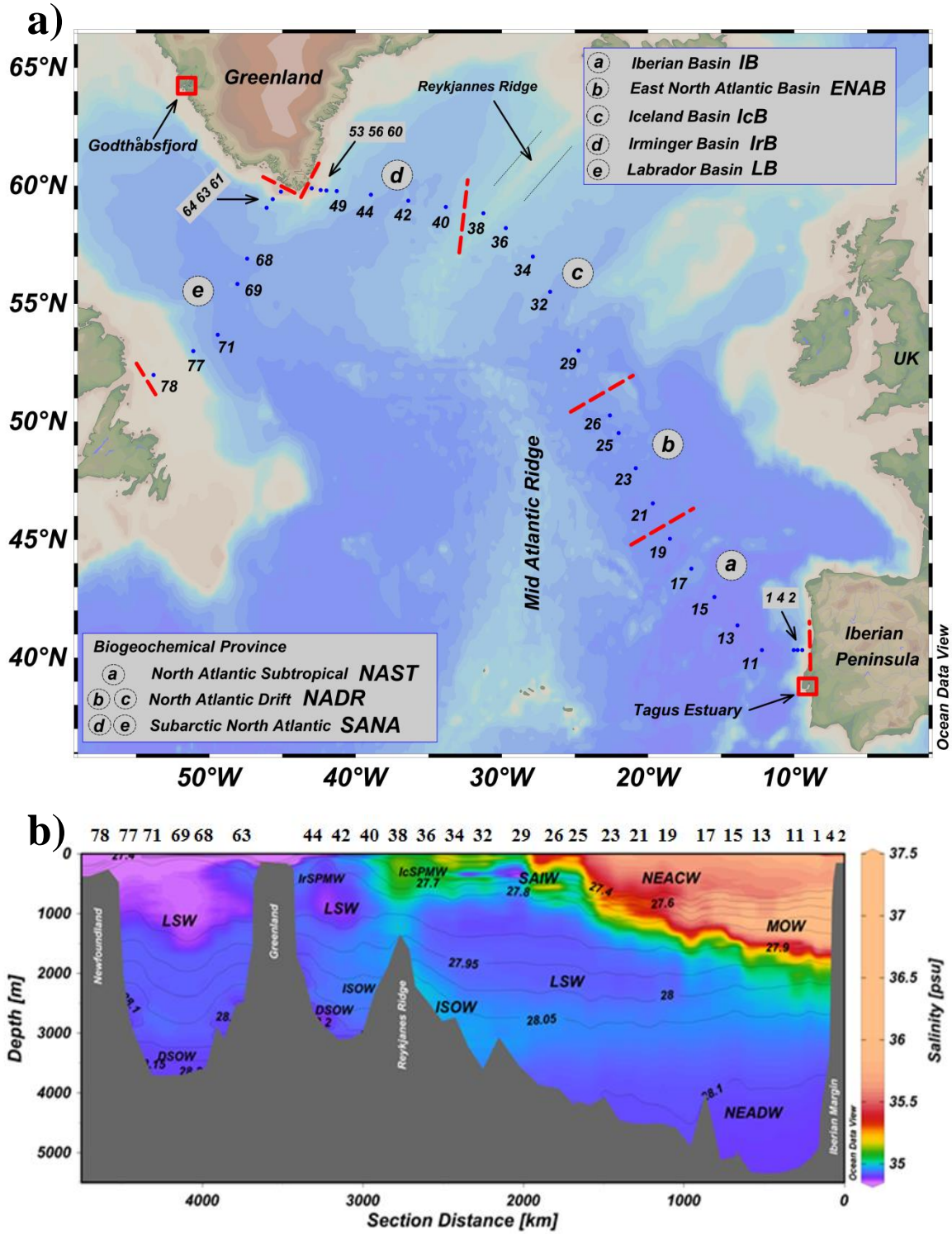


Figure 3.1: a) The cruise track along the North Atlantic and the Labrador Sea. b) Cross-section plot of salinity along GEOVIDE. Annotations represent main water masses in the study region. Isolines represent layers of equal neutral density (σ^{θ}). DSOW, Denmark Strait Overflow Water; ISOW, Iceland Scotland Overflow Water; LSW, Labrador Sea Water; MOW, Mediterranean Outflow Water; NEACW, North East Atlantic Central Water; NEADW, North East Atlantic Deep Water; IcSPMW, Iceland Sub Polar Mode Water; IrSPMW, Irminger Sub Polar Mode Water; SAIW, Sub Arctic Intermediate Water. Plots created in Ocean Data View (Schlitzer, 2017).

The main water masses used in the discussion of the dAl distribution are the (i) MOW which originates in the Mediterranean Sea, is present at intermediate layers (~500 to 2600 m) on the most eastern part of the section and decreases in salinity and density with increasing distance from Gibraltar (Baringer and Price, 1997); (ii) Iceland Scotland and Denmark Strait Overflow Waters (ISOW and DSOW, respectively) which are cold and saline water masses (ISOW= θ of 2.6°C, salinity of 34.98; DSOW= θ of 1.3°C, salinity of 34.90) formed in the Norwegian and Nordic Seas and produced during the overflow across the sills in the Faroe Bank Channel and the Iceland-Faroe ridge for the ISOW, and across the Denmark Strait into the IrB for the DSOW (Read, 2000; Swift et al., 1980; Tanhua et al., 2005; Van Aken and De Boer, 1995); (iii) East North Atlantic Central Water which originates in the North Atlantic subtropical gyre by subduction of surface waters (Pollard et al., 1996); (iv) North East Atlantic Deep Water (NEADW) which is enriched in Si(OH)_4 and NO_3^- and is depleted in O_2 and (v) Labrador Sea Water (LSW) which is formed by freshening, cooling and deep convection of the sub-polar mode water in the Labrador Sea (Talley and McCartney, 1982). A detailed description of the water masses and mixing figures, obtained through an extended optimum multiple parameter (eOMP) analysis can be found in García-Ibáñez et al. (2018).

3.2 The surface distribution of dissolved aluminium along the GEOVIDE transect: influences of atmospheric deposition, phytoplankton community structure and freshwater sources

Figure 3.2 shows average dAl concentrations in surface waters (> 50 m depth) along the cruise track, except for stations above the Iberian and Greenland shelves. The latter stations are shown in Figures 3.3 and 3.4. Dissolved Al concentrations ranged

between 0.54 nM (Station 26) and 30.99 nM (Station 2). Average surface dAl concentrations decreased from 3.3 ± 1.7 nM ($n=5$) in the IB (Stations 1, 2, and 4 are excluded due to elevated dAl concentrations from inputs by the Tagus estuary) to 3.2 ± 0.8 nM ($n=4$) in the ENAB (Stations 21 to 26) and 2.8 ± 1.2 nM ($n=5$) in the IcB (Stations 29 to 38), to 1.7 ± 0.7 nM ($n=4$) and 1.7 ± 0.6 nM ($n=3$) in the IrB and LB (Stations 53, 56, 60, 61, and 64 are excluded due to elevated dAl concentrations related to inputs from Greenland), respectively. However, within analytical errors, no significant difference was observed between basins. Our low surface dAl values agreed with literature values for the ENAB (Barrett et al., 2015; Kramer et al., 2004; Measures et al., 2008; Ussher et al., 2013) and IrB (Middag et al., 2015b), and coincided with low pAl concentrations- except over the Greenland shelf (See subsection 3.2.4) (Figure 3.4).

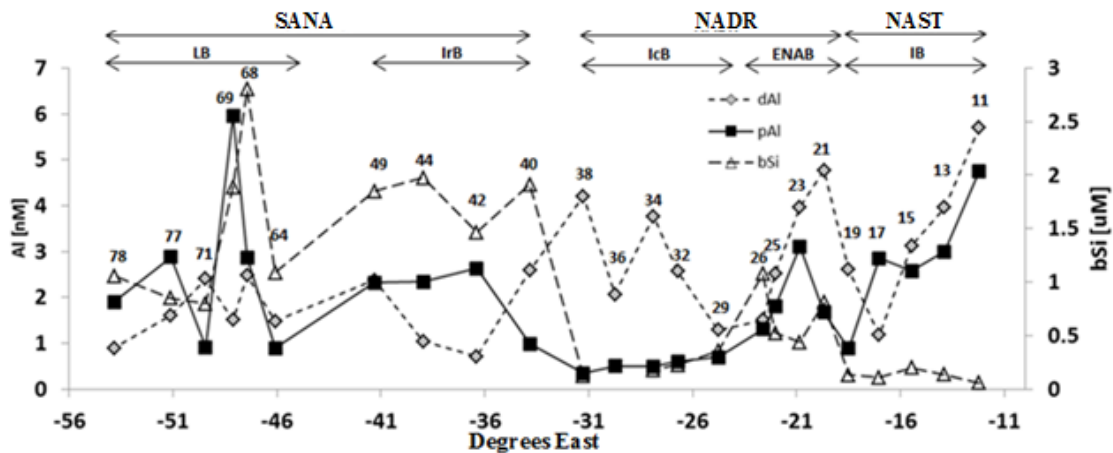


Figure 3.2: Average surface distribution (<50 m) of dissolved Al (dAl), particulate Al (pAl) (Gourain et al., special issue) and biogenic Si (bSi) (Sarhou et al., special issue) along the GEOVIDE section. Note that stations over the Iberian and Greenland shelf are not included as they are presented in Figures 3.3 and 3.4. LB, Labrador basin; IrB, Irminger Basin; IcB, Iceland Basin; ENAB, East North Atlantic Basin; IB, Iberian basin; SANA, Subarctic North Atlantic; NADR, North Atlantic Drift; NAST, North Atlantic Subtropical.

3.2.1 Atmospheric deposition

In the North Atlantic atmospheric aerosol loading decline, in a westward and northward direction, with increasing distance from African dust source regions (e.g. Sahara and Sahel) (Duce et al., 1991; Jickells et al., 2005). The low dAl surface concentrations observed (Figure 3.2) in the different basins suggest a low aerosol deposition to the study area, which is consistent with low aerosol deposition fluxes reported for the GEOVIDE cruise by Shelley et al. (2017).

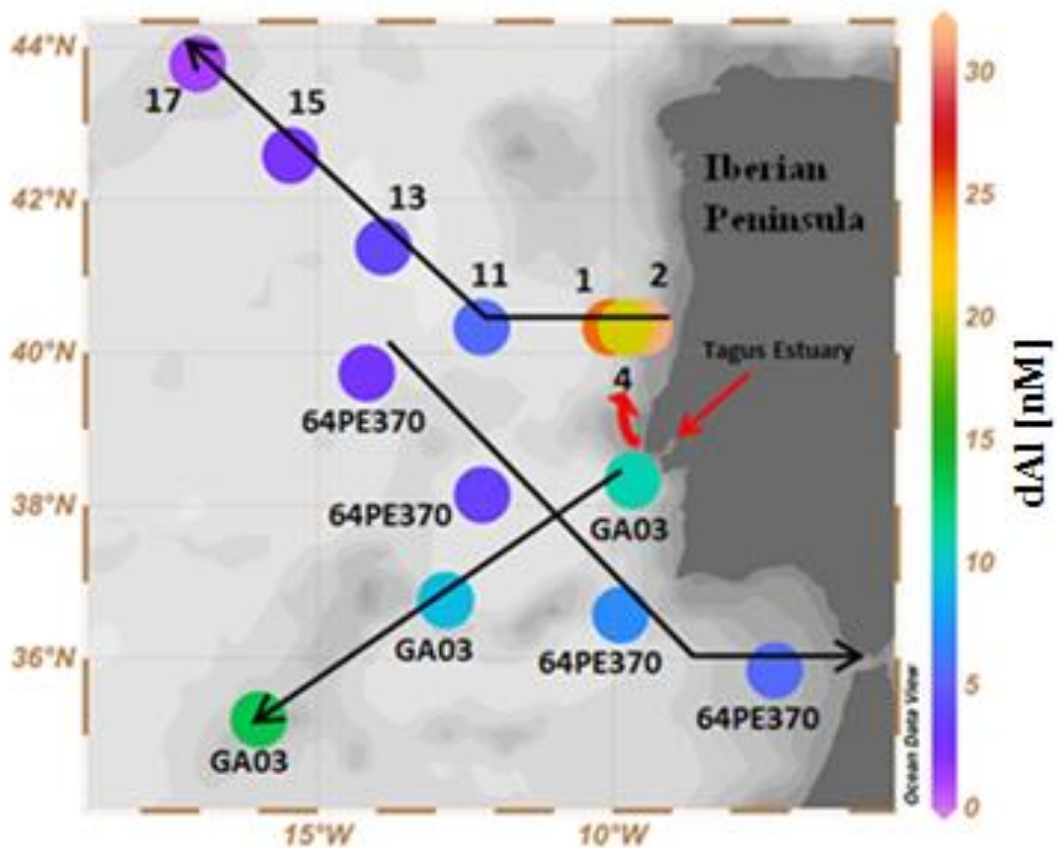


Figure 3.3: Surface concentration of dAl in the Iberian basin during GEOVIDE. GA03 refers to GEOTRACES section GA03 (Measures et al., 2015). 64PE370 refers to GEOTRACES section GA04N (Rolison et al., 2015). Black arrows show the cruise tracks. Red arrows show the location of the Tagus estuary and the northward direction of the Tagus plume. Plot created in Ocean Data View (Schlitzer, 2017).

Aerosol deposition is considered as a major source of Al to the surface ocean and modelling studies on global dust deposition indicate a tenfold decrease in atmospheric dust deposition fluxes between Portugal and the Labrador Sea (5 to 0.5 g m⁻² yr⁻¹, values from Mahowald et al., 2005) (Han et al., 2008; Jickells et al., 2005; Mahowald et al., 2005; van Hulst et al., 2014; van Hulst et al., 2013). We performed a one way ANOVA analysis of surface dAl and pAl for the different basins to determine whether atmospheric deposition was the dominant control on surface Al distributions, expecting a decrease in concentrations from east to west. However, no significance difference was observed (at the p<0.05 level) in surface dAl and pAl between the different basins (dAl: [F (3, 17)=0.89, p=0.46]; pAl: [F (3, 17)=1.79, p=0.18]). Hence additional processes must have controlled the surface distribution of Al along the section.

3.2.2 Dynamic equilibrium between dissolved and particulate Al phases

Biogenic opal production and biogenic particles play an important role in the removal of dAl in the surface ocean as a result of the high particle surface affinity of dAl (Moran and Moore, 1988b). Removal of dAl by particles therefore represents a mechanism which reduces dAl and increases pAl concentrations in surface waters (Moran and Moore, 1988a). During the GEOVIDE cruise, Chl a concentrations increased from the NAST (0.2 to 0.6 mg m⁻³), via the NADR (0.5 to 1.3 mg m⁻³) to the SANA region (up to 5.5 mg m⁻³ at station 61) (Tonnard et al., b, special issue). Along the GEOVIDE transect, diatoms were the dominant phytoplankton taxa (>40% of total phytoplankton community) in the ENAB, IrB, and LB while coccolithophorids were dominant (50% total phytoplankton community) in the IcB (Tonnard et al., b, special issue).

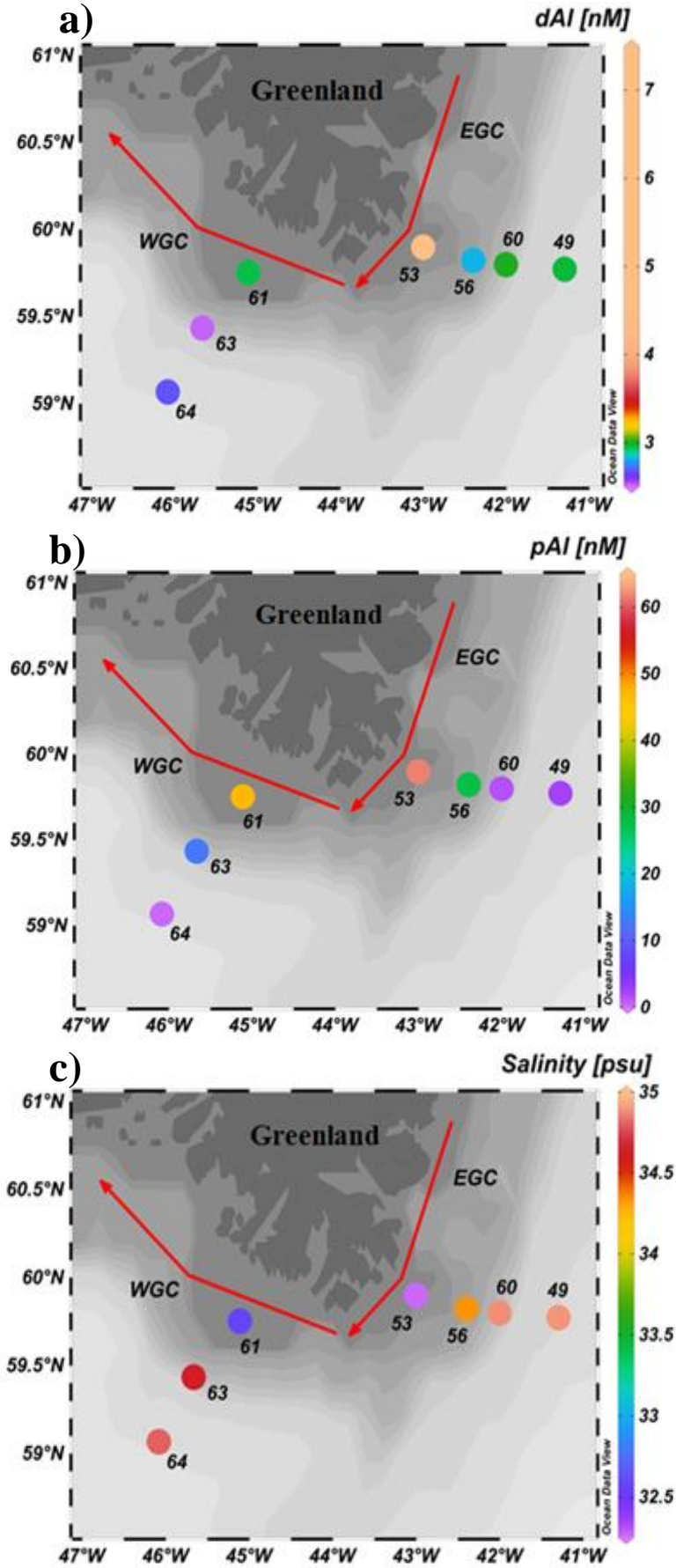


Figure 3.4: Surface concentration around the southern tip of Greenland of: a) dAl [nM]; b) pAl [nM] (Gourain et al., special issue); c) Salinity. Red arrows represent the main surface currents. EGC and WGC stand for East Greenland Current and West Greenland Current, respectively. Plot created in Ocean Data View (Schlitzer, 2017).

Elevated bSi and pAl concentrations and low dAl concentrations coincided with diatom dominated phytoplankton communities for the ENAB, IrB, and LB (Figure 3.2). In contrast, elevated dAl and low bSi and pAl concentrations coincided with coccolithophore dominated phytoplankton communities for the IcB (Figure 3.2). The latter could suggest a preferential scavenging of dAl by diatoms rather than by coccolithophorids. This conclusion is supported by increased pAl to dAl ratios where surface waters were dominated by diatoms (Figure 3.5), as possibly a consequence of active dAl incorporation into siliceous shells (Gehlen et al., 2002) or scavenging of dAl onto biogenic opal (Moran and Moore, 1988a). One way ANOVA analysis was performed for the pAl to dAl ratio in the surface waters (>50 m) in each of the four basins which showed strong dAl to Si(OH)₄ correlations with depth (LB, IrB, IcB and ENAB, see section 3.3.1). The ANOVA test showed significant differences (at the $p < 0.01$ level) between basins [$F(3, 38) = 7.9$, $p = 0.0003$]. Post hoc comparisons using the Tukey HSD test showed significant differences between the LB and IcB ($p < 0.01$) and ENAB ($p < 0.05$), and between the IrB and IcB ($p < 0.01$). No significant difference was observed between the IrB and LB and ENAB ($p = 0.86$ and 0.28 , respectively), and between ENAB and IcB ($p = 0.3$). Taken together, our results indicate that when diatoms were abundant, as in the IrB and LB (>60% of total phytoplankton community, Tonnard et al., b, special issue), the ratio between pAl and dAl significantly increases due to dAl sorption onto biogenic opal surfaces and the transfer of Al from the dissolved to the particulate fraction. Similar observations have been reported for laboratory studies and in the field where dAl decreased as a function of diatom growth and/or the presence of enhanced quantities of biogenic particles (Hydes, 1979; Kremling, 1985; Kremling and Hydes, 1988; Measures et al., 1986; Measures et al., 1984; Orians and Bruland, 1986; Stoffyn,

1979; van Bennekom, 1981). In addition, the transfer from dAl to pAl has been observed in coastal regions (Brown et al., 2010; Moran and Moore, 1988a) and the North Atlantic (Barrett et al., 2015). Considering the low aerosol deposition, reduced fluvial inputs into the tested basins (ENAB, IcB, IrB and LB), and elevated levels of bSi, we conclude that the observed differences in pAl to dAl ratios were mainly related to the of abundance diatoms.

3.2.3 The Iberian shelf surface waters: Influence of the Tagus estuary

Enhanced surface water (ca. 15 m) dAl concentrations were observed on the Iberian shelf (stations 1, 2 and 4), with average dAl concentrations of 25.5 ± 5.5 nM ($n=3$) (Figure 3.3) that decreased westwards, reaching 5.6 nM at station 11 (Figure 3.3). Previous GEOTRACES cruises close to the Iberian Peninsula, GA03 (Measures et al., 2015) and GA04N (Rolison et al., 2015), observed average surface water dAl concentrations of 11.1 ± 2 nM ($n=3$) and 4.7 ± 2 nM ($n=4$), respectively (Figure 3.3). Higher surface dAl concentrations were observed for the GA01 than for the GA03 or GA04N cruises, despite atmospheric aerosol deposition of Al being one order of magnitude lower during GA01 compared to GA03 (Shelley et al., 2015; Shelley et al., 2017). Possible sources which could explain the elevated surface dAl concentrations are shelf sediment resuspension, wet deposition, and riverine inputs. Shelf sediment resuspension is unlikely to be the reason for the elevated dAl concentrations as deep profiles for stations 2 and 4 (Figure 3.6) showed that the elevated levels of dAl observed in bottom waters were not a source for surface waters since minimum dAl values were observed between maximum surface and deep dAl values. Salinity profiles for GEOVIDE showed salinity minima (<35) in surface water for stations 1, 2, and 4 (Figure 3.7), indicating a freshwater source.

No evidence of freshwater input was observed at station 11, located just west of station of 1. A plausible explanations for the observed distribution in salinity are therefore wet deposition and/or river inputs. Wet deposition events were registered between stations 1 and 4 (Shelley et al., 2017a). Yet, the shape of the salinity profiles of stations 1 to 4 seem unlikely to have been caused solely by recent wet deposition as the differences in salinity were observed up to a depth of 45 m. GA01 ship's ADCP data (Figure 3.8) showed that surface waters near the Iberian Peninsula flowed in a northward direction. Therefore, we suggest that the additional source of dAl to surface waters originated from the Tagus estuary located approximately 175 km south from stations 1, 2 and 4. Elevated concentrations of dissolved Fe in the Tagus outflow and strong correlations for salinity against dAl and dFe (Tonnard et al., 2018) observed during the GA01 cruise supports a riverine source of dAl.

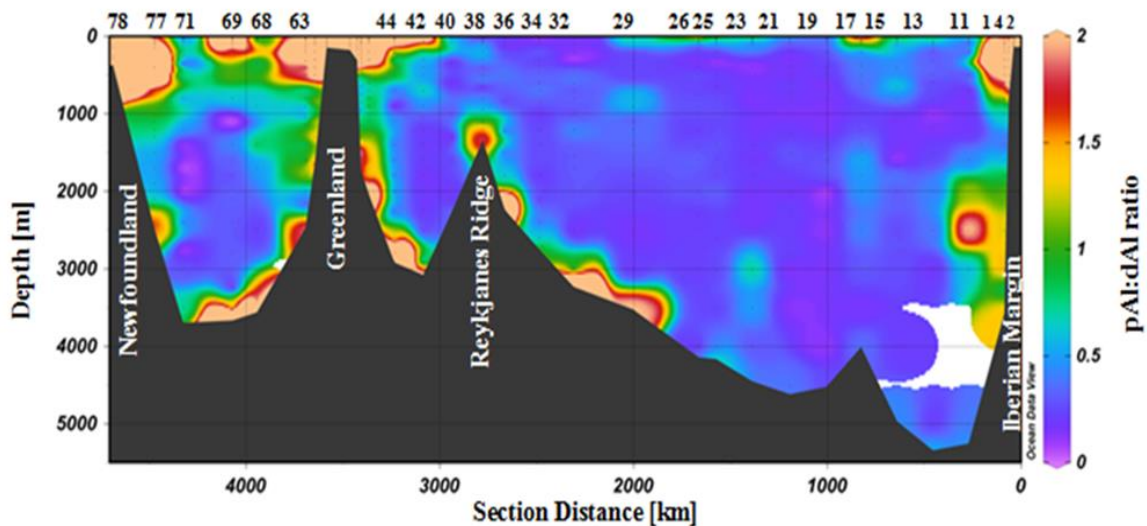


Figure 3.5: Cross-section plot of the pAl to dAl ratio (mol : mol) over the full depth of the water column. Plots created in Ocean Data View (Schlitzer, 2017).

However, we note that the wet deposition events registered between stations 1 and 4 during the GA01 cruise (Shelley et al., 2017) formed an additional freshwater source of dAl to surface waters which was superimposed on the Tagus input. Our results indicate that a fraction of riverine dAl can be advected offshore, as observed previously in the Bay of Bengal (Grand et al., 2015), Gulf of Alaska (Brown et al., 2010), and coastal waters of Oregon and Washington (Brown and Bruland, 2009), despite removal of dAl in estuaries (Hydes, 1979; Maring and Duce, 1987).

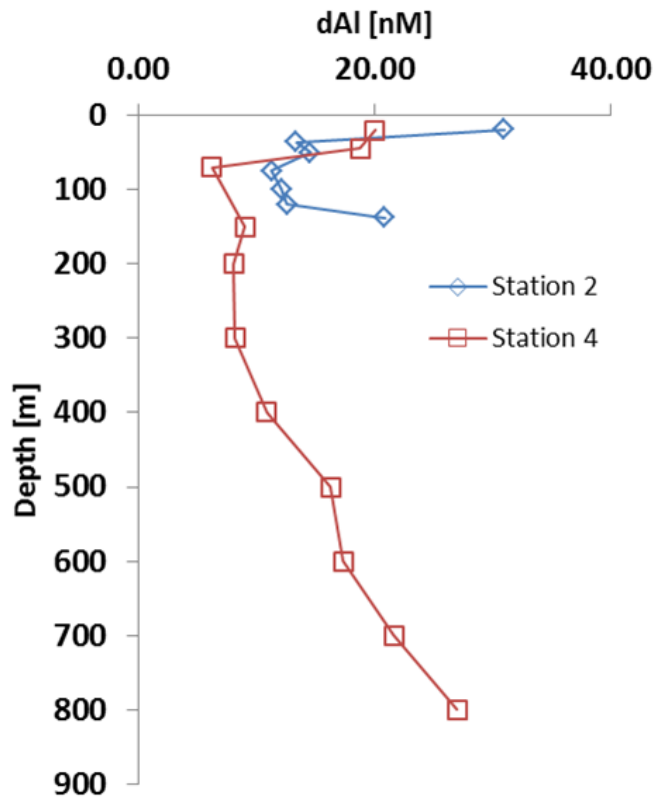


Figure 3.6: Deep profiles for dAl over the Iberian shelf.

3.2.4 The Greenland shelf surface waters: Influence of glacial runoff and ice melt

Concentrations of dAl in surface water samples collected on the Greenland shelf ranged between 2 to 7 nM, and coincided with reduced salinities (down to 32.2) and enhanced pAl concentrations (up to 62 nM) (Figure 3.4 a, b and c). Linear regressions between dAl, pAl and salinity for surface samples collected SE and SW of Greenland had coefficients of $R^2 > 0.89$ (Table 3.1). Aluminium concentrations increased with reduced salinity potentially indicating a freshwater Al source (ice melt, glacial runoff or sea-ice melt). However, as was the case for the Iberian Shelf, it is challenging to distinguish between multiple terrestrially derived dAl sources which co-occur in near-shore waters. Both, sea-ice melt and a smaller fraction of

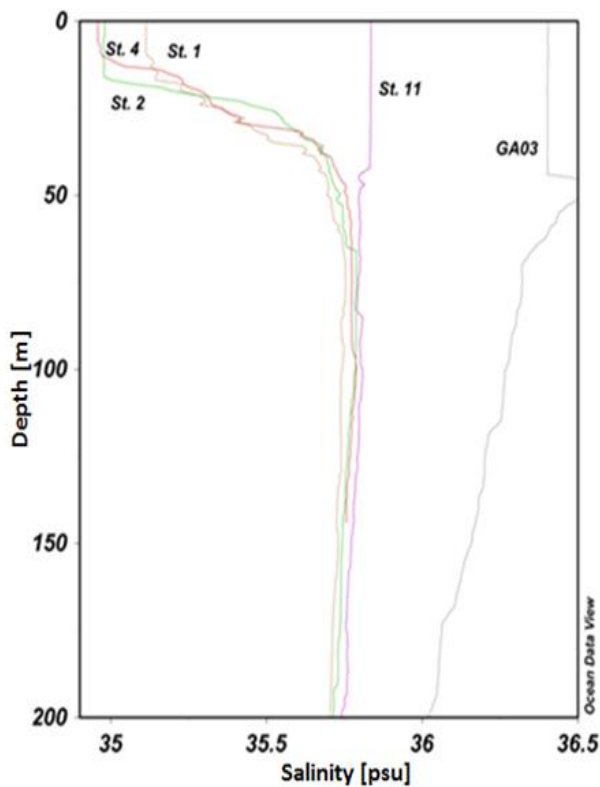


Figure 3.7: Salinity profiles showing an influence of fresh water for stations 1, 2 and 4. Profile labelled GA03 (Measures et al., 2015) shows the salinity profile for the closest station to the Tagus estuary (For reference on the location of the profile labelled GA03 please refer to Figure 3.3). Plot created in Ocean Data View (Schlitzer, 2017).

runoff (inclusive of tundra runoff, glacial discharge and meltwater from calved ice) are carried by the East Greenland Current (EGC), which flows southwards parallel to the eastern coast of Greenland (Bacon et al., 2002; Martin and Wadhams, 1999; Woodgate et al., 1999).

Freshwater endmembers (salinity 0) for Al were determined from linear regressions between dAl, pAl and salinity for the eastern stations (49, 53, 56 and 60; dAl 60.5 ± 9.9 nM and pAl 773.7 ± 125.6 nM) and western stations (61, 63 and 64; dAl 6.2 ± 1.2 nM and pAl 675.1 ± 124.7 nM) on the Greenland shelf (Table 3.1). These endmember estimates will be considered conservative as they do not incorporate Al scavenging processes. To gain some insight into what sources may have contributed most strongly to our high Al signals in surface waters off the Greenland shelf, we analysed a collection of iceberg and fjord samples from west Greenland. Mean total dissolvable Al (unfiltered) iceberg and fjord concentrations were 55 ± 2 nM and 12.8 ± 6 μ M, respectively (Table 3.2).

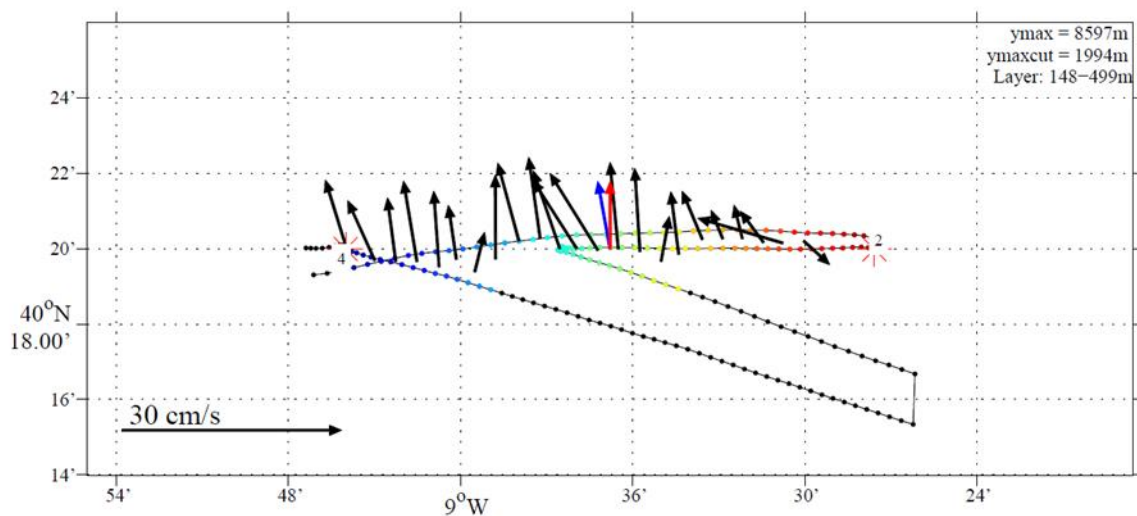


Figure 3.8: ADCP data between stations 4 and 2 during the GEOVIDE transect. The ADCP data showed a northward direction of the surface currents.

Freshwater Al endmembers (dAl+pAl) derived from our shelf stations were an order of magnitude higher than the mean tdAl measured in iceberg samples. Total dissolvable Al must by definition be <pAl due to the weaker leaching procedure applied. Yet given the large difference, the Al values off Greenland appear to be related to the input from terrestrial runoff enriched with glacially derived sediment, with this enrichment occurring either downstream of glaciers in pro-glacial environments or in near-shore environments where sediment plumes can result in high trace element concentrations throughout the year (Hopwood et al., 2016). This is consistent with a similar elevated Fe signal on the Greenland shelf. Similar observations of elevated Al were made downstream of a glacier catchment in Cumberland Bay (Schlosser et al., 2017), and attributed to suspended glacial flour as the main source for enhanced pAl concentrations. An alternative low salinity dAl signal could come from sea-ice, which contributes a total freshwater input to the EGC approximately equal to that of terrestrial runoff (Sutherland et al., 2009). Whilst sea-ice dAl concentrations are not available for this study/region, Lannuzel et al. (2011) reported median dAl and pAl concentrations in sea ice (pack ice) of 2.6 and 10.7 nmol L⁻¹. We therefore anticipate that local ice-melt (from sea-ice and icebergs) formed a minor contributor to the shelf dAl signal compared to terrestrial runoff.

Table 3.1: Correlations between salinity (S) and dAl and pAl for the eastern and western transects off Greenland. Endmember salinity 0 estimations for dAl and pAl.

Transect	Correlation S vs dAl	R ²	Correlation S vs pAl	R ²	Endmember S=0 dAl – pAl [nM]
Eastern flank	dAl = -1.6586 S + 60.5	0.94	pAl = - 22.018 S + 773.7	0.95	60.5 ± 9.9 - 773.7 ± 125.6
Western flank	dAl = -0.1013 S + 6.2	0.89	pAl = -19.272 S + 675.1	0.97	6.2 ± 1.2 - 675.1 ± 124.7

Samples	[TdAl]
Ice 1	65.91
Ice 2	35.65
Ice 3	29.92
Ice 4	29.31
Ice 5	59.31
Ice 6	62.89
Ice 7	52.48
Ice 8	112.85
Ice 9	52.50
Ice 10	45.56
Ice 11	60.59
Fjord 1	4.09
Fjord 2	7.46
Fjord 3	17.73
Fjord 4	20.10
Fjord 5	14.65
Fjord 6	13.16

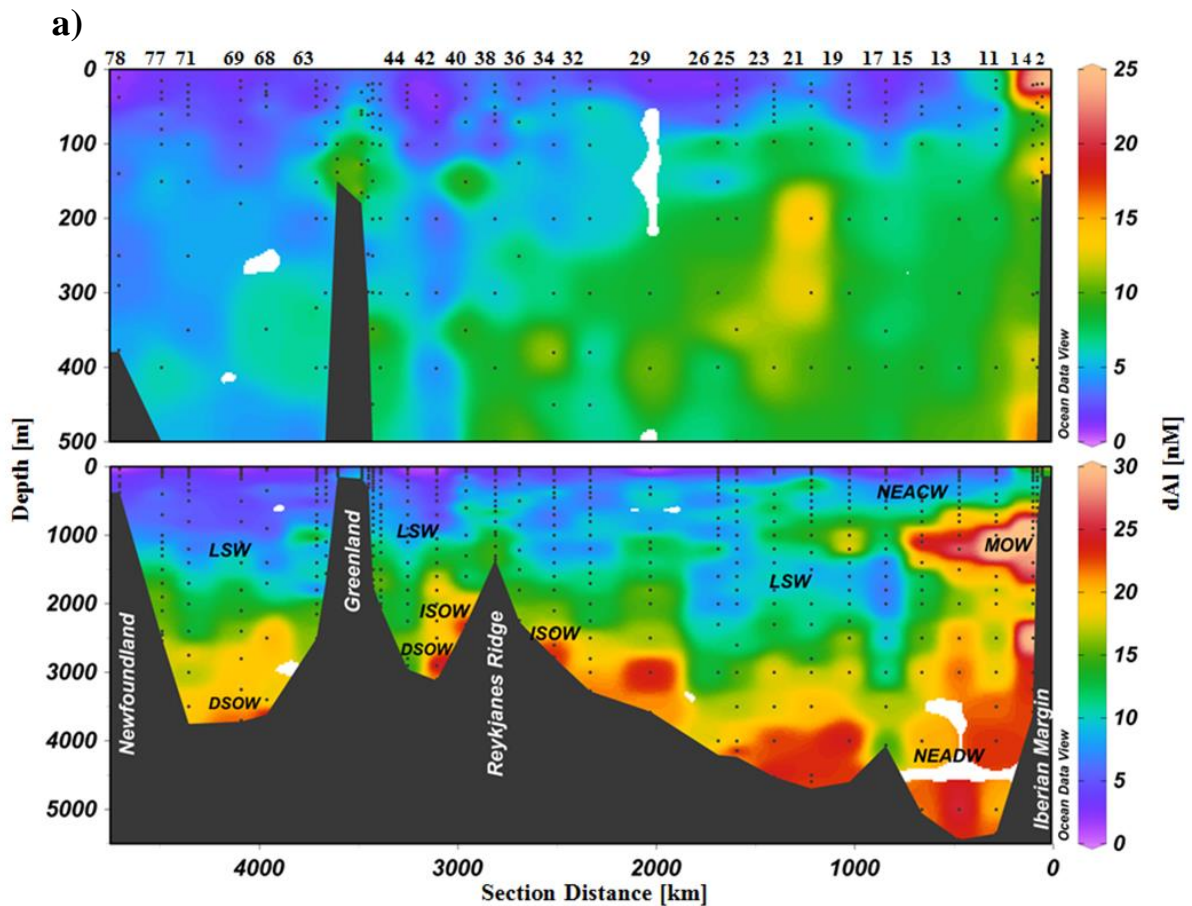
Table 3.2: Concentrations of total dissolvable Al (TdAl) in iceberg (ice) and fjord samples in Godthåbsfjord (SW Greenland). Iceberg samples are in the nM range and fjord samples are in the μM range. Ice samples were collected at 66.7°N 50.7°W while fjord samples were collected at ca. 64.7°N 50.6°W

3.3 Overview of the water column distribution of dAl

The section of dAl showed low concentrations in surface waters and an increase with depth (Figure 3.9a, b, c), therefore resembling a nutrient type distribution. The IB formed an exception with maximum dAl (up to 38 nM) observed at intermediate depths associated with the MOW (Figure 3.9a, b,c and Figure 3.10) (see section 3.4.1). Average dAl depth profiles as well as maximum,

minimum, median and quartile (1st and 3rd) dAl values per basin are presented in Figure 3.9b. In sub-surface waters between 50 and 500 m depth the median dAl concentrations were lowest in the LB (4.3 nM) and highest in the ENAB (7.6 nM) associated with East North Atlantic Central Waters (Figure 3.9c), with an overall median concentration along the full transect of 5.9 nM (n=132). In the IB observed dAl in sub surface waters compare well with GEOTRACES GA04N (Rolison et al., 2015) (median 7.3 nM for GA01 and 8.2 nM for GA04N), although they are lower than for GA03 (Measures et al., 2015) (median 16.4 nM) (Figure 3.9b). GA01 and GA04N cruises sampled the region in May 2015 and May 2013, respectively, while GA03 sampled in October 2010. The region is known to receive enhanced atmospheric aerosol deposition (Mahowald et al., 2005). A possible explanation for the difference between GA01 and GA04N with GA03 may be that dAl is

accumulated in surface waters during June to September; thus, following the late summer-autumn bloom in the Iberian Basin it is possible that the excess of dAl accumulated in surface waters is removed by particles produced by the bloom and then released in sub-surface waters. However, this explanation remains speculative. Sub-surface dAl in the IrB compared well with the GA02 data (Middag et al., 2015b) (Figure 3.9b). In deep waters, sampled between 500 and 2500 m, the median dAl concentration was lowest in the LB (6.6 nM) and highest in the IB (15.7 nM), with a median concentration along the full GEOVIDE transect of 10.3 nM (n=206). In the IB differences were found in mid waters (Figure 3.9b) between GEOVIDE (median 16.5 nM), GA04N (median 23.8 nM), and GA03 (Median 32.7 nM).



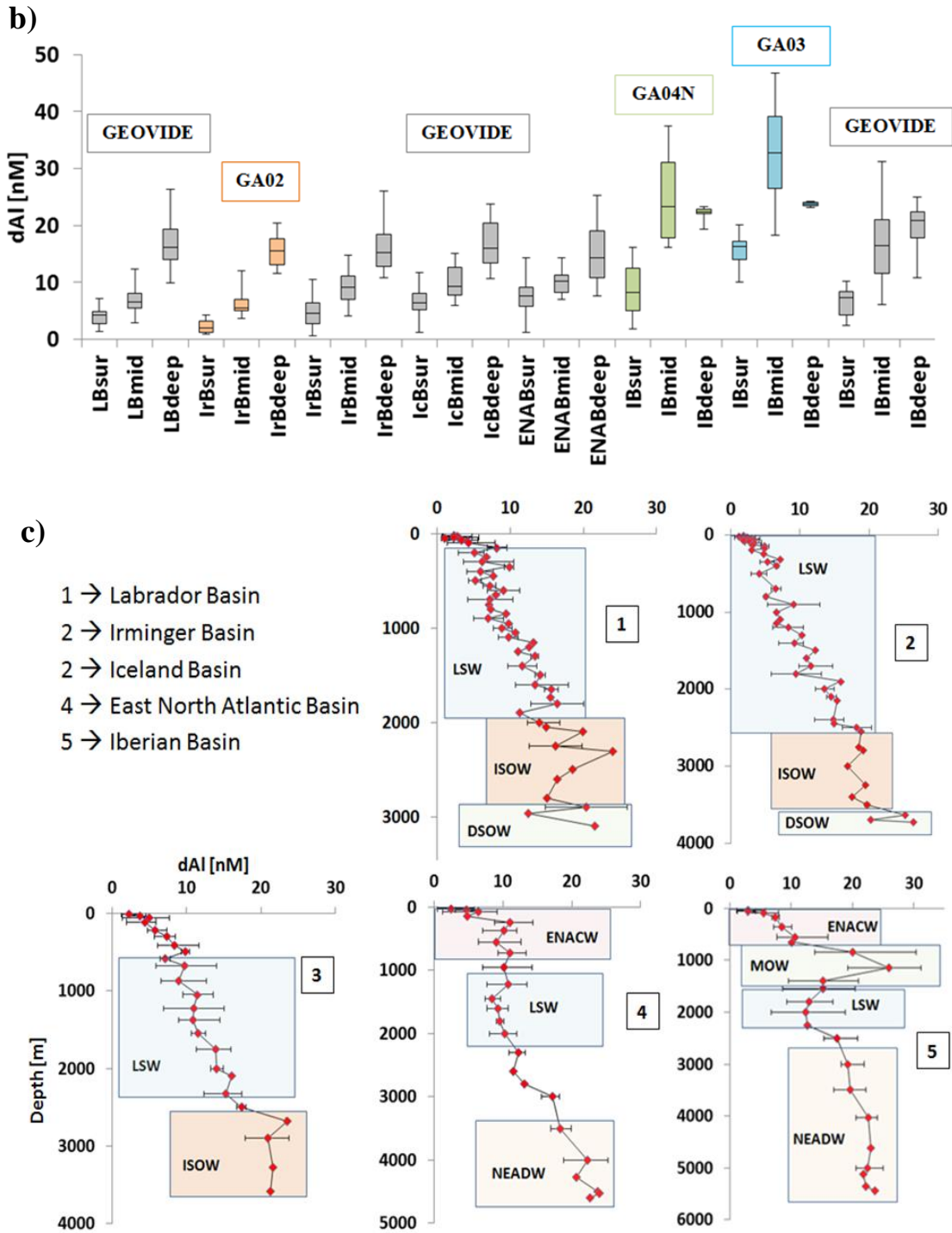


Figure 3.9: a) Cross-section plot of dAI concentrations [nM] over the full depth of the water column. Numbers represent the station numbers. On the Greenland shelf, stations numbers are as follow: From right to left 49, 60, 56, 53, 61, 63 and 64. Discrete sampling depths are indicated by filled black dots. For reference to water masses please refer to Figure 3.1b. b) Box-Whiskers plots for the different basins relative to depth. Sur: 50-500 m; Mid: 500-2500; Deep: 2500-seafloor. Numbers represent number of observations. Note that for the IrB and LB sur, mid and deep stand for 50-300, 300-1500 and 1500-seafloor as these basins are less deep. Orange, green, and blue boxes are data from GEOTRACES cruise GA02 (Middag et al., 2015b), GA04N (Rolison et al., 2015) and GA03 (Measures et al., 2015), respectively. c) Average dAI depth profiles (see section 3.1 for stations).

These are linked to a stronger presence of MOW for GA03 and GA04N than for GEOVIDE (see section 3.4.1). Below 2500 m, the median dAl concentration was lowest in the ENAB (14.4 nM) and highest in the IB (20.9 nM) associated with North East Atlantic Deep Water, with a median concentration along the full transect of 16.7 nM (n=134). Deep concentrations were comparable between GEOVIDE, GA04N, GA03 and GA02 (Figure 3.9b), and displayed similar concentrations on the eastern and western part of the transect as noted before by Middag et al. (2015b) at a latitude of ca. 40°N.

3.3.1 Remineralization versus scavenging in the North Atlantic and Labrador Sea

In the remote oligotrophic regions of the North Atlantic Ocean with enhanced Saharan dust inputs, dAl shows enhanced surface water concentrations with depletion at depth (Measures et al., 2015), typical for a scavenged type element (Bruland et al., 2014). A scavenged type distribution for dAl has also been described for the Pacific Ocean (Orians and Bruland, 1985). In contrast, a nutrient type depth distribution of dAl has been reported for the Arctic Ocean (Middag et al., 2009), Mediterranean Sea (Hydes et al., 1988; Rolison et al., 2015b), North Atlantic (40°-50°N) (Barrett et al., 2012; Measures et al., 2008) and high latitude North Atlantic (Middag et al., 2015b) and these distributions coincided with strong correlations between dAl and Si(OH)_4 (Hydes et al., 1988; Middag et al., 2015b; Middag et al., 2009; Rolison et al., 2015b). Dissolved Al is thought to be removed from surface waters onto particle surfaces (Moore and Millward, 1984; Orians and Bruland, 1985), including diatom cells (Gehlen et al., 2002) and subsequently released at depth during the recycling of biogenic particles and desorption from non-biogenic

particles. In our study region, diatoms dominate the phytoplankton communities at the early stage of the spring bloom (Brown et al., 2003), and are an important producer of biogenic silica (bSi) (Nelson et al., 1995). This, along with other biogenic particles, is a main carrier for scavenged Al (Moran and Moore, 1988b; Stoffyn, 1979). Elevated bSi concentrations and associated high export rates of bSi were measured using in situ pumps in the ENAB (up to 1.19 μM bSi), and in the IrB and LB (up to 4.27 and 4.63 μM bSi, respectively) (Lemaitre et al., special issue). Dissolved Al and Si(OH)_4 displayed strong correlations with depth in all basins (ENAB, IcB, IrB and LB) ($R^2 > 0.76$), except in the IB ($R^2 = 0.2$) which featured Al enrichment from the MOW (See section 3.4.1), the Tagus estuary and the Iberian shelf/margin (see section 3.2.1 and 3.4.2). The large production of opal and other biogenic particles (e.g. CaCO_3 from coccolithophorids) (Lemaitre et al., special issue), the strong correlation between dAl and Si(OH)_4 with depth, and the increase in dAl concentrations with depth (Fig. 7a and b, see section 3.3) suggest that in the water column the net remineralization of dAl from particles was larger than the net removal of dAl from scavenging. However, it should be noted that dAl removal by diatom production is not necessarily the only reason for the nutrient type distribution. Whilst we did not observe enhanced pAl concentrations where coccolithophorids were dominant (e.g. IcB; section 3.2.2), we assume that also other biogenic and non-biogenic particles (e.g. CaCO_3 , organic carbon, lithogenic particles, zooplankton fecal pellets) will contribute to the vertical export of surface dAl into the deep ocean. Advection and mixing of water masses with different pre-formed dAl concentrations will also influence water column distributions of dAl, as observed for water masses with low dAl concentrations (e.g. DSOW) in comparison

with overlying waters (e.g. ISOW; see section 3.4.2). Enhanced sediment resuspension can furthermore add dAl to bottom waters (See section 3.4.2).

3.4. Dissolved Al enrichment at depth

3.4.1 Mediterranean outflow water (MOW)

The Mediterranean Sea receives large inputs of aerosols which result in elevated surface dAl concentrations of up to 174 nM, as reported by Hydes et al. (1988). The presence of the MOW was indicated by a mid-depth maximum in salinity (>36) (Figure 3.1b), low oxygen concentrations ($<171 \mu\text{M}$, data not shown) and a dAl maximum (Figure 3.9a and c) at stations 11 to 29, relative to surrounding water masses. The highest dAl concentration (38.7 nM) in the outflow water was observed at station 1 (ca. 900 m deep), in agreement with observations made along GA03 for station USGT10-1 (depth 876 m – dAl = 38.8 nM) (Measures et al., 2015). Figure 3.11 displays dAl and pAl versus salinity in the MOW for a neutral density surface layer (γ^n) between 27.6 and 27.8 kg m^{-3} , corresponding to a MOW core depth, based on highest salinity values, between 1000 and 1200 m. In addition, dAl versus salinity for cruises GA03 and GA04N are plotted. The data used in the linear regressions, cover a distance of 1800 km from station 11 to station 29. The coefficients of determination (R^2) observed for dAl and pAl against salinity are 0.95 and 0.67 (Figure 3.11), respectively. The linear correlation between dAl and pAl and salinity, and the shape of the vertical distribution of dAl at station 11 (Figure 3.10) indicate that the MOW is highly enriched in dAl and represents a major source of dAl to mid-depth waters in the North Atlantic. In addition, the good correlation between dAl and salinity, and the steady decline of dAl in a westerly direction along

the neutral density surface layer 27.7 kg m^{-3} , suggest that the dAl content of MOW waters is mainly controlled by mixing with surrounding water masses and only to a minor degree by the remineralisation of biogenic particles. Due to this, dAl is a quantitative tracer for MOW.

3.4.2 Sediment resuspension

Sediment resuspension and transport due to physical forcings, such as internal waves, tides and currents, and diffusion of Al-rich pore waters, are all deemed to increase Al levels in bottom waters (Stoffyn-Egli, 1982; Van Beueskom et al., 1997). Enhanced dAl levels have been observed as a result of continental margin inputs for the Drake Passage (Middag et al., 2012) and European shelf (de Jong et al., 2007; Moran and Moore, 1991).

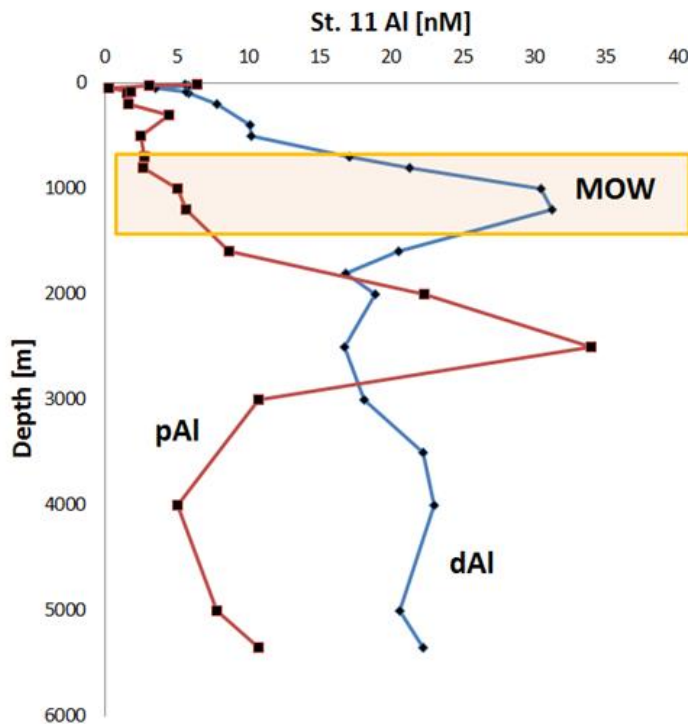


Figure 3.10: Profiles of dissolved and particulate Al [nM] at station 11. The orange box represents the approximate depth of the Mediterranean overflow Water (MOW). The high particulate Al observed at ca. 2500 m depth is associated with inputs from the Iberian margin.

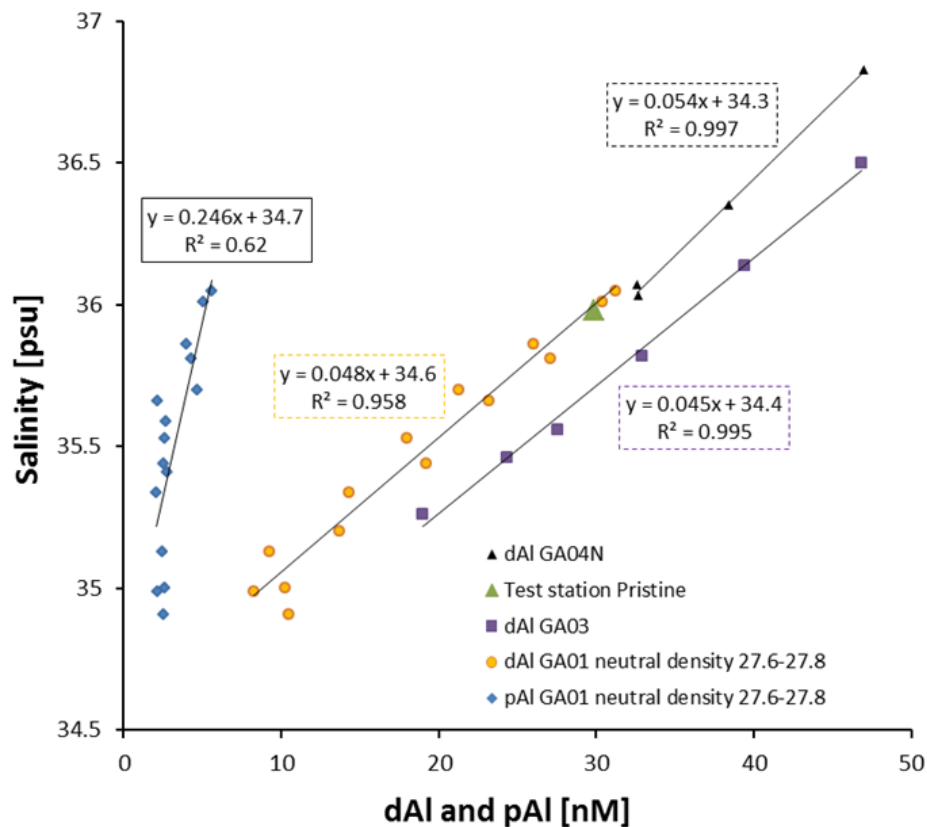


Figure 3.11: Dissolved Al and particulate Al (pAl) (Gourain *et al.*, special issue) concentrations against salinity for the Mediterranean Outflow Water (MOW) between the neutral density layer 27.6 and 27.8 kg m^{-3} . GA03 (Measures *et al.*, 2015), GA04N (Rolison *et al.*, 2015) and test station Pristine (Rijkenberg *et al.*, 2015).

Moreover, in the North Atlantic, resuspension of sediments associated with benthic nepheloid layers has been shown to elevate dAl concentrations in comparison to overlying waters (Middag *et al.*, 2015b; Moran and Moore, 1991; Sherrell and Boyle, 1992). On the Iberian and Greenland shelves and margins we observed both enhanced dAl concentrations and pAl to dAl ratios (Figure 3.9 and 3.9a). In contrast, on the Newfoundland shelf no enhanced dAl concentrations were observed. On the Iberian shelf and margin enhanced dAl concentrations were observed near the seafloor (station 2: up to 21 nM at a depth of 140 m; station 4: up to 27 nM at a depth of 800 m) associated with enhanced pAl concentrations of up to 1.5 μM at station 2 (Figure 3.13) (Gourain *et al.*, special issue). Likely, the Portugal current (Coelho *et al.*, 2002; Huthnance *et al.*, 2002), and poleward (Frouin *et al.*, 1990) and

equatorward upper slope currents (Hall et al., 2000) caused the sediment resuspension responsible for the observed enhanced dAl levels. On the Greenland margin and shelf, elevated dAl concentrations were measured at stations 53 and 61 (station 53: up to 17.4 nM at a depth=180 m) and coincided with high pAl concentrations (Up to 73.2 nM). The East Greenland Current (EGC) and West Greenland Current (WGC) are known to produce sediment resuspension. Additionally, Mienert et al. (1993) showed that sediments are transported across the shelf from melt water and runoff. In contrast, on the Newfoundland shelf and margin (Station 78), no enhanced dAl levels were observed near the seafloor (Figure 3.6). However, a large input of pAl was observed (station 78), and pAl concentrations increased from 94.6 nM at a depth of 140 m to 550 nM at the seafloor (377 m) (Gourain et al., special issue). Dissolved Al could be scavenged by resuspended particles; thus showing lower levels where elevated pAl levels were observed. Thus, the enhanced pAl levels could be attributed to sediment resuspension events caused by the south flowing Labrador Current (Mertz et al., 1993), possibly in combination with eddies that could also transfer terrigenous inputs into the Labrador Sea (Chanut et al., 2008; Hátún et al., 2007).

Enhanced dAl concentrations in the bottom layers of several basins (Iceland, Irminger, Labrador) accompanied by enhanced attenuation signals from the beam transmissometer were indicative of the presence of benthic nepheloid layers which are typically caused by strong bottom currents (e.g. ISOW and DSOW) (Eittrheim et al., 1976). Figure 3.12 shows dAl and transmissometry profiles for stations 26, 42, 69 and 77 (Figure 3.13 shows pAl for the same stations). Enhanced dAl concentrations near the seafloor coincided with enhanced pAl (Gourain et al., special issue) and a beam attenuation signal. In contrast, at station 42 dAl concentrations

decreased near the seafloor. Based on the eOMP analysis (Garcia Ibanez et al., 2018), the waters at 2900 m depth (dAl 25.1 nM) had an ISOW contribution of 66% and a residual contribution of DSOW of 2%. In contrast, near the seafloor the contribution of DSOW increased to 91% with a residual ISOW contribution of 6%. Thus, the low dAl concentrations near the seafloor were probably related to low dAl DSOW in comparison with overlaying dAl-rich ISOW as reported by Middag et al. (2015b). Enhanced dAl concentrations with no concomitant decrease in transmissometry (station 77) could indicate that dAl was released from pore waters.

Overall, the observed enhanced Al concentrations suggest that along the GEOVIDE section continental shelves and margins acted as a source of Al to adjacent waters. However, dAl concentrations did not always increase when enhanced pAl concentrations were present which implies that the release/sorption mechanisms from shelf and deep sea sediments may be different. These results suggest that, occasionally, scavenging of dAl onto resuspended particles may be a dominant process rather than partial dissolution of Al from resuspended sediments. However, the mechanisms controlling either a net dissolution or scavenging of Al from or by resuspended particles remain unclear. Moreover though, the general increase in Al concentrations in bottom layers suggests that these areas act as a potential source of Al to the North Atlantic Deep Water as observed in previous studies (Measures et al., 2015; Middag et al., 2015b; Moran and Moore, 1991).

3.4.3 Hydrothermal activity

Hydrothermal activity was assessed at station 38 over the Mid Atlantic Ridge. Hydrothermal activity has been reported as a source of dAl to the deep ocean in the Pacific and Atlantic (Measures et al., 2015; Resing et al., 2015). No enhanced dAl (Figure 3.9A) or dFe (Tonnard et al., 2018) concentrations were evident, although Achterberg et al. (2018) observed enhanced dFe over the Reykjanes ridge and attributed this to a possible combination of hydrothermal sources and sediment resuspension. However, enhanced concentrations in particulate Al (up to 28 nM), Fe, Ti and Mn and a pFe to pAl ratio similar to the ratio in fresh mid-ocean ridge basalts were observed at station 38 (Gourain et al., special issue). Therefore, the minor pAl signature observed at station 38 could be partly related to hydrothermal inputs and resuspension of newly formed oceanic crust.

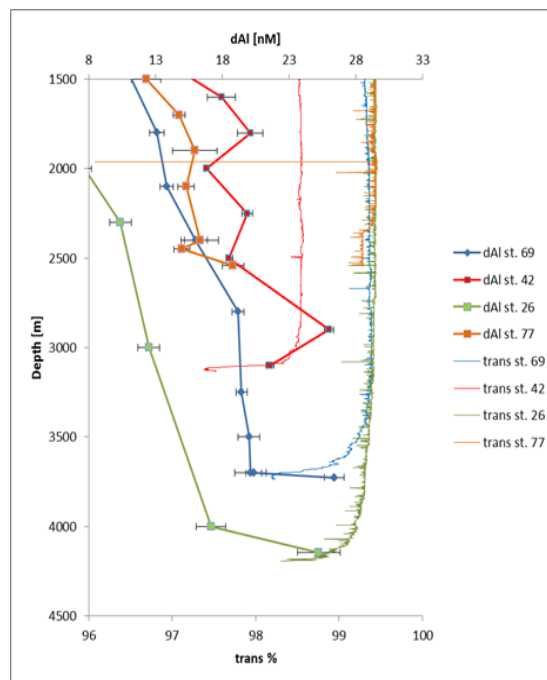


Figure 3.12: Dissolved Al [nM] and beam transmissometer [%] profiles for stations 26, 42, 69 and 77.

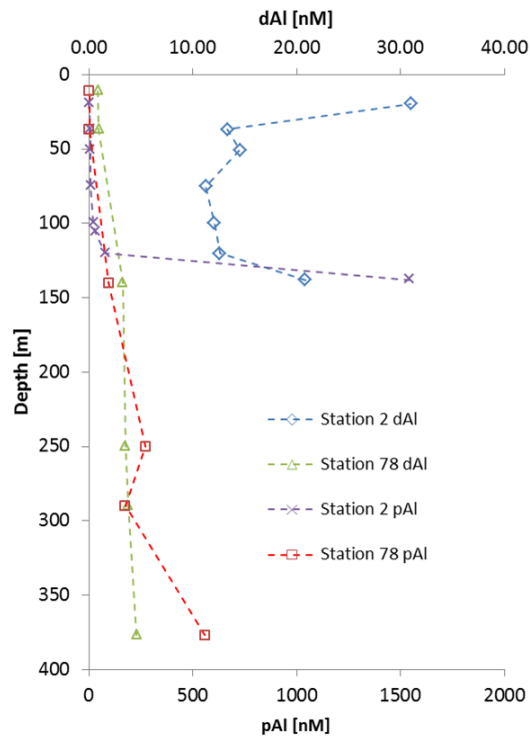


Figure 3.13: Profiles for dAl and pAl (Gourai et al., special issue) for the Iberian (Station 2) and the Newfoundland shelves (Station 78).

4. Conclusions

The dAl distribution in seawater is controlled by the relative strength of its sources and removal processes. At large basin scales, along the GEOVIDE section, the dAl distribution was mostly determined by low aerosol depositions, removal onto biogenic particles and the remineralization of biogenic particles at depth. Yet we show that at smaller regional scales, local sources such as rivers and glacial runoff controlled the dAl signatures. Additionally, sediment resuspension events and the processes of sorption/desorption of dAl onto/from particles were important mechanisms determining the dAl concentrations at sediment-water interface. Our results highlight the importance of phytoplankton (particularly diatom) abundance and dynamics for determining the interaction between dissolved and particulate Al phases in surface waters.

Overall, the AI distribution along the GEOVIDE section, in addition to other recent discoveries from the GEOTRACES Programme, highlights the complex nature of dAI biogeochemical cycling in seawater as it can resemble a scavenged type or a nutrient type element. The large sets of parameters measured on each GEOTRACES cruise will allow us, in the coming years, to examine the global ocean dAI cycling from a holistic perspective.

Acknowledgments

We are greatly thankful to the captain, Gilles Ferrand, and crew of the N/O Pourquoi Pas? for their help during the *GEOVIDE* mission. Many thanks to T. Browning for valuable comments which helped to improve the manuscript. We would like to give a special thanks to Pierre Branellec, Michel Hamon, Catherine Kermabon, Philippe Le Bot, Stéphane Leizour, Olivier Ménage (Laboratoire de Physique des Océans et Spatiale), Fabien Pérault and Emmanuel de Saint Léger (Division Technique de l'INSU, Brest, France) for their technical expertise during clean CTD deployments and to Catherine Schmechtig for the GEOVIDE database management. We also acknowledge Emilie Grosteffan, Manon Le Goff, Morgane Galinari, and Paul Tréguer for the analysis of nutrients. Greg Cutter is also thanked for his help in setting up the new French clean sampling system. This work was supported by GEOMAR, a PhD Fellowship of the Department of Scientific Politics of the Basque government to JLMB, the French National Research Agency (ANR-13-BS06-0014, ANR-12-PDOC-0025-01), the French National Centre for Scientific Research (CNRS-LEFE-CYBER), the LabexMER (ANR-10-LABX-19), and IFREMER. We thank the Helmholtz Association for financing the publication costs for this manuscript.

References

Achterberg, E. P., Steigenberger, S., Marsay, C. M., LeMoigne, F. A., Painter, S. C., Baker, A. R., Connelly, D. P., Moore, C. M., Tagliabue, A., and Tanhua, T.: Iron Biogeochemistry in the High Latitude North Atlantic Ocean, *Scientific reports*, 8, 1283, 2018.

Aminot, A. and K erouel, R.: Dosage automatique des nutriments dans les eaux marines: m ethodes en flux continu, Editions Quae, 2007.

Bacon, S., Reverdin, G., Rigor, I. G., and Snaith, H. M.: A freshwater jet on the east Greenland shelf, *Journal of Geophysical Research: Oceans*, 107, 2002.

Baringer, M. O. N. and Price, J. F.: Mixing and spreading of the Mediterranean outflow, *Journal of Physical Oceanography*, 27, 1654-1677, 1997.

Barrett, P. M., Resing, J. A., Buck, N. J., Landing, W. M., Morton, P. L., and Shelley, R. U.: Changes in the distribution of Al and particulate Fe along A16N in the eastern North Atlantic Ocean between 2003 and 2013: Implications for changes in dust deposition, *Marine Chemistry*, 177, 57-68, 2015.

Brown, L., Sanders, R., Savidge, G., and Lucas, C. H.: The uptake of silica during the spring bloom in the Northeast Atlantic Ocean, *Limnology and Oceanography*, 48, 1831-1845, 2003.

Brown, M. T. and Bruland, K. W.: Dissolved and particulate aluminum in the Columbia River and coastal waters of Oregon and Washington: Behavior in near-field and far-field plumes, *Estuarine, Coastal and Shelf Science*, 84, 171-185, 2009.

Brown, M. T. and Bruland, K. W.: An improved flow-injection analysis method for the determination of dissolved aluminum in seawater, *Limnol. Oceanogr. Methods*, 6, 87-95, 2008.

Brown, M. T., Lippitt, S. M., and Bruland, K. W.: Dissolved aluminum, particulate aluminum, and silicic acid in northern Gulf of Alaska coastal waters: Glacial/riverine inputs and extreme reactivity, *Marine Chemistry*, 122, 160-175, 2010.

Bruland, K., Middag, R., and Lohan, M.: Controls of trace metals in seawater. In 'Treatise on Geochemistry' (Eds H. Holland and K. Turekian.) pp. 19-51. Elsevier: Amsterdam, Netherlands, 2014.

Carpenter, J. H.: The accuracy of the Winkler method for dissolved oxygen analysis, *Limnology and Oceanography*, 10, 135-140, 1965.

Chanut, J., Barnier, B., Large, W., Debreu, L., Penduff, T., Molines, J. M., and Mathiot, P.: Mesoscale eddies in the Labrador Sea and their contribution to convection and restratification, *Journal of Physical Oceanography*, 38, 1617-1643, 2008.

Chou, L. and Wollast, R.: Biogeochemical behavior and mass balance of dissolved aluminum in the western Mediterranean Sea, *Deep Sea Research Part II: Topical Studies in Oceanography*, 44, 741-768, 1997.

Coelho, H., Neves, R., White, M., Leitao, P., and Santos, A.: A model for ocean circulation on the Iberian coast, *Journal of Marine Systems*, 32, 153-179, 2002.

de Jong, J. T., Boyé, M., Gelado-Caballero, M. D., Timmermans, K. R., Veldhuis, M. J., Nolting, R. F., Van den Berg, C. M., and de Baar, H. J.: Inputs of iron, manganese and aluminium to surface waters of the Northeast Atlantic Ocean and the European continental shelf, *Marine Chemistry*, 107, 120-142, 2007.

Duce, R., Liss, P., Merrill, J., Atlas, E., Buat-Menard, P., Hicks, B., Miller, J., Prospero, J., Arimoto, R., and Church, T.: The atmospheric input of trace species to the world ocean, *Global biogeochemical cycles*, 5, 193-259, 1991.

Eitrem, S., Thorndike, E. M., and Sullivan, L.: Turbidity distribution in the Atlantic Ocean, *Deep Sea Research and Oceanographic Abstracts*, 23, 1115-1127, 1976.

Frouin, R., Fiúza, A. F. G., Ambar, I., and Boyd, T. J.: Observations of a poleward surface current off the coasts of Portugal and Spain during winter, *Journal of Geophysical Research: Oceans*, 95, 679-691, 1990.

García-Ibáñez, M. I., Pérez, F. F., Lherminier, P., Zunino, P., Mercier, H., and Tréguer, P.: Water mass distributions and transports for the 2014 GEOVIDE cruise in the North Atlantic, *Biogeosciences*, 15, 2075-2090, 2018.

Gehlen, M., Beck, L., Calas, G., Flank, A.-M., Van Bennekom, A., and Van Beusekom, J.: Unraveling the atomic structure of biogenic silica: evidence of the structural association of Al and Si in diatom frustules, *Geochimica et Cosmochimica Acta*, 66, 1601-1609, 2002.

Gourain, Planquette, H., Cheize, M., Menzel, J. L., Boutorh, J., Shelley, R., Contreira, L. P., Lemaitre, N., Lacan, F., Lherminier, P., and Sarthou, G.: Particulate trace metals along the GEOVIDE section, 2017. 2017.

Grand, M. M., Measures, C. I., Hatta, M., Hiscock, W. T., Landing, W. M., Morton, P. L., Buck, C. S., Barrett, P. M., and Resing, J. A.: Dissolved Fe and Al in the upper 1000 m of the eastern Indian Ocean: A high-resolution transect along 95°E from the Antarctic margin to the Bay of Bengal, *Global Biogeochemical Cycles*, 29, 375-396, 2015.

Guerzoni, S., Molinaroli, E., and Chester, R.: Saharan dust inputs to the western Mediterranean Sea: depositional patterns, geochemistry and sedimentological implications, *Deep Sea Research Part II: Topical Studies in Oceanography*, 44, 631-654, 1997.

Hall, I., Schmidt, S., McCave, I., and Reyss, J.: Particulate matter distribution and disequilibrium along the Northern Iberian Margin: implications for particulate organic carbon export, *Deep Sea Research Part I: Oceanographic Research Papers*, 47, 557-582, 2000.

Hall, I. R. and Measures, C.: The distribution of Al in the IOC stations of the North Atlantic and Norwegian Sea between 52° and 65° North, *Marine chemistry*, 61, 69-85, 1998.

Han, Q., Moore, J. K., Zender, C., Measures, C., and Hydes, D.: Constraining oceanic dust deposition using surface ocean dissolved Al, *Global biogeochemical cycles*, 22, 2008.

Hátún, H., Eriksen, C. C., and Rhines, P. B.: Buoyant eddies entering the Labrador Sea observed with gliders and altimetry, *Journal of Physical Oceanography*, 37, 2838-2854, 2007.

Hopwood, M. J., Connelly, D. P., Arendt, K. E., Juul-Pedersen, T., Stinchcombe, M. C., Meire, L., Esposito, M., and Krishna, R.: Seasonal changes in Fe along a glaciated Greenlandic fjord, *Frontiers in Earth Science*, 4, 15, 2016.

Huthnance, J. M., Van Aken, H. M., White, M., Barton, E. D., Le Cann, B., Coelho, E. F., Fanjul, E. A., Miller, P., and Vitorino, J.: Ocean margin exchange—water flux estimates, *Journal of Marine Systems*, 32, 107-137, 2002.

Hydes, D., De Lange, G., and De Baar, H.: Dissolved aluminium in the Mediterranean, *Geochimica et Cosmochimica Acta*, 52, 2107-2114, 1988.

Hydes, D. J.: Aluminum in seawater: Control by inorganic processes, *Science*, 205, 1260-1262, 1979.

Hydes, D. J.: Seasonal variation in dissolved aluminium concentrations in coastal waters and biological limitation of the export of the riverine input of aluminium to the deep sea, *Continental Shelf Research*, 9, 919-929, 1989.

Jeandel, C., Peucker-Ehrenbrink, B., Jones, M. T., Pearce, C. R., Oelkers, E. H., Godderis, Y., Lacan, F., Aumont, O., and Arsouze, T.: Ocean margins: The missing term in oceanic element budgets?, *Eos, Transactions American Geophysical Union*, 92, 217-218, 2011.

Jickells, T. D., An, Z. S., Andersen, K. K., Baker, A. R., Bergametti, G., Brooks, N., Cao, J. J., Boyd, P. W., Duce, R. A., Hunter, K. A., Kawahata, H., Kubilay, N.,

laRoche, J., Liss, P. S., Mahowald, N., Prospero, J. M., Ridgwell, A. J., Tegen, I., and Torres, R.: Global iron connections between desert dust, ocean biogeochemistry, and climate, *Science*, 308, 67-71, 2005.

Koning, E., Gehlen, M., Flank, A.-M., Calas, G., and Epping, E.: Rapid post-mortem incorporation of aluminum in diatom frustules: Evidence from chemical and structural analyses, *Marine Chemistry*, 106, 208-222, 2007.

Kramer, J., Laan, P., Sarthou, G., Timmermans, K. R., and de Baar, H. J. W.: Distribution of dissolved aluminium in the high atmospheric input region of the subtropical waters of the North Atlantic Ocean, *Marine Chemistry*, 88, 85-101, 2004.

Kremling, K.: The distribution of cadmium, copper, nickel, manganese, and aluminium in surface waters of the open Atlantic and European shelf area, *Deep Sea Research Part A. Oceanographic Research Papers*, 32, 531-555, 1985.

Kremling, K. and Hydes, D.: Summer distribution of dissolved Al, Cd, Co, Cu, Mn and Ni in surface waters around the British Isles, *Continental Shelf Research*, 8, 89-105, 1988.

Mahowald, N. M., Baker, A. R., Bergametti, G., Brooks, N., Duce, R. A., Jickells, T. D., Kubilay, N., Prospero, J. M., and Tegen, I.: Atmospheric global dust cycle and iron inputs to the ocean, *Global Biogeochemical Cycles*, 19, 2005.

Maring, H. B. and Duce, R. A.: The impact of atmospheric aerosols on trace metal chemistry in open ocean surface seawater, 1. Aluminum, *Earth and Planetary Science Letters*, 84, 381-392, 1987.

Martin, T. and Wadhams, P.: Sea-ice flux in the East Greenland Current, *Deep Sea Research Part II: Topical Studies in Oceanography*, 46, 1063-1082, 1999.

Mawji, E. and Schlitzer, R. and Dodas, E. M. and Abadie, C. and Abouchami, W. and Anderson, R. F. and Baars, O. and Bakker, K. and Baskaran, M. and Bates, N. R. and Bluhm, K. and Bowie, A. and Bown, J. and Boye, M. and Boyle, E. A. and Branellec, P. and Bruland, K. W. and Brzezinski, M. A. and Bucciarelli, E. and Buesseler, K. and Butler, E. and Cai, P. and Cardinal, D. and Casciotti, K. and Chaves, J. and Cheng, H. and Chever, F. and Church, T. M. and Colman, A. S. and Conway, T. M. and Croot, P. L. and Cutter, G. A. and de Baar, H. J. W. and de Souza, G. F. and Dehairs, F. and Deng, F. and Dieu, H. T. and Dulaquais, G. and Echegoyen-Sanz, Y. and Lawrence Edwards, R. and Fahrbach, E. and Fitzsimmons, J. and Fleisher, M. and Frank, M. and Friedrich, J. and Fripiat, F. and Galer, S. J. G. and Gamo, T. and Solsona, E. G. and Gerringa, L. J. A. and Godoy, J. M. and Gonzalez, S. and Grossteffan, E. and Hatta, M. and Hayes, C. T. and Heller, M. I. and Henderson, G. and Huang, K.-F. and Jeandel, C. and Jenkins, W. J. and John, S. and Kenna, T. C. and Klunder, M. and Kretschmer, S. and Kumamoto, Y. and Laan, P. and Labatut, M. and Lacan, F. and Lam, P. J. and Lannuzel, D. and le Moigne, F. and Lechtenfeld, O. J. and Lohan, M. C. and Lu, Y. and Masqué, P. and McClain, C.

R. and Measures, C. and Middag, R. and Moffett, J. and Navidad, A. and Nishioka, J. and Noble, A. and Obata, H. and Ohnemus, D. C. and Owens, S. and Planchon, F. and Pradoux, C. and Puigcorbé, V. and Quay, P. and Radic, A. and Rehkämper, M. and Remenyi, T. and Rijkenberg, M. J. A. and Rintoul, S. and Robinson, L. F. and Roeske, T. and Rosenberg, M. and van der Loeff, M. R. and Ryabenko, E. and Saito, M. A. and Roshan, S. and Salt, L. and Sarthou, G. and Schauer, U. and Scott, P. and Sedwick, P. N. and Sha, L. and Shiller, A. M. and Sigman, D. M. and Smethie, W. and Smith, G. J. and Sohrin, Y. and Speich, S. and Stichel, T. and Stutsman, J. and Swift, J. H. and Tagliabue, A. and Thomas, A. and Tsunogai, U. and Twining, B. S. and van Aken, H. M. and van Heuven, S. and van Ooijen, J. and van Weerlee, E. and Venchiarutti, C. and Voelker, A. H. L. and Wake, B. and Warner, M. J. and Woodward, E. M. S. and Wu, J. and Wyatt, N. and Yoshikawa, H. and Zheng, X.-Y. and Xue, Z. and Zieringer, M. and Zimmer, L. A.: The GEOTRACES Intermediate Data Product 2014, Marine Chemistry, 177, Part 1, 1-8, 2015.

Measures, C., Brown, M., and Vink, S.: Dust deposition to the surface waters of the western and central North Pacific inferred from surface water dissolved aluminum concentrations, *Geochemistry, Geophysics, Geosystems*, 6, 2005.

Measures, C. and Edmond, J.: Aluminium in the South Atlantic: steady state distribution of a short residence time element, *Journal of Geophysical Research: Oceans* (1978–2012), 95, 5331-5340, 1990.

Measures, C., Edmond, J., and Jickells, T.: Aluminium in the northwest Atlantic, *Geochimica et Cosmochimica Acta*, 50, 1423-1429, 1986.

Measures, C., Grant, B., Khadem, M., Lee, D., and Edmond, J.: Distribution of Be, Al, Se and Bi in the surface waters of the western North Atlantic and Caribbean, *Earth and planetary science letters*, 71, 1-12, 1984.

Measures, C., Hatta, M., Fitzsimmons, J., and Morton, P.: Dissolved Al in the zonal N Atlantic section of the US GEOTRACES 2010/2011 cruises and the importance of hydrothermal inputs, *Deep Sea Research Part II: Topical Studies in Oceanography*, 116, 176-186, 2015.

Measures, C., Landing, W., Brown, M., and Buck, C.: High-resolution Al and Fe data from the Atlantic Ocean CLIVAR-CO2 Repeat Hydrography A16N transect: Extensive linkages between atmospheric dust and upper ocean geochemistry, *Global Biogeochemical Cycles*, 22, 2008.

Measures, C. and Vink, S.: On the use of dissolved aluminum in surface waters to estimate dust deposition to the ocean, *Global biogeochemical cycles*, 14, 317-327, 2000.

Measures, C. I. and Brown, E. T.: Estimating Dust Input to the Atlantic Ocean Using Surface Water Aluminium Concentrations. In: *The Impact of Desert Dust Across the Mediterranean*, Guerzoni, S. and Chester, R. (Eds.), Springer Netherlands, Dordrecht, 1996.

Mertz, G., Narayanan, S., and Helbig, J.: The freshwater transport of the Labrador Current, *Atmosphere-Ocean*, 31, 281-295, 1993.

Middag, R., Baar, H. d., Laan, P., and Huhn, O.: The effects of continental margins and water mass circulation on the distribution of dissolved aluminum and manganese in Drake Passage, *Journal of Geophysical Research: Oceans* (1978–2012), 117, 2012.

Middag, R., de Baar, H. J. W., Laan, P., and Bakker, K.: Dissolved aluminium and the silicon cycle in the Arctic Ocean, *Marine Chemistry*, 115, 176-195, 2009.

Middag, R., Séférian, R., Conway, T., John, S., Bruland, K., and de Baar, H.: Intercomparison of dissolved trace elements at the Bermuda Atlantic Time Series station, *Marine Chemistry*, doi: 10.1016/j.marchem.2015.06.014, 2015a. 2015a.

Middag, R., Van Hulst, M., Van Aken, H., Rijkenberg, M., Gerringa, L., Laan, P., and De Baar, H.: Dissolved aluminium in the ocean conveyor of the West Atlantic Ocean: effects of the biological cycle, scavenging, sediment resuspension and hydrography, *Marine Chemistry*, 177, 69-86, 2015b.

Middag, R., van Slooten, C., de Baar, H. J. W., and Laan, P.: Dissolved aluminium in the Southern Ocean, *Deep Sea Research Part II: Topical Studies in Oceanography*, 58, 2647-2660, 2011.

Mienert, J., Thiede, J., Kenyon, N., and Hollender, F. J.: Polar continental margins: studies off East Greenland, *EOS, Transactions American Geophysical Union*, 74, 225-236, 1993.

Moore, R. M. and Millward, G. E.: Dissolved-particulate interactions of aluminium in ocean waters, *Geochimica et Cosmochimica Acta*, 48, 235-241, 1984.

Moran, S. and Moore, R.: Temporal variations in dissolved and particulate aluminum during a spring bloom, *Estuarine, Coastal and Shelf Science*, 27, 205-215, 1988a.

Moran, S. B. and Moore, R. M.: Evidence from mesocosm studies for biological removal of dissolved aluminium from sea water, *Nature*, 335, 706-708, 1988b.

Moran, S. B. and Moore, R. M.: The potential source of dissolved aluminum from resuspended sediments to the North Atlantic Deep Water, *Geochimica et Cosmochimica Acta*, 55, 2745-2751, 1991.

Orians, K. J. and Bruland, K. W.: The biogeochemistry of aluminum in the Pacific Ocean, *Earth and planetary science letters*, 78, 397-410, 1986.

Orians, K. J. and Bruland, K. W.: Dissolved aluminium in the central North Pacific, *Nature*, 316, 427-429, 1985.

Planquette, H. and Sherrell, R. M.: Sampling for particulate trace element determination using water sampling bottles: methodology and comparison to in situ pumps, *Limnology and Oceanography: methods*, 10, 367-388, 2012.

Prospero, J. M. and Carlson, T. N.: Vertical and areal distribution of Saharan dust over the western equatorial North Atlantic Ocean, *Journal of Geophysical Research*, 77, 5255-5265, 1972.

Read, J.: CONVEX-91: water masses and circulation of the Northeast Atlantic subpolar gyre, *Progress in Oceanography*, 48, 461-510, 2000.

Resing, J. A. and Measures, C. I.: Fluorometric Determination of Al in Seawater by Flow Injection Analysis with In-Line Preconcentration, *Analytical Chemistry*, 66, 4105-4111, 1994.

Resing, J. A., Sedwick, P. N., German, C. R., Jenkins, W. J., Moffett, J. W., Sohst, B. M., and Tagliabue, A.: Basin-scale transport of hydrothermal dissolved metals across the South Pacific Ocean, *Nature*, 523, 200-203, 2015.

Rijkenberg, M. J. A., de Baar, H. J. W., Bakker, K., Gerringa, L. J. A., Keijzer, E., Laan, M., Laan, P., Middag, R., Ober, S., van Ooijen, J., Ossebaar, S., van Weerlee, E. M., and Smit, M. G.: "PRISTINE", a new high volume sampler for ultraclean sampling of trace metals and isotopes, *Marine Chemistry*, 177, Part 3, 501-509, 2015.

Roberson, C. E. and Hem, J. D.: Solubility of aluminum in the presence of hydroxide, fluoride, and sulfate, USGPO, 1969.

Rolison, J., Middag, R., Stirling, C., Rijkenberg, M., and De Baar, H.: Zonal distribution of dissolved aluminium in the Mediterranean Sea, *Marine Chemistry*, 177, 87-100, 2015.

Rudnick, R. and Gao, S.: Composition of the continental crust, *Treatise on geochemistry*, 3, 659, 2003.

Schlosser, C., Klar, J. K., Wake, B. D., Snow, J. T., Honey, D. J., Woodward, E. M. S., Lohan, M. C., Achterberg, E. P., and Moore, C. M.: Seasonal ITCZ migration dynamically controls the location of the (sub)tropical Atlantic biogeochemical divide, *Proceedings of the National Academy of Sciences*, 111, 1438-1442, 2014.

Shelley, R. U., Morton, P. L., and Landing, W. M.: Elemental ratios and enrichment factors in aerosols from the US-GEOTRACES North Atlantic transects, *Deep Sea Research Part II: Topical Studies in Oceanography*, 116, 262-272, 2015.

Shelley, R. U., Roca-Martí, M., Castrillejo, M., Masqué, P., Landing, W. M., Planquette, H., and Sarthou, G.: Quantification of trace element atmospheric deposition fluxes to the Atlantic Ocean (> 40° N; GEOVIDE, GEOTRACES GA01) during spring 2014, *Deep Sea Research Part I: Oceanographic Research Papers*, 119, 34-49, 2017.

Sherrell, R. M. and Boyle, E. A.: The trace metal composition of suspended particles in the oceanic water column near Bermuda, *Earth and Planetary Science Letters*, 111, 155-174, 1992.

Statham, P. J., Skidmore, M., and Tranter, M.: Inputs of glacially derived dissolved and colloidal iron to the coastal ocean and implications for primary productivity, *Global Biogeochemical Cycles*, 22, 2008.

Stoffyn-Egli, P.: Dissolved aluminium in interstitial waters of recent terrigenous marine sediments from the North Atlantic Ocean, *Geochimica et Cosmochimica Acta*, 46, 1345-1352, 1982.

Stoffyn, M.: Biological control of dissolved aluminum in seawater: experimental evidence, *Science*, 203, 651-653, 1979.

Stoffyn, M. and Mackenzie, F. T.: Fate of dissolved aluminum in the oceans, *Marine chemistry*, 11, 105-127, 1982.

Sutherland, D. A., Pickart, R. S., Peter Jones, E., Azetsu-Scott, K., Jane Eert, A., and Ólafsson, J.: Freshwater composition of the waters off southeast Greenland and their link to the Arctic Ocean, *Journal of Geophysical Research: Oceans*, 114, 2009.

Swift, J. H., Aagaard, K., and Malmberg, S.-A.: The contribution of the Denmark Strait overflow to the deep North Atlantic, *Deep Sea Research Part A. Oceanographic Research Papers*, 27, 29-42, 1980.

Talley, L. D. and McCartney, M. S.: Distribution and Circulation of Labrador Sea Water, *Journal of Physical Oceanography*, 12, 1189-1205, 1982.

Tanhua, T., Olsson, K. A., and Jeansson, E.: Formation of Denmark Strait overflow water and its hydro-chemical composition, *Journal of Marine Systems*, 57, 264-288, 2005.

Tonnard, M., Planquette, H., Bowie, A. R., van der Merwe, P., Gallinari, M., Desprez de Gésincourt, F., Germain, Y., Gourain, A., Benetti, M., Reverdin, G., Tréguer, P., Boutorh, J., Cheize, M., Menzel Barraqueta, J. L., Pereira-Contreira, L., Shelley, R., Lherminier, P., and Sarthou, G.: Dissolved iron in the North Atlantic Ocean and Labrador Sea along the GEOVIDE section (GEOTRACES section GA01), *Biogeosciences Discuss.*, 2018, 1-53, 2018.

Ussher, S. J., Achterberg, E. P., Powell, C., Baker, A. R., Jickells, T. D., Torres, R., and Worsfold, P. J.: Impact of atmospheric deposition on the contrasting iron biogeochemistry of the North and South Atlantic Ocean, *Global Biogeochemical Cycles*, doi: 10.1002/gbc.20056, 2013. n/a-n/a, 2013.

Van Aken, H. and De Boer, C.: On the synoptic hydrography of intermediate and deep water masses in the Iceland Basin, *Deep Sea Research Part I: Oceanographic Research Papers*, 42, 165-189, 1995.

van Bennekom, A. J.: On the role of aluminium in the dissolution kinetics of diatom frustules, 445-455, 1981.

Van Beueskom, J., Van Bennekom, A., Tréguer, P., and Morvan, J.: Aluminium and silicic acid in water and sediments of the Enderby and Crozet Basins, *Deep Sea Research Part II: Topical Studies in Oceanography*, 44, 987-1003, 1997.

van Hulst, M. M. P., Sterl, A., Middag, R., de Baar, H. J. W., Gehlen, M., Dutay, J. C., and Tagliabue, A.: On the effects of circulation, sediment resuspension and biological incorporation by diatoms in an ocean model of aluminium*, *Biogeosciences*, 11, 3757-3779, 2014.

van Hulst, M. M. P., Sterl, A., Tagliabue, A., Dutay, J. C., Gehlen, M., de Baar, H. J. W., and Middag, R.: Aluminium in an ocean general circulation model compared with the West Atlantic Geotraces cruises, *Journal of Marine Systems*, 126, 3-23, 2013.

Vink, S. and Measures, C. I.: The role of dust deposition in determining surface water distributions of Al and Fe in the South West Atlantic, *Deep Sea Research Part II: Topical Studies in Oceanography*, 48, 2787-2809, 2001.

Vrieling, E. G., Poort, L., Beelen, T. P., and Gieskes, W. W.: Growth and silica content of the diatoms *Thalassiosira weissflogii* and *Navicula salinarum* at different salinities and enrichments with aluminium, *European journal of phycology*, 34, 307-316, 1999.

Woodgate, R. A., Fahrbach, E., and Rohardt, G.: Structure and transports of the East Greenland Current at 75 N from moored current meters, *Journal of Geophysical Research: Oceans*, 104, 18059-18072, 1999.

Chapter 4

Atmospheric deposition fluxes over the Atlantic Ocean: A GEOTRACES case study

This manuscript has been submitted to Biogeosciences

Jan-Lukas Menzel Barraqueta¹, Jessica K. Klar^{2,3}, Martha Gledhill¹, Christian Schlosser¹, Rachel Shelley^{4,5,6}, Helene Planquette⁵, Bernhard Wenzel¹, Geraldine Sarthou⁵, Eric P. Achterberg¹

¹ *GEOMAR, Helmholtz Centre for Ocean Research Kiel, Germany*

² *Ocean and Earth Science, National Oceanography Centre, University of Southampton European Way, Southampton SO14 3ZH, UK*

³ *LEGOS, Université de Toulouse, CNES, CNRS, IRD, UPS, 14 Avenue Edouard Belin, 31400 Toulouse, France*

⁴ *Department of Earth, Ocean and Atmospheric Science, Florida State University, 117 N Woodward Ave, Tallahassee, Florida, 32301, USA*

⁵ *Laboratoire des Sciences de l'Environnement Marin, UMR 6539 LEMAR (CNRS/UBO/IRD/IFREMER), Institut Universitaire Européen de la Mer, Technopôle Brest-Iroise, Plouzané 29280, LEMAR, UMR 6539, Plouzané, France*

⁶ *School of Geography, Earth and Environmental Sciences, University of Plymouth, Drake Circus, Plymouth, PL4 8AA, UK*

Abstract

Atmospheric deposition is an important source of micronutrients to the ocean, but atmospheric deposition fluxes remain poorly constrained in most ocean regions due to the limited number of field observations of wet and dry atmospheric inputs. Here we present the distribution of dissolved aluminium (dAl), as a tracer of atmospheric inputs, in surface waters of the Atlantic Ocean along GEOTRACES sections GA01, GA06, GA08, and GA10. We used the surface mixed layer concentrations of dAl to calculate atmospheric deposition fluxes using a simple steady state model. We have optimized the aerosol Al fractional solubility, dAl residence time within the surface mixed layer and depth of the surface mixed layer for each separate cruise to calculate the atmospheric deposition fluxes. We calculated the lowest deposition fluxes of 0.15 ± 0.1 and 0.27 ± 0.13 $\text{g m}^{-2} \text{yr}^{-1}$ for the South and North Atlantic Ocean ($>40^\circ\text{S}$ and $>40^\circ\text{N}$), respectively, and highest fluxes of 1.8 and 3.09 $\text{g m}^{-2} \text{yr}^{-1}$ for the South East Atlantic and tropical Atlantic Ocean, respectively. Overall, our estimations are comparable to atmospheric dust deposition model estimates and reported field-based atmospheric deposition estimates. We note that our estimates diverge from atmospheric dust deposition model flux estimates in regions influenced by riverine Al inputs and in upwelling regions. As dAl is a key trace element in the GEOTRACES Programme, the approach presented in this study allows calculations of atmospheric deposition fluxes at high spatial resolution for remote ocean regions.

1 Introduction

Atmospheric deposition is a major source of micronutrients, especially iron, to the surface ocean (Martin et al., 1991; Moore et al., 2004). Aerosol deposition of iron in the tropical and subtropical North Atlantic stimulates N₂ fixation (Moore et al., 2009), and in high latitude waters with high nitrate low chlorophyll conditions it can enhance primary productivity (Baker et al., 2013). Consequently, atmospheric deposition is considered to support up to 50% of global export production (Jickells et al., 2014). Therefore, by supplying growth-limiting elements to marine microorganisms, atmospheric deposition can have important direct impacts on the marine carbon cycle and indirectly influence global climate (Mahowald et al., 2014).

The size distribution of mineral dust is considered a continuum. However, mineral dust is often described to have a bimodal size distribution and thus aerosols are classified into a fine (radius 0.1 - 1 μM) or coarse mode (radius 1 - 2.5 μM) (Maring et al., 2003). The classification facilitates us to assign aerosol deposition velocities for the aerosol size classes for the quantification of dry deposition fluxes (Slinn and Slinn, 1980). Mineral dust mobilization mainly depends on vegetation cover, surface soil moisture content, and wind friction speed (Mahowald et al., 2014; Zender et al., 2003). Once mobilized by wind and lofted into the troposphere, mineral dust can be transported thousands of kilometres from source regions following major air mass movements. In the North Atlantic the trade winds transport dust from North Africa to the Caribbean and Americas (Prospero et al., 2010) in about one week (Ott et al., 1991). Along the transport path of atmospheric aerosols, the size distribution of aerosol tends to decrease with increasing distance from the source regions. Chemical and physical transformation processing of aerosol in clouds, such as photo-reduction

and dissolution, can enhance the fraction of trace metals that are released upon deposition into the surface ocean (Duce and Tindale, 1991). Thus, the degree of atmospheric processing can be a critical factor in determining the impact of atmospheric deposition on marine ecosystems (Baker and Croot, 2010; Mahowald et al., 2011).

In the Atlantic Ocean, mineral dust deposition is highest in tropical regions located downwind of the major aerosol source regions of the Sahara Desert and Sahel (Jickells et al., 2005; Prospero and Carlson, 1972). Moreover, the Intertropical Convergence Zone (ITCZ) in the Atlantic Ocean (located at $\sim 5 - 10^\circ\text{N}$ in winter and summer, respectively) features intense wet deposition which effectively strip the aerosols from the atmosphere, thereby depositing trace elements to the surface ocean in solution (Kim and Church, 2002; Schlosser et al., 2014). Other important mineral dust source regions include the Namib Desert and Patagonia for the South Atlantic Ocean (Chance et al., 2015; Mahowald et al., 2005; Wagener et al., 2008). In remote marine areas such as the far North and South Atlantic, removed from major desert dust sources, aerosols are of a mixture of marine origin, shipping emissions, industrial and agricultural emissions from the continents (Baker et al., 2013; Chance et al., 2015; Shelley et al., 2017a), seasonal emissions of proglacial till (Bullard et al., 2016) and occasional volcanic ash emissions (Achterberg et al., 2013). In addition, aerosols in these remote regions may also have a mineral dust component, depending on the meteorological conditions (Prospero, 1996a).

Atmospheric deposition flux determination has a relatively high uncertainty (Zender et al., 2003) due to large inter-annual and inter-seasonal variabilities. Several approaches are used to calculate atmospheric deposition fluxes from geochemical

tracers or proxies (Anderson et al., 2016). Geochemical methods determine atmospheric deposition fluxes from elemental concentrations in aerosols and/or rain, or chemical concentrations or signatures of tracers of atmospheric deposition in seawater (Anderson et al., 2016). A commonly used geochemical method to determine total (wet + dry) deposition fluxes is to measure elemental concentrations in aerosols collected on filters and in rain water, and multiplying the aerosol concentration data with deposition velocities (dry deposition flux) and the rainwater concentration data by a precipitation rate (wet deposition flux) (Baker et al., 2003; Prospero, 1996a; Shelley et al., 2017b). Atmospheric dry deposition fluxes are subject to a 2-3 fold uncertainty due to the use of a single deposition velocity in the flux calculation (Duce et al., 1991) thus not taking into account the varying deposition velocity of different mineral dust sizes. However, when size segregated sampling approaches are used more than one deposition velocity is applied, thereby decreasing the uncertainty in the calculated deposition flux. The uncertainty may be even larger for wet deposition fluxes because of the uncertainties associated with precipitation rates and scavenging ratios (Shelley et al., 2017a). A different approach that tries to reduce the uncertainties associated with the deposition velocity and precipitation rates uses the inventory of ^7Be in the surface mixed layer and the ratio of trace elements to ^7Be in aerosols to calculate atmospheric deposition fluxes on seasonal timescales (Kadko et al., 2015; Kadko and Prospero, 2011). Other approaches used to determine atmospheric fluxes of trace elements use particles collection by sediment traps (Jickells et al., 1998; Kohfeld and Harrison, 2001) or analyse mineral dust tracers in surface ocean waters (Dammshäuser et al., 2011). Modern atmospheric models take into account aerosol characteristics (e.g. size distribution, particle type) and field observations to estimate atmospheric deposition

fluxes (Mahowald et al., 2005; Zender et al., 2003; Zhang et al., 2015). Often, modelling approaches simulate atmospheric deposition fluxes more accurately in regions downwind from the main aerosol sources (Huneus et al., 2011; Wagener et al., 2008) because the aerosol characteristics, due to extensive datasets in these regions, are better constrained in proximity to their source. Modelled atmospheric deposition fluxes rely on satellite-derived climatologies which suffer from interferences from cloud coverage.

In this manuscript we present surface ocean dAl concentration data for the Atlantic Ocean and use these to calculate atmospheric deposition fluxes using the MADCOW model (Measures and Brown, 1996). The strength of this approach is that it can be used to fill gaps where there are relatively few direct aerosol observations and that with just one parameter it allows the calculation of total atmospheric deposition fluxes (wet+dry). This study compares the MADCOW model outputs with field and model-derived atmospheric deposition flux estimates from the North to the South Atlantic Ocean. We provide some of the first atmospheric deposition fluxes based on high-resolution surface mixed layer concentrations of dAl for remote regions including the Labrador Sea, South East Atlantic and South Atlantic Ocean (ca. 40°S). Our results are discussed in light of the assumptions and limitations of the MADCOW model, and compared to available atmospheric deposition flux estimates from modelling and geochemical approaches.

2 Methods

2.1 Regional, sampling, and processing settings

Seawater samples for dAl were collected during the GEOTRACES section cruises GA01, GA06, GA08, and GA10 (Figure 4.1). GEOTRACES section GA01 sailed aboard the research vessel *Pourquoi Pas?* on 15 May (2014) from Lisbon (Portugal) and arrived on 30 June (2014) in St. John's (Canada). GEOTRACES section GA06 sailed aboard RRS *Discovery* on 7 February (2011) from Tenerife (Canary Islands, Spain) and returned on 19 March (2011) to Tenerife. GEOTRACES section GA08, on board FS *Meteor*, sailed from Walvis Bay (Namibia) on 14 November (2015) and returned there on 27 December (2015). GEOTRACES section GA10, on board RRS *James Cook*, sailed on 24 December (2011) from Port Elizabeth (South Africa) and arrived on 27 January (2012) in Montevideo (Uruguay). The four expeditions crossed several biogeochemical provinces (Longhurst, 2010) In total, seawater samples were collected at 108 stations, with 32 stations sampled during GA01, 14 stations during GA06, 52 stations during GA08 and 18 stations during GA10. Although the different teams used slightly different CTD set ups for sampling the seawater (Table 4.2), all samples were collected using trace metal clean CTD rosettes and following the GEOTRACES sampling protocols (Cutter et al., 2017). All seawater samples for the determination of dAl were collected in 125 mL low density polyethylene bottles (LDPE; Nalgene) cleaned using a three-step wash protocol (Cutter et al., 2017). After collection, the samples were acidified to pH1.8 with ultra clean hydrochloric acid (UpA, Romil) and double bagged until analysis. Analysis of dAl during GA01, GA06, and GA10 used the flow injection analysis (FIA) method developed by Resing and Measures (1994) and further modified by Brown and Bruland

(2008). Dissolved Al during GA08 cruise was analysed using the batch lumogallium method (Hydes and Liss, 1976). The analytical figures of merit for the dAl datasets can be found in Table 4.2.

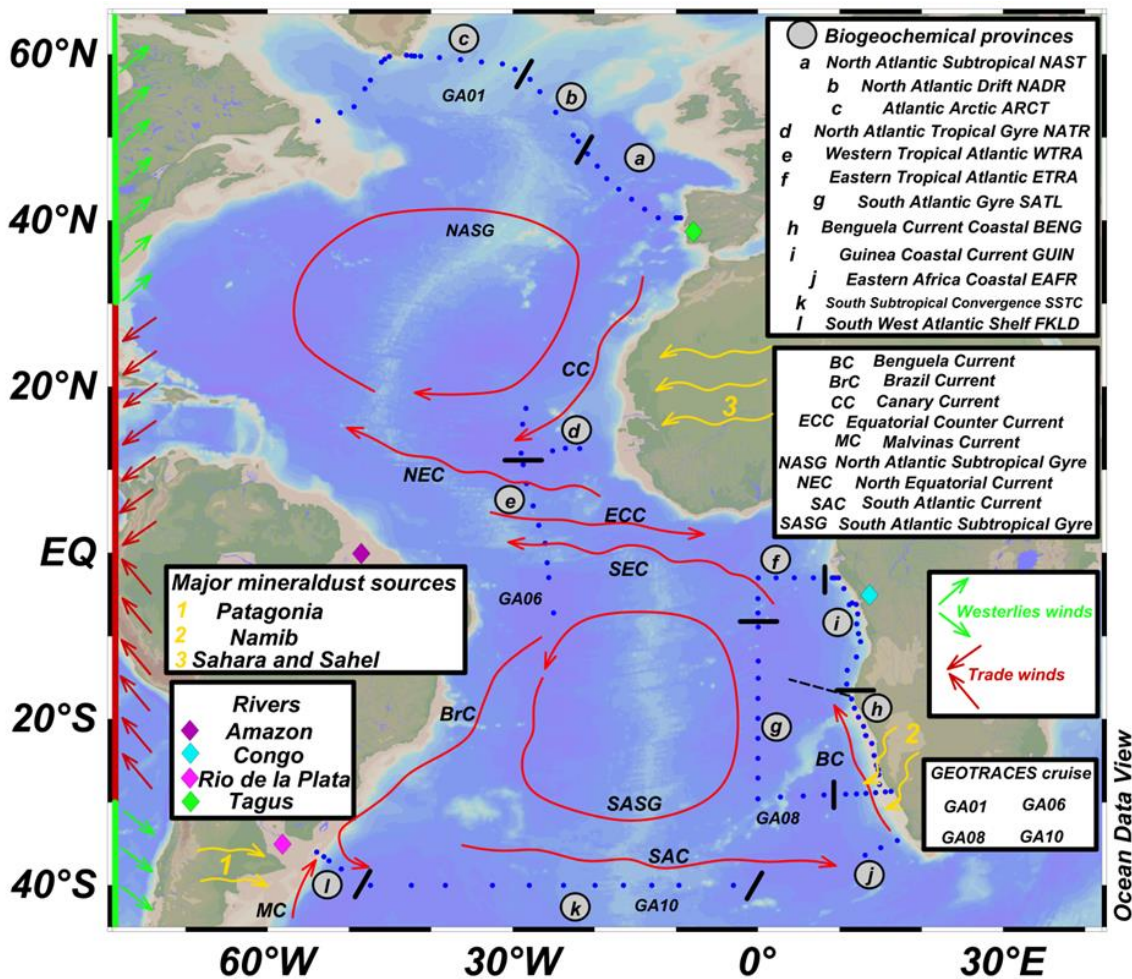


Figure 4.1: Map showing the location of the four GEOTRACES cruises. Red lines represent the main surface ocean currents. The diamonds represent rivers. Yellow arrows represent approximate areas which act as the main mineral dust sources to the Atlantic ocean (Prospero et al., 2002). The yellow solid lines represent the area where maximum rainfall is associated with the ITCZ. Black lines divide different biogeochemical provinces used in this study which are labelled with letters. For station numbers for each cruise please refer to Figure 4.2.

Chapter 4

Table 4.1 Biogeochemical provinces and their principal characteristics used in this study from Longhurst (2010)

Region	Acronym	Cruise	North boundary	South Boundary	East Boundary	West Boundary	Ecology	Physical properties
North Atlantic Subtropical	NAST	GA01	42°N SE flowing Azores Current	25-30°N Subtropical convergence	Canary current	Gulf Stream	Seasonal mixing, low productivity spring bloom (April-June)	Northern part of the anticyclonic gyre, light westerly winds and eddy fields in north, Moderate winter mixing (MLD 100-150 m)
North Atlantic Drift	NADR	GA01	56°N Oceanic Polar Front and Subarctic Front	42 °N Meeting of NAD with southeast flowing Azores Current	European shelf break	45°W	Spring stratification and high production bloom (mid-April, 39-50 °N)	West wind drift, deep winter mixing (MLD < 200 m)
Atlantic Arctic	ARCT	GA01	Spitzbergen	Flemish Cap	North America	45 ° W	Large spring phytoplankton blooms.	Comprises the two cyclonic Subpolar Gyres of the North Atlantic Ocean. Deep winter mixing.
North Atlantic Tropical Gyral	NATR	GA06	~30 °N Subtropical convergence	10-12 °N Conjunction of Northern Equatorial Current and Countercurrent	Canary current	Bahama Islands	No spring bloom, low productivity and chlorophyll	Weak winter mixing, shallow MLD (15-120 m)
Western Tropical Atlantic	WTRA	GA06	~10°N Northern Equatorial Countercurrent	~ 4°S South Equatorial Current	20 °W	Brazilian shelf	No spring bloom and high spatial variability in production. High chlorophyll with high nutrient concentrations	Easterly trade winds and intertropical convergence zone (ITCZ), upwelling and seasonally variable Northern Equatorial Countercurrent
Eastern Tropical Atlantic	ETRA	GA08	5-10° N	5-10°S	15° W shelfbreak front along the north-south coast from Cameroon to Congo	shelf-edge front of the east-west coast of West Africa (Guinea to Nigeria)	Enhanced chlorophyll	Southeasterly trade-winds, ITCZ above the northwest corner in winter. Seasonally varying MLD as a consequence of changes in zonal wind stress.

Chapter 4

South Atlantic Gyral	SATL	GA08	~ 4°S South Equatorial Current	~40 °S Subtropical Convergence Province (raised chlorophyll by ~0.3 mg m ⁻³)	Benguela current	Brazil current	Low surface chlorophyll. Highly productive eddies near boundaries	Shallow winter mixing, anticyclonic gyre, trade winds dominate, high pressure cell (20-30 °S). Greatest MLDs (<100 m) at ~ 20 °S. Westerly Brazil current south of gyre (35-42 °S)
Guinea Current Coastal	GUIN	GA08	12°N Cape Roxo	18° S Cape Frio	West African tropical coast along Congo and Angola	Shelf edge front at ca. 2-3° N 4° W	Oligotrophic area.	Shallow mixed layer above sharp and permanent thermocline. Strongly seasonal reversal of wind patterns.
Benguela Coastal Current	BENG	GA08	18° S	Cape of Good Hope	Southwestern Africa shelf	SATL region	High primary productivity.	Agulhas retroflexion area. Large upwelling area
Eastern Africa Coastal	EAFR	GA10	5°S Coastal boundary of Indian Ocean	Cape of Good Hope	Western boundary currents	BENG	High seasonal variability in chlorophyll concentrations	. Shelf region with seasonal variability. Retroflexion of the Agulhas Current.
South Subtropical Convergence	SSTC	GA10	35° S South Atlantic Gyre	45° S ACC	FKLD	EAFR	High nutrient low chlorophyll. Enhanced phytoplankton biomass in austral spring and midsummer.	Between anticyclonic circulation of the South Atlantic and cyclonic circulation of the Antarctic circumpolar Current. Strong convergence and downwelling occurring
South West Atlantic Shelf	FKLD	GA10	38° S Mar del Plata	55° S Tierra del Fuego	Argentine shelf and Falklands plateau	SSTC	High seasonal variability in chlorophyll concentrations	Two singularities: Subantarctic Front and confluence of Brazil Current and Malvinas Current.

2.2 Atmospheric deposition flux determinations: The MADCOW model

The MADCOW (Measurement of Aluminium for Dust Calculation in Ocean Waters) model (Measures and Vink, 2000; Measures and Brown, 1996) determines atmospheric deposition fluxes to the surface ocean from the concentration of dAl in the surface mixed layer. The primary model assumption is that dAl in the surface waters is in steady state with respect to inputs from soluble Al provided by the dissolution of mineral dust on contact with seawater and rain deposition, and removal via scavenging of Al onto particle surfaces, and subsequent transfer to depth by sinking. The model itself is provided by the following equation (1):

$$G = \frac{[Al] \times MLD}{\tau \times S \times D} \quad (1)$$

Where G is the total dust flux in $\text{g m}^{-2} \text{yr}^{-1}$, $[Al]$ is the concentration of dAl (nM) in the surface mixed layer, MLD is the depth of the mixed layer in meters (m), τ is the residence time in years (yr), S is the fractional solubility of Al in dust (%), and D is the concentration of Al in dust (mol g^{-1}). We describe how each parameter is derived for each of the cruises in the following sections and describe the assumptions used by the MADCOW model for the determination of the atmospheric deposition fluxes.

2.2.1 Quantification of surface mixed layer depths

We used two different MLDs. First, a measured mixed layer depth (MLD_m) was obtained for each station using a potential density difference criterion $\Delta\sigma_\theta = 0.125 \text{ kg m}^{-3}$ (Monterey and Levitus, 1997) calculated from the salinity and temperature retrieved from the sensors mounted in the CTDs. Second, annual (MLD_{ar}) and seasonal (MLD_{wi}, MLD_{sp}, MLD_{su} and MLD_{au}, for winter, spring, summer, and autumn, respectively) MLDs were extracted for each station of the four cruises in a 1 x 1 degree bin in latitude and longitude from the Argo mixed layer climatology (<http://mixedlayer.ucsd.edu/>) (Holte et al., 2017).

Table 4.2: Sampling and analysis approaches used for each of the cruise

Cruise	Sampling CTD	Bottle	Filter type	Pore size	Air vs N ₂	Reference material	Values measured reference material (nM)
GA01	Trace metal clean Rosette (TMR, General Oceanics Inc. Model 1018 Intelligent Rosette)	GO-FLO	Sartobran 300, Sartorius	0.2 μM	N ₂ (0.5 bar)	GD Safe S	17.79 \pm 0.26 (n=4) 1.85 \pm 0.33 (n=9)
GA06	Titanium frame clean CTD Rosette	10 L Teflon coated OTE	AcroPak Supor filter capsule (Pall Corp.)	0.2 μM	Oxygen free N ₂ (0.1-0.5 bar)	GD GS	18.8 \pm 0.8 (n=4) 28 \pm 5 (n=7)
GA08	Trace metal clean CTD Rosette	12 L GO-FLO (OTE)	Acropak 500 cartridge filters (Pall Corp.)	0.2-0.8 μM	N ₂ (0.2 bar)	GS	27.8 \pm 0.2 (n=4)
GA10	Titanium frame clean CTD Rosette	10 L Teflon coated OTE	AcroPak Supor polyethersulfone membrane filter capsules (Pall Corp.)	0.2 μM	High purity air (1.7 bar)	SAFe S SAFe D2	1.68 \pm 0.49 (n=3) 0.89 \pm 0.09 (n=4)

2.2.2 Fractional solubility of aluminium

Seasonal (April to June and September to November) Al fractional solubilities were obtained from the compilation of Baker et al. (2013), based on aerosol samples collected at high spatial resolution over several years in the Atlantic Ocean. The soluble fraction was based on the results of an ammonium acetate leach at pH 4.7 for 1-2 h, following Sarthou et al. (2003). Baker et al. (2013) divided the Atlantic Ocean into various regions and sub-regions (Figure 4.3) based on air mass back trajectories and the relative contribution of the air masses over the two seasons in each region. In the supplementary information we provide an explanatory note on the relative contribution of each air mass for each region which we then compiled in Table 4.3. They calculated the fractional Al solubility for each sub region. Baker et al. (2013) provide a good spatial coverage of the Atlantic Ocean, thus allowing us to assign values of Al fractional solubility for different biogeochemical regions (Figure 4.1) based on field observations. However, the aerosols Al fractional solubility might not be representative over an annual timescale due to, for example, the pulses of Saharan dust and where the mineral dust falls which is related to the position of the ITCZ. Yet, it is still the largest dataset on aerosol Al fractional solubility over the Atlantic Ocean. We produced a single weighted averaged aerosol Al fractional solubility percentage value for each area of interest based on the Al fractional solubility for each air mass to the relative contribution of that air mass to a certain area (Table 4.3). Furthermore, we assumed that the chosen Al solubility was representative for the whole annual cycle as our atmospheric aerosol deposition flux estimates are given in $\text{g m}^{-2} \text{y}^{-1}$. As the compilation of Baker et al. (2013) does not cover regions north of 50°N in the North Atlantic, we used Al fractional solubilities from Shelley et al. (2017a) derived from aerosol samples collected during the GA01 cruise.

Chapter 4

Table 4.3: Definition of the regions based on baker et al., (2013) to derive Al fractional solubility. Figure 4.3 shows the location of the aerosol source region and air mass type sub-regions. The last column displays the weighted average for Al fractional solubility. The different air mass types are as follow: NAr, North Atlantic remote; NAm, North America; SAf, South African; SAr, South Atlantic remote; SAbb, South African burning biomass; Sah, Saharan; SAm, South American.

Cruise	Stations	Aerosol source region	Air mass type sub-region	Air mass type %	Al fractional solubility percentage
GA01	1 to 26	2	2a	NAr 77 European 15 NAm 8	11.6
GA01	29 to 71	-	-	NAr	21
GA01	77 and 78	-	-	Canadian	14.5
GA06	7 to 9	3	3b	SAf 47 SAr 44 SAbb 7	5.8
GA06	10	4	4a	SAf 82 SAbb 17	5.5
GA06	11.5 to 18	3	3a	NAr 31 Sah 21 SAf 25 SAbb 16	5
GA06	19 and 20	2	2d	Sah 48 NAr 46 Eur 6	8.6
GA08	1 to 5 & 30 to 52	4	4c	SAr 81 SAf 14 SAbb 5	10.3
GA08	6 to 29	4	4b	SAf 44 SAbb 31 SAr 25	7.7
GA10	1 to 3	4	4d	SAr 94	10.9
GA10	7 to 24	5	5b	SAr 52 SAm 45	13.9

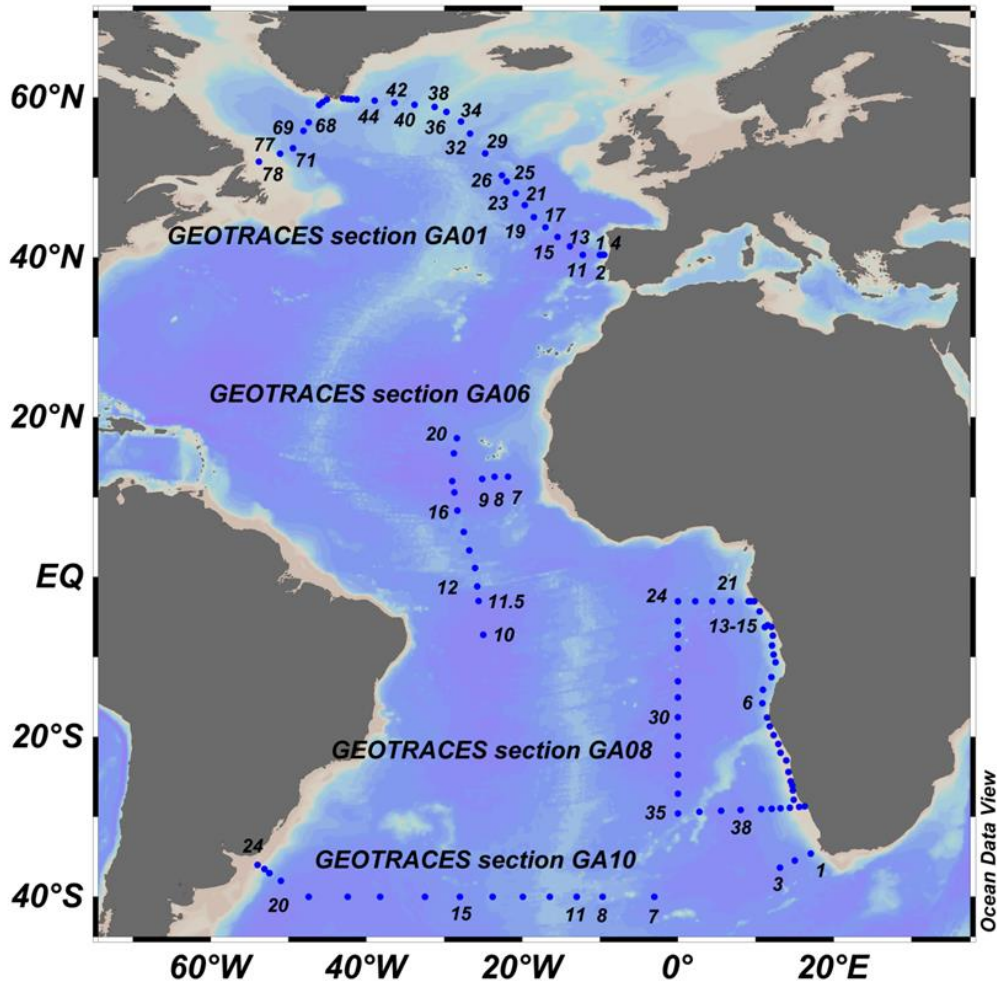


Figure 4.2: Map showing the cruise locations and the station numbers

2.2.3 Al residence time in the surface mixed layer

The residence time is defined as the ratio of the dAl inventory in the surface mixed layer to the rate of input or removal. Residence times of dAl in the surface mixed layer were obtained from Han et al. (2008) and were derived using model simulations using the Biogeochemical Elemental Cycling (BEC) ocean model (Moore et al., 2004). The dAl residence times provided by Han et al. (2008) take into account Al sources to the surface mixed layer from atmospheric deposition, advection, and mixing. We have chosen the residence times from Han et al. (2008) as they are based on an extensive surface water dAl observational database, including a total of 41 research expeditions (22 in the Atlantic Ocean) up to the year

2002. The MADCOW model used in our study does not account for advection and mixing processes which, for example, occurs in equatorial regions as waters of higher dAl concentrations are advected into low dAl concentration waters (van Hulst et al., 2013). Thus, the use of modelled residence times which account for advection and mixing sources could partially counterbalance the error associated with our modelled atmospheric deposition fluxes

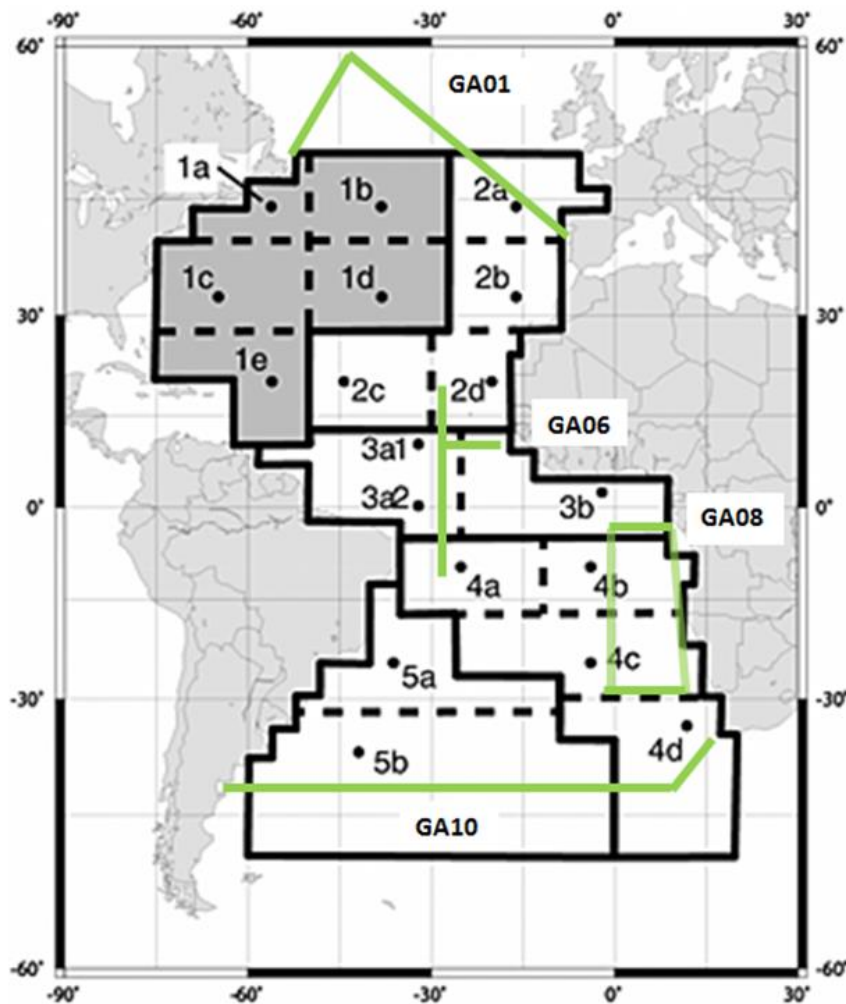


Figure 4.3: Atmospheric sub-regions used to define aerosol Al fractional solubility. The cruise tracks for GA01, GA06, GA08 and GA10 are plotted as green solid lines. Modified from (Baker et al., 2013).

3. Results and Discussion

3.1 Mixed layer depth (MLD)

The surface mixed layer is considered a quasi-homogenous layer based on physical properties (salinity and temperature). The properties display gradients at the bottom of the layer. The bottom depth of the surface mixed layer varies due to atmospheric forcing, with turbulent mixing caused by wind stress (Risien and Chelton, 2008), convection caused by heat exchange (Yu and Weller, 2007), in addition to salinity changes due to evaporation and precipitation at the surface (Schanze et al., 2010). Thus, the thickness of the MLD is an indication of the amount of water that directly interacts with the atmosphere.

Figure 4.4 shows a box whisker plot with the quantified MLDs for each of the four study regions. Table S4.1 shows the calculated MLDs for each station and Figure 4.5 shows a comparison plot for each cruise between MLDms, MLDar, MLDmw (mixed layer depth original MADCOW model) and the Argo average MLD during the season when each cruise took place.

In the North Atlantic (GA01) and South Atlantic (GA10) Ocean, large differences were observed between median MLDms and MLDar with a difference of 77 and 20 m, respectively. Smaller differences were detected between median MLDms and MLDar in the tropical (GA06) and Southeast Atlantic (GA08) Ocean with a difference of 7 and 10 m, respectively. Maximum MLDar and MLDms were greatest in the North Atlantic (up to 218 m), followed by the South Atlantic (106 m) and the South East Atlantic (83 m) and tropical Atlantic (66 m). The large difference, both in maximum MLDar and in the difference between the median MLDms and MLDar,

between the North Atlantic Ocean and the other three study areas was due to strong deep mixing taking place in the North Atlantic Ocean during winter (Kara et al., 2003). In the tropical Atlantic Ocean, the MLD is largely controlled by changes in temperature (net heat flux) and salinity (evaporation to precipitation ratios) (Chahine, 1992; Webster, 1994). In our study, deeper MLDs relative to shallower MLDs imply that higher quantities of atmospheric aerosols need to be supplied to a specific region in order to maintain the observed dAl concentrations in the MLD.

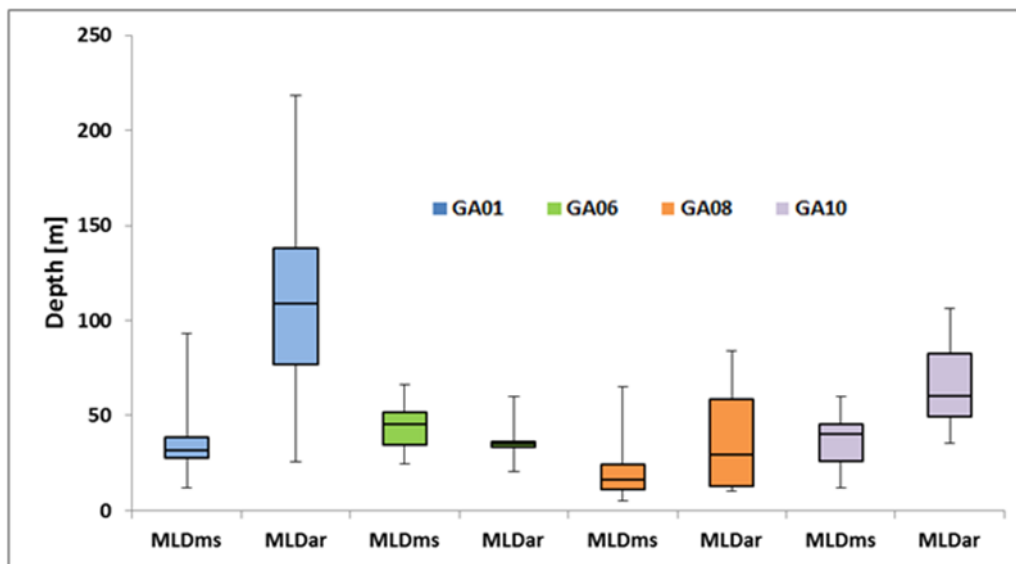


Figure 4.4: Box whisker plot for the MLD determined using in situ measurements (MLDms) and mixed layer climatology (MLDar) (<http://mixedlayer.ucsd.edu/>) (Holte et al., 2017).

3.2 Distributions of dAl in the surface mixed layer

Figure 4.6 shows the average dAl concentration in the surface mixed layer along the four sections. Occasionally, when no sample was collected, the closest underway surface water sample collected with a towfish was used. A detailed description for the surface mixed layer dAl concentrations of the four cruises relative to physical and biological parameters is given in the following sections. Overall, a large range in

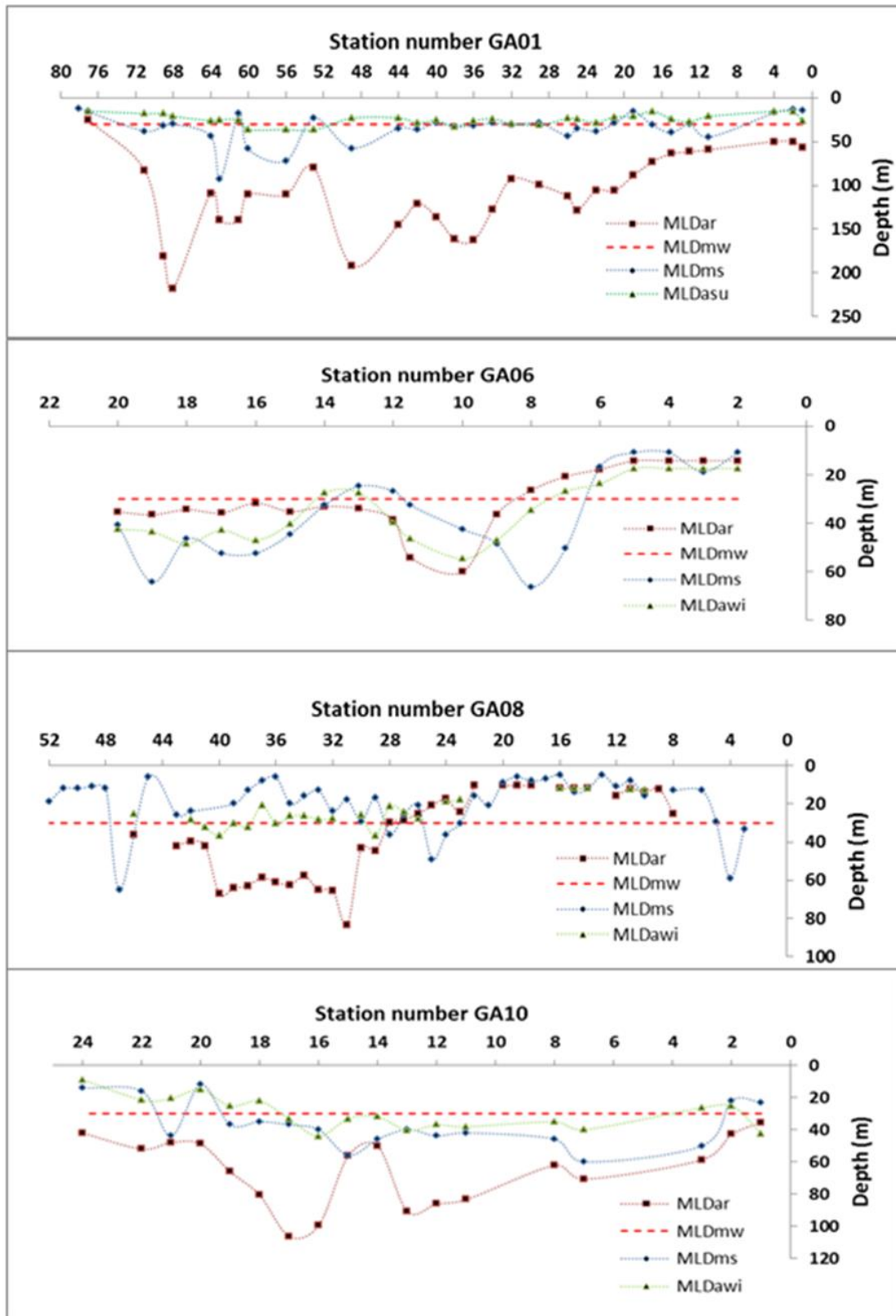


Figure 4.5: Depth of the surface mixed layer (MLD). MLDar refers to the annual average MLD from the Argo project (Holte et al., 2017). MLDms refers to in situ MLD measured on each cruise. MLDasu or MLDaw represent the summer or winter average MLD from the Argo project. MLDmw represent the MLD used in the original application of the MADCOW model (30 m) (Measures et al., 2015).

surface dAl concentrations was observed, ranging between <0.5 nM and 784 nM (median 5.1 nM; n=108 stations). The highest dAl concentrations were observed in the tropical Atlantic Ocean between 1-15°N and ca. 26°W, and in coastal waters off Portugal, Greenland, Argentina, Angola, Democratic Republic of Congo, and Gabon in association with the highest atmospheric inputs and continental inputs (rivers, glacial flour, and ice melt). In contrast, low dAl concentrations (<5 nM) due to low atmospheric deposition and/or scavenging of dAl by particles were found in the North Atlantic (GA01), in the Southeast Atlantic (GA08), and in the South Atlantic Ocean (GA10).

3.2.1 Dissolved aluminium in the surface mixed layer of the North Atlantic Ocean (GA01)

Along GEOTRACES GA01 section in the North Atlantic (Figure 4.1), highest (>15 nM) dAl surface mixed layer concentrations were found in the North Atlantic Subtropical Gyre region (NAST) off Portugal (stations 1, 2 and 4) and are attributed to riverine inputs from the Tagus estuary (Menzel Barraqueta et al., 2018). An additional source of dAl off Portugal involves episodic deposition of mineral dust originating from the Sahara and Sahel regions (Prospero, 1996a), and wet deposition events as observed during the GA01 cruise (Shelley et al., 2017a). Enhanced dAl surface mixed layer concentrations (>5 nM) were also observed in the Atlantic Arctic region (ARCT) off Southeast and Southwest Greenland (stations 53 and 61) as a consequence of runoff and ice melt, respectively (Menzel Barraqueta et al., 2018). In addition, enhanced dust inputs delivered from proglacial tills in Greenland occur from June to September (Bullard et al., 2016), coinciding with the time of sample collection off Greenland. Excluding the stations with continental Al inputs,

mixed layer dAl concentrations were low, reflecting low contributions of atmospheric deposition (median dAl=2.9 nM), and were not significantly different from east to west due to differences in the intensity of biological removal processes as described by Menzel Barraqueta et al. (2018). A more detailed explanation on the surface distribution for dAl along the GA01 cruise is given in Menzel Barraqueta et al. (2018). Similarly low concentrations of dAl were observed during the CLIVAR A16N line along 22°W longitude in the eastern North Atlantic in 2003 (Measures et al., 2008), and when re-occupied in 2013 (Barrett et al., 2015), and in the Irminger Basin during GEOTRACES GA02 (Middag et al., 2015).

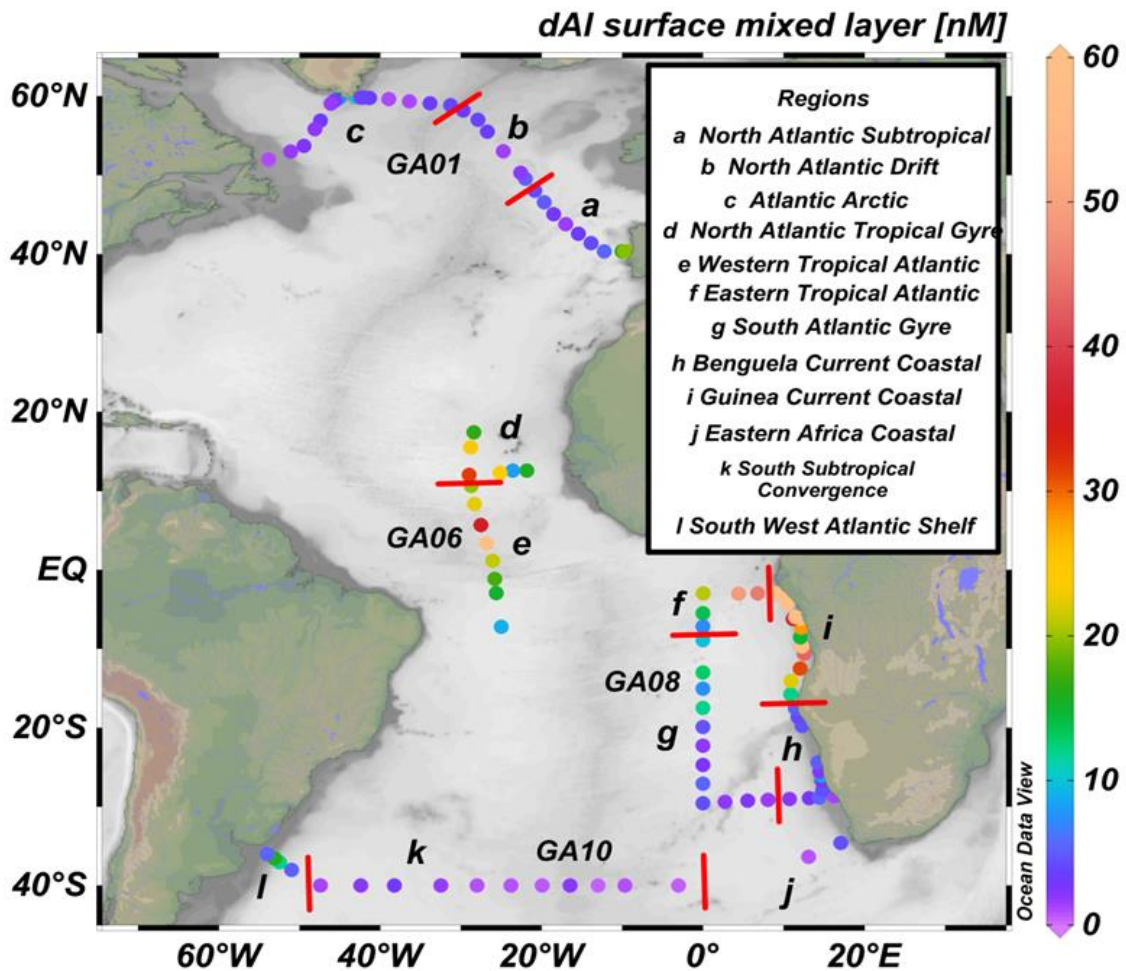


Figure 4.6: Surface mixed layer dAl concentrations (nM) for the cruises used in this study. Red lines divide the different biogeochemical provinces used in this study.

3.3.2 Dissolved aluminium in the surface mixed layer of the tropical Atlantic Ocean (GA06)

The tropical Atlantic has a large coverage of dAl measurements, compiled in Han et al. (2008), related to the importance of dust delivering micronutrients (e.g. Fe) to the surface ocean. Along the GEOTRACES GA06 section, dAl concentrations were high and ranged from 8 nM in the North Atlantic Tropical Gyre region (NATR) to 67 nM in the Western Tropical Atlantic region (WTRA). In the southern part of the section at $\sim 8^{\circ}\text{S}$, at the boundary between the South Atlantic Gyre (SAG) and the South Equatorial Current (SEC) in the WTRA (Figure 4.1), dAl displayed low concentrations (~ 8.8 nM) with elevated salinity (36.54) (Figure 4.7). The latter region is known to have low rainfall, high rates of evaporation (Yoo and Carton, 1990) and receives large volumes of mineral dust deposition (Prospero, 1996b). Vink and Measures (2001) observed similarly low levels of dAl (8 nM) but somewhat further south at 15°S . Similarly, on the westward transect at ca. 12.5°N , low dAl concentrations were observed (down to 8 nM), associated with enhanced removal of dAl by biogenic particles. Enhanced primary production as a consequence of upwelling of nutrient-rich deep water resulted in a high abundance of biogenic particles; Measures et al. (2015) reported similar conditions for the region.

High dAl concentrations (15-28 nM) were found north of 3°S and were related to enhanced deposition of mineral dust as the sampling stations were located along the flow path of the trade winds that carry mineral dust from the Sahara and Sahel regions (Mahowald et al., 2005; Prospero et al., 2002). Maximum concentrations of dAl (up to 68 nM) were observed at ca. 3°N , 26°W (station 14) and coincided with

reduced salinity (down to 35) (Figure 4.7), suggesting freshwater inputs from rainfall occurring in the ITCZ. The ITCZ was positioned between ca. 3°S and 3°N with the core situated at 1°N during the cruise period (Schlosser et al., 2014). Precipitation in the ITCZ effectively scavenges dust from the atmosphere and supplies Al to surface waters in wet deposition (Schlosser et al., 2014). Similarly high dAl concentrations (e.g. up to 74 nM) (Van Der Loeff et al., 1997) for the region have been reported (Barrett et al., 2015; Bowie et al., 2002; Dammshäuser et al., 2011; Measures et al., 2015; Measures et al., 2008; Measures and Vink, 2000; Pohl et al., 2011; Schlosser et al., 2014), and also attributed to wet deposition. However, spatial variability in the distribution of dAl in the tropical Atlantic Ocean is a consequence of the sporadic and seasonal nature of mineral dust plumes with dust pulses varying in intensity on a daily basis (Patey et al., 2015) and with seasonal migration of the ITCZ.

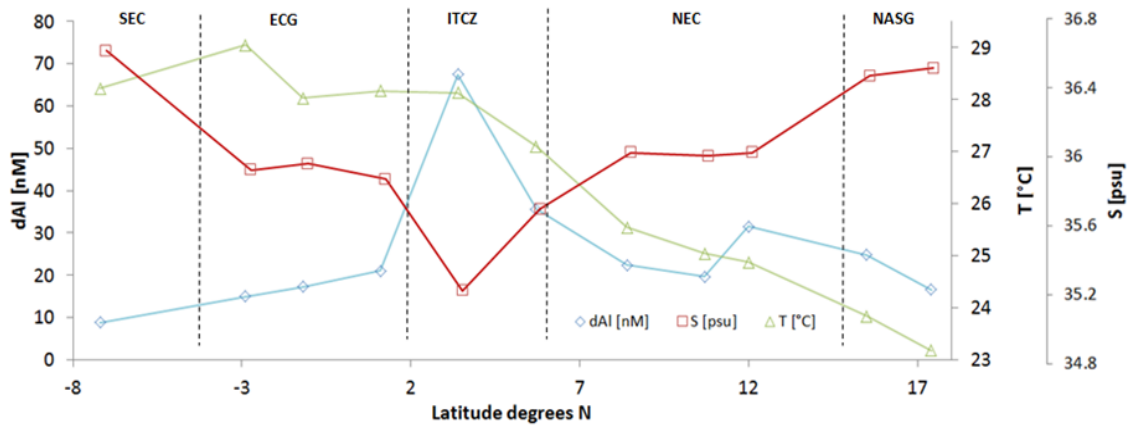


Figure 4.7: Distribution of dAl (nM), salinity and temperature for the northward transect in the tropical Atlantic (GA06). SEC, South Equatorial Current; ECG, Equatorial Gyre; ITCZ, Intertropical Convergence Zone; NEC, North Equatorial Current; NASG, North Atlantic Subtropical Gyre.

3.3.3 Dissolved aluminium in the surface mixed layer of the South East Atlantic Ocean (GA08)

Along GEOTRACES section GA08 in the South East Atlantic, dAl concentrations ranged from 1.2 (station 45) to 784 nM (station 15) (median 9 nM; n=44). The lowest dAl concentrations were found south of 20°S at stations along the prime meridian and at ca. 30°S and 1° to 10°E as a consequence of low aerosol deposition to the South Atlantic Gyre (SAG) region. Similar low concentrations of surface dAl associated with low productivity waters in the South Atlantic Gyre have been reported (Measures, 1995). Low dAl concentrations (down to 1.3 nM) were observed during GA08 in the Benguela Coastal Current (BENG) region off Namibia coinciding with high Chl a concentrations (Figure 4.8) and thus enhanced dAl scavenging onto biogenic particles (Figure 4.3). The enhanced scavenging of dAl by particles is supported by elevated concentrations of total dissolvable Al (unfiltered) during the AMT-6 cruise (Bowie et al., 2002). Bowie et al. (2002) argued that the enhanced total dissolvable Al was a consequence of Al-rich upwelled waters. Significant correlations between enhanced biogenic particles, and low dAl and high pAl concentrations have recently been reported (Menzel Barraqueta et al., 2018), indicating the control of biogenic particles on Al cycling in surface waters. The highest dAl concentrations (up to 784 nM) were observed along the SW African coast north of 6°S (stations 14 to 23) in the Guinean Current Coastal region (GUIN) and were associated with freshwater inputs from the Congo River. Similar observations were made by van Bennekom and Jager (1978), and enhanced levels of dAl (up to 50 nM) associated with inputs from the Congo river have been reported as far as 1200 km (6°S 0°E) from the river mouth (Van Der Loeff et al., 1997). Between the Congo River mouth (6°S) and the Angola-Benguela frontal zone (ca.

11°S) (Figure 4.1) elevated dAl was observed (20–40 nM) (Figure 4.6). Possible sources for the elevated dAl concentrations are urban emissions and atmospheric mineral dust from West Africa. Prospero (1996a) argued that when the ITCZ migrates south of the equator, additional southward transfer to the Gulf of Guinea of atmospheric dust from the Sahara and the Sahel regions can occur during austral summer. In addition, the low Chl a concentrations in the GUIN region would facilitate dAl accumulation in the surface mixed layer due to a lack of adsorption onto biogenic particles.

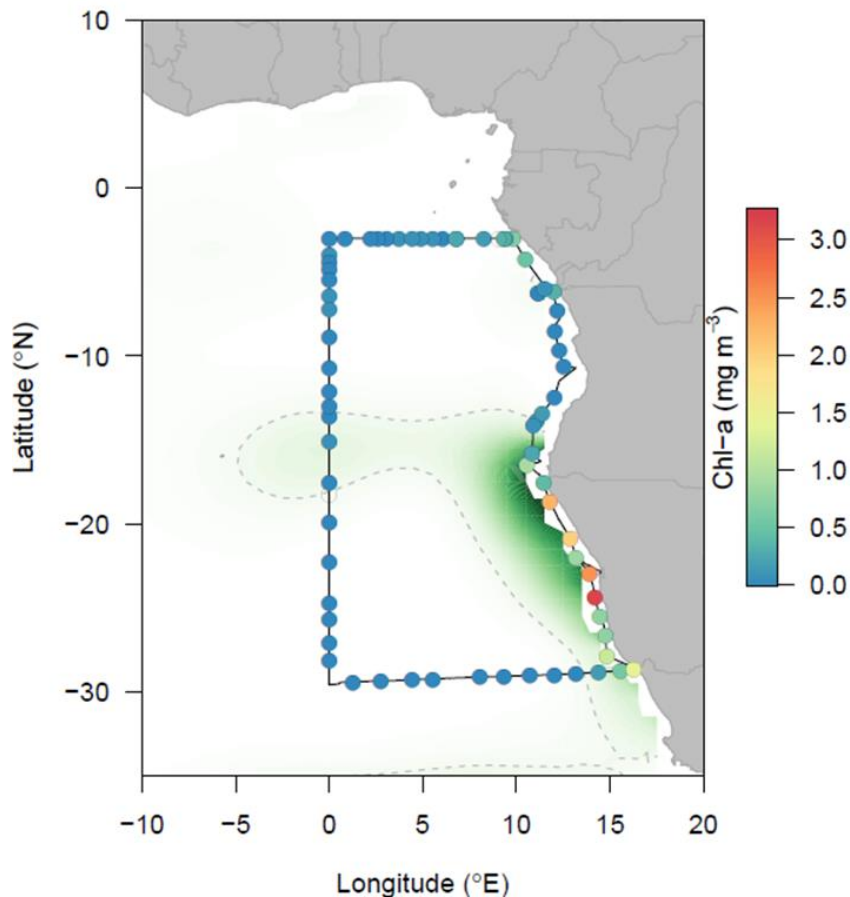


Figure 4.8: Chlorophyll a values for GEOTRACES section GA08. Data are from Dr. Tom Browning.

3.3.4 Dissolved aluminium in the surface mixed layer of the South Atlantic Ocean (GA10)

Along GEOTRACES section GA10 in the South Atlantic Ocean, dAl concentrations were generally low and ranged between 0.3 nM in the SAC and 15.8 nM on the Argentine shelf (median = 1.6 nM; n=17) (Figure 4.6). Highest concentrations (up to 16 nM) were observed on the South West Atlantic Shelf region (FKLD). The FKLD is thought to be influenced by dAl inputs from the River de la Plata, shelf sources, and possibly atmospheric deposition from Patagonian sources (Chance et al., 2015; Jickells et al., 2005; Mahowald et al., 2005; Wagener et al., 2008). A decrease in salinity is observed in the FKLD (Figure 4.9). However, the correlation between surface salinity and dAl for the FKLD is weak ($R^2=0.13$; n=4) and suggests a minor influence on Al concentrations from freshwater sources. Thus, it is unlikely that the River de la Plata was a major source of dAl at the time of the cruise. An additional input of dAl could be associated from the advection Al rich waters of the southward flowing Brazil Current (Vink and Measures, 2001). However, this feature has been observed somewhat further north at 34°S and the influence of the Brazil Current at our latitude may be counterbalanced by the northward flowing Malvinas Current (Figure 4.1). Similar dAl concentrations in the vicinity of the South American continent were observed during expedition ANT IX/1 (Van Der Loeff et al., 1997) and AMT-3 (Bowie et al., 2002) and attributed to recent dust deposition. In the South Subtropical Convergence region (SSTC), the dAl concentrations were low (<5 nM), reflecting low Al inputs from atmospheric deposition (Mahowald et al., 2005) and/or removal via particle scavenging in SSTC along ca. 40° S. Our observations agree with measurements of low concentration of dAl in the high latitude South Atlantic (Middag et al., 2011).

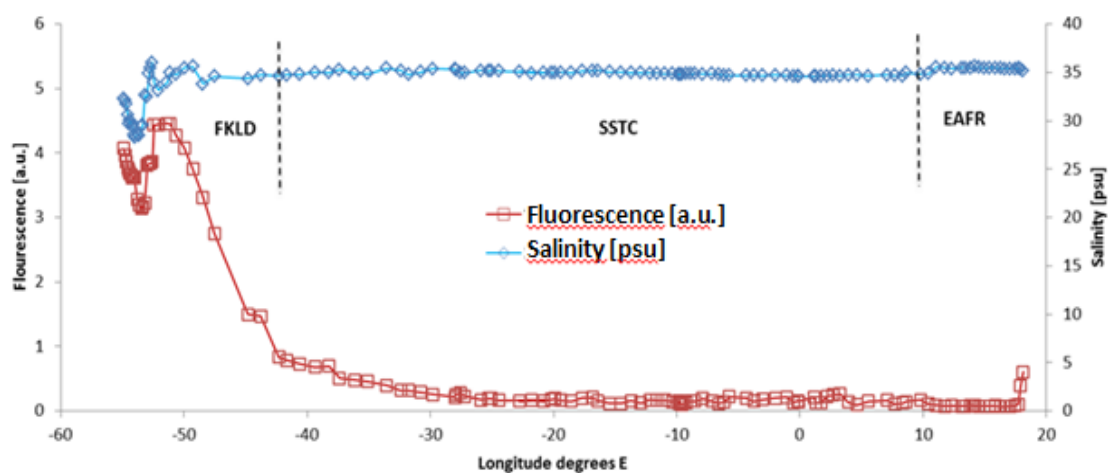


Figure 4.9: Salinity and fluorescence measurements from the ship sensors along the South Atlantic (GA10). FKLD, South West Atlantic Shelf region; SSTC, South Subtropical Convergence region; EAFR, Eastern Africa Coastal region.

3.3 Fractional solubility of aluminium ($Al_{sol\%}$)

The fractional solubility of trace metals from aerosols is controlled by: 1) chemical processing during atmospheric transport which is influenced by the balance of acid species (enhanced by anthropogenic sources e.g. fossil fuel combustion) (Ito, 2015; Sholkovitz et al., 2012) and the phase partitioning of NH_3 (Hennigan et al., 2015) and; 2) composition and type of particle; aerosols from different sources have different mineralogies and size distributions which influence the solubility of metals (Baker and Jickells, 2017). Reported aerosol Al fractional solubilities in aerosols span a large range from 0.5% to 100% (Baker et al., 2006; Buck et al., 2010; Measures et al., 2010; Prospero et al., 1987; Shelley et al., 2017a). One of the reasons for this large range is likely the lack of standardisation in aerosol leaching methods (Aguilar-Islas et al., 2010). An up to twentyfold (1 to $20 \text{ g m}^{-2} \text{ yr}^{-1}$) difference between atmospheric deposition fluxes estimated from Al fractional solubility values following two different aerosol leaching methods has been reported by Anderson et al. (2016). However, based on aerosol Fe solubility experiments, the

largest differences resulted from aerosols from different sources (Aguilar-Islas et al., 2010; Fishwick et al., 2014).

In an early study which used dAl concentrations in the surface mixed layer to derive atmospheric deposition fluxes, Measures and Brown (1996) choose an Al fractional solubility range of 1.5% to 5% for the tropical Atlantic, with the upper limit derived from aerosols and rain data by Prospero et al. (1987). Measures and Brown (1996) discussed that the chosen upper boundary for Al fractional solubility may have been too low, as earlier studies (Maring and Duce, 1987) reported an Al fractional solubility of 9%, attributed to cloud processing during long-range atmospheric transport to the mid-Pacific Ocean, and thus not directly applicable to tropical Atlantic aerosols.

As our study region spans the entire Atlantic Ocean, we expect a large range in Al fractional solubility due to multiple aerosol sources (Baker and Jickells, 2017; Baker et al., 2006). Table 4.3 shows the Al fractional solubility for each region and sub-region (Figure 4.3) and the relative abundance of air mass back trajectories. The aerosol Al fractional solubility partially reflects the different aerosol sources. The lowest Al fractional solubility values (5-7.7%) were calculated for the NTRA and WTRA in the tropical Atlantic (GA06) and for the GUIN and BENG region in the Southeast Atlantic (GA08) due to the dominance of mineral dust. The highest Al fractional solubility (11.6-21%) was calculated at high latitudes (GA01 and GA10) and in the SATL (GA08) which was likely due to the greater distances from aerosol source regions and/or higher degree of atmospheric processing that these aerosols have undergone during transport (e.g. Shelley et al., 2018). Overall, the Al fractional solubility used in this study ranged from 5% to 21%. The higher the Al fractional

solubility value, the less aerosol material is required to maintain the observed dAl surface mixed layer concentrations.

3.4 Residence time of dissolved aluminium

The residence time of dAl in the surface mixed layer is a balance between atmospheric, riverine and sedimentary inputs, and removal processes which are dominated by scavenging of dAl by biogenic particles (Orians and Bruland, 1986). Short residence times are associated with regions of enhanced mineral dust deposition (Dammshäuser et al., 2011; Schüßler et al., 2005) such as the tropical North Atlantic and regions of enhanced biological activity (primary productivity) such as the North Atlantic (north of 40°N). In contrast, long Al residence times are associated with regions of low mineral dust deposition and low biological activity (Dammshäuser et al., 2011; Jickells, 1999) such as the South Atlantic subtropical gyre. The residence time of dAl in the upper ocean has been estimated to range from ~0.2 to more than 17 yr (Dammshäuser et al., 2011; Jickells, 1999; Jickells et al., 1994; Orians and Bruland, 1986) and up to 73 yr in modelling studies (Han et al., 2008). In this study, we used short Al residence times in the surface mixed layer for the North Atlantic (GA01), tropical Atlantic (GA06), along the upwelling regions in the Southeast Atlantic (GA08), and for the South Atlantic along the South Subtropical Convergence region (SSTC) (GA10). Longer Al residence times were used for the Southeast Atlantic Ocean, more precisely along the prime meridian as a consequence of low removal rates removal due to low primary productivity and low atmospheric deposition. Overall, the Al residence times used in this study (Table 4.4), and derived for each biogeochemical province from the estimates provided in Han et al. (2008), ranged between 0.75 and 3 years.

3.5 Application of the MADCOW model to derive total atmospheric deposition fluxes in the study area

3.5.1 MADCOW input parameter assumptions

The original MADCOW model (Measures and Brown, 1996) assumed a uniform residence time of 5 yr for dAl in the surface mixed layer, an invariant content of Al in dust of 8%, a fixed MLD of 30 m, and an aerosol Al fractional solubility between 1.5% and 5%. The total dust deposition was calculated by multiplying the concentration of dAl in the mixed layer by 0.133 and 0.04 (factors for unit conversion) for a solubility of 1.5% and 5%, respectively. Our study region spans the whole Atlantic Ocean, with a range in MLDs, fractional Al solubilities, and residence times of Al in the surface mixed layer. The different input parameters used for the atmospheric deposition flux calculations for each of the four study regions can be found in Table 4.4 and relate to the factors described in Sections 2 and 3. Mixed layer depths were deeper for GA01 and GA10, and shallower for GA06 and GA08. The residence time of dAl in the surface mixed layer along the four transects was quite uniform and ranged from 0.75 to 3 years. The largest variability was noted for the aerosol Al fractional solubility due to inter-annual and inter-seasonal variability in the contribution of different aerosol sources, incomplete spatial coverage, wet to dry deposition balance, etc. As a consequence, for each cruise we have chosen a lower and upper limit of Al fractional solubility. As such we obtained an upper and lower range in atmospheric deposition fluxes for each cruise. The total range on aerosol Al fractional solubility used in this study was 5% to 20%, which is up to 3x and 4x higher than the lower and upper limit used by Measures and Brown

(1996). Higher Al fractional solubilities were used for GA01 and GA10 and lower values for GA08 and GA06.

Table 4.4: Input values to estimate total atmospheric aerosol deposition fluxes using the MADCOW model. MLD, average between the median MLDms and MLDar; τ , dAl residence time derived from Han et al. (2008) for the different biogeochemical provinces; Alsol%, Al fractional solubility percentage calculated from Baker et al. (2013). For reference to the biogeochemical provinces please refer to Table 4.1.

Cruise	MLD (m)	τ (yr)	Alsol% range (%)
GA01	57	1.25 (NAST and NADR) 0.75 (ARCT)	11.6-20
GA06	36	1.25 (NATR and WTRA)	5-8.6
GA08	20	0.75 (BENG, GUIN, and ETRA) 3 (SATL)	7.7-10.3
GA10	47	1.5 (EAFR) 1 (SSTC and FKLD)	10.9-13.9

3.6 Atmospheric deposition fluxes

Figure 4.10 shows the average atmospheric deposition flux (wet + dry) for each station. In addition, Figure 4.11 shows a comparison of calculated average total atmospheric aerosol deposition fluxes (this study) and total atmospheric deposition fluxes for each station extracted from the composite model of Mahowald et al. (2005). In Table 4.5, we present our total atmospheric deposition fluxes values for each biogeochemical province compared to the model estimates from Mahowald et al. (2005) and (Duce et al., 1991). Overall we found good agreement along GA01, GA08, and GA10. Weaker agreement was found in the tropical Atlantic along

GA06. In the following sections we describe our atmospheric deposition fluxes in more detail.

3.6.1 Atmospheric deposition fluxes to the North Atlantic and Labrador Sea (GA01)

In the North Atlantic, along the GA01 section, our calculated atmospheric deposition fluxes ranged from $1.75 \pm 0.71 \text{ g m}^{-2} \text{ yr}^{-1}$ (St. 2) near the Iberian Peninsula in the NAST region to $0.12 \pm 0.05 \text{ g m}^{-2} \text{ yr}^{-1}$ (St. 78) above the Newfoundland margin in the ARCT region. The average atmospheric deposition flux was $0.49 \pm 0.46 \text{ g m}^{-2} \text{ y}^{-1}$ (Figure 4.10 and 4.11).

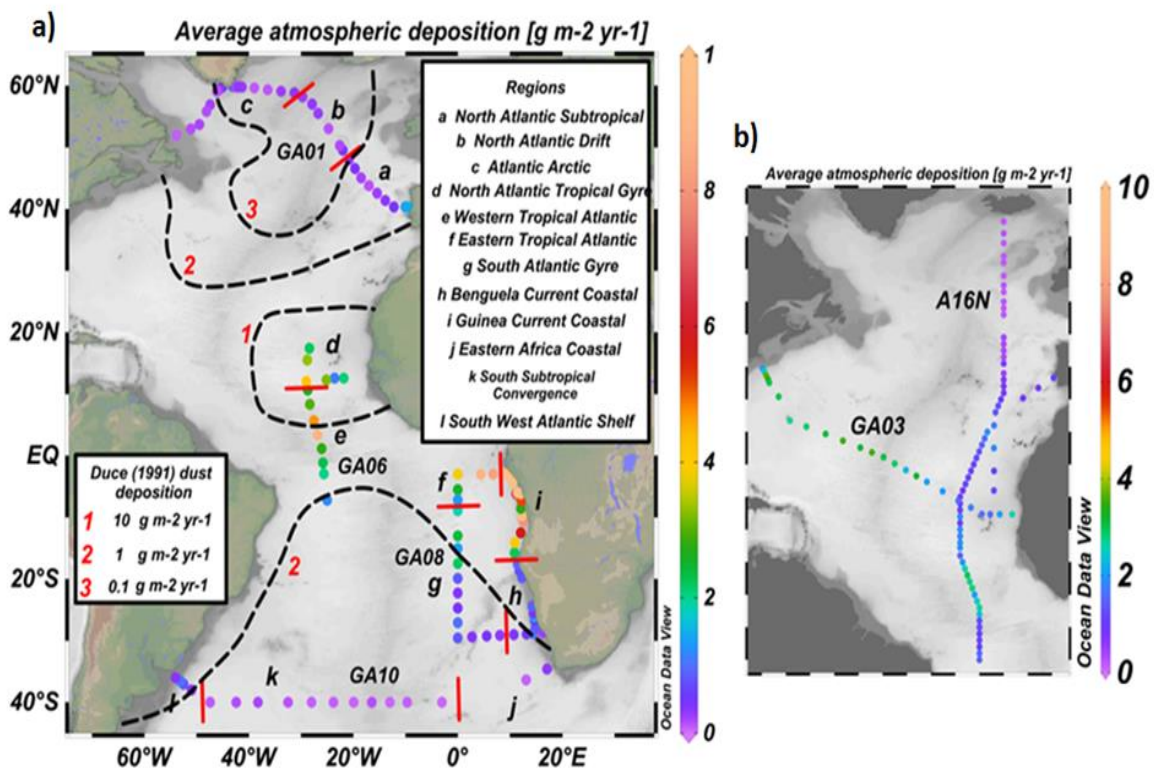


Figure 4.10: a) Average atmospheric deposition fluxes determined for the four GEOTRACES cruises. b) Average atmospheric deposition fluxes determined from GEOTRACES GA03 and A16N-2003 cruises are plotted (Measures et al., 2015). Black dashed lines defined boundaries of atmospheric aerosol deposition from (Duce et al., 1991).

The highest atmospheric deposition fluxes were calculated in the vicinity of land masses (i.e. Iberian Peninsula and Greenland) and could be partly due to overestimations by the MADCOW model. An overestimation would arise if there were additional Al sources, rather than Al being input solely from atmospheric deposition. The coastal stations near the Iberian Peninsula received additional Al inputs from the Tagus estuary (Menzel Barraqueta et al., 2018), while the coastal stations near Greenland are influenced by additional Al inputs from glacial run-off and ice melt (Menzel Barraqueta et al., 2018). With these stations removed, the average atmospheric deposition flux along GA01 decreased to $0.28 \pm 0.12 \text{ g m}^{-2} \text{ yr}^{-1}$ (n=24).

Table 4.5: Average atmospheric deposition fluxes estimated for each biogeochemical province. For reference on the different regions please refer to table 4.1. The deposition fluxes are given in $\text{g m}^{-2} \text{ yr}^{-1}$. Mahowald and Duce refer to the atmospheric deposition flux results provided in Mahowald et al., (2005) and Duce et al., (1991), respectively. GUIN refers to deposition results affected with addition Al inputs from the Congo River plume.*

Cruise	Biogeochemical province	Deposition (this study)	Mahowald	Duce
GA01	NAST	0.71 ± 0.65	1.05 ± 0.24	0.1 - 1
GA01	NADR	0.28 ± 0.12	0.52 ± 0.1	0.01 - 0.1
GA01	ARCT	0.27 ± 0.13	0.35 ± 0.03	0.01 - 1
GA06	NATR	2.2 ± 1.2	10 ± 1.3	10 - 100
GA06	WTRA	3.8 ± 2.7	4.4 ± 3.2	1 - 100
GA08	ETRA	2.65 ± 1.84	0.89 ± 0.36	1 - 10
GA08	GUIN*	26.2 ± 43.42	1.04 ± 0.9	1 - 10
	GUIN	2.67 ± 1.96		
GA08	BENG	0.36 ± 0.18	5.2 ± 4.16	1 - 10
GA08	SATL	0.17 ± 0.18	0.22 ± 0.09	0.1 - 1
GA10	EAFR	0.21 ± 0.22	0.28 ± 0.14	0.1 - 1
GA10	SSTZ	0.15 ± 0.1	0.44 ± 0.34	0.1 - 1
GA10	FKLD	1.23 ± 0.67	1.17 ± 0.16	1 - 10

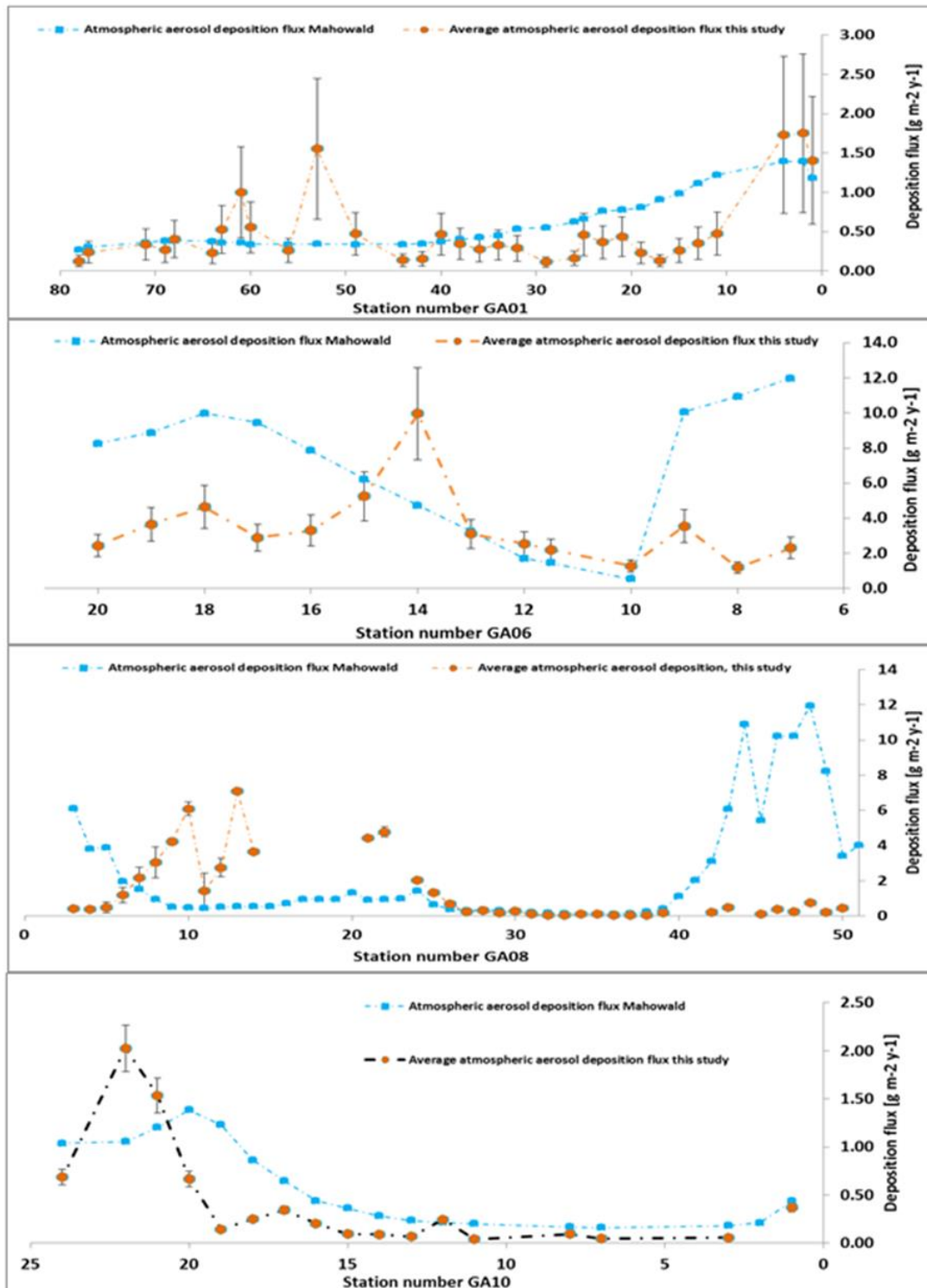


Figure 4.11: Total average atmospheric deposition fluxes (this study) and model atmospheric deposition estimates from Mahowald et al. (2005).

Although the atmospheric deposition fluxes near the Iberian Peninsula were high relative to the rest of the transect, they are comparable to modelled atmospheric deposition fluxes (Mahowald et al., 2005) (Table 4.5 and Figure 4.11). Measures et al. (2015) reported an atmospheric deposition flux of ca. $0.91 \text{ g m}^{-2} \text{ yr}^{-1}$ (station USGT10-02) close to the Iberian Peninsula along GEOTRACES section GA03 (Figure 4.10b), which is somewhat lower than our average deposition flux for stations 1, 2 and 4 ($1.63 \pm 0.08 \text{ g m}^{-2} \text{ yr}^{-1}$). Our calculated fluxes derived from dAl at coastal stations near the Iberian Peninsula may be on the high end of the scale due to additional Al inputs from the Tagus estuary which did not influence the nearby stations sampled by Measures et al. (2015). In the NAST we derived an average dust flux for stations 21, 23 and 25 of $0.42 \pm 0.17 \text{ g m}^{-2} \text{ yr}^{-1}$ which is in good agreement with calculated atmospheric deposition fluxes for the same region during the 2003 CLIVAR A16N cruise (Measures et al., 2015) using aerosol Al concentrations from Buck et al. (2010) (Figure 4.10b). Shelley et al. (2017b) reported atmospheric deposition fluxes for a suite of elements for the GA01 cruise using two different approaches; 1) aerosol and precipitation concentration data (which they termed “traditional approach”) and 2) ^7Be in aerosols and the surface mixed layer. They divided the GA01 section into two areas: (i) Area 1 = west of 30° W ; (ii) Area 2 = east of 30° W (Figure 4.1). For Area 1 they derived atmospheric deposition fluxes of 0.03 and $0.1 \text{ g m}^{-2} \text{ yr}^{-1}$ using the traditional and ^7Be approaches, respectively. For Area 2, the atmospheric deposition fluxes were 0.19 and $0.14 \text{ g m}^{-2} \text{ yr}^{-1}$ for the traditional and ^7Be approaches, respectively. With the MADCOW model we calculated average atmospheric deposition fluxes of 0.27 ± 0.16 and $0.3 \pm 0.12 \text{ g m}^{-2} \text{ yr}^{-1}$ for Area 1 and 2, respectively. The average modelled flux estimates for the same areas from Mahowald et al., 2005 were 0.36 ± 0.03 and $0.76 \pm 0.32 \text{ g m}^{-2} \text{ yr}^{-1}$.

It is encouraging that the different flux results are of a similar order of magnitude, although the dust flux estimates derived from Mahowald et al. (2005) were always highest. It is possible that the dust deposition model (Mahowald et al., 2005) may have overestimated atmospheric deposition in the North Atlantic (north of 50°N) due to the limited number of field observations available at the time. Interestingly, a higher atmospheric aerosol deposition flux was calculated with the MADCOW model than with either the aerosol approach or the ^7Be method. This could be due to the different timescales over which each approach integrates. The MADCOW model approach integrates the total atmospheric deposition flux over a period of ca. 1 yr prior (based on our choice of dAl surface mixed layer residence time) to the GA01 cruise, while the ^7Be approach integrates over a period of 3 months, and the aerosol approach provides a snapshot over a period of days. The elevated atmospheric deposition flux for the traditional compared to the ^7Be approach in area 2 was attributed to ^7Be scavenging onto biogenic particles near the Iberian Peninsula (Shelley et al., 2017).

3.6.2 Atmospheric deposition fluxes to the Tropical Atlantic (GA06)

Overall, the atmospheric deposition fluxes calculated for the tropical Atlantic using MADCOW are generally of the same order of magnitude compared to modelled atmospheric deposition fluxes (Mahowald et al., 2005) (Table 4.5 and Figure 4.11). Along GA06, the calculated atmospheric deposition fluxes ranged from $1.19 \pm 0.45 \text{ g m}^{-2} \text{ yr}^{-1}$ at station 8 to $9.96 \pm 3.72 \text{ g m}^{-2} \text{ yr}^{-1}$ at station 14 (Figure 4.2 and 4.6). The average calculated atmospheric deposition flux along the cruise was $3.46 \pm 2.18 \text{ g m}^{-2} \text{ yr}^{-1}$. Large discrepancies are observed between our MADCOW model results and the modelled atmospheric deposition fluxes of Duce et al. (1991) (Figure 4.10) and

Mahowald et al. (2005) (Figure 4.11). The largest differences are found in the NATR, along the East-West transect and north of 8°N (Figure 4.11 and Table 4.5). Along the East-West transect (Station 7 to 9), at ca. 12°N, and north of 8°N, our atmospheric deposition fluxes ranged between 1.19 ± 0.44 and 3.54 ± 1.32 $\text{g m}^{-2} \text{yr}^{-1}$ while modelled dust fluxes were above $8 \text{ g m}^{-2} \text{yr}^{-1}$ and reach up to $12 \text{ g m}^{-2} \text{yr}^{-1}$ (station 7).

The discrepancy could result from differences in the solubility of aerosols in the east and west of the basin. A combination of more soluble aerosols transported from mineral dust sources regions in North Africa via the trade winds to the western tropical Atlantic and from American sources may result in higher levels of dAl in the western tropical Atlantic than in the eastern tropical Atlantic (Measures et al., 2015; Sedwick et al., 2007). In addition, the Mahowald model uses extensive field data and monthly satellite retrievals over many years. Thus, the latter model may better capture the high degree of inter-annual and inter-seasonal variability in dust. Whilst there is more dust being deposited in the eastern tropical Atlantic than in the western tropical Atlantic, MADCOW calculates higher atmospheric deposition fluxes in the western tropical Atlantic than in the eastern tropical Atlantic (this study and Measures et al., 2008; 2015). These results do not match the observations (from field data and satellite retrievals) and suggests that the MADCOW model is not able to accurately determine atmospheric deposition fluxes in the tropical North Atlantic Ocean. In contrast, in the WTRA, our average atmospheric deposition flux of 3.82 ± 2.72 $\text{g m}^{-2} \text{yr}^{-1}$ agrees very well with modelled atmospheric deposition fluxes (4.4 ± 3.2 $\text{g m}^{-2} \text{yr}^{-1}$) (Duce et al., 1991; Mahowald et al., 2005).

3.6.3 Atmospheric deposition fluxes to the Southeast Atlantic (GA08)

The MADCOW model most likely overestimates atmospheric deposition fluxes to the GUIN region north of 6°S with fluxes ranging between 38 to 163 g m⁻² yr⁻¹. We have omitted stations 14 to 21 from the average atmospheric deposition flux, as they are strongly influenced by additional dAl inputs from the Congo River (Figure 4.1 and 4.6). Following this removal, atmospheric deposition fluxes along GA08 (Figure 4.10) ranged from 0.04±0.01 g m⁻² yr⁻¹ in the South Atlantic Gyre region (SATL) to 7.08±1.44 g m⁻² yr⁻¹ in the Guinea Current Coastal region (GUIN) at ca. 12°S. The average calculated atmospheric deposition flux to the Southeast Atlantic was 1.33±1.85 g m⁻² yr⁻¹. The MADCOW model may underestimate atmospheric deposition fluxes in the BENG region, which is influenced by eastern boundary upwelling processes, supplying nutrients from deep to surface waters and resulting in enhanced primary productivity with high levels of Chl a (Figure 4.8). The BENG region receives mineral dust inputs from the Namib Desert (Prospero et al., 2002), but the large abundance of biogenic particles likely result in low surface dAl concentrations (<7 nM) (Figure 4.6) due to enhanced scavenging. Mahowald et al. (2005) calculated an average atmospheric deposition flux for the BENG region of 5.2±4.16 g m⁻² yr⁻¹ with deposition values of up to 11.96 g m⁻² yr⁻¹ (station 48). However, our atmospheric deposition fluxes for this region are rather low with an average of 0.36±0.18 g m⁻² yr⁻¹. In contrast, our MADCOW derived atmospheric deposition fluxes in the SATL region (0.17±0.18 g m⁻² yr⁻¹) are in close agreement with model estimates (0.22±0.09 g m⁻² yr⁻¹).

3.6.4 Atmospheric deposition fluxes to the South Atlantic Ocean (GA10)

Along GA10, the calculated atmospheric deposition fluxes ranged from $0.15 \pm 0.1 \text{ g m}^{-2} \text{ yr}^{-1}$ in the South Subtropical Convergence (SSTC) region to $1.23 \pm 0.67 \text{ g m}^{-2} \text{ yr}^{-1}$ in the South West Atlantic Shelf (FKLD) region off Argentina. The average atmospheric deposition flux calculated along the 40°S section was $0.21 \text{ g m}^{-2} \text{ yr}^{-1}$. The highest atmospheric deposition flux was estimated in the FKLD, downwind from South America with Patagonian dust reported as the main source of mineral dust to the South Atlantic Ocean (Johnson et al., 2010; Wagener et al., 2008). Our atmospheric deposition fluxes in the FKLD agree with model estimates for the same region from Mahowald et al. (2005) (Table 4.5) and Wagener et al. (2008). Some discrepancies exist between the region of maximum atmospheric deposition. Indeed, Wagener et al. (2008) acknowledged this issue stating that the largest uncertainty in their estimates occurred downwind from South America as their field data from this sector were collected on cruises in the South Pacific and South Indian Oceans. The lowest atmospheric aerosol deposition was found along the SSTC region ($0.15 \pm 0.1 \text{ g m}^{-2} \text{ yr}^{-1}$) and were somewhat lower than model results (Mahowald et al., 2005) ($0.44 \pm 0.34 \text{ g m}^{-2} \text{ yr}^{-1}$) but identical within the calculated uncertainties. In the EAFR, we calculated an average atmospheric deposition flux of $0.21 \pm 0.22 \text{ g m}^{-2} \text{ yr}^{-1}$. The latter flux agrees very well with total atmospheric deposition fluxes for the same region calculated from aerosol samples collected on the Falkland Islands ($0.18 \text{ g m}^{-2} \text{ yr}^{-1}$) (Chance et al., 2015) and with model results ($0.28 \pm 0.14 \text{ g m}^{-2} \text{ yr}^{-1}$) (Mahowald et al., 2005). It is possible that the South Atlantic Ocean also receives additional mineral dust inputs from South African sources although Patagonian dust is considered the major source of aerosols to this region (Gaiero et al., 2003; Wagener et al., 2008).

4 Conclusions

Dissolved Al concentrations in the surface ocean are a balance between input and removal processes. In this context, we can use the concentration of dAl in the mixed layer along with the residence time of dAl in the mixed layer to calculate atmospheric deposition fluxes. Overall, in oceanic regions beyond the shelf break, we found good agreement between our calculated MADCOW atmospheric deposition fluxes and modelled atmospheric deposition fluxes (Mahowald et al., 2005). The agreement between our MADCOW deposition flux calculations and model results was poor in regions with additional Al inputs (e.g. river run off, ice melt, and benthic) and strong Al removal by biogenic particles in upwelling regions. Away from the main aerosol sources to the Atlantic Ocean, we found that our atmospheric deposition fluxes were lower than model fluxes which may suggest that these regions receive less atmospheric inputs than models indicate. As such, this work provides new constraints for models of atmospheric deposition for the largely under-sampled regions of the Atlantic Ocean (e.g. Labrador Sea, South Atlantic and Southeast Atlantic Ocean). Specifically, Mahowald et al. (2008) note that there are few aerosol measurements reported for the region between 30° and 60°S, due to a lack of island site for deployment of aerosol samplers and the remoteness of the region presenting logistical challenges for research cruises. In the GEOTRACES Programme, a concerted effort has been made to cover these under-sampled regions of the ocean. Dissolved Al is a key trace element of the GEOTRACES Programme and as such it is measured on all the GEOTRACES cruises which implies a major strength of the approach used in this study. We acknowledge that there are regions of the Atlantic for which the application of the MADCOW model has limitations (i.e. tropical Atlantic Ocean). In these regions, more work is needed to constrain

parameters such as aerosol Al fractional solubility and the residence time of Al within the surface mixed layer. Realistic residence time values would significantly improve our atmospheric deposition flux results. We suggest that forthcoming expeditions should use more than one technique to calculate atmospheric deposition fluxes as different methods provide us with complimentary information. The new Intermediate Data Product from the GEOTRACES Programme along with upcoming dAl datasets will give us a better coverage of under-sampled regions which combined with historical data will help us to refine atmospheric deposition fluxes (i.e. capturing seasonal and inter-annual variability).

Acknowledgments

We are greatly thankful to the captains and crews of expeditions GA01, GA06, GA08 and GA10 for their support during the cruises. We would like to give a special thanks to Pierre Branellec, Michel Hamon, Catherine Kermabon, Philippe Le Bot, Stéphane Leizour, Olivier Ménage, Fabien Pérault and Emmanuel de Saint Léger for their technical expertise during GA01 clean CTD deployments and to Catherine Schmechtig for the GA01 database management. Greg Cutter is also strongly acknowledged for his help in setting up the new French clean sampling system. A special thank goes to the trace metal colleagues on board GA01, GA06, GA08, and GA10. This work was funded by a PhD fellowship to Jan-Lukas Menzel Barraqueta from the Department of Scientific Politics of the Basque Government, with further financial support from GEOMAR Helmholtz Center for Ocean Research Kiel. GEOTRACES GA01 was led by France, GA06 and GA08 by the UK, and GA10 by Germany. Part of this work was supported by the French National Research Agency (ANR-13-BS06-0014, ANR-12-PDOC-0025-01), the French

Chapter 4

National Centre for Scientific Research (CNRS-LEFE-CYBER), the LabexMER (ANR-10-LABX-19), and Ifremer.

Supplementary information

Text S1

Fractional Al solubility in the North Atlantic (GA01)

In the North Atlantic, section GA01, we used a combination of in Al fractional solubility ($Al_{sol\%}$) estimates from aerosols collected during the cruise (Shelley et al., 2017a) for stations north of 50°N and $Al_{sol\%}$ estimates from the compilation of Baker et al. (2013) for stations south of 50°N. For stations 1 to 26 we used an $Al_{sol\%}$ of 11.6 % as the stations fall into aerosol source region 2 and air mass type sub-region 2a. Sub region 2a is dominated by North Atlantic remote (76.8%) and European (15.2%) air mass types with a small and residual contribution of North American (7.8%) and Saharan (0.25%) air mass types, respectively. From station 29 to 71 we averaged all the aerosol $Al_{sol\%}$ estimates as all the air mass types for the aerosol samples collected (n=9) between the previous mentioned stations had a North Atlantic remote air mass provenance yielding a final $Al_{sol\%}$ of 21%. The last two stations (77 and 78) were located between aerosol samples geo17 and geo18 which had a Canadian air mass type origin with an average $Al_{sol\%}$ of 14.5%.

Fractional Al solubility in the tropical Atlantic (GA06)

For the tropical Atlantic, section GA06, we selected four different $Al_{sol\%}$ values. For the eastward transect (stations 7 to 9) an $Al_{sol\%}$ of 5.8% was selected as the stations were located in the aerosol source region number 3. Air mass provenance within sub-region 3b were Southern African (46.5%) and South Atlantic remote (43.6%), with a small contribution of Southern African biomass burning (7.1%) and Sahara

(2.7%) air mass types and a residual contribution of North Atlantic remote (0.2%) air mass type. The most southern station (station 10) was located within source region 4 and air mass provenance within sub-region 4a. Sub-region 4a was dominated by Southern African (82.1%) and Southern African biomass burning (16.9%) air mass types with an additional small contribution of Southern Atlantic remote (1.1%) air mass type, thus yielding an $Al_{sol\%}$ of 5.5%. Similar to station 10, for the northward transect (St. 11.5 to 18) we used an $Al_{sol\%}$ of 5%. This northward transect was located in aerosol source region 3, although the air mass type provenance was a combination between sub regions 3a1 and 3a2. Sub-region 3a (3a1+3a2) had a mixed air mass type provenance, with North Atlantic remote (30.5%), Sahara (20.7%), Southern African (24.9%) and Southern Atlantic biomass burning (15.5%) dominating the air mass types. A small contribution of Southern Atlantic remote (9.1%) and European (0.2%) was also present. The most northern stations (St. 19 and 20) had the highest $Al_{sol\%}$ with a value of 8.6% as they were located in aerosol source region 2 and air mass type provenance sub-region 2d, which is dominated by Sahara (48.1%) and North Atlantic remote (45.7%) air mass types. Sub-region 2d also had a small and residual contribution of European (6%) and North American (0.3%) air mass types, respectively.

Fractional Al solubility in the South East Atlantic (GA08)

In the South East Atlantic, section GA08, two different $Al_{sol\%}$ were used. Both were located in aerosol source region 4. Stations 1 to 5 and 30 to 52 were located in air mass type sub-region 4c. Sub-region 4c was dominated by Southern Atlantic remote (81.2%) and South African (13.5%) air mass types with smaller contributions of Southern Africa burning biomass (4.9%) and South American (0.5%) air mass types,

yielding an average $Al_{sol\%}$ of 10.3%. Stations 6 to 29 were located in air mass type sub-region 4b, where the dominant air type masses were Southern Africa (44.2%), Southern Africa burning biomass (30.8%) and Southern Atlantic remote (25.1%). Average $Al_{sol\%}$ for sub-region 4b was 7.7%.

Fractional Al solubility in the South Atlantic Ocean (GA10)

For the Southern Ocean (GA10), two different $Al_{sol\%}$ were used. On the eastern part of the transect, stations 1 to 3, we used a value of 10.9 % which is mainly due to 94.3% of the air masses types having a South Atlantic remote areas origin with an average $Al_{sol\%}$ of 11.3%. West of station 3, stations 7 to 24, we used an $Al_{sol\%}$ of 13.9% which is mainly due to the combined effect of 52% and 45% of the air masses coming from South Atlantic marine remote areas and South America with an average $Al_{sol\%}$ of 14.1% and 14.5%, respectively.

Table S4.1: Calculated MLD (m), measured dAl concentrations (nM), and derived atmospheric aerosol deposition estimates ($g\ m^{-2}yr^{-1}$) for each of the stations along the four cruises.

Cruise	Station number	MLD	dAl	Deposition flux
GA01	1	35.8	15.8	1.2
GA01	2	31.4	19.6	1.5
GA01	4	33.4	19.4	1.4
GA01	11	52.1	5.3	0.4
GA01	13	45.9	4.0	0.3
GA01	15	51.9	2.9	0.2
GA01	17	52.1	1.5	0.1
GA01	19	52.4	2.6	0.2
GA01	21	67.5	4.9	0.4
GA01	23	72.1	4.1	0.3
GA01	25	82.0	5.2	0.4
GA01	26	78.2	1.8	0.1
GA01	29	64.3	1.3	0.1
GA01	32	62.0	3.2	0.2
GA01	34	78.5	3.7	0.3
GA01	36	97.5	3.1	0.2
GA01	38	97.4	3.9	0.3
GA01	40	82.5	3.1	0.2
GA01	42	78.7	1.1	0.1
GA01	44	89.9	0.9	0.1
GA01	49	124.5	3.2	0.2
GA01	53	51.6	10.4	0.8
GA01	56	91.3	1.8	0.1
GA01	60	84.6	3.7	0.3
GA01	61	78.9	6.7	0.5
GA01	63	116.4	3.6	0.3
GA01	64	76.1	1.5	0.1
GA01	68	124.1	2.8	0.2
GA01	69	106.5	1.8	0.1
GA01	71	60.6	2.3	0.2
GA01	77	20.7	1.6	0.1
GA01	78	12.0	0.9	0.1
GA06	7	35.6	15.6	2.2
GA06	8	46.4	8.1	1.1
GA06	9	42.4	24.0	3.4

Chapter 4

GA06	10	51.3	8.8	1.2
GA06	11.5	43.4	15.0	2.1
GA06	12	32.6	17.3	2.5
GA06	13	29.4	21.0	3.0
GA06	14	32.9	67.5	9.6
GA06	15	39.9	35.6	5.1
GA06	16	42.1	22.4	3.2
GA06	17	44.1	19.7	2.8
GA06	18	40.5	31.5	4.5
GA06	19	50.4	24.8	3.5
GA06	20	38.0	16.6	2.4
GA08	1	-	-	-
GA08	2	-	-	-
GA08	3	33.0	4.4	0.8
GA08	4	59.0	4.0	0.7
GA08	5	29.0	4.9	0.9
GA08	6	13.0	12.0	2.2
GA08	7	25.2	22.0	4.1
GA08	8	12.2	31.0	5.7
GA08	9	13.5	43.0	7.9
GA08	10	14.1	62.0	11.4
GA08	11	11.8	14.5	2.7
GA08	12	11.0	28.0	5.2
GA08	13	8.5	72.0	13.3
GA08	14	12.0	37.0	6.8
GA08	15	13.0	784.6	163.2
GA08	16	5.0	269.0	56.0
GA08	17	8.7	261.0	54.3
GA08	18	9.2	211.0	43.9
GA08	19	8.2	209.0	43.5
GA08	20	9.0	186.0	38.7
GA08	21	15.8	44.9	8.3
GA08	22	20.2	48.6	9.0
GA08	23	23.8	32	6.7
GA08	24	28.4	20.8	3.8
GA08	25	37.2	13.6	2.5
GA08	26	24.8	7.0	1.3
GA08	27	28.0	9.8	1.8
GA08	28	40.4	12.8	2.4
GA08	29	30.0	7.3	1.3
GA08	30	56.4	11.8	2.2
GA08	31	41.7	4.5	0.8
GA08	32	44.6	1.8	0.3
GA08	33	35.4	2.3	0.4

Chapter 4

GA08	34	39.2	5.3	1.0
GA08	35	40.5	4.3	0.8
GA08	36	32.3	1.9	0.3
GA08	37	35.5	2.2	0.4
GA08	38	38.6	1.5	0.3
GA08	39	43.6	1.9	0.4
GA08	40	-	-	-
GA08	41	42.0	2.5	0.5
GA08	42	31.8	5.4	1.0
GA08	43	34.0	3.3	0.6
GA08	44	6.0	1.2	0.2
GA08	45	36.1	4.3	0.8
GA08	46	65.0	2.9	0.5
GA08	47	12.0	8.3	1.5
GA08	48	11.0	2.2	0.4
GA08	49	12.0	4.9	0.9
GA08	50	12.0	4.7	0.8
GA08	51	19.0	4.5	0.7
GA10	1	29.3	4.4	0.3
GA10	2	32.4	4.2	0.4
GA10	3	54.4	0.7	0.0
GA10	7	65.4	0.4	0.0
GA10	8	54.1	0.7	0.1
GA10	11	62.8	0.3	0.0
GA10	12	65.1	1.9	0.1
GA10	13	65.4	0.5	0.0
GA10	14	48.1	0.7	0.1
GA10	15	56.2	0.7	0.1
GA10	16	69.9	1.6	0.1
GA10	17	71.8	2.7	0.2
GA10	18	57.9	2.0	0.1
GA10	19	51.6	1.1	0.1
GA10	20	30.5	5.2	0.3
GA10	21	46.0	12.0	0.8
GA10	22	34.0	15.8	1.0
GA10	24	28.1	5.4	0.3

References

Achterberg, E. P., Moore, C. M., Henson, S. A., Steigenberger, S., Stohl, A., Eckhardt, S., Avendano, L. C., Cassidy, M., Hembury, D., and Klar, J. K.: Natural iron fertilization by the Eyjafjallajökull volcanic eruption, *Geophysical Research Letters*, 40, 921-926, 2013.

Aguilar-Islas, A. M., Wu, J., Rember, R., Johansen, A. M., and Shank, L. M.: Dissolution of aerosol-derived iron in seawater: Leach solution chemistry, aerosol type, and colloidal iron fraction, *Marine Chemistry*, 120, 25-33, 2010.

Anderson, R. F., Cheng, H., Edwards, R. L., Fleisher, M. Q., Hayes, C. T., Huang, K.-F., Kadko, D., Lam, P. J., Landing, W. M., Lao, Y., Lu, Y., Measures, C. I., Moran, S. B., Morton, P. L., Ohnemus, D. C., Robinson, L. F., and Shelley, R. U.: How well can we quantify dust deposition to the ocean?, *Philosophical Transactions of the Royal Society A: Mathematical, Physical and Engineering Sciences*, 374, 2016.

Baker, A., Adams, C., Bell, T., Jickells, T., and Ganzeveld, L.: Estimation of atmospheric nutrient inputs to the Atlantic Ocean from 50° N to 50° S based on large-scale field sampling: Iron and other dust-associated elements, *Global Biogeochemical Cycles*, 27, 755-767, 2013.

Baker, A. R. and Croot, P. L.: Atmospheric and marine controls on aerosol iron solubility in seawater, *Marine Chemistry*, 120, 4-13, 2010.

Baker, A. R. and Jickells, T. D.: Atmospheric deposition of soluble trace elements along the Atlantic Meridional Transect (AMT), *Progress in Oceanography*, 158, 41-51, 2017.

Baker, A. R., Jickells, T. D., Witt, M., and Linge, K. L.: Trends in the solubility of iron, aluminium, manganese and phosphorus in aerosol collected over the Atlantic Ocean, *Marine Chemistry*, 98, 43-58, 2006.

Baker, A. R., Kelly, S. D., Biswas, K. F., Witt, M., and Jickells, T. D.: Atmospheric deposition of nutrients to the Atlantic Ocean, *Geophysical Research Letters*, 30, 2296, 2003.

Barrett, P. M., Resing, J. A., Buck, N. J., Landing, W. M., Morton, P. L., and Shelley, R. U.: Changes in the distribution of Al and particulate Fe along A16N in the eastern North Atlantic Ocean between 2003 and 2013: Implications for changes in dust deposition, *Marine Chemistry*, 177, 57-68, 2015.

Bowie, A. R., Whitworth, D. J., Achterberg, E. P., Mantoura, R. F. C., and Worsfold, P. J.: Biogeochemistry of Fe and other trace elements (Al, Co, Ni) in the

upper Atlantic Ocean, Deep Sea Research Part I: Oceanographic Research Papers, 49, 605-636, 2002.

Brown, M. T. and Bruland, K. W.: An improved flow-injection analysis method for the determination of dissolved aluminum in seawater, *Limnol. Oceanogr. Methods*, 6, 87-95, 2008.

Buck, C. S., Landing, W. M., Resing, J. A., and Measures, C. I.: The solubility and deposition of aerosol Fe and other trace elements in the north atlantic ocean: observations from the A16N CLIVAR/CO 2 repeat hydrography section, *Marine Chemistry*, 120, 57-70, 2010.

Bullard, J. E., Baddock, M., Bradwell, T., Crusius, J., Darlington, E., Gaiero, D., Gasso, S., Gisladottir, G., Hodgkins, R., and McCulloch, R.: High-latitude dust in the Earth system, *Reviews of Geophysics*, 54, 447-485, 2016.

Chahine, M. T.: The hydrological cycle and its influence on climate, *Nature*, 359, 373, 1992.

Chance, R., Jickells, T. D., and Baker, A. R.: Atmospheric trace metal concentrations, solubility and deposition fluxes in remote marine air over the south-east Atlantic, *Marine Chemistry*, 177, 45-56, 2015.

Dammshäuser, A., Wagener, T., and Croot, P. L.: Surface water dissolved aluminum and titanium: Tracers for specific time scales of dust deposition to the Atlantic?, *Geophysical Research Letters*, 38, 2011.

Duce, R., Liss, P., Merrill, J., Atlas, E., Buat-Menard, P., Hicks, B., Miller, J., Prospero, J., Arimoto, R., and Church, T.: The atmospheric input of trace species to the world ocean, *Global biogeochemical cycles*, 5, 193-259, 1991.

Duce, R. A. and Tindale, N. W.: Atmospheric Transport of Iron and Its Deposition in the Ocean, *Limnology and Oceanography*, 36, 1715-1726, 1991.

Fishwick, M. P., Sedwick, P. N., Lohan, M. C., Worsfold, P. J., Buck, K. N., Church, T. M., and Ussher, S. J.: The impact of changing surface ocean conditions on the dissolution of aerosol iron, *Global Biogeochemical Cycles*, 28, 1235-1250, 2014.

Gaiero, D. M., Probst, J. L., Depetris, P. J., Bidart, S. M., and Leleyter, L.: Iron and other transition metals in Patagonian riverborne and windborne materials: geochemical control and transport to the southern South Atlantic Ocean, *Geochimica et Cosmochimica Acta*, 67, 3603-3623, 2003.

Han, Q., Moore, J. K., Zender, C., Measures, C., and Hydes, D.: Constraining oceanic dust deposition using surface ocean dissolved Al, *Global biogeochemical cycles*, 22, 2008.

Hennigan, C., Izumi, J., Sullivan, A., Weber, R., and Nenes, A.: A critical evaluation of proxy methods used to estimate the acidity of atmospheric particles, *Atmospheric Chemistry and Physics*, 15, 2775, 2015.

Holte, J., Talley, L. D., Gilson, J., and Roemmich, D.: An Argo mixed layer climatology and database, *Geophysical Research Letters*, 2017. 2017.

Huneus, N., Schulz, M., Balkanski, Y., Griesfeller, J., Prospero, M., Kinne, S., Bauer, S., Boucher, O., Chin, M., and Dentener, F.: Global dust model intercomparison in AeroCom phase I, *Atmospheric Chemistry and Physics*, 11, 7781-7816, 2011.

Hydes, D. and Liss, P.: Fluorimetric method for the determination of low concentrations of dissolved aluminium in natural waters, *Analyst*, 101, 922-931, 1976.

Ito, A.: Atmospheric processing of combustion aerosols as a source of bioavailable iron, *Environmental Science & Technology Letters*, 2, 70-75, 2015.

Jickells, T.: The inputs of dust derived elements to the Sargasso Sea; a synthesis, *Marine Chemistry*, 68, 5-14, 1999.

Jickells, T., Boyd, P., and Hunter, K. A.: Biogeochemical impacts of dust on the global carbon cycle. In: *Mineral Dust*, Springer, 2014.

Jickells, T., Church, T., Veron, A., and Arimoto, R.: Atmospheric inputs of manganese and aluminium to the Sargasso Sea and their relation to surface water concentrations, *Marine chemistry*, 46, 283-292, 1994.

Jickells, T., Dorling, S., Deuser, W., Church, T., Arimoto, R., and Prospero, J.: Airborne dust fluxes to a deep water sediment trap in the Sargasso Sea, *Global Biogeochemical Cycles*, 12, 311-320, 1998.

Jickells, T. D., An, Z. S., Andersen, K. K., Baker, A. R., Bergametti, G., Brooks, N., Cao, J. J., Boyd, P. W., Duce, R. A., Hunter, K. A., Kawahata, H., Kubilay, N., laRoche, J., Liss, P. S., Mahowald, N., Prospero, J. M., Ridgwell, A. J., Tegen, I., and Torres, R.: Global iron connections between desert dust, ocean biogeochemistry, and climate, *Science*, 308, 67-71, 2005.

Johnson, M. S., Meskhidze, N., Solmon, F., Gassó, S., Chuang, P. Y., Gaiero, D. M., Yantosca, R. M., Wu, S., Wang, Y., and Carouge, C.: Modeling dust and soluble iron deposition to the South Atlantic Ocean, *Journal of Geophysical Research: Atmospheres*, 115, 2010.

Kadko, D., Landing, W. M., and Shelley, R. U.: A novel tracer technique to quantify the atmospheric flux of trace elements to remote ocean regions, *Journal of Geophysical Research: Oceans*, 120, 848-858, 2015.

Kadko, D. and Prospero, J.: Deposition of ^{7}Be to Bermuda and the regional ocean: environmental factors affecting estimates of atmospheric flux to the ocean, *Journal of Geophysical Research: Oceans*, 116, 2011.

Kara, A. B., Rochford, P. A., and Hurlburt, H. E.: Mixed layer depth variability over the global ocean, *Journal of Geophysical Research: Oceans*, 108, 2003.

Kim, G. and Church, T. M.: Wet deposition of trace elements and radon daughter systematics in the South and equatorial Atlantic atmosphere, *Global biogeochemical cycles*, 16, 2002.

Kohfeld, K. E. and Harrison, S. P.: DIRTMAP: the geological record of dust, *Earth-Science Reviews*, 54, 81-114, 2001.

Longhurst, A. R.: *Ecological geography of the sea*, Academic Press, 2010.

Mahowald, N., Albani, S., Kok, J. F., Engelstaeder, S., Scanza, R., Ward, D. S., and Flanner, M. G.: The size distribution of desert dust aerosols and its impact on the Earth system, *Aeolian Research*, 15, 53-71, 2014.

Mahowald, N., Ward, D. S., Kloster, S., Flanner, M. G., Heald, C. L., Heavens, N. G., Hess, P. G., Lamarque, J.-F., and Chuang, P. Y.: Aerosol impacts on climate and biogeochemistry, *Annual review of environment and resources*, 36, 2011.

Mahowald, N. M., Baker, A. R., Bergametti, G., Brooks, N., Duce, R. A., Jickells, T. D., Kubilay, N., Prospero, J. M., and Tegen, I.: Atmospheric global dust cycle and iron inputs to the ocean, *Global Biogeochemical Cycles*, 19, 2005.

Mahowald, N. M., Engelstaedter, S., Luo, C., Sealy, A., Artaxo, P., Benitez-Nelson, C., Bonnet, S., Chen, Y., Chuang, P. Y., and Cohen, D. D.: Atmospheric iron deposition: global distribution, variability, and human perturbations, 2008.

Maring, H., Savoie, D., Izaguirre, M., Custals, L., and Reid, J.: Mineral dust aerosol size distribution change during atmospheric transport, *Journal of Geophysical Research: Atmospheres*, 108, 2003.

Maring, H. B. and Duce, R. A.: The impact of atmospheric aerosols on trace metal chemistry in open ocean surface seawater, 1. Aluminum, *Earth and Planetary Science Letters*, 84, 381-392, 1987.

Martin, J. H., Gordon, M., and Fitzwater, S. E.: The case for iron, *Limnology and Oceanography*, 36, 1793-1802, 1991.

Measures, C.: The distribution of Al in the IOC stations of the eastern Atlantic between 30°S and 34°N , *Marine chemistry*, 49, 267-281, 1995.

Measures, C., Hatta, M., Fitzsimmons, J., and Morton, P.: Dissolved Al in the zonal N Atlantic section of the US GEOTRACES 2010/2011 cruises and the importance of hydrothermal inputs, *Deep Sea Research Part II: Topical Studies in Oceanography*, 116, 176-186, 2015.

Measures, C., Landing, W., Brown, M., and Buck, C.: High-resolution Al and Fe data from the Atlantic Ocean CLIVAR-CO₂ Repeat Hydrography A16N transect: Extensive linkages between atmospheric dust and upper ocean geochemistry, *Global Biogeochemical Cycles*, 22, 2008.

Measures, C., Sato, T., Vink, S., Howell, S., and Li, Y.: The fractional solubility of aluminium from mineral aerosols collected in Hawaii and implications for atmospheric deposition of biogeochemically important trace elements, *Marine Chemistry*, 120, 144-153, 2010.

Measures, C. and Vink, S.: On the use of dissolved aluminum in surface waters to estimate dust deposition to the ocean, *Global biogeochemical cycles*, 14, 317-327, 2000.

Measures, C. I. and Brown, E. T.: Estimating Dust Input to the Atlantic Ocean Using Surface Water Aluminium Concentrations. In: *The Impact of Desert Dust Across the Mediterranean*, Guerzoni, S. and Chester, R. (Eds.), Springer Netherlands, Dordrecht, 1996.

Menzel Barraqueta, J. L., Schlosser, C., Planquette, H., Gourain, A., Cheize, M., Boutorh, J., Shelley, R., Pereira Contreira, L., Gledhill, M., Hopwood, M. J., Lherminier, P., Sarthou, G., and Achterberg, E. P.: Aluminium in the North Atlantic Ocean and the Labrador Sea (GEOTRACES GA01 section): roles of continental inputs and biogenic particle removal, *Biogeosciences Discuss.*, 2018, 1-28, 2018.

Middag, R., Van Hulten, M., Van Aken, H., Rijkenberg, M., Gerringa, L., Laan, P., and De Baar, H.: Dissolved aluminium in the ocean conveyor of the West Atlantic Ocean: effects of the biological cycle, scavenging, sediment resuspension and hydrography, *Marine Chemistry*, 177, 69-86, 2015.

Middag, R., van Slooten, C., de Baar, H. J. W., and Laan, P.: Dissolved aluminium in the Southern Ocean, *Deep Sea Research Part II: Topical Studies in Oceanography*, 58, 2647-2660, 2011.

Monterey, G. I. and Levitus, S.: Seasonal variability of mixed layer depth for the world ocean, US Department of Commerce, National Oceanic and Atmospheric Administration, National Environmental Satellite, Data, and Information Service, 1997.

Moore, C. M., Mills, M. M., Achterberg, E. P., Geider, R. J., LaRoche, J., Lucas, M. I., McDonagh, E. L., Pan, X., Poulton, A. J., and Rijkenberg, M. J.: Large-scale

distribution of Atlantic nitrogen fixation controlled by iron availability, *Nature Geoscience*, 2, 867-871, 2009.

Moore, J. K., Doney, S. C., and Lindsay, K.: Upper ocean ecosystem dynamics and iron cycling in a global three-dimensional model, *Global Biogeochemical Cycles*, 18, 2004.

Orians, K. J. and Bruland, K. W.: The biogeochemistry of aluminum in the Pacific Ocean, *Earth and planetary science letters*, 78, 397-410, 1986.

Ott, S., Ott, A., Martin, D., and Young, J.: Analysis of a trans-Atlantic Saharan dust outbreak based on satellite and GATE data, *Monthly Weather Review*, 119, 1832-1850, 1991.

Patey, M. D., Achterberg, E. P., Rijkenberg, M. J., and Pearce, R.: Aerosol time-series measurements over the tropical Northeast Atlantic Ocean: Dust sources, elemental composition and mineralogy, *Marine Chemistry*, 174, 103-119, 2015.

Pohl, C., Croot, P. L., Hennings, U., Daberkow, T., Budeus, G., and Loeff, M. R. v. d.: Synoptic transects on the distribution of trace elements (Hg, Pb, Cd, Cu, Ni, Zn, Co, Mn, Fe, and Al) in surface waters of the Northern- and Southern East Atlantic, *Journal of Marine Systems*, 84, 28-41, 2011.

Prospero, J.: Saharan dust transport over the North Atlantic Ocean and Mediterranean: an overview. In: *The impact of desert dust across the Mediterranean*, Springer, 1996a.

Prospero, J. M.: The atmospheric transport of particles to the ocean, *Scope-scientific committee on problems of the environment international council of Scientific unions*, 57, 19-52, 1996b.

Prospero, J. M. and Carlson, T. N.: Vertical and areal distribution of Saharan dust over the western equatorial North Atlantic Ocean, *Journal of Geophysical Research*, 77, 5255-5265, 1972.

Prospero, J. M., Ginoux, P., Torres, O., Nicholson, S. E., and Gill, T. E.: Environmental characterization of global sources of atmospheric soil dust derived from the nimbus7 toms absorbing aerosol product, rev, 2002.

Prospero, J. M., Landing, W. M., and Schulz, M.: African dust deposition to Florida: Temporal and spatial variability and comparisons to models, *Journal of Geophysical Research: Atmospheres*, 115, n/a-n/a, 2010.

Prospero, J. M., Nees, R. T., and Uematsu, M.: Deposition rate of particulate and dissolved aluminum derived from Saharan dust in precipitation at Miami, Florida, *Journal of Geophysical Research: Atmospheres*, 92, 14723-14731, 1987.

Resing, J. A. and Measures, C. I.: Fluorometric Determination of Al in Seawater by Flow Injection Analysis with In-Line Preconcentration, *Analytical Chemistry*, 66, 4105-4111, 1994.

Risien, C. M. and Chelton, D. B.: A global climatology of surface wind and wind stress fields from eight years of QuikSCAT scatterometer data, *Journal of Physical Oceanography*, 38, 2379-2413, 2008.

Sarthou, G., Baker, A. R., Blain, S., Achterberg, E. P., Boye, M., Bowie, A. R., Croot, P., Laan, P., de Baar, H. J. W., Jickells, T. D., and Worsfold, P. J.: Atmospheric iron deposition and sea-surface dissolved iron concentrations in the eastern Atlantic Ocean, *Deep Sea Research Part I: Oceanographic Research Papers*, 50, 1339-1352, 2003.

Schanze, J. J., Schmitt, R. W., and Yu, L.: The global oceanic freshwater cycle: A state-of-the-art quantification, *Journal of Marine Research*, 68, 569-595, 2010.

Schlosser, C., Klar, J. K., Wake, B. D., Snow, J. T., Honey, D. J., Woodward, E. M. S., Lohan, M. C., Achterberg, E. P., and Moore, C. M.: Seasonal ITCZ migration dynamically controls the location of the (sub)tropical Atlantic biogeochemical divide, *Proceedings of the National Academy of Sciences*, 111, 1438-1442, 2014.

Schüßler, U., Balzer, W., and Deeken, A.: Dissolved Al distribution, particulate Al fluxes and coupling to atmospheric Al and dust deposition in the Arabian Sea, *Deep Sea Research Part II: Topical Studies in Oceanography*, 52, 1862-1878, 2005.

Sedwick, P. N., Sholkovitz, E. R., and Church, T. M.: Impact of anthropogenic combustion emissions on the fractional solubility of aerosol iron: Evidence from the Sargasso Sea, *Geochemistry, Geophysics, Geosystems*, 8, 2007.

Shelley, R. U., Landing, W. M., Ussher, S. J., Planquette, H., and Sarthou, G.: Characterisation of aerosol provenance from the fractional solubility of Fe (Al, Ti, Mn, Co, Ni, Cu, Zn, Cd and Pb) in North Atlantic aerosols (GEOTRACES cruises GA01 and GA03) using a two stage leach, *Biogeosciences Discuss.*, 2017, 1-31, 2017a.

Shelley, R. U., Roca-Martí, M., Castrillejo, M., Masqué, P., Landing, W. M., Planquette, H., and Sarthou, G.: Quantification of trace element atmospheric deposition fluxes to the Atlantic Ocean (> 40° N; GEOVIDE, GEOTRACES GA01) during spring 2014, *Deep Sea Research Part I: Oceanographic Research Papers*, 119, 34-49, 2017b.

Sholkovitz, E. R., Sedwick, P. N., Church, T. M., Baker, A. R., and Powell, C. F.: Fractional solubility of aerosol iron: Synthesis of a global-scale data set, *Geochimica et cosmochimica acta*, 89, 173-189, 2012.

Slinn, S. and Slinn, W.: Predictions for particle deposition on natural waters, *Atmospheric Environment* (1967), 14, 1013-1016, 1980.

van Bennekom, A. J. and Jager, J. E.: Dissolved aluminium in the Zaire river plume, *Netherlands Journal of Sea Research*, 12, 358-367, 1978.

Van Der Loeff, M. R., Helmers, E., and Kattner, G.: Continuous transects of cadmium, copper, and aluminium in surface waters of the Atlantic Ocean, 50°N to 50°S: correspondence and contrast with nutrient-like behaviour, *Geochimica et Cosmochimica Acta*, 61, 47-61, 1997.

van Hulst, M. M. P., Sterl, A., Tagliabue, A., Dutay, J. C., Gehlen, M., de Baar, H. J. W., and Middag, R.: Aluminium in an ocean general circulation model compared with the West Atlantic Geotraces cruises, *Journal of Marine Systems*, 126, 3-23, 2013.

Vink, S. and Measures, C. I.: The role of dust deposition in determining surface water distributions of Al and Fe in the South West Atlantic, *Deep Sea Research Part II: Topical Studies in Oceanography*, 48, 2787-2809, 2001.

Wagener, T., Guieu, C., Losno, R., Bonnet, S., and Mahowald, N.: Revisiting atmospheric dust export to the Southern Hemisphere ocean: Biogeochemical implications, *Global Biogeochemical Cycles*, 22, 2008.

Webster, P. J.: The role of hydrological processes in ocean-atmosphere interactions, *Reviews of Geophysics*, 32, 427-476, 1994.

Yoo, J.-M. and Carton, J. A.: Annual and interannual variation of the freshwater budget in the tropical Atlantic Ocean and the Caribbean Sea, *Journal of physical Oceanography*, 20, 831-845, 1990.

Yu, L. and Weller, R. A.: Objectively analyzed air-sea heat fluxes for the global ice-free oceans (1981-2005), *Bulletin of the American Meteorological Society*, 88, 527-539, 2007.

Zender, C. S., Bian, H., and Newman, D.: Mineral Dust Entrainment and Deposition (DEAD) model: Description and 1990s dust climatology, *Journal of Geophysical Research: Atmospheres* (1984-2012), 108, 2003.

Zhang, Y., Mahowald, N., Scanza, R., Journet, E., Desboeufs, K., Albani, S., Kok, J., Zhuang, G., Chen, Y., and Cohen, D.: Modeling the global emission, transport and deposition of trace elements associated with mineral dust, *Biogeosciences (BG)*, 12, 5771-5792, 2015.

Chapter 5

The dissolved aluminium plume of the Congo River

This manuscript is in preparation for *Geophysical Research Letters*

Jan-Lukas Menzel Barraqueta¹, Eric P. Achterberg¹, Stephan Krisch¹, Bernhard Wenzel¹, Martha Gledhill¹, Pablo Lodeiro¹, Martin Frank¹, Mark Hopwood¹, Christian Schlosser¹

¹ *GEOMAR, Helmholtz Centre for Ocean Research Kiel, Germany*

Abstract

The distribution of dissolved aluminium (dAl) was investigated in surface ocean waters along the flow path of the Congo River plume. The dAl concentrations were highest in the vicinity of the river mouth, reaching $1.7 \mu\text{mol L}^{-1}$ at the lowest salinity (24) and extended as far as 1300 km offshore into the tropical South Atlantic Ocean. Dissolved Al correlated negatively with salinity in subsurface samples (ca-15-20 m depth) obtained using a trace metal clean CTD rosette ($R^2=0.95$) and surface samples (3-4 m depth) collected using a towfish ($R^2=0.84$), suggesting a conservative behavior in the plume. Colloid formation or organic complexation are possible mechanisms that prevented of removal by particle scavenging of dAl, with this stabilization likely facilitated by dissolved organic matter concentrations in the Congo River. This study shows that the riverine dAl signal can be detected far away from its riverine source and indicates the importance of high resolution surface water sampling using a towfish. The Congo River accounts for an estimated 7.5% of the global riverine dAl flux, making this river with its globally second largest discharge volume, an important source for this element.

1 Introduction

Rivers are a major source to the ocean of particulate materials and dissolved compounds, including nutrients, metals and metalloids (Carey et al., 2002), supplying ca. $20 \times 10^3 \text{ Gt yr}^{-1}$ (Meybeck, 1976). The riverine elemental fluxes to the oceans depend on factors such as the extent of weathering in catchments and anthropogenic inputs to the rivers (Zhang and Liu, 2002).

The Congo is the second largest river in the world in terms of drainage basin size ($3.7 \times 10^6 \text{ km}^2$) and average water discharge rate ($45,000 \text{ m}^3 \text{ s}^{-1}$), after the Amazon (Laraque et al., 2009; Spencer et al., 2014). Total annual river water discharge to the ocean is estimated to be around $37,400 \text{ km}^3 \text{ yr}^{-1}$ (Baumgartner, 1975). The Congo River exhibits a bimodal seasonal hydrological cycle with maximum discharges occurring in November-December and May, and minimum discharges in March and August (Eisma and van Bennekom, 1978). The discharge peaks are related to latitudinal shifts of the Intertropical Convergence Zone (ITCZ) (Bouillon et al., 2012), and consequently enhanced precipitation in the drainage basins of the northern Congo tributaries (November-December), and increased discharge of the southern tributaries (May) (Coynel et al., 2005). River biogeochemistry is closely related to the variability in catchment area and differences in terrigenous source. Total dissolved solute concentrations in the Congo River are among the lowest of all major rivers (ca. 37 mg L^{-1}) and about four times lower than the median global river value (150 mg L^{-1}) (Gaillardet et al., 1999). In contrast, the Congo River is enriched in dissolved Si, trace metals, and dissolved organic carbon (DOC) (Spencer et al., 2014).

The remoteness and low population density of the Congo River catchment area, and regional political instability (Prunier, 2008), make the Congo River the most understudied large river of the world. Anthropogenic impacts such as industrial logging, land use changes, settlement expansion, and the extraction of mineral oil and gas in near coastal waters may affect river discharges and biogeochemical processes in the estuary and beyond (Laporte et al., 2007). The latter impacts can induce fluctuations in environmental conditions which may influence trace metal fluxes to the ocean. Therefore, elemental studies within the Congo River and plume are urgently required (Spencer et al., 2014).

Aluminium in the coastal waters and oceans originates from mineral dust deposition (Measures and Vink, 2000), efflux from sediments, and riverine discharges including runoff from sulfidic and urban soils and industrial emissions (Harford et al., 2011; Powell and Martens, 2005). Dissolved aluminium in the oceans is used as a tracer for mineral dust deposition (Measures and Brown, 1996) and water mass mixing (Measures and Edmond, 1990). Globally, dAl concentrations in river waters range from 50 nM to $>5\mu\text{M}$ with an average dAl concentration of $1.18\ \mu\text{M}$ (Gaillardet et al., 2003). In estuarine mixing zones, physicochemical variables such as salinity, suspended organic matter, temperature, pH, ionic strength, and dissolved O_2 influence the rates of sorption/desorption, dissolution/precipitation, and flocculation, which are the key processes controlling the cycling of trace metals in estuarine waters (Morel et al., 1991). Dissolved aluminium is reported to be efficiently removed in estuarine regions due to its high particle affinity at high ionic strength and pH. Most dAl is considered to be removed below at low salinities (< 15) (Brown and Bruland, 2009; Hydes and Liss, 1977), with only a small fraction (ca. 40%) reaching coastal waters (Brown and Bruland, 2009). The main

mechanisms responsible for the removal of dAl from solution during estuarine mixing are flocculation of riverine microcolloids (Sholkovitz, 1978) and adsorption onto suspended sediment particles (Morris et al., 1986).

The aim of this work is to examine the behaviour of dAl in the Congo Plume and evaluate its input to the South Atlantic Ocean. We present dAl data from subsurface samples (ca. 15-20 m depth) obtained using a trace metal clean CTD rosette ($R^2=0.95$) and surface samples (3-4 m depth) collected using a towfish along with salinity as a freshwater tracer, sampled in the region from the river mouth to as far as 1700 km offshore. We discuss the possible dAl sources to and stabilization mechanisms in waters of the study region.

2 Materials and Methods

We present new data from GEOTRACES cruise GA08 (Meteor cruise M121) in the Southeast Atlantic conducted in austral summer: 15 November to 26 December, 2015 (Figure 1). Surface seawater was pumped from ca. 3 m depth with a towfish directly into a trace metal clean laboratory container. Full water column profile samples were obtained using GO-FLO bottles (Ocean Test Equipment) attached to a trace metal clean rosette frame. Samples for trace metal analysis were collected in 125 mL acid cleaned low density polyethylene bottles (Nalgene) and acidified to a pH of ~ 1.8 by adding HCl (Ultra-pure-Acid UpA, Romil) as described in (Menzel Barraqueta et al., 2018). Dissolved Al was analysed following the batch Lumogallion method of Hydes and Liss (1976). All samples were analysed in a clean laboratory (ISO 5) at GEOMAR.

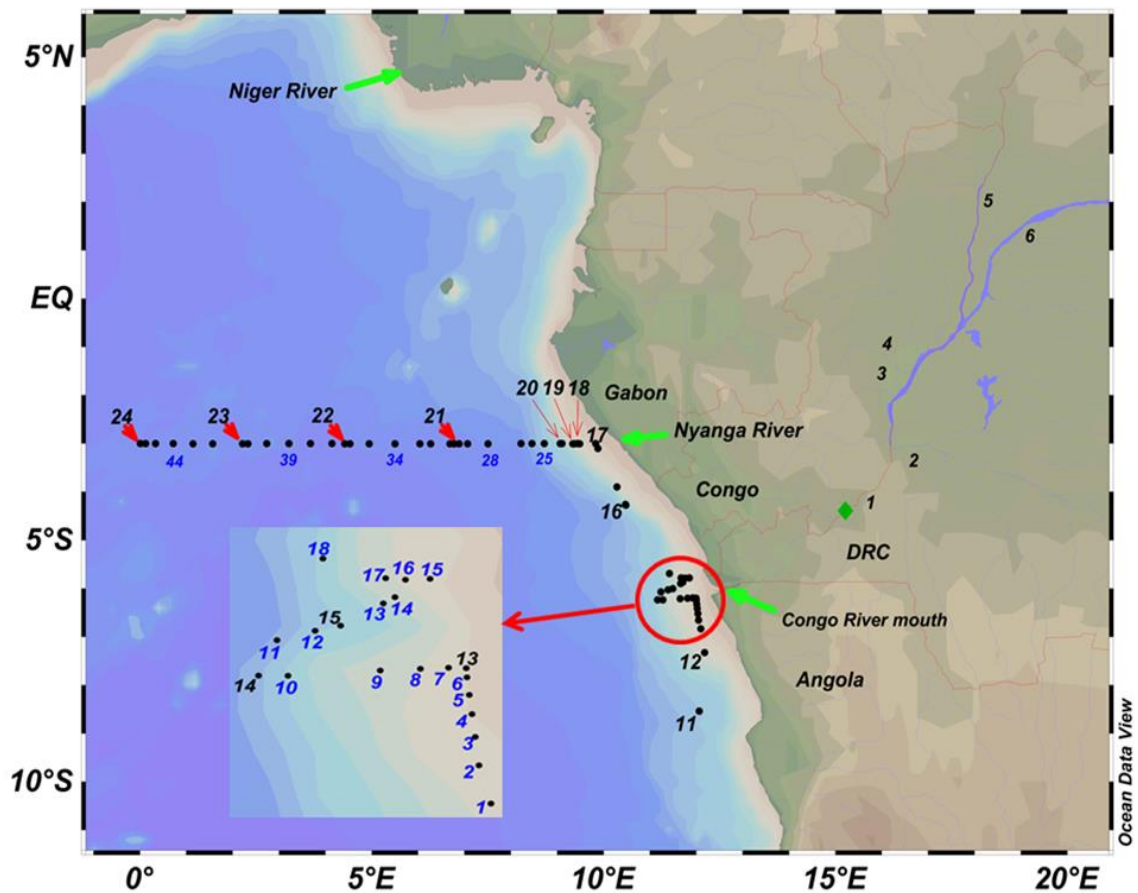


Figure 5.1: Map showing the locations of CTD casts (numbers 11 to 24) and towfish samples (blue numbers 1 to 46). Black numbers (1 to 6) show dAl sampling sites in the northern and southern tributaries draining in the Congo Basin (Dupre et al., 1996). Green diamond shows the location of the cities Brazzaville and Kinshasa. Thick green arrows show the position of the Congo, Nyanga, and Niger River mouths. DRC: Democratic Republic of Congo.

Acidified samples were buffered offline to a pH between 5.1 and 5.2 with a 2M ammonium acetate buffer (Romil, UpA). Buffered samples were spiked with a 2 mgL⁻¹ lumogallion (TCI) solution, prepared in 2 M ammonium acetate buffer. After spiking, samples were heated for 1.5 h at 80°C in an oven (Heratherm, Thermo Scientific) and left to cool down overnight to room temperature to facilitate the formation of a fluorescent Al complex. Samples were measured using a fluorescence spectrophotometer (Cary Eclipse, Agilent) with an excitation and emission wavelength of 465 and 555 nm, respectively. All samples were analysed in duplicate and concentrations calculated from the peak heights via standard addition as

described in Chapter 2. GEOTRACES reference seawater (GS) was run and yielded a mean dAl concentration of 27.8 ± 0.2 nM ($n=4$). The obtained value is within error identical to the GEOTRACES consensus values of 27.5 ± 0.2 nM (May 2013) (www.geotraces.org).

3 Results and discussion

3.1 Extension of the Congo River plume

Salinities ranged from 33.6 to 36 (Figure 5.2). Evidence of freshwater inputs ($S=35.4 \pm 0.2$) and elevated suspended particle concentrations (transmission= $97.35 \pm 0.09\%$; $n=2$) was observed south of the Congo River mouth, at ca. 8.5°S 12°E (St. 11 and 12). A shallow ($\sim 6\text{m}$) surface lens of reduced salinities (below 33.2) and reduced transmission (down to 72%) was observed at St. 13, perpendicular to the river mouth, in an offshore direction (St. 13 to 15) and expanded northwards. This is in accordance with the general NW extension of the Congo river plume during austral summer (Hopkins et al., 2013) and with observations made by Cadée (1984) and Pak et al. (1984) of freshwater signals reaching 8°E and 8.15°S showing inter-seasonal and intra-annual variability in the transfer direction of the Congo River Plume. Modelled plume dispersion analysis for the Congo River Plume for the season when our study took place (November-December) also show a narrow freshwater lens flowing south (Denamiel et al., 2013). At St. 16 (215 km north and 170 km west of the river mouth) the shallow surface water lens of reduced salinity and transmission persisted and became deeper ($z=14$ m) further north at 3°S 9.8°E (St.17).

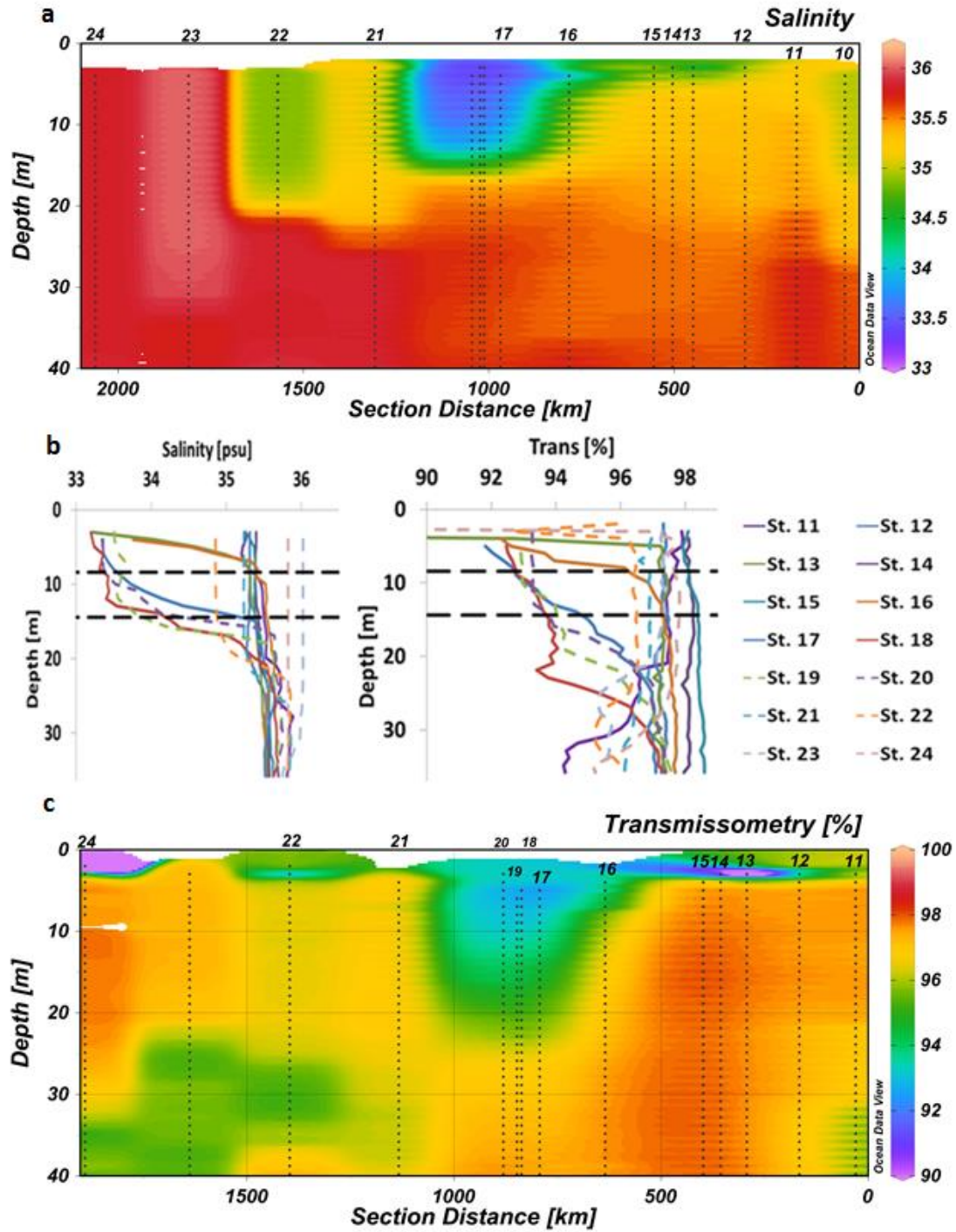


Figure 5.2: a) and c) Section plot for salinity and transmission [%] data for the CTD casts. b) Profiles for salinity and transmission for the CTD casts. Horizontal black dashed lines represent the approximate depths at which the shallowest subsurface water sample was taken.

This deepening of the freshwater lens may have been associated with advection of freshwater inputs from the Nyanga River which feeds the Congo plume at ca. 3°S (Figure 5.1) (Denamiel et al., 2013). Along 3°S, the plume was still present at 4.4°E (St. 22) based on salinity data. Station 21 did not show any influence of freshwater addition, indicating that the Congo River plume at that point, was formed by wind driven fresh water filaments (Hopkins et al., 2013). Salinity data from the ship's flow-through seawater system ($z=5$ m) revealed reduced salinities (<35) up to 3.6°E and 3°S and minimum salinities (<26) north of the river mouth at ca 4°S 10°E (Figure 5.3). Based on measurements of the $^{224}\text{Ra}/^{228}\text{Ra}$ ratios, Vieira et al. (unpublished data) estimated that the Congo River freshwater plume spreads in a northward direction at a velocity of 21 cm s^{-1} between 6°S 11.5°E (Congo River mouth) and ca. 4°S 10.5°E (Figure 5.1).

3.2 Dissolved Al in the Congo plume

Elevated concentrations of dAl coincided with low salinities (Figure 5.3). Dissolved Al correlated negatively with salinity ($R^2=0.95$ $n=14$ for CTD samples for the salinity range 33.89 to 36.0; $R^2=0.84$ $n=42$ for towfish samples for the salinity range 24.35 to 35.81) (Figure 5.4). The mean dAl concentrations for the salinity ranges 24-30, 30-34, and >34 were $1.2\pm 0.49 \mu\text{M}$ ($n=3$), $0.3\pm 0.22 \mu\text{M}$ ($n=12$), and $71\pm 152 \text{ nM}$ ($n=41$), respectively. Maximum dAl concentrations of up to $1.7 \mu\text{M}$ were measured in the lowest salinity samples (down to 24, Fish 14 in Figure 5.3). Likewise, maximum dFe (up to $1.2 \mu\text{M}$) and dMn (up to 54 nM) concentrations coincided with lowest salinities (data not shown). Similar coincidence was found for the Tagus estuary plume (Tonnard et al., 2018).

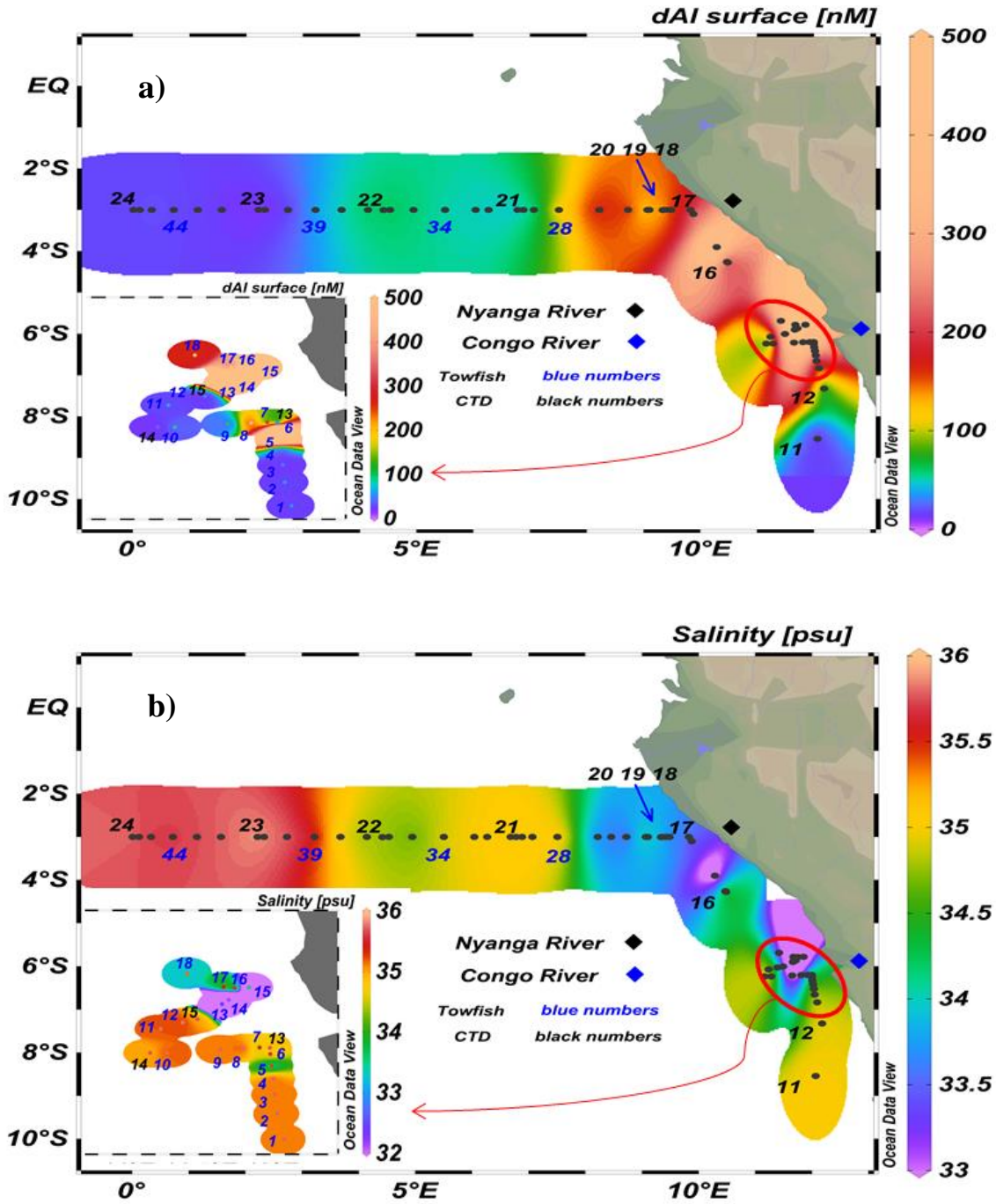


Figure 5.3: a) Dissolved Al for the Congo Plume; b) salinity for the Congo River Plume

That the observations for maximum dAl, dFe, and dMn coincided with the lowest salinity, indicates a common origin and control on transport mechanisms. Dupré et al. (1996) found a significant correlation between dAl and dFe concentrations in river waters of the Congo Basin. Dissolved Al concentrations (CTD sampling) were highest at St. 17 which may have been influenced by additional freshwater Al inputs from the Nyanga River. Elevated concentrations of dAl (up to 49 nM) at reduced salinities (34.8) are noticeable up to station 22 at ca. 3°S 4.4°E. Van Der Loeff et al. (1997) reported dAl concentrations (up to 50 nM) at ca. 6°S 0°E and suggested an influence from the Congo River plume. van Bennekom and Jager (1978) measured dAl concentrations of 29.6 nM ($S > 35.2$) in the vicinity of the Congo River mouth, which agree well with our dAl concentrations (29.3 ± 8.6 nM, $n=18$) for the same region. Our dAl concentrations above salinity 34 are similar to average dAl concentrations in the Conway estuarine plume (average of 55 nM) (Hydes and Liss, 1977).

The observed strong correlation between dAl and salinity indicates that dAl behaves conservatively in the salinity region above 33.9, with physical mixing determining the dAl distribution along the plume. Strong correlation between dAl and salinity has been reported for the Yakutak, Columbia, Copper and Tamar River plumes (Brown and Bruland, 2009; Brown et al., 2010; Morris et al., 1986) (Figure 5.4) and in the Tagus estuary plume Tonnard et al. (2018). However, dAl concentrations from the towfish (salinities > 24) displayed a weaker correlation with salinity, indicating a weaker stabilization of dAl at lower salinities.

The dAl concentration (1.7 μM) at salinity 24 for GA08 was somewhat higher than dAl (0.94 μM) observed at a salinity of 24.5 in the Congo River plume by van

Bennekom and Jager (1978). The difference could be caused by variations in estuarine conditions which feature dynamic dissolution processes of e.g. authigenic aluminosilicates, which are produced through diagenetic processes in reducing sediments and mobilized during tidal activity as observed in the Tamar estuary (Mackin and Aller, 1984; Morris et al., 1986). van Bennekom and Jager (1978) suggested a net addition of dAl within the Congo estuary rather than net removal of dAl as reported for the Chikugogawa (Hosokawa et al., 1970) and Conway (Hydes and Liss, 1977) estuaries. A change in soil weathering conditions along the Congo River watershed cannot be excluded in the time gap between both expeditions (40 years) as inter-decadal variations in river discharge due to differences in precipitation have been noticed (Laraque et al., 2009).

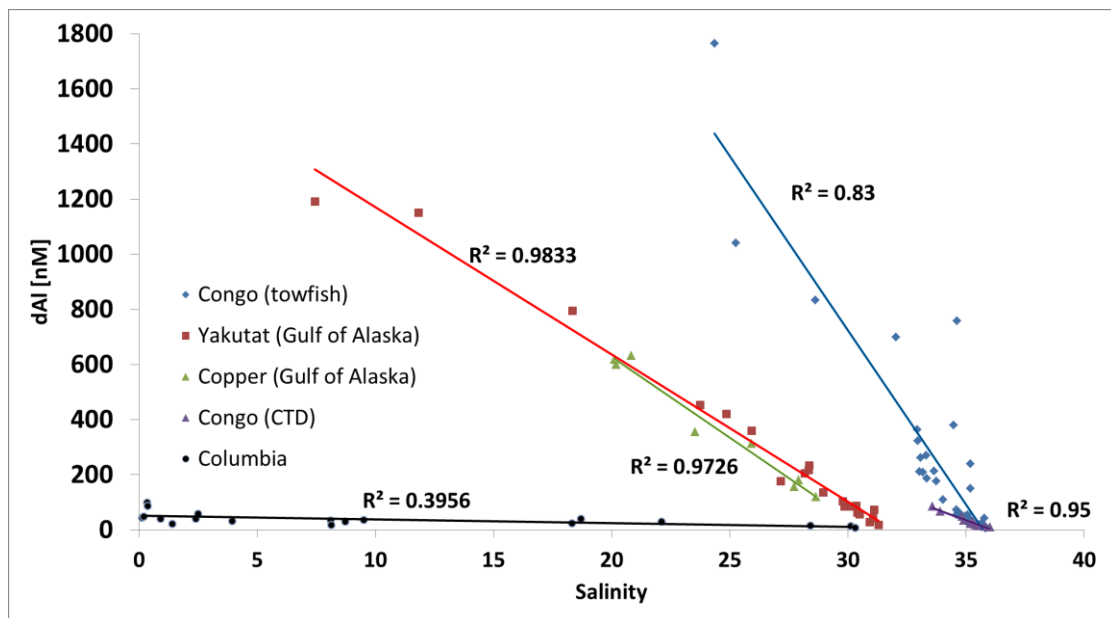


Figure 5.4: Dissolved aluminium against salinity for this study and the Yakutat, Copper, and Columbia estuaries (Brown and Bruland, 2009; Brown et al., 2010)

Inter-seasonal variations in dFe concentrations at salinity 0, ca. 10 km upstream of the river mouth (unpublished data), indicate the influence of high and low flushing periods of the Congo River. The latter likely applies to dAl as the dissolved concentrations of Al and Fe in the Congo River show a significant correlation, and thus a similar behavior (Dupré et al., 1996). Our measured dAl concentrations in the plume waters can be considered a lower limit. This is due to sampling occurring during the Congo River water discharge peak, thus containing higher suspended particle loads and concomitant a potential removal of dAl from solution by adsorption (Angel et al., 2015; Morris et al., 1986).

3.3 Dissolved aluminium in the Congo River and worldwide rivers

The dissolved Al freshwater endmember (salinity 0) was estimated to be $4.5 \pm 0.4 \mu\text{M}$ based on the linear correlation between dAl and salinity (both datasets together). Upstream of the major cities of the Congo watershed (Brazzaville and Kinshasa, 11.5 million inhabitants, number 1 in Figure 5.1) the observed dAl concentration was $2.8 \mu\text{M}$ (Dupré et al., 1996), with dAl concentrations for the major tributaries ranging between $0.44\text{--}14.2 \mu\text{M}$ (Dupré et al., 1996). Our results therefore are within the range determined by Dupré et al. (1996). Trace element concentrations (e.g. dAl) in the Congo River are among the highest in the world for rivers (Dupré et al., 1996; Gaillardet et al., 2003). For the published data for other major rivers (Table 5.1), only the Yellow River, the most turbid river in the world (Zhang and Huang, 1993), shows higher dAl concentrations ($5.9 \mu\text{M}$) (Zhang et al., 1999). Rivers with water discharges in the same order of magnitude as the Congo River and the Amazon River (water discharge one order of magnitude higher than the Congo River) show dAl concentrations below $1.48 \mu\text{M}$ (Table 5.1 and references therein).

Table 5.1: Average concentration of dAl, DOC, water discharge, and estimated dAl flux for different rivers assuming conservative mixing behaviour.

River	Mean water discharge ($\text{m}^3 \text{s}^{-1}$)	Average dAl (μM)	Average DOC (mgL^{-1})	Riverine dAl flux (ktyr^{-1})	Reference
Amazon	209000	1.48	5	263	<i>Gibbs, 1972</i>
Columbia	7500	0.07	2.7	0.4	<i>Brown and Bruland, 2009</i>
Congo	45000	2.8	8.45	107	<i>Dupre et al., 1996</i>
Congo*	45000	4.5	-	44-175	<i>This study</i>
Conway	19	0.95	-	1.5×10^{-5}	<i>Hydes and Liss, 1976</i>
Danube	7130	0.4	4.8	2.4	<i>Guieu and Martin, 2002</i>
Mississippi	17792	1.1	8	16.7	<i>Taylor et al., 1995</i>
Niger	5590	0.16	2.1	0.76	<i>van Bennekom and Jager, 1978</i>
Pearl	11100	1.24	0.97	11.7	<i>Zhang et al., 1999</i>
St. Lawrence	10100	1.18	3.7	10.5	<i>Takayanaki and Gobeil, 2000</i>
Yangtze	30166	0.61	1.85	15.6	<i>Zhang et al., 1999</i>
Yellow	2571	5.9	3.2	12.9	<i>Zhang et al., 1999</i>
Average	37400	1.7	4.1	1.8	

The latter values are similar to the average world river dAl concentration (Meybeck, 1988). In contrast, lowest dAl concentrations (0.2 and 0.1 μM) were measured in the Niger (van Bennekom and Jager, 1978) and Columbia River (Brown and Bruland, 2009), respectively. Brown and Bruland (2009) attributed the low dAl concentrations in the Columbia River to enhanced presence of suspended particles and enhanced river flow (12000 m^3s^{-1} in comparison to a mean annual flow of 7300 m^3s^{-1}).

Elevated dAl concentrations in fresh waters have been attributed to high levels of DOC which can lead to enhanced fraction of dAl associated with organic complexes (Perdue et al., 1976) such as colloidal humic acids (Bruland et al., 2014). The amount of DOC in rivers is influenced by the river discharge (e.g. flushing effect), basin slope, and amount of soil carbon in the catchment area. The soil organic pool is partly transferred as DOC to rivers. High levels of DOC in the Congo River are thus a consequence of the Congo Basin draining humid and tropical rainforest regions of Africa (Martins and Probst, 1991) in combination with a strong flushing effect. Both, soil organic carbon and annual river water discharge, display globally significant correlations with river DOC flux ($R^2=0.6$ and $R^2=0.93$, respectively) which leads to the highest worldwide DOC flux found between 0° and 30°S (Li et al., 2017).

The high dAl signal of the Congo River plume in comparison to other rivers (e.g. Figure 5.4, Table 5.1) may be associated the Congo Basin draining and thus mobilizing high levels/amounts of organic matter (e.g. DOC) (van Bennekom and Jager, 1978).

Thus the elevated DOC concentrations (8.5 mg L^{-1}) of the Congo River could lead to enhanced fraction of dAl associated with organic matter, either due to Al-organic ligand complexation, or association of organic matter in Al colloidal material as suggested for the Columbia River by Brown and Bruland (2009).

3.4 Congo River dissolved aluminium flux and comparison of dissolved aluminium fluxes

Riverine trace metal fluxes to the ocean are difficult to estimate and are subject to uncertainties in the range of 20%, due to undersampling of representative river systems and the inaccuracy of historical river trace metal data (Bruland et al., 2014). Using the average Congo River water discharge ($45000 \text{ m}^3\text{s}^{-1}$) and assuming a conservative mixing from freshwater to oceanic waters we estimated a dAl riverine flux of $109 \pm 65 \text{ Kt yr}^{-1}$. Taking into account the average river dAl concentration ($1.7 \text{ }\mu\text{M}$, $n=11$, compiled in this study) and the global river water discharge, we estimated a global river dAl flux of 1.45 Mtyr^{-1} which agrees well with the estimation made by Chester (2009) of 1.24 Mtyr^{-1} . Other major sources of dAl to the ocean are atmospheric deposition and hydrothermal vents, representing Al fluxes (dAl + particulate Al) of 35.77 Mtyr^{-1} and 9.71 Ktyr^{-1} , respectively. Additional Al sources to the ocean from the shelf and sediments are likely important, but remain unquantified (Rauch and Pacyna, 2009).

Taken together, this suggests that the Congo River is a major source of dAl to the ocean, accounting for 7.5% of the global riverine dAl flux. Despite the Amazon River having a freshwater discharge one order of magnitude larger than the Congo River, the estimated dAl flux (263 ktyr^{-1}) is of the same order of magnitude as for

the Congo River. Together (Amazon + Congo) they account for 25% of the global riverine dAl flux to the ocean.

4 Conclusions

The Congo River is the second largest riverine source of dAl (7.5% of total dAl flux) to the global ocean, and the advection of dAl in the Congo River plume can be detected up to 1300 km away from the river mouth. The Congo River Plume presents high dAl concentrations which in combination with the high levels of DOC of the Congo River suggest that dAl may be stabilized and kept in solution through colloidal association and/or organic complexation. This study indicated that sampling very shallow water with a towfish revealed long-range offshore transport of dAl within the Congo River Plume which can be omitted when sampling with a regular CTD.

Acknowledgments

We thank the crew and officers of FS Meteor and our colleagues K. Kunde, G. Merschel, and R. Zitoun for their help during M121. This work was funded by a PhD Fellowship of the Department of Scientific Politics of the Basque government to JLMB and supported by GEOMAR. Cruise M121 was funded by the DFG. The authors declare no competing financial interests.

References

- Angel, B. M., Apte, S. C., Batley, G. E., and Golding, L. A.: Geochemical controls on aluminium concentrations in coastal waters, *Environmental Chemistry*, 13, 111-118, 2015.
- Baumgartner, F.: The world water balance: mean annual global, continental and maritime precipitation, *Evaporation and Runoff*, 179, 1975.
- Bouillon, S., Yambélé, A., Spencer, R., Gillikin, D., Hernes, P., Six, J., Merckx, R., and Borges, A.: Organic matter sources, fluxes and greenhouse gas exchange in the Oubangui River (Congo River basin), *Biogeosciences*, 9, 2045-2062, 2012.
- Brown, M. T. and Bruland, K. W.: Dissolved and particulate aluminum in the Columbia River and coastal waters of Oregon and Washington: Behavior in near-field and far-field plumes, *Estuarine, Coastal and Shelf Science*, 84, 171-185, 2009.
- Brown, M. T., Lippitt, S. M., and Bruland, K. W.: Dissolved aluminum, particulate aluminum, and silicic acid in northern Gulf of Alaska coastal waters: Glacial/riverine inputs and extreme reactivity, *Marine Chemistry*, 122, 160-175, 2010.
- Bruland, K., Middag, R., and Lohan, M.: Controls of trace metals in seawater. In 'Treatise on Geochemistry'.(Eds H. Holland and K. Turekian.) pp. 19–51. Elsevier: Amsterdam, Netherlands, 2014.
- Cadée, G.: Particulate and dissolved organic carbon and chlorophyll a in the Zaire River, estuary and plume, *Netherlands Journal of Sea Research*, 17, 426-440, 1984.
- Carey, A. E., Nezat, C. A., Lyons, W. B., Kao, S. J., Hicks, D. M., and Owen, J. S.: Trace metal fluxes to the ocean: The importance of high-standing oceanic islands, *Geophysical research letters*, 29, 2002.
- Chester, R.: *Marine geochemistry*, John Wiley & Sons, 2009.
- Coynel, A., Seyler, P., Etcheber, H., Meybeck, M., and Orange, D.: Spatial and seasonal dynamics of total suspended sediment and organic carbon species in the Congo River, *Global Biogeochemical Cycles*, 19, 2005.
- Denamiel, C., Budgell, W. P., and Toumi, R.: The Congo River plume: Impact of the forcing on the far-field and near-field dynamics, *Journal of Geophysical Research: Oceans*, 118, 964-989, 2013.

Dupré, B., Gaillardet, J., Rousseau, D., and Allègre, C. J.: Major and trace elements of river-borne material: the Congo Basin, *Geochimica et Cosmochimica Acta*, 60, 1301-1321, 1996.

Eisma, D. and van Bennekom, A. J.: The Zaire river and estuary and the Zaire outflow in the Atlantic Ocean, *Netherlands Journal of Sea Research*, 12, 255-272, 1978.

Gaillardet, J., Dupré, B., Louvat, P., and Allègre, C.: Global silicate weathering of silicates estimated from large river geochemistry, *Chemical Geology, Special issue Carbon Cycle*, 7, 3-30, 1999.

Gaillardet, J., Viers, J., and Dupré, B.: Trace elements in river waters, *Treatise on geochemistry*, 5, 605, 2003.

Harford, A., Hogan, A., Tsang, J., Parry, D., Negri, A., Adams, M., Stauber, J., and Van Dam, R.: Effects of alumina refinery wastewater and signature metal constituents at the upper thermal tolerance of: 1. The tropical diatom *Nitzschia closterium*, *Marine pollution bulletin*, 62, 466-473, 2011.

Hopkins, J., Lucas, M., Dufau, C., Sutton, M., Stum, J., Lauret, O., and Channelliere, C.: Detection and variability of the Congo River plume from satellite derived sea surface temperature, salinity, ocean colour and sea level, *Remote Sensing of Environment*, 139, 365-385, 2013.

Hosokawa, I., Ohshima, F., and Kondo, N.: On the concentrations of the dissolved chemical elements in the estuary water of the Chikugogawa river, *Journal of Oceanography*, 26, 1-5, 1970.

Hydes, D. and Liss, P.: The behaviour of dissolved aluminium in estuarine and coastal waters, *Estuarine and Coastal Marine Science*, 5, 755-769, 1977.

Hydes, D. and Liss, P.: Fluorimetric method for the determination of low concentrations of dissolved aluminium in natural waters, *Analyst*, 101, 922-931, 1976.

Laporte, N. T., Stabach, J. A., Grosch, R., Lin, T. S., and Goetz, S. J.: Expansion of industrial logging in Central Africa, *Science*, 316, 1451-1451, 2007.

Laraque, A., Bricquet, J. P., Pandi, A., and Olivry, J. C.: A review of material transport by the Congo River and its tributaries, *Hydrological processes*, 23, 3216-3224, 2009.

Li, M., Peng, C., Wang, M., Xue, W., Zhang, K., Wang, K., Shi, G., and Zhu, Q.: The carbon flux of global rivers: A re-evaluation of amount and spatial patterns, *Ecological Indicators*, 80, 40-51, 2017.

Mackin, J. E. and Aller, R. C.: Diagenesis of dissolved aluminum in organic-rich estuarine sediments, *Geochimica et Cosmochimica Acta*, 48, 299-313, 1984.

Martins, O. and Probst, J.: Biogeochemistry of major African rivers: carbon and mineral transport, 1991. 1991.

Measures, C. and Edmond, J.: Aluminium in the South Atlantic: steady state distribution of a short residence time element, *Journal of Geophysical Research: Oceans* (1978–2012), 95, 5331-5340, 1990.

Measures, C. and Vink, S.: On the use of dissolved aluminum in surface waters to estimate dust deposition to the ocean, *Global biogeochemical cycles*, 14, 317-327, 2000.

Measures, C. I. and Brown, E. T.: Estimating Dust Input to the Atlantic Ocean Using Surface Water Aluminium Concentrations. In: *The Impact of Desert Dust Across the Mediterranean*, Guerzoni, S. and Chester, R. (Eds.), Springer Netherlands, Dordrecht, 1996.

Menzel Barraqueta, J. L., Schlosser, C., Planquette, H., Gourain, A., Cheize, M., Boutorh, J., Shelley, R., Pereira Contreira, L., Gledhill, M., Hopwood, M. J., Lherminier, P., Sarthou, G., and Achterberg, E. P.: Aluminium in the North Atlantic Ocean and the Labrador Sea (GEOTRACES GA01 section): roles of continental inputs and biogenic particle removal, *Biogeosciences Discuss.*, 2018, 1-28, 2018.

Meybeck, M.: Total mineral dissolved transport by world major rivers/Transport en sels dissous des plus grands fleuves mondiaux, *Hydrological Sciences Journal*, 21, 265-284, 1976.

Morel, F., Dzombak, D., and Price, N.: Heterogeneous reactions in coastal waters, *Ocean margin processes in global change*, 1991. 165-180, 1991.

Morris, A., Howland, R., and Bale, A.: Dissolved aluminium in the Tamar Estuary, southwest England, *Geochimica et Cosmochimica Acta*, 50, 189-197, 1986.

Pak, H., Zaneveld, J., and Spinrad, R.: Vertical distribution of suspended particulate matter in the Zaire river, estuary and plume, *Netherlands journal of sea research*, 17, 412-425, 1984.

Perdue, E. M., BECK, K. C., and REUTER, J. H.: Organic complexes of iron and aluminium in natural waters, *Nature*, 260, 418, 1976.

Powell, B. and Martens, M.: A review of acid sulfate soil impacts, actions and policies that impact on water quality in Great Barrier Reef catchments, including a case study on remediation at East Trinity, *Marine Pollution Bulletin*, 51, 149-164, 2005.

Prunier, G.: Africa's world war: Congo, the Rwandan genocide, and the making of a continental catastrophe, Oxford University Press, 2008.

Rauch, J. N. and Pacyna, J. M.: Earth's global Ag, Al, Cr, Cu, Fe, Ni, Pb, and Zn cycles, *Global Biogeochemical Cycles*, 23, 2009.

Sholkovitz, E. R.: The flocculation of dissolved Fe, Mn, Al, Cu, Ni, Co and Cd during estuarine mixing, *Earth and Planetary Science Letters*, 41, 77-86, 1978.

Spencer, R., Stubbins, A., and Gaillardet, J.: Geochemistry of the Congo River, estuary and plume, *Biogeochemical Dynamics at Large River-Coastal Interfaces: Linkages With Global Climate Change*, 2014. 554-584, 2014.

Tonnard, M., Planquette, H., Bowie, A. R., van der Merwe, P., Gallinari, M., Desprez de Gésincourt, F., Germain, Y., Gourain, A., Benetti, M., Reverdin, G., Tréguer, P., Boutorh, J., Cheize, M., Menzel Barraqueta, J. L., Pereira-Contreira, L., Shelley, R., Lherminier, P., and Sarthou, G.: Dissolved iron in the North Atlantic Ocean and Labrador Sea along the GEOVIDE section (GEOTRACES section GA01), *Biogeosciences Discuss.*, 2018, 1-53, 2018.

van Bennekom, A. J. and Jager, J. E.: Dissolved aluminium in the Zaire river plume, *Netherlands Journal of Sea Research*, 12, 358-367, 1978.

Van Der Loeff, M. R., Helmers, E., and Kattner, G.: Continuous transects of cadmium, copper, and aluminium in surface waters of the Atlantic Ocean, 50°N to 50°S: correspondence and contrast with nutrient-like behaviour, *Geochimica et Cosmochimica Acta*, 61, 47-61, 1997.

Zhang, J. and Liu, C.: Riverine composition and estuarine geochemistry of particulate metals in China—weathering features, anthropogenic impact and chemical fluxes, *Estuarine, coastal and shelf science*, 54, 1051-1070, 2002.

Synthesis and future recommendations

Synthesis and future recommendations

This work focused on the biogeochemical cycling of dAl in surface waters and water column of the Atlantic Ocean. The study of dAl in seawater is important as the element is used as a tracer for lithogenic inputs into the ocean (Measures and Brown, 1996) and water masses identification (Measures and Edmond, 1990). The suitability of dAl as a tracer of atmospheric aerosol deposition was assessed on two cruises in the North Atlantic Ocean and two cruises in the South Atlantic Ocean. This study has contributed to two of the key mission goals of the GEOTRACES project (Anderson et al., 2007; Anderson et al., 2014): (i) it has identified processes which control the distribution of dAl in the North Atlantic Ocean (Chapter 3), tropical Atlantic, Southeast Atlantic and South Atlantic Ocean (Chapter 4), and (ii) it has estimated atmospheric aerosol deposition (Chapter 5) and riverine fluxes (Chapter 6) of dAl to the ocean.

Chapter 3 investigated at high spatial resolution the distribution of dAl in the North Atlantic along GEOTRACES section GA01. This produced the largest high-resolution vertical and lateral dataset of dAl that exists in the North Atlantic Ocean (>40°N) and the first large dataset in the Labrador Sea. Over 500 seawater samples were collected at 32 stations between the Iberian Peninsula (Portugal) and Newfoundland (Canada). This dataset resolves a major deficiency in understanding, at high spatial resolution, the biogeochemical cycling of dAl in the North Atlantic Ocean and Labrador Sea. This work is under review as Menzel Barraqueta et al. (2018). A particularly novel finding from this work was that diatoms directly influence the transfer of dAl onto or into particulate Al in surface waters, as low concentrations of dAl and enhanced pAl to dAl ratios coincided with elevated pAl

and bSi concentrations. The latter has been acknowledged by many authors in the past (Middag et al., 2009; Orians and Bruland, 1985) but in these previous studies no pAl and bSi data were provided to explicitly demonstrate this mechanism. Also, the sole presence of elevated levels of bSi and pAl do not unambiguously prove the presence of diatoms, but additional HPLC diagnostic pigment data coupled with CHEMTAX analysis allowed the determination of the relative abundance of phytoplankton types within the whole phytoplankton community. The CHEMTAX results (Tonnard et al., in prep) showed that in the regions where we observed low levels of dAl and elevated levels of pAl and bSi diatoms were the dominant phytoplankton species.

An additional important finding was that dAl displayed, in general, a recycled type distribution along the section, whereas in other regions of the Atlantic Ocean dAl was found to display a scavenged type distribution (Measures et al., 2015; Middag et al., 2015). This recycled distribution seems to be coupled with surface uptake and the dissolution of diatoms frustules, as strong correlations between dAl and silicate are observed in depth profiles. However, the strong correlations between dAl and Si were not observed everywhere, as noted for the Iberian Basin, where additional sources of dAl from Mediterranean Overflow Waters and inputs from sediment resuspension with concomitant desorption of dAl from particles are proposed to be responsible for low correlations between dAl and Si. This has also been reported for the Pacific (Orians and Bruland, 1986) and Indian (Thi Dieu Vu and Sohrin, 2013) Oceans where continuous scavenging of dAl from the water column coincides with continuous addition of Si through remineralization; thus decoupling the dAl - Si relationship as a function of water mass age.

Finally, this study showed the importance of local dAl sources such as river runoff and ice melt in controlling the distribution of dAl in surface waters near continents. This study has also given evidence of dAl release from pore waters, as elevated levels of dAl were found close to the seafloor without concomitant increase in pAl concentrations. Interestingly, during this investigation it has been observed that sediments resuspension can act as both a source of dAl, through desorption of Al from the resuspended particles, or as a sink of dAl through scavenging of dAl by the resuspended particles. It was also noticed that during this study a major conservative source of dAl to mid depth waters of the Iberian Basin was additional Al inputs from Mediterranean Overflow Waters. In contrast, no hydrothermal source was observed over the Reyjannes Ridge.

Chapter 4 assess of the potential use of dAl as an atmospheric deposition tracer over the Atlantic Ocean. In this chapter the distribution of dAl in the surface mixed layer of the entire Atlantic basin was studied using a synthesis of data from the GEOTRACES Programme. These new datasets have now filled in gaps for regions where no, or limited, dAl data were available (Figure 6.1). The dAl distribution in surface waters showed marked regional differences, which are a consequence of varying degrees of Al sources and sinks in surface waters. These new datasets provide a baseline for future modelling studies, to test and improve the mechanisms that influence the biogeochemical cycling of Al in surface waters. The latter issue is critical if accurate estimates of atmospheric aerosol inputs to seawater are required, as a range of oceanic atmospheric aerosol deposition models use the concentrations of dAl in surface waters to derive deposition estimates. This chapter endeavoured to implement reasonable aerosol Al fractional solubilities for each study area according to new and extended datasets on aerosol Al fractional solubility (Baker et al., 2013;

Baker and Jickells, 2017; Baker et al., 2006). Aerosol Al fractional solubility is a vital parameter to estimate atmospheric aerosol deposition fluxes, and was addressed with caution as previous studies (Grand et al., 2014; Measures and Brown, 1996) used aerosol Al fractional solubilities that were 2 to 3 fold lower than proposed in the literature in this study. Having such a large dataset of surface dAl concentrations has allowed for the first time to calculate atmospheric deposition fluxes for remote regions of the North Atlantic, South Atlantic and Southeast Atlantic Ocean from observational field data. The atmospheric deposition fluxes provided in this chapter show, generally, a good agreement with prior modelling studies (Duce et al., 1991; Mahowald et al., 2005). However, it is important to notice that in remote regions far from main mineral dust sources the atmospheric deposition fluxes are generally lower than modelling inputs but in the same order of magnitude. Also it was shown that in regions where the surface water dAl concentrations are affected by enhanced inputs from non-mineral dust sources or enhanced removal by suspended ocean particles, the atmospheric deposition fluxes using dAl from surface waters are not reliable.

Chapter 5 presented the distribution of dAl within the Congo River plume in the Southeast Atlantic Ocean. Prior to this study, this area was undersampled, with only a few studies presenting surface dAl concentrations (Bowie et al., 2002; Van Der Loeff et al., 1997) and deep profiles of dAl concentrations (Measures, 1995). This study represents the largest dataset of dAl in this region and is the first dataset that has traced the influence that the Congo River plume has on dAl concentrations, which extends as far as 1300 km from the river mouth. Another study, some 40 years ago, showed the influence on dAl of the Congo River plume but only close to the river mouth (van Bennekom and Jager, 1978). This chapter showed, based on the

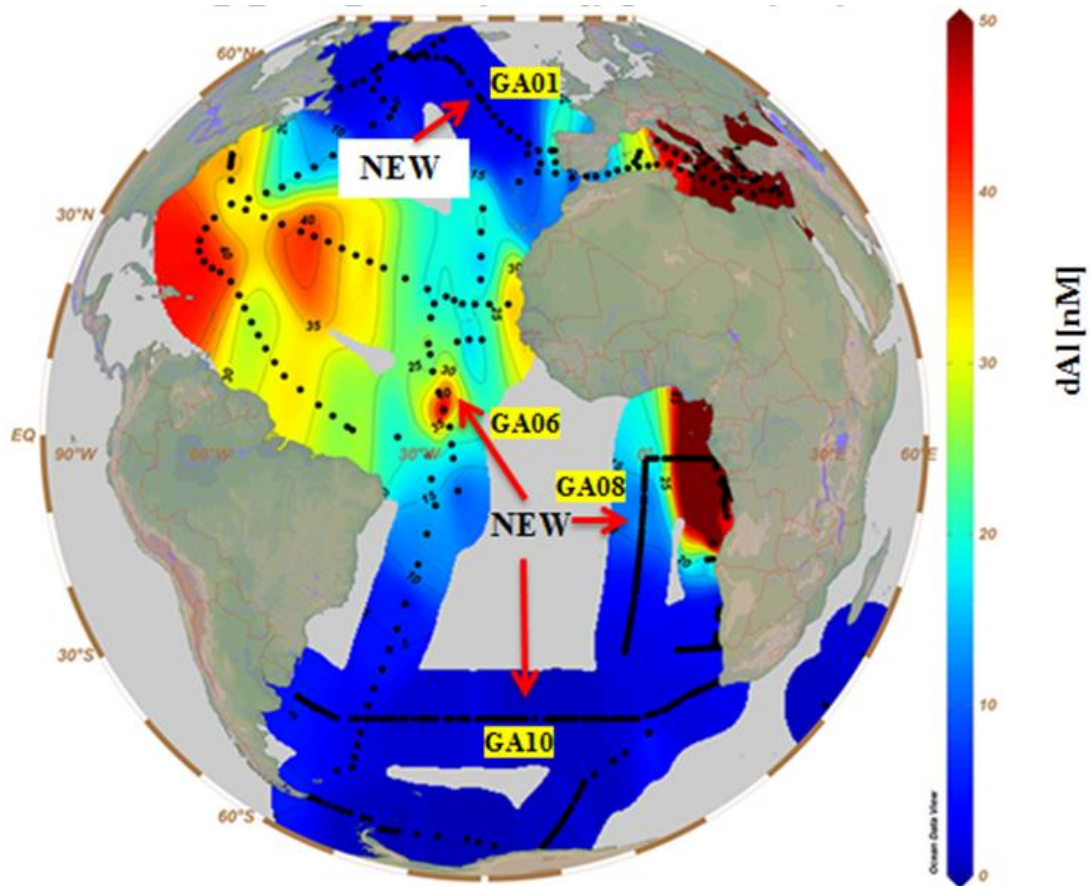


Figure 6.1: Surface dAl concentrations in the Atlantic Ocean, Mediterranean and Labrador Sea. New datasets are marked with GA01, GA06, GA08, and GA10. GA02, GA03, GA04N are data from Middag *et al.* (2015), Measures *et al.* (2015), Rolison *et al.* (2015), respectively.

plume extension, that the Congo River is a major source of dAl to surface waters of the South East Atlantic.

During this study we have calculated the approximate flux of dAl from the Congo River into the Southeast Atlantic Ocean and determined that the Congo River accounts for ca. 7.5 % of the global world river to ocean dAl flux. Of note is the critical importance demonstrated in this study of using a near-surface trace metal clean sampling system (towfish) (Achterberg, 2000), as the Congo River Plume flows as a shallow surface lens of freshwater, meaning that dAl signatures would have been missed entirely if only sampling using a CTD system with bottles closed

at ~15-20 m were used. The input of dAl from the Congo River Plume showed a conservative behaviour, as a strong correlation was found between salinity and dAl. However, this study also suggested that the elevated concentrations of dAl could be maintained or could be influenced by enhanced dissolved organic carbon and the presence of humic acids.

Overall, this study investigated the mechanisms that control the distribution of dAl in the Ocean and the sources and sinks of this element to and within the Ocean. A graphic representation of all the topics mentioned during chapters 3, 4, and 5 is given in Figure 6.2. In the latter figure we observed the different sources of Al to the ocean which are dry and wet atmospheric aerosol deposition, river-glacial runoff, Ice and sea ice melt, deep slope convection, diffusion from pore waters, hydrothermal activity, resuspension of sediments from the shelf, margins, and seafloor. We can also observe the cycling of dAl in the water column. The processes associated with dAl cycling in the ocean are dissolution from atmospheric aerosols deposited into surface waters, adsorption of dAl into abiotic particles, passive-active uptake of dAl onto biogenic particles and desorption of dAl from biogenic and non-biogenic particles. The processes within the ocean that distributes dAl into different water mass layers are also described (upwelling, deep water mass formation, and advection).

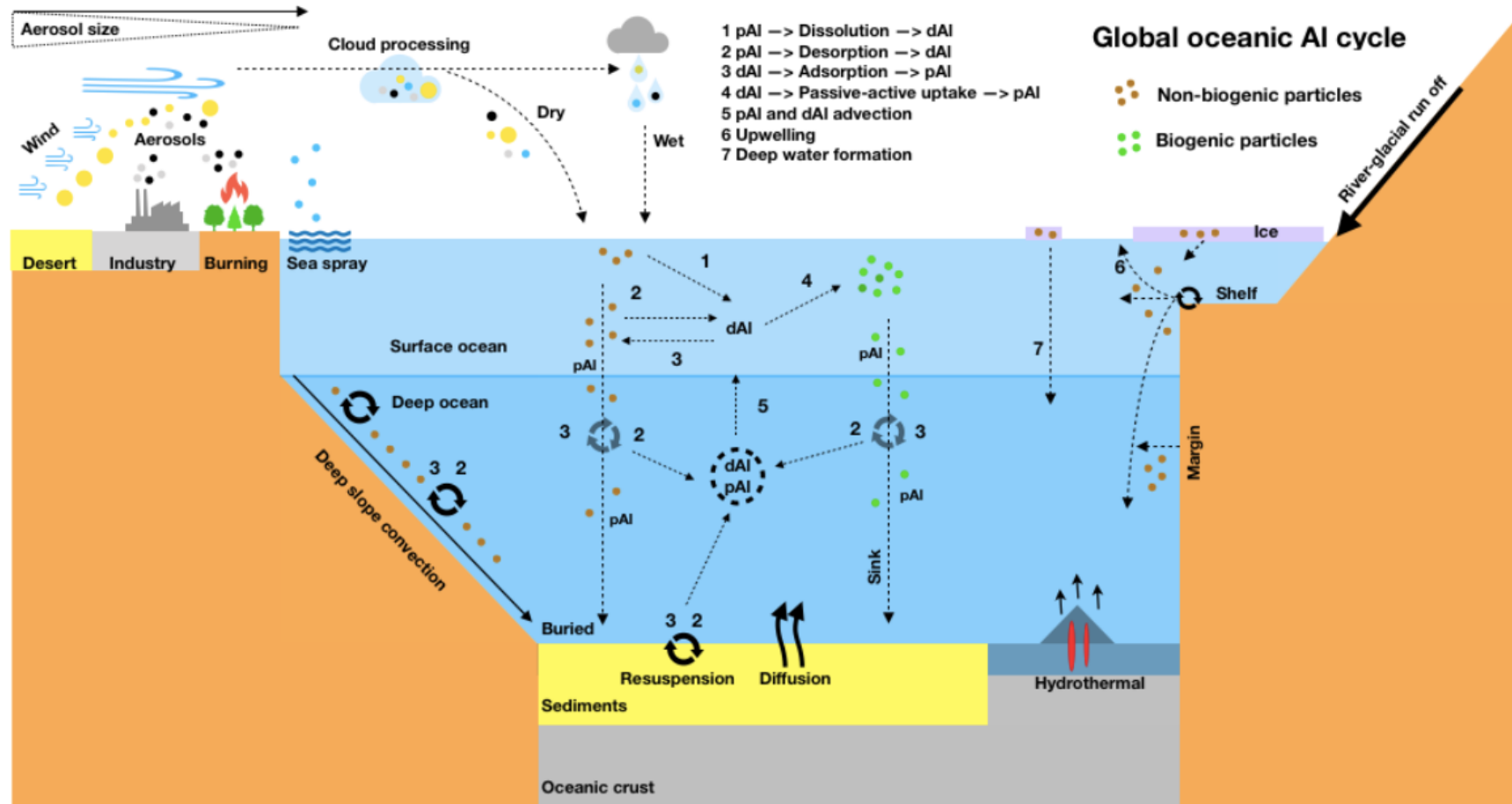


Figure 6.2: Global biogeochemical cycle of Al in the ocean.

Future recommendations

In the coming years the biogeochemical cycling of dAl should be investigated from a holistic point of view. The large inventory of chemical, physical, and biological parameters measured coincidentally during GEOTRACES cruises will help to understand the cycling of dAl in the ocean from new perspectives. For example, from the results given in chapter 4, it is clear that the behaviour of dAl in regions of enhanced primary productivity is closely related to phytoplankton bloom dynamics and community composition. In regions of low atmospheric aerosol deposition it is now clear that the relationship between the dissolved and the particulate phase of Al are closely related to the phytoplankton species assemblage that is present. In particular it is clear that biogenic silica is a major carrier for dAl into deep waters. This raises the question of whether the dAl is being actively taken up by diatoms or if there is a preferential passive uptake of dAl into or onto diatoms frustules compared to other particles. Therefore more studies, both in the field and in laboratory experiments, should aim to address these issues. To what extent different phytoplankton types affect the distribution of dAl in surface waters and in the water column remains unclear, as for example the potential role that other biogenic particles (e.g. CaCO_3 from coccolithophores or zooplankton faecal pellets) could have in the removal of dAl from surface waters and subsequent release of dAl with depth. The latter requires further investigation. There is still no knowledge on how dAl behaves in combination with pAl and biogenic particles during pre-bloom, bloom and post-bloom conditions. Also, there is little known about the role that soluble and colloidal Al fractions play within the transfer from the dissolved to the particulate fraction (Dammshäuser and Croot, 2012). Studies focusing on colloidal

Al have often been performed in estuaries and rivers but not in the open ocean. The role of soluble and colloidal phases has been extensively studied for iron and now is the turn of other metals such Al. Future research cruises in regions of high primary productivity should measure the different dissolved phases as well as the particulate phase in order to understand how the predominantly removal mechanism works. More emphasis need to be placed in measuring additional chemical parameters such as biogenic silica and particulate inorganic carbon, as combining these parameters will better enable mechanistic explanations for how and why dAl and pAl vary during phytoplankton blooms.

More emphasis needs to be put on identifying and constraining the sources of dAl to surface waters in order to reduce errors associated with atmospheric deposition fluxes. This is particularly pertinent for improving global biogeochemical models that use atmospheric deposition fluxes derived from dAl distributions (Gehlen et al., 2003; Han et al., 2008). In particular dAl sources from sediment resuspension and water mass advection should be further investigated, as few data exist in the literature. The latter would better constrain the residence times of dAl in the surface mixed layer, which is a key parameter to determine atmospheric deposition fluxes using surface water dAl concentrations. The residence time of dAl in the surface mixed layer is difficult to assess and many times a circular approach is being used when estimating atmospheric deposition. Specifically this arises from the use of residence times that themselves have been derived using model atmospheric deposition fluxes derived from dAl. Thus it is clear that more research is needed to assess residence times without using modelled atmospheric deposition estimates derived from dAl. Also, more emphasis needs to be placed on identifying the role of mineral dust deposition in adding dAl to surface waters or removing dAl from

surface waters (Ye and Völker, 2017). Although there has been a considerable progress in the assessment of the aerosol Al fractional solubility (notably in the Atlantic Ocean) there remains a lack of these estimations in the Pacific and Indian Oceans. The assessment of the parameters which affect the aerosol Al fractional solubility such as aerosol provenance and cloud processing should be addressed in more detail, especially in remote regions. Given the uncertainties of atmospheric deposition fluxes, it is highly recommended to use a multi tracer approach in order to reduce errors and allow for more precise atmospheric deposition flux calculations. Again, it is critical to have precise estimates of atmospheric deposition from the field so that global biogeochemical models which incorporate the role of atmospheric deposition can better constrain these inputs.

From results given in Chapter 6 it is clear that more importance need to be put into investigations of the role of organic complexation on the cycling of dAl in transition waters from freshwaters to saline waters. It seems that the concentrations of dAl in plume waters could be closely related to dissolved organic matter (e.g. humic and fulvic acids). Further research expeditions sampling river plumes should use near-surface sampling systems as it has been proved that regular sampling with trace metal clean bottles at ~10–20 m may not sample the plume and this would be a missed opportunity for that specific research expedition. It is also important, however difficult to do, to have continuous measurements of dAl with seawater sampled from a towfish. This method has been previously used (Vink et al., 2000) and should be implemented by more research groups as it would provide large sets of information on the fine scale mechanisms which control the distribution of dAl in surface waters. The latter is important for adequately interpreting large scale dAl surface distribution

References

Achterberg, E. P.: Automated techniques for real-time shipboard determination of dissolved trace metals in marine surface waters, *International Journal of Environment and Pollution*, 13, 249-261, 2000.

Anderson, R., Henderson, G., Adkins, J., Andersson, P., Eisenhauer, A., Frank, M., and Oschlies, A.: GEOTRACES-An international study of the global marine biogeochemical cycles of trace elements and their isotopes, *Chemie der Erde-Geochemistry*, 67, 85-131, 2007.

Anderson, R. F., Mawji, E., Cutter, G. A., MEASURES, C. I., and Jeandel, C.: GEOTRACES: changing the way we explore ocean chemistry, *Oceanography*, 27, 50-61, 2014.

Baker, A., Adams, C., Bell, T., Jickells, T., and Ganzeveld, L.: Estimation of atmospheric nutrient inputs to the Atlantic Ocean from 50° N to 50° S based on large-scale field sampling: Iron and other dust-associated elements, *Global Biogeochemical Cycles*, 27, 755-767, 2013.

Baker, A. R. and Jickells, T. D.: Atmospheric deposition of soluble trace elements along the Atlantic Meridional Transect (AMT), *Progress in Oceanography*, 158, 41-51, 2017.

Baker, A. R., Jickells, T. D., Witt, M., and Linge, K. L.: Trends in the solubility of iron, aluminium, manganese and phosphorus in aerosol collected over the Atlantic Ocean, *Marine Chemistry*, 98, 43-58, 2006.

Bowie, A. R., Whitworth, D. J., Achterberg, E. P., Mantoura, R. F. C., and Worsfold, P. J.: Biogeochemistry of Fe and other trace elements (Al, Co, Ni) in the upper Atlantic Ocean, *Deep Sea Research Part I: Oceanographic Research Papers*, 49, 605-636, 2002.

Dammshäuser, A. and Croot, P. L.: Low colloidal associations of aluminium and titanium in surface waters of the tropical Atlantic, *Geochimica et Cosmochimica Acta*, 96, 304-318, 2012.

Duce, R., Liss, P., Merrill, J., Atlas, E., Buat-Menard, P., Hicks, B., Miller, J., Prospero, J., Arimoto, R., and Church, T.: The atmospheric input of trace species to the world ocean, *Global biogeochemical cycles*, 5, 193-259, 1991.

Gehlen, M., Heinze, C., Maier-Reimer, E., and Measures, C. I.: Coupled Al-Si geochemistry in an ocean general circulation model: A tool for the validation of oceanic dust deposition fields?, *Global Biogeochemical Cycles*, 17, 2003.

Grand, M. M., Buck, C. S., Landing, W. M., Measures, C. I., Hatta, M., Hiscock, W. T., Brown, M., and Resing, J. A.: Quantifying the Impact of Atmospheric Deposition on the Biogeochemistry of Fe and Al in the Upper Ocean A Decade of Collaboration with the US CLIVAR-CO₂ Repeat Hydrography Program, *OCEANOGRAPHY*, 27, 62-65, 2014.

Han, Q., Moore, J. K., Zender, C., Measures, C., and Hydes, D.: Constraining oceanic dust deposition using surface ocean dissolved Al, *Global biogeochemical cycles*, 22, 2008.

Mahowald, N. M., Baker, A. R., Bergametti, G., Brooks, N., Duce, R. A., Jickells, T. D., Kubilay, N., Prospero, J. M., and Tegen, I.: Atmospheric global dust cycle and iron inputs to the ocean, *Global Biogeochemical Cycles*, 19, 2005.

Measures, C.: The distribution of Al in the IOC stations of the eastern Atlantic between 30° S and 34° N, *Marine chemistry*, 49, 267-281, 1995.

Measures, C. and Edmond, J.: Aluminium in the South Atlantic: steady state distribution of a short residence time element, *Journal of Geophysical Research: Oceans (1978–2012)*, 95, 5331-5340, 1990.

Measures, C., Hatta, M., Fitzsimmons, J., and Morton, P.: Dissolved Al in the zonal N Atlantic section of the US GEOTRACES 2010/2011 cruises and the importance of hydrothermal inputs, *Deep Sea Research Part II: Topical Studies in Oceanography*, 116, 176-186, 2015.

Measures, C. I. and Brown, E. T.: Estimating Dust Input to the Atlantic Ocean Using Surface Water Aluminium Concentrations. In: *The Impact of Desert Dust Across the Mediterranean*, Guerzoni, S. and Chester, R. (Eds.), Springer Netherlands, Dordrecht, 1996.

Menzel Barraqueta, J. L., Schlosser, C., Planquette, H., Gourain, A., Cheize, M., Boutorh, J., Shelley, R., Pereira Contreira, L., Gledhill, M., Hopwood, M. J., Lherminier, P., Sarthou, G., and Achterberg, E. P.: Aluminium in the North Atlantic Ocean and the Labrador Sea (GEOTRACES GA01 section): roles of continental inputs and biogenic particle removal, *Biogeosciences Discuss.*, 2018, 1-28, 2018.

Middag, R., de Baar, H. J. W., Laan, P., and Bakker, K.: Dissolved aluminium and the silicon cycle in the Arctic Ocean, *Marine Chemistry*, 115, 176-195, 2009.

Middag, R., Van Hulten, M., Van Aken, H., Rijkenberg, M., Gerringa, L., Laan, P., and De Baar, H.: Dissolved aluminium in the ocean conveyor of the West Atlantic Ocean: effects of the biological cycle, scavenging, sediment resuspension and hydrography, *Marine Chemistry*, 177, 69-86, 2015.

Orians, K. J. and Bruland, K. W.: The biogeochemistry of aluminum in the Pacific Ocean, *Earth and planetary science letters*, 78, 397-410, 1986.

Orians, K. J. and Bruland, K. W.: Dissolved aluminium in the central North Pacific, *Nature*, 316, 427-429, 1985.

Thi Dieu Vu, H. and Sohrin, Y.: Diverse stoichiometry of dissolved trace metals in the Indian Ocean, *Scientific Reports*, 3, 1745, 2013.

van Bennekom, A. J. and Jager, J. E.: Dissolved aluminium in the Zaire river plume, *Netherlands Journal of Sea Research*, 12, 358-367, 1978.

Van Der Loeff, M. R., Helmers, E., and Kattner, G.: Continuous transects of cadmium, copper, and aluminium in surface waters of the Atlantic Ocean, 50°N to 50°S: correspondence and contrast with nutrient-like behaviour, *Geochimica et Cosmochimica Acta*, 61, 47-61, 1997.

Vink, S., Boyle, E. A., Measures, C. I., and Yuan, J.: Automated high resolution determination of the trace elements iron and aluminium in the surface ocean using a towed Fish coupled to flow injection analysis, *Deep Sea Research Part I: Oceanographic Research Papers*, 47, 1141-1156, 2000.

Ye, Y. and Völker, C.: On the Role of Dust-Deposited Lithogenic Particles for Iron Cycling in the Tropical and Subtropical Atlantic, *Global Biogeochemical Cycles*, 31, 1543-1558, 2017.

Acknowledgments

First of all a big thank you goes to my primary supervisor Eric P. Achterberg which gave me the opportunity to do my master thesis and afterwards my PhD. I will not forget the 6 years in the Achterberg's group. Also, I would like to thank Christian and Martha for insightful help during my PhD. A big thank you goes to the post-doc office (Tom, Mark, Aaron, Pablo) for always willing to help. Another big thank you goes to Helene Planquette who since my first cruise took care of me and taught me all about trace metals. You have been a great support during the critical phases of this work.

It has been nearly five years in Kiel and now it is time to start a new chapter in life. During the time in Kiel many people were part of my life, some of them will continue to be part of it and others have left a mark in my life.

Muchas gracias a todos los kielers. Hemos vivido grandes momentos que se quedaran en la memoria para siempre. Bodas, barbacoas, festivales, nacimientos..... Se os echara de menos. Muchas gracias a todos los que durante estos años me han aguantado y a la vez han compartido risas y agradables momentos.

Sara, muchas gracias por aguantarme muchos años y por tu ayuda con los codigos!!Cuida bien de Maui!

Ese Guille y Angie. Ya esta. Conseguido!! Nos veremos por el mundo o en nuestra capital favorita!

Ein großes danke schön für die HTC Mannschaft. Vielen Dank dass ich bei euch mitspielen könnte!

This thesis is dedicated to my parents, Pilar and Siegmar. You always taught me freedom and from you I learned to be a good person. You always have supported me in any decision I took without questioning it. Much of what I am nowadays is due to you both.

A massive thank you for all the support, for putting up with me during all the last steps of the PhD goes to Jessica. You are an amazing woman and from now on we will live all the adventures that have waited because of the PhD.

-- Make love, not war --

-- Mach Liebe, nicht Krieg --

-- Haz el amor, no la guerra --

Statement of declaration

I declare that I have produced the PhD thesis

"Biogeochemical cycle of dissolved aluminium in the Atlantic Ocean"

independently and without improper external assistance and that I have identified all word-for-word quotations of other authors, as well as comments based closely on other authors' ideas, and I have listed the relevant sources.

Moreover, I assure that the PhD thesis has been written under compliance of the rules for good scientific practice of the German Research association and that the PhD thesis has not been submitted before to an examination procedure.

Jan-Lukas Menzel Barraqueta

Kiel, 28.04.2018

List of Figures

- 1.1 Locations where dissolved iron has been analysed below 2000 m depth
- 1.2 GEOTRACES cruise sections plan
- 1.3 Dissolved aluminium IDP 2017
- 1.4 Modelled atmospheric dust deposition
- 1.5 Distribution of dissolved aluminium with depth in the Atlantic Ocean
- 1.6 Global satellite chlorophyll a
- 2.1 Surface sampling with towfish
- 2.2 Deep sampling with CTD
- 2.3 Clean container seawater sampling
- 2.4 Flow Injection Analyser (FIA)
- 2.5 Matlab output for FIA
- 2.6 FIA data processing spreadsheet
- 2.7 Calibration Batch Lumogallion method
- 3.1 GA01 cruise map and salinity section
- 3.2 Surface dissolved and particulate aluminium, and biogenic silica (GA01)
- 3.3 Surface dissolved aluminium in the Iberian basin
- 3.4 Surface dissolved aluminium in Greenland
- 3.5 Section particulate to dissolved aluminium ratio (GA01)
- 3.6 Deep profiles of dissolved aluminium (Iberian shelf)
- 3.7 Salinity profiles (Iberian shelf)
- 3.8 ADCP (Iberian basin)
- 3.9 Section plot of dissolved aluminium, Box whisker plot, and average dissolved aluminium profiles with depth (GA01).
- 3.10 Deep profile of dissolved and particulate aluminium (station 11 GA01)
- 3.11 Dissolved aluminium against salinity for Mediterranean Outflow Waters

- 3.12 Deep profiles for dissolved aluminium and transmissometry (GA01)
- 3.13 Deep profiles dissolved and particulate aluminium on the shelf
- 4.1 Map Atlantic Ocean with cruises
- 4.2 Map Atlantic Ocean with station numbers
- 4.3 Atmospheric sub-regions to define aerosol aluminium fractional solubility
- 4.4 Box Whisker plot surface mixed layer depth
- 4.5 Comparisons of surface mixed layer depth for each cruise
- 4.6 Surface mixed layer dissolved aluminium concentrations
- 4.7 Surface distribution of dissolved aluminium, temperature, and chlorophyll a GA06
- 4.8 Chlorophyll a for cruise GA08
- 4.9 Salinity and fluorescence for cruise GA10
- 4.10 Average atmospheric deposition fluxes for cruise GA01, GA06, GA08, and GA10
- 4.11 Comparison of calculated atmospheric deposition fluxes and modelled atmospheric deposition fluxes for GA01,GA06,GA08, and GA10
- 5.1 Map cruise GA08
- 5.2 Sections and deep profiles for salinity and transmissometry for the Congo River Plume
- 5.3 Dissolved aluminium and salinity in the Congo River Plume
- 5.4 Correlation between salinity and dissolved aluminium for different rivers
- 6.1 Surface dissolved aluminium concentrations in the Atlantic Ocean
- 6.2 Global biogeochemical cycle of aluminium in the ocean

List of Tables

- 1.1 Key trace elements and isotopes (GEOTRACES Programme)
- 3.1 Aluminium freshwater endmembers (Greenland)
- 3.2 Total dissolvable aluminium in Ice and Fjord samples
- 4.1 Biogeochemical provinces for cruises GA01, GA06, Ga08, and GA10
- 4.2 Sampling and analysis approaches for cruises GA01, GA06, GA08, and GA10
- 4.3 Aerosol Al fractional solubility for the different sub-regions
- 4.4 Inputs values for estimation of atmospheric deposition fluxes
- 4.5 Average atmospheric deposition flux for each biogeochemical province
- S4. 1 Calculated mixed layer depth, measured dissolved aluminium, and atmospheric deposition flux for each station
- 5.1 Average dissolved organic carbon, dissolved aluminium, water discharge, and dissolved aluminium flux for major rivers in the world.

List of Abbreviations

ADCP	Acoustic Doppler Current Profiler
ANOVA	Analysis of Variance
BEC	Biogeochemical Elemental Cycling
BENG	Benguela Coastal Current
BODC	British Oceanographic Data Centre
BSi	biogenic silica
CaCO ₃	Calcium Carbonate
Chl a	Chlorophyll a
CTD	Sampling device
dAl	Dissolved aluminium
DOC	Dissolved organic carbon
DRC	Democratic Republic of Congo
DSOW	Denmark Strait Overflow Water
EAFR	Eastern Africa Coastal
ECG	Equatorial Gyre
EGC	East Greenland Current
ENAB	Eastern North Atlantic Basin
FIA	Flow Injection Analysis
FKLD	South West Atlantic Shelf
GA01	GEOTRACES section
GA02	GEOTRACES section
GA03	GEOTRACES section
GA04N	GEOTRACES section
GA06	GEOTRACES section
GA08	GEOTRACES section
GA10	GEOTRACES section
GD	GEOTRACES deep
GS	GEOTRACES surface reference seawater
Gt	Giga tonne
GUIN	Guinean Current Coastal
HCl	hydrochloric acid
IB	Iberian Basin
IcB	Iceland Basin
IcSPMW	Iceland Sub Polar Mode Water
IDP	Intermediate Data Product
IrB	Irminger Basin
IrSPMW	Irminger Sub Polar Mode Water
ISOW	Iceland Scotland Overflow Water
ITCZ	Intertropical Convergence Zone
LB	Labrador Basin
LDPE	low density polyethylene
LSW	Labrador Sea Water
MADCOW	Model of Aluminium for Dust Calculation in Oceanic Waters
MLD	mixed layer depth

MOC	meridional overturning circulation
MOW	Mediterranean Outflow Water
NAm	North America
NAr	North Atlantic remote
NASG	North Atlantic Subtropical Gyre
NAST	North Atlantic Subtropical
NATR	North Atlantic Tropical Gyre
NEACW	North East Atlantic Central Water
NEADW	North East Atlantic Deep Water
NEC	North Equatorial Current
pAl	particulate Al
PES	polyethersulfone
PTFE	polytetrafluorethylene
PVC	polyvinylchloride
SAbb	South African burning biomass
SAC	South Atlantic Current
Saf	South African
SaFe S	Reference Seawater
SAG	South Atlantic Gyre
Sah	Saharan
SAIW	Sub Arctic Intermediate Water
SAm	South American
SANA	Subarctic North Atlantic
SAr	South Atlantic remote
SEAO	Southeast Atlantic Ocean
SEC	South Equatorial Current
SSTC	South Subtropical Convergence
TdAl	total dissolvable Al
TMR	Trace Metal Clean Rosette
UpA	ultra-pure acid
WGC	West Greenland Current
WTRA	Western Tropical Atlantic
μM	micromolar

Curriculum Vitae

Jan-Lukas Menzel Barraqueta

Date of birth: 19.07.1986

Place of birth: Gatika (Basque Country)

Nationality: German-Spanish

Education

- 2014-2018 PhD candidate at GEOMAR Helmholtz Centre for Ocean Research Kiel
Dissertation title: “*The biogeochemical cycle of dissolved aluminium in the Atlantic Ocean*”
PI: Eric Pieter Achterberg
Co-supervisors: Christian Schlosser and Martha Gledhill
- 2011-2013 European Master in Marine Environment and Resources
University of Bordeaux, University of the Basque Country, University of Southampton (National Oceanographic Centre Southampton)
Master thesis title: “*Carbonate chemistry and acidification in the North East Atlantic*”
PI: Eric Pieter Achterberg
- 2005-2011 Marine sciences Diplom at University of Vigo, Spain

Research at Sea

- 2015 GEOTRACES GA08 section on board RV Meteor
- 2014 GEOTRACES GA01 section on board RV Pourquoi Pas?
- 2013 Extended Ellet Line on board RV James Cook

Publications

- 1) Menzel Barraqueta, J.-L., Schlosser, C., Planquette, H., Gourain, A., Cheize, M., Boutorh, J., Shelley, R., Pereira Contreira, L., Gledhill, M., Hopwood, M. J., Lherminier, P., Sarthou, G., and Achterberg, E. P.: Aluminium in the North Atlantic Ocean and the Labrador Sea (GEOTRACES GA01 section): roles of continental inputs and biogenic particle removal, *Biogeosciences Discuss.*, <https://doi.org/10.5194/bg-2018-39>, in review, 2018.
- 2) Menzel Barraqueta, J.-L., Jessi K., Klar., Rachel Shelley, Martha Gledhill, Christian Schlosser, Bernhard Wenzel, Helene Planquette, Geraldine Sarthou, Eric Achterberg. Atmospheric deposition fluxes over the Atlantic Ocean: A GEOTRACES case study. Submitted to *Biogeoscience discussions*
- 3) Tonnard, M., Planquette, H., Bowie, A. R., van der Merwe, P., Gallinari, M., Desprez de Gésincourt, F., Germain, Y., Gourain, A., Benetti, M., Reverdin, G., Tréguer, P., Boutorh, J., Cheize, M., Menzel Barraqueta, J.-L., Pereira-Contreira, L., Shelley, R., Lherminier, P., and Sarthou, G.: Dissolved iron in

the North Atlantic Ocean and Labrador Sea along the GEOVIDE section (GEOTRACES section GA01), *Biogeosciences Discuss.*, <https://doi.org/10.5194/bg-2018-147>, in review, 2018.

- 4) Zurbrick, C. M., Boyle, E. A., Kayser, R., Reuer, M. K., Wu, J., Planquette, H., Shelley, R., Boutorh, J., Cheize, M., Contreira, L., Menzel Barraqueta, J.-L., and Sarthou, G.: Dissolved Pb and Pb isotopes in the North Atlantic from the GEOVIDE transect (GEOTRACES GA-01) and their decadal evolution, *Biogeosciences Discuss.*, <https://doi.org/10.5194/bg-2018-29>, in review, 2018.
- 5) Humphreys, M., Griffiths, A., Achterberg, E., Holliday, N.P., Rerolle, V., **Menzel Barraqueta, J.L**, Couldrey, M., Oliver, K., Hartman, S., Esposito, M., Boyce, A., 2016. Multidecadal accumulation of anthropogenic and remineralised dissolved inorganic carbon along the Extended Ellett Line in the northeast Atlantic Ocean. *Glob. Biogeochem. Cycles* 30, 293–310.
<http://dx.doi.org/10.1002/2015GB005246>

